UNIVERSITY OF STRATHCLYDE

Department of Electronic and Electrical Engineering

EM Field Effects on the Surface of Polluted HV Insulators

Hossam Abd -Elsattar Gouda

PhD Thesis

October 2003

With all love

To the soul of my father

Abd El-sattar

The man who taught me how to be a man

Also, to my wife Soha and my sons

Mohamed and Youssef

I

Summary

Outdoor high voltage power plant is exposed to environmental pollution which is an important cause of failure. Knowledge of conditions leading to flashover is essential to design insulation levels. Discharges on the surface of polymeric insulators are one of the ageing mechanisms responsible for eventual failure. In this thesis, we examine water droplets on insulator surfaces. Chapter 1 discusses pollution on the surface of high voltage insulators, and chapter 2 considers water droplets on insulator surfaces. Chapter 3 reviews recent work in this area. Chapter 4 presents the aims of the present work to examine partial discharges at the edge of water droplets and to investigate droplet vibration with an applied ac field. Chapter 5 identifies the apparatus and procedures that were developed. Chapter 6 describes an experimental study of electrical breakdown at the edges of sessile water droplets on a PE surface subject to ac electrical stress up to of 2.0MV/m at 50 Hz. The study involves observing the motion of water droplets using a high-speed video camera operating at 3000 frames per second whilst electrically detecting any partial discharge activity. The significance of droplet vibration on electrical stress enhancement is investigated along with the effects on partial discharge activity. Chapter 7 describes test sample geometry and electric field modeling using finite element analysis. Chapters 8 and 9 describe an experimental study of breakdown at a sessile water droplet on a planar, polymeric, insulating surface subject to ac stress, parallel to the insulator surface, up to 2.0MV/m. The contact angle between droplet and surface was varied by controlling the physical properties of the droplet and by inclining the insulator plane from the horizontal. A theoretical model is developed which shows that it is possible to sustain partial discharges in the air around a droplet above the polymer surface.

ACKNOWLEDGMENTS

This research was supported partly by the Egyptian Ministry of Defence. I am grateful to the Egyptian Armed Force for the sponsorship of tuition fees and living expenses of myself during the period of study. It has been a remarkable in linking British and Egyptian cultures.

I must thank the providence of **GOD** that gave me the chance to work under the supervision of Dr. Bruce H Crichton. I appreciate very much his valuable scientific guidance and constructive criticism during the undertaking of this thesis. Also, I wish to express my deepest thanks and gratitude for his help in the analysis of the computed results in this work and his encouragement to complete this thesis.

I would also like to thank professor Brain Culshaw, head of the Electronic and Electrical Engineering department at the University of Strathclyde, for providing excellent environment and facilities for performing this research. In addition, I owe gratitude to the reprographic team, Elizabeth Allan and Isabel Mungall, for their logistics support. They always wear a smile, which is unforgettable. I wish to thank Maureen Cooper for her great help.

I would also like to thank Dr. R Anthony Fouracre for his great support, providing me with recent publications, and for his valuable advice. My greatful thanks got to workshop team for their fruitful help in preparing the samples and models for my experimental work, especially Joseph Mc Kechnie. Also, I wish to express my deepest thanks to John Mackersie, Martin D Judd and John Wilson for their significant technical help in preparing my experimental work.

Finally, I would like to thank my wife Soha for her patience and support through the difficult years of my PhD. Thanks for going through the adventure with me, for feeding me and cheering me up, for keeping me up to date with the news about Egypt... and for

believing in me all the times and under all circumstances. I would like to record my great indebtedness and gratitude to my sons Mohamed and Youssef for their smiles all the time and my family in Egypt for their endless prayers, encouragement, and support especially my mother Nadia and my brother Mohamed Shehata. It may not be possible for me to return their endless love and sacrifice.

Many thanks go to anyone else who has helped me either explicitly or implicitly.

Hossam A. Gouda

October 2003

Table of Contents

Chapter 1

Introduction Pollution on HV insulation

1.1 General

Surface pollution of insulators is one of the most important causes of failure in the transport of electric energy. Pollution phenomena constitute a serious problem, which must be taken into account in the design, the dimensioning and operation of HV insulating structures [1]. Consequently, knowledge of the conditions that lead to flashover is essential to properly design the insulation level of an electric power system against pollution. The particles deposited on the surface of outdoor insulators form a non-uniform mixture of different soluble and non-soluble substances, which, under certain conditions, modify the electrical performance of insulators. In such circumstances, a complex process is originated and its final stage may be the flashover of the insulators.

Outdoor high voltage power plant, such as insulators, bushings, surge arresters and current transformers, etc. are exposed to various environmental conditions during their service life. In industrial, coastal and desert areas, for example, the surface of an insulator can become heavily polluted [2]. The deposit of pollutants on insulating surfaces may cause considerable diminution of the dielectric strength of the system [3]. In addition to normal operating stress, HV transmission systems are also submitted to numerous other stresses of various origins, e.g. mechanical, electrical and environmental. Among the main electrical stresses are, those caused by lighting and switching over-voltages and those resulting from the flashover of polluted insulators [4].

Under severe environmental conditions, when a pollution layer (dry or wet) is deposited on an insulator surface, leakage current begins to flow, which may lead to a total flashover [5]. Contamination flashover may occur during periods of wet weather and may cause power outages, which pose a particular threat to the reliability of the

power supply [6]. The performance of an HV insulator under polluted conditions is quite different from that under pollution-free condition [7].

Considering the importance of pollution problems, continuous and intensive laboratory studies and field investigations have been taking place worldwide for many years. In chapter 3, a review is given of previous work especially relevant to the present investigation. The work involves not only experimental investigations but also mathematical modeling to understand the different aspects of the contamination flashover mechanism [8].

Despite this previous work, in recent years the importance of the research on insulator pollution has increased considerably with the rise in typical transmission line voltage. Pollution performance of insulators will be of major significance for the co-ordination of insulation in UHV (Ultra High Voltage) transmission lines. Research on insulator pollution is directed primarily at understanding the physics of the growth of discharges and to the development of mathematical models, which can predict accurately the critical leakage current [9].

The pollution flashover on external insulator is extremely complex and many variables are involved during the development of the phenomenon. Some of these variables: are the polarity of voltages, type and nature of the contaminant, particle size, non-uniform wetting effect, surface conductivity, washing, wind, length, diameter and profile of the insulator, etc [10]. The most significant ones, causing the pollution flashover to be complex are: the insulator shapes, the pollutant deposit on the insulator surface and the wetting of the pollution layer [11]. A review of these factors is given in the following sections of this thesis.

1.2 Insulating Materials

High voltages are used for wide variety of application, covering power systems, industries and research laboratories. The potential benefits of electrical energy supplied to a large number of consumers have resulted in the development of complex electrical apparatus. The development of electrical energy utilization has led to increasing transmission voltage. The diverse conditions under which high voltage apparatus is used necessitates careful design of its insulation. The principal media of insulation are gases, vacuum, solids, and liquids or, more usually combinations of these. For achieving reliability and economy, knowledge of the causes of deterioration is essential, and the tendency to increase the voltage stress for optimum design calls for judicious selection of insulation in relation to the dielectric strength, corona discharges and other relative factors. There are four principal areas where insulation must be applied i.e.:

a) Between HV conductor and earth (phase to earth).

b) Between HV conductors of different phases (phase to phase).

c) Between turns in a coil (inter-turn).

d) Between the coils of the same phase (inter-coil).

The insulation is primarily meant to resist electrical stresses, however, it should also be able to withstand certain other stresses, for example, mechanical and thermal stresses which the insulation encounters during manufacture, storage and operation.

Usually the performance of the insulation depends on its operating temperature, where the higher the temperature the higher will be the rate of its chemical deterioration. Therefore it is necessary to determine the maximum temperature for an insulation which will ensure safe operation over its expected life. Thus the insulating materials are rated into different classes according to their operating temperature limits.

One important matter in the study of electrical insulation is to determine the condition of the insulating material before breakdown. There are several methods and instruments by which the quality of insulation can be monitored so as to avoid

unexpected breakdown. Among the most important electrical properties of insulating materials to be measured are: electrical strength, surface flashover strength, volume and surface resistivity, and dissipation factor and dielectric permittivity.

The present study is concerned primarily with solid insulating materials; especially the polymeric insulating materials used extensively in many high-voltage power transmissions applications. Polymers are favoured by manufacturer because they are cheap, easy to fabricate into complicated shapes and sizes, tough and lightweight. Furthermore their electrical properties are generally superior to those of alternative materials in term of resistivity, surface conductivity and dielectric losses [12].

1.3 Polymeric Insulators

Over the years the use of polymeric materials in electric power applications has increased steadily. They currently represent 60% to 70% of newly installed HV insulators in North America [13]. Special interest has been paid to the use of polymeric materials for high voltage outdoor insulators. Some of the major advantages of the polymeric insulators over the traditional ceramic ones are their light weight and good hydrophobicity (water-repellence). As a consequence, they are easier and cheaper to store, transport and install. However, polymeric materials are more prone to deterioration and chemical alterations, which can seriously reduce the reliability and lifetime of insulators in service. The weather-exposed part of polymeric insulator should possess high hydrophobicity in order to give maximum performance (see chapter 2). Necessary demands on materials for such usage are an ability to withstand discharges in wet, salty, acidic, tropical or arctic environment. Difficult environment conditions can, however, cause a permanent or temporary loss of hydrophobicity. Polymeric insulators are therefore today often pessimistically designed for an assumed reduced hydrophobic, i.e. hydrophilic, state. This means that the benefits of using a polymeric material instead of porcelain and glass are not utilised to their full potential. Properly used, these materials can offer advantages such as more compact design, reduced maintenance and lower total operating cost.

1.4 Types of Outdoor Insulators

A practical high-voltage insulator is actually a system of components consisting of the dielectric, terminal electrodes or end-fitting and internal parts that help attach the dielectric to the electrodes. There is quite a variety in the details of these components and in construction methods. Insulators are commonly identified largely by the dielectric material employed. There are three main groups of dielectrics that have been used for outdoor HV insulator construction and lead to the well-known nomenclature of porcelain, glass and polymeric insulators. Porcelain insulators are also commonly known by other names, such as, composite (in Europe) and nonceramic (in North America) [14].

Porcelain and glass insulators have been used for many decades whereas the wide-spread use of polymeric outdoor insulation is relatively recent. The most widely used type of porcelain and glass insulator worldwide, is the cap and pin type where each unit or bell is connected to each other by metal hardware. Fig (1.1) shows photographs of outdoor lines using the gap and pin suspension porcelain insulator and composite insulators. This illustrates the typical configurations and exposure which outdoor insulators are subject to.

High voltage porcelain insulators are glazed, thereby imparting a smooth, glossy surface of uniform color to the insulator. This has two important functions. The first is to increase the strength of porcelain. It is well known that failure of brittle materials generally starts from microscopic surface defect. The glaze not only fills these microscopic defects, thereby preventing their propagation, but also has a slightly lower thermal expansion coefficient than the porcelain which induces superficial macroscopic compressive stresses. The resulting strength improvement over unglazed porcelain is about 30%. The second function is to provide a smooth surface, which is more easily cleaned by rain or during insulator washing and cleaning operations [15]. Polymeric materials are known to suffer from surface erosion and tracking when exposed to such conditions [13].

1.5 Uses of Outdoor insulators

Insulators used on overhead lines are called line insulators. Insulators used in stations for supporting bus work and related switchgear are referred to as station insulators. They are used as bushings in apparatus in order to enable connection of the enclosed energized terminals to overhead system. Station insulators are used as external housings on measuring devices such as instrument transformers, and protective equipment, e.g., surge arresters. In underground networks, they are used with the terminations, which enable the transition of an overhead line to an underground cable [16].

Line insulators are called by several names, depending on the function. Insulators used for suspending the overhead conductor from the tower are known as suspension insulators. Insulators used on structures where the lines terminate or originate, or where the direction of a line changes, are known as dead-end insulators (in North America) and tension insulators (in Europe or elsewhere). Suspension and dead-end insulators are mounted on cross-arms connected to the pole. Fig (1.2) illustrates the use of insulators in various applications [15]. Polymeric insulators are being widely adopted for all types of applications.

1.6 Stresses Encountered in Service

Outdoor insulators are subjected to a variety of stresses, including mechanical, electrical and environmental stresses, which act in unison. The exact nature and magnitude of these stresses varies significantly and depends on the details of insulator design, application and location. For example, suspension and dead end insulators encounter a tensile load due to weight and tension of the conductor. Fig (1.3) shows a typical dead-end insulator. It has a fiberglass core with a polymeric sheath and weathersheds. The surfaces show a wide range of orientations from horizontal to vertical. Wind and ice imposes additional loading. Insulators used for supporting station apparatus encounter a compressive mechanical load. Line post insulators are subject to a cantilever or bending load in supporting the conductor. In addition, transient-loading

conditions can be generated. Torsional or twisting type of load can be experienced by line insulators during line construction. Vibrational loads are imposed on insulators due to conductor vibration and movement. Shock (or impact) loading is possible during natural events like earthquakes, ice shedding, or man made events like the impact of vehicles on poles and vandalism (gun shots) [15]. Surface pollution may be affected by such mechanical stresses. For example, liquid pollution would be affected by vibration. The term "string efficiency" is used as a general reference to the mechanical performance of suspension insulators.

Electrical stresses include the steady-state stress imposed by power frequency normal operating voltage. Voltage surges generated by lighting or switching operation impose a higher, albeit, momentary stress on the insulator. In the event of an insulator flashover, the insulator is subjected to a large fault current (several kA) at power frequency in the form a power arc which, persists until the protection isolates the fault.

Outdoors environmental conditions vary over a wide range. Temperature affects the insulation properties of all materials as the conductivity usually increases with temperature. For polymers that are organic materials, ultra-violet (UV) radiation from sunlight can break certain chemical bonds, and/or cause cross-linking on the surface, resulting in surface degradation. Moisture in any form (rain, dew, fog, melting ice and snow) lowers the surface insulation resistance significantly from the dry state. In the presence of contamination, the surface resistance is reduced even more drastically. Altitude or the elevation above sea level affects the insulation properties. Higher altitudes reduce the air density, hence, weakening the surface insulating strength. These stresses could be acting on insulators in various combinations. Hence it is clear that the insulators have to perform under a wide range of surface of service conditions. Needless to say, only insulators that are designed to take all these stresses into account will work satisfactorily in the field for many years [17]. Hence, research into how insulators function under polluted conditions remains an important field of activity.

1.6.1 Electrical Performance

The insulator's dielectric material is largely responsible for the electrical performance of the insulator. It is important to distinguish between the bulk or volume properties, and surface properties. The volume dielectric strength is determined by defects in the form of impurities and voids. These defects provide sites for electrical stress concentration, which could lead to formation of permanent failure path within the dielectric. Failures along the bulk of material are usually permanent in nature and are called punctures [15]. The surface dielectric strength is determined largely by surface deposits and moisture.

Resistivity values, for the bulk material which are indicative of the dielectric strength, are typically $> 10^{10}\ \Omega/mm^2$. High surface resistance may also obtained under dry conditions. However, in the presence of humidity, surface resistance values are lowered by several orders of magnitude, and are even further lowered in the presence of ionic contaminants on the surface [15].

For dielectric materials that do not contain large voids or impurities the electric stress required for failure via the surrounding air medium is much lower than for bulk failure. The arc produced by such a flashover is usually away from the surface of the dielectric. Therefore, as far as flashover is concerned, porcelain, glass and composite insulators are self-restoring types of insulation. However, such discharges may affect the surface by altering its hydrophobicity, for example, by emitting UV light and so breaking chemical bonds, as mentioned above. This effect may also occur in the presence of partial discharges near the surface.

Whether an insulator fails by surface flashover or by puncture depends on the magnitude and duration of the electric stress applied, insulator dimensions and defects in the material. Puncture breakdown will take place at the point where the voltage curve of surface flashover intersects that of internal breakdown, as illustrated in Fig (1.4). Breakdown requires the formation of an ionized channel, and this channel has to be

established within the duration of the applied voltage. If the insulator is defective (i.e. has large voids or impurities), puncture can be caused by extremely short duration, large magnitude pulses. Lighting surges, which have a risetime in the microsecond range, do not cause puncture if the insulator is sound. Similarly, switching surges normally do not cause puncture. Both lighting and switching surges can cause surface flashover if they have adequate magnitude, even under dry conditions. Longer duration stresses, such as imposed by power frequency, do not result in a puncture, except, perhaps, in the very long term. A flashover is possible, however, in a wet and contaminated environment [15].

1.7 Shapes of Outdoor Insulators

Flashover due to surges is usually determined by the shortest gap in air between the conductors supporting as insulator. This spacing is called the dry arc distance, see Fig (1.5). Moisture has little effect on the flashover voltage due to lighting surges. The flashover voltage under surges is, however, dependent on the dry arc distance. Flashover under contaminated conditions depends on the leakage or creepage distance which is also illustrated in Fig (1.5).

If the dielectric material is not altered during service, electrical characteristics like power frequency wet withstand or flashover, lighting and switching surges are defined by dry arc distance. The shape or profile of the dielectric determines the leakage distance and is important for the insulator's contamination performance.

In order to increase the leakage distance, and to help keep certain sections of the insulator dry, it is common to see corrugations on the underside of porcelain and glass cap and pin insulators. The required dry arcing and leakage distance is obtained by stacking several units, the number being dependent on the voltage level, contamination severity and the profile of the insulator. Many shapes of porcelain and glass insulators have been developed as shown in Fig (1.6) of which the common ones are the standard (A), fog type(C) and the aerodynamic (H) profiles [15].

1.8 Environmental Pollution of Outdoor Insulators

When contamination is present, the response of external insulation to power frequency becomes an important consideration and may dictate external insulation design. It is known that flashover of insulation generally occurs when the surface is contaminated [18]. The surface pollution can take a number of forms, including:

- Wetting by fog, dew, rain, snow or sea spray. This wetting may be affected by dissolved contaminants contained in the wetting agent, including salt and other chemical pollutants. Such pollution tends to form thin layers distributed over parts of the surface.
- Contamination by natural air-borne particles such as dust, sands or soot. In this case the pollution can be in the form of discrete particles scattered over large areas of the insulator surface.

1.9 The Pollution Problem

High voltage systems often contain insulating bodies in a gaseous environment. If a contamination layer develops on the surface of such an insulator, its electric strength can be enormously reduced. Above all, this is the case for insulation of overhead transmission lines or outdoor switching stations, the long-term behavior of which under atmospheric pollution is of great significance to the operating security of high voltage networks [19].

The severity and frequency of breakdown of insulators due to pollution varies considerably with climate and environment. The problem is that insulators, which are designed carefully to have surface with creepage paths long enough to prohibit voltage breakdown have their properties completely changed by pollution. For example, the pollutants of the surfaces of insulators in desert areas are mainly sand and salty water which can form a conductive path on the surface. The particles constituting the pollutants are deposited from the environment onto the surfaces. The processes, which lead to deposition, are quite diverse, they include: gravitation force, electrostatic

attraction, dielectrophoric migration of high permittivity particles, evaporation of solutions, condensation of solution (dew) and aerodynamic catch [20].

In a recent paper [21] the effects of pollution in arid climates is discussed. It is considered that the resistance of the polluted regions is dependent upon the chemical constituents, the thickness of the deposited layer, the ambient temperate, and the humidity, the dimensions and shape of insulators.

Air movement can cause rotating flow or vortex generation. This effect is particularly important in the portion of the insulator, which is ribbed. In service, the severity of pollution depends on many factors such as: velocity, direction of wind, grain size and type of the contaminant, temperature, humidity and rate of wetting, rainfall, thermal conduction, and corona discharges on the surfaces. The surface becomes conducting under certain conditions and this may initiate breakdown. In comparatively clean regions where rainfall is plentiful, the insulator pollutants are washed off and breakdown problems due to pollution are rare [20].

Surface damage can result from the deposited chemicals and their reactions, which produce sulfuric and nitric acids. These acids increase the exposed area of pollution and react with the surface producing deterioration, which promotes creeping surface discharges when the voltage is applied.

These surface discharges produce ionization in the ambient air and hence ozone. Ozone will be active to oxdize nitrogen, which increases the concentration of nitric acid in the presence of humidity. In turn the nitric acid affects the surface and increases the leakage current.

This leakage current, with its high resistance leakage path, results in heating that dries the region and may promote formation of an electric arc. Such an arc will burn the

region and raise its temperature, which increases the rate of deterioration towards complete failure [21].

The problem of pollution in insulators design has to be seen in the context that it is very desirable to produce high voltage insulators with high electric strength, long life-time and high string efficiency but with minimum weight and size. These requirements give rise to conflicting constraints.

1.10 The Contamination Problem

Determining the performance of insulators under contaminated conditions is the underlying factor that determines insulation design for outdoor applications. Contamination has an unavoidable role to play in every outdoor insulator application. This fact was recognized from the very beginning of outdoor power delivery. There are long-established standardized contamination tests for porcelain and glass insulators, but not for the relatively recent composite insulators [15]. Even for porcelain and glass insulators, there are instances where discrepancies between laboratory predictions and field experience arise. Thus, it is of continuing importance to have a good understanding of the fundamental contamination flashover phenomena if only to understand the advantages and limitations of laboratory testing in relation to application in the field.

As described earlier, the most significant electrical stresses on HV insulation can be divided into lighting overvoltages, switching overvoltages, and abnormal voltage gradients caused by contamination deposited on the insulator surfaces. The lighting and switching surge problems can be adequately addressed by the use of zinc oxide surge arresters and sulfur hexafluoride (SF_6) circuit breakers [15]. This leaves insulation pollution as the most important outdoor insulation problem still outstanding, and this is particularly the case for the more recent polymeric materials. This fact is one of the significant reasons for undertaking the work of this thesis.

1.11 Contamination Flashover Phenomenon

The events leading to contamination flashover of outdoor insulators are shown in Fig (1.7). For a given contamination severity and voltage, this illustrates whether the insulator flashes over or not depends on the insulator materials and design.

1.11.1 Accumulation of contamination

The main forces acting on a dust particle near an energized insulator are gravity, wind and electric field. Of these, the most dominant is wind. The force due to the electric field (E) is composed of two components: a force proportional to E, and a force proportional to E^2 due to divergence of the electric field (see section 2.2). On insulators used an ac lines the first component of these forces averages to zero over a whole cycle due to the alternating nature of the voltage, but the second component – field divergence always result in positive force whose magnitude increases with the normal electric field. On insulators used for dc lines, both components of the magnitude of the forces exerted on a dust particle are shown in Table (1.3). The most dominating force for insulator contamination is wind, followed by electric field stress (for dc). On both ac and dc insulators, as the electric field is non-uniform and concentrated more near the HV terminal, it is common to see this section of the insulator more contaminated than the rest. There are many types of contaminants in the field. The types and amount accumulated on the insulator depends on the service area.

The most common is sand (SiO_2). Common salt (NaCl) contamination is problem for insulators close to the coast. Gypsum ($CaSO_4$) is another common contaminant for inland insulators. Calcium chloride ($CaCl_2$) is the salt used on roadways in colder locations to prevent icing on roads following a snowfall. A combination of vehicular traffic and wind cause deposition of this salt on the insulator surface. In agricultural areas, phosphates and nitrates of nitrogen and ammonia are commonly noticed on insulator [15].

1.11.2 Insulator Wetting

During service the insulator can become wet during rain, wind assisted spray, dew or fog. Wetting by rain and spray is by simple water particle impingement. The surface of an insulator exposed to rain/spray can be expected to be wetted more easily than protected surfaces. If the rain persists long enough, the entire insulator can become wet. Wetting during dew and fog is by the process of condensation, which depends on the temperature difference between the insulator surface and the ambient. Water vapor will condense on the insulator surface for as long as the surface temperature is below that of the ambient. Condensation will cease when the temperature difference vanishes. The profile of the insulator has little influence on condensation wetting.

The insulator material has a significant effect on wetting in service. One important difference between inorganic porcelain and glass materials and the organic polymer materials used for composite insulator is their wettability. The strong electrostatic bonds between the silicon and oxygen in porcelain and glass contribute to a high value of surface free energy, which is a thermodynamic quantity that determines the strength of adhesion of the surface with water. Hence porcelain and glass insulators are readily wettable. Polymers, on the other hand, are weakly bonded at the molecular level, and this provides them with low values of surface energy. This property is responsible for composite insulators resisting the formation of a continuous water layer to a far greater extent than porcelain and glass insulators. The property of resisting water film formation is referred to as hydrophobicity. The surface resistance of an insulator with a hydrophobic surface is far higher than one with a wettable or hydrophilic surface [15]. These aspects of surface behaviour will be examined in more detail in chapter 2.

For a given insulator material, the surface resistance is lowered to a greater degree by condensation wetting than by collision wetting. Condensation wetting is characterized by uniform distribution of tiny water droplets, whereas collision wetting by rain is characterized by bigger water drops that are also further apart. Wind assisted spray wetting can produce a pattern similar to condensation wetting, depending on the wind speed.

The reduction in surface resistance of the insulator under wet condition is a function of the solubility of the contaminant. Among all the salt, NaCl is the most readily soluble salt, but is not the most frequently encountered contaminant (except near the coast). Hence this salt can be expected to provide the highest leakage current. Gypsum and sand are insoluble, and other salts, which are among likely to be observed on insulators, are soluble to different degrees.

1.11.3 Dry Band Arcing

A wet insulator with contaminating has a conductive layer. Electric stress results in a leakage current which causes heating of the electrolytic layer. The power dissipation, which is a function of the current density, this is higher in the narrow parts of the insulator, such as near the pin of porcelain and glass insulators, and on shank of composite insulators. Water is evaporated in this region leaving small annular bands, called dry bands. The formation of dry bands causes a significant change in the voltage distribution along the insulator. The bulk of the voltage now appears across the narrow bands. Consequently the electric stress across the dry bands is higher than the withstand value of the dry band, causing an arc to develop across this band. The arc current is limited by the resistance of the surface layer in series with the dry band. Several dry band arcs can develop in an insulator, but one of them will dominate [15].

The dry band arcs are usually self-limiting. The current in the dry band arc is only a few milliamper's, and requires substantial voltage to support it. This factor, combined with the large surface resistance, causes dry band arcs to be arrested or extinguished. However, under certain conditions such as, low surface resistance caused by high levels of contamination, or voltage surge, presence of ionized gases in the vicinity of the insulator. Then, with the wind assisted motion of the arc, the dry band can elongate long enough to bridge the gap between the insulator terminals causing a flashover.

1.12 Artificial Contamination Test

Artificial contamination laboratory tests have been the subject of research in standard-writing organization, such as the IEC and IEEE/ANSI, for more than years. This has led to the standardization of the two test methods for evaluation porcelain and class insulators, the salt-fog test and the clean-fog test. Both these tests are performed within enclosed chambers.

The quality of laboratory testing can be assessed by three measures: repeatability, reproducibility, and representivity. Repeatability refers to the ability of the test to produce the same (within reasonable limits) results every time the test is performed in one laboratory. Reproducibility refers to the ability to obtain the same results (again with reasonable limits) when the tests are performed in other laboratories. Representivity refers to the ability of the laboratory test to duplicate service or field conditions [15].

1.13 Pollution Test

Testing insulators for their contamination behaviour must take the physical mechanisms during development of flashover into particular account. Deposition of the contamination layer on the insulator can be done either before beginning the voltage test or during the test. In the case of natural pollution, formation of the contamination layer depends on whether the voltage was on or not during increasing pollution [22]. Because of the effect of the electric field on the thickness and distribution of the contamination layer, the results can vary considerably. Natural pollution has the advantage that the site conditions are accurately realized, but too much time is required and the reproducibility is poor. In artificial pollution the contamination layer is deposited before or during the test, where the requirement is to realize as closely as possible the natural pollution condition at the future site [23].

1.14 Flashover Models of polluted insulators

The flashover of a given polluted insulator under ac stress is the final stage of complicated mechanisms. There are three cases of ac flashover mechanism can be distinguished: -

1- Immediate flashover of the pollution band similar to the flashover phenomena under dc voltage;
2- Flashovers on several consecutive voltage cycles in which case the problem of the arc re-ignition is posed each time the current passes thorough zero;
3- No flashover, that is the case in which, despite the heating effect which, may increase the conductivity of the surface layer, the applied voltage is insufficient to induce a flashover [2].

Despite the complexity of the mechanisms involved in the discharge (arc) phenomena, numerous models describing the flashover processes of a polluted insulator have been proposed. A common feature of all these models is a simplified representation of a propagation arc consisting of a partial arc in series with the resistance of the not bridged section of polluted layer. Most of these models are limited to the static state under dc voltage and then extended to the ac case, with no consideration of the re-ignition process. Therefore, they cannot be considered as a complete model that can predict the entire temporal evaluation of the flashover process.

1.15 Types of flashover models

The Mathematical dynamic models allowing to compute the parameters describing the evaluation of the flashover. The mathematical model may be an equivalent electrical network. In this case the flashover or the discharge can be modeled as a resistance in parallel with a capacitance, which respectively represents the arc resistance and the accumulation of the charge at the arc head. A complete characterization will consist of a description of the arc channel by RLC (R, L, C are respectively the resistance, the inductance and the capacitance of the channel [2, 24, 25].

Another type of model is to describe the system by two electrodes (the type of the electrodes may be cylindrical, circular, rectangular, etc.) with the insulation sample between the two electrodes. The length of the insulation sample is varied according the type of the test, the nature of the pollution layer and the electrical stress. This model is used widely to calculate the flashover, leakage current and other discharge phenomena as in for example references [4, 26, 27 and 28].

The flashover, discharge and leakage current can be controlled in an environmental chamber and the type of pollution of interest can be set over the insulation sample. Also in this arrangement the temperature, humidity and chamber volume can be controlled and chosen as described in references [29, 30, 31, and 32].

1.16 Summary

The material presented in this chapter has identified the broad range of issues which are significant for insulator performance. From these the question of the behaviour of water pollution on the surface of polymeric insulators would appear to be one of some importance. The performance of the relatively recent polymeric materials when polluted by the water on their surfaces has not been as extensively studied as other materials. In recognition of this, a review of this area of interest was undertaken. This is presented in the following chapters 2 and 3.

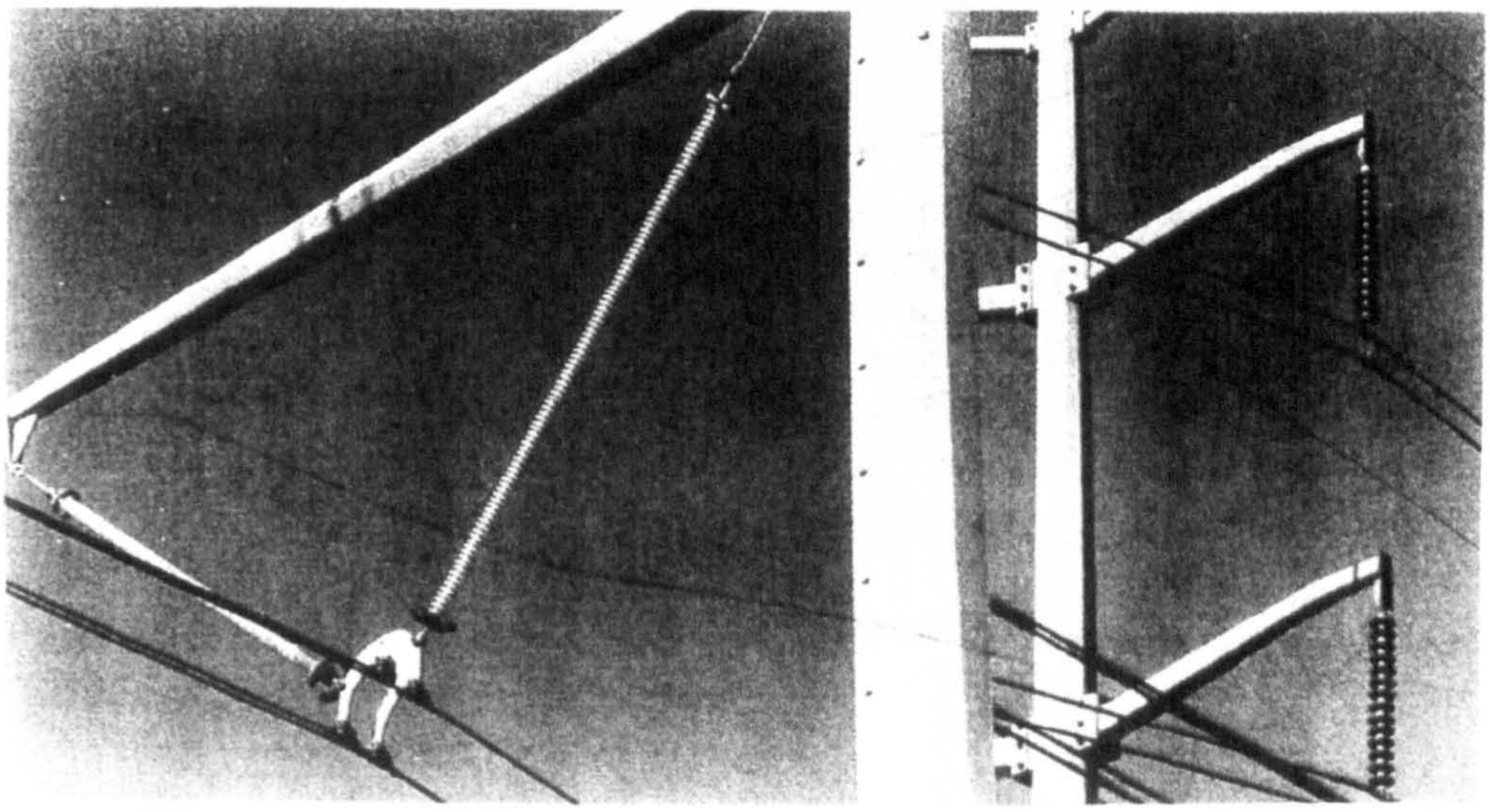

Fig (1.1): 500 kV line using composite insulators (left) and a 230 kV line using cap and pin porcelain insulators (right)

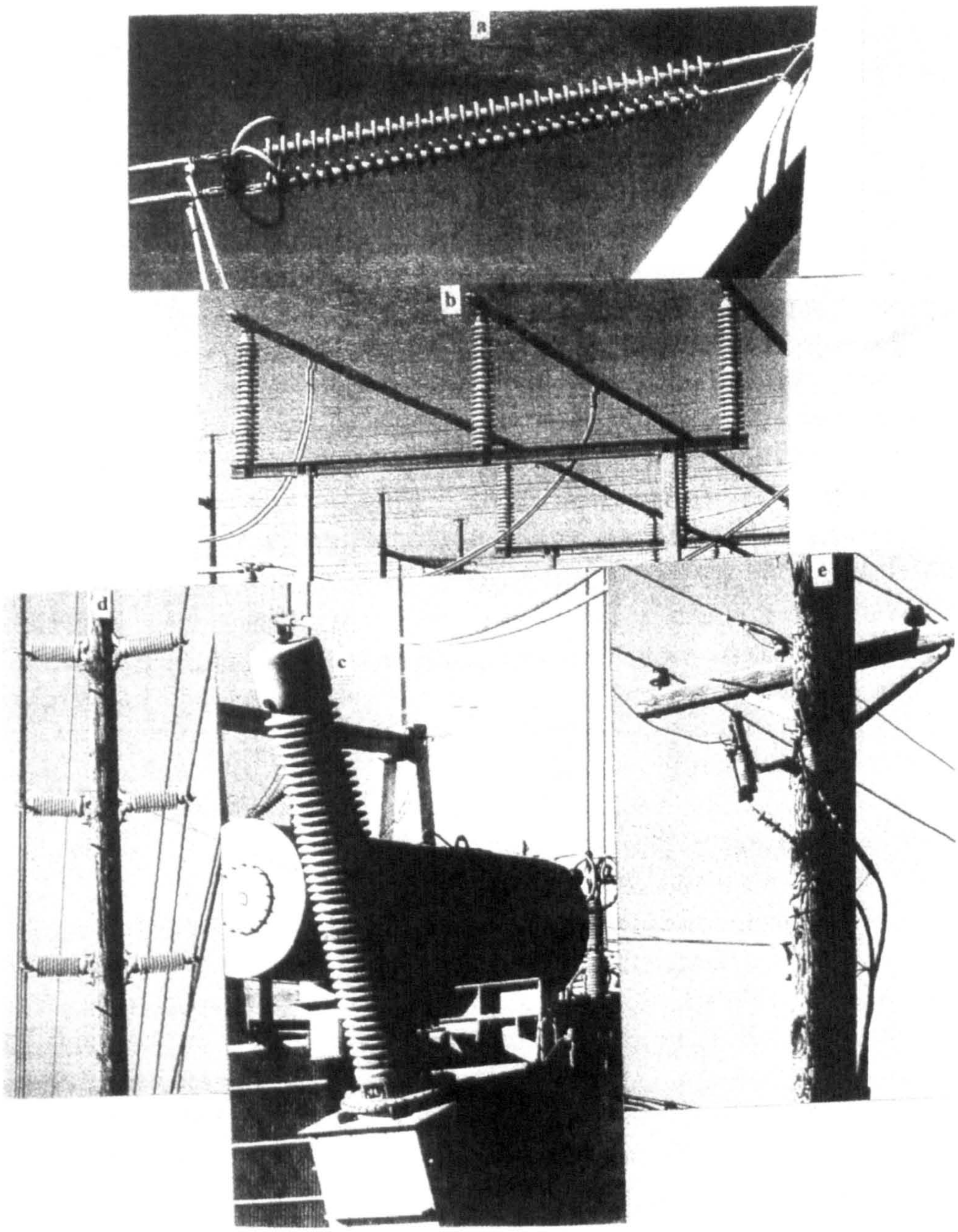

Fig (1.2): photographs of dead-end (a) and station post (b) porcelain insulators, porcelain apparatus bushing (c), porcelain line post (d) and polymer cable terminations (e).

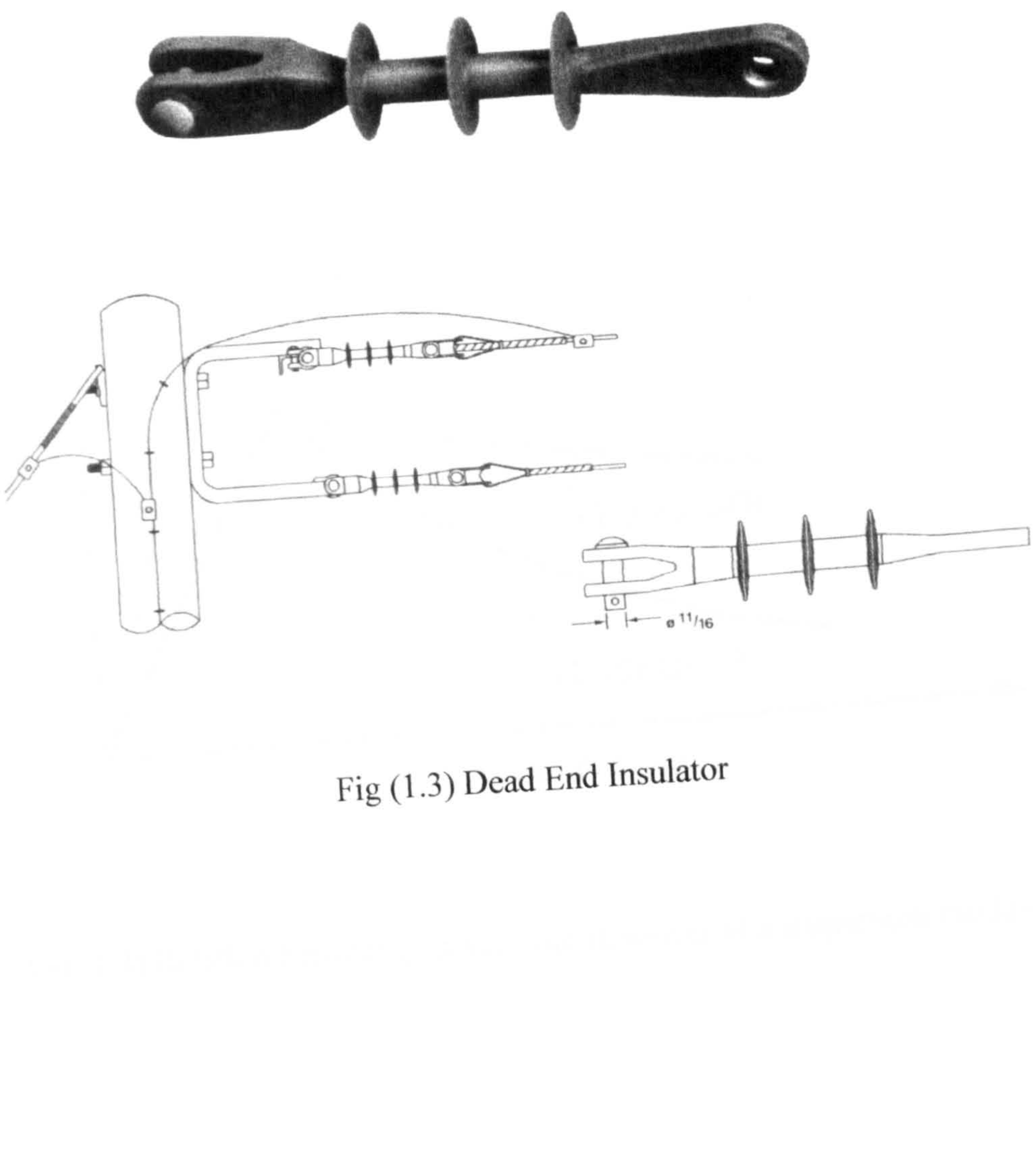

Fig (1.3) Dead End Insulator

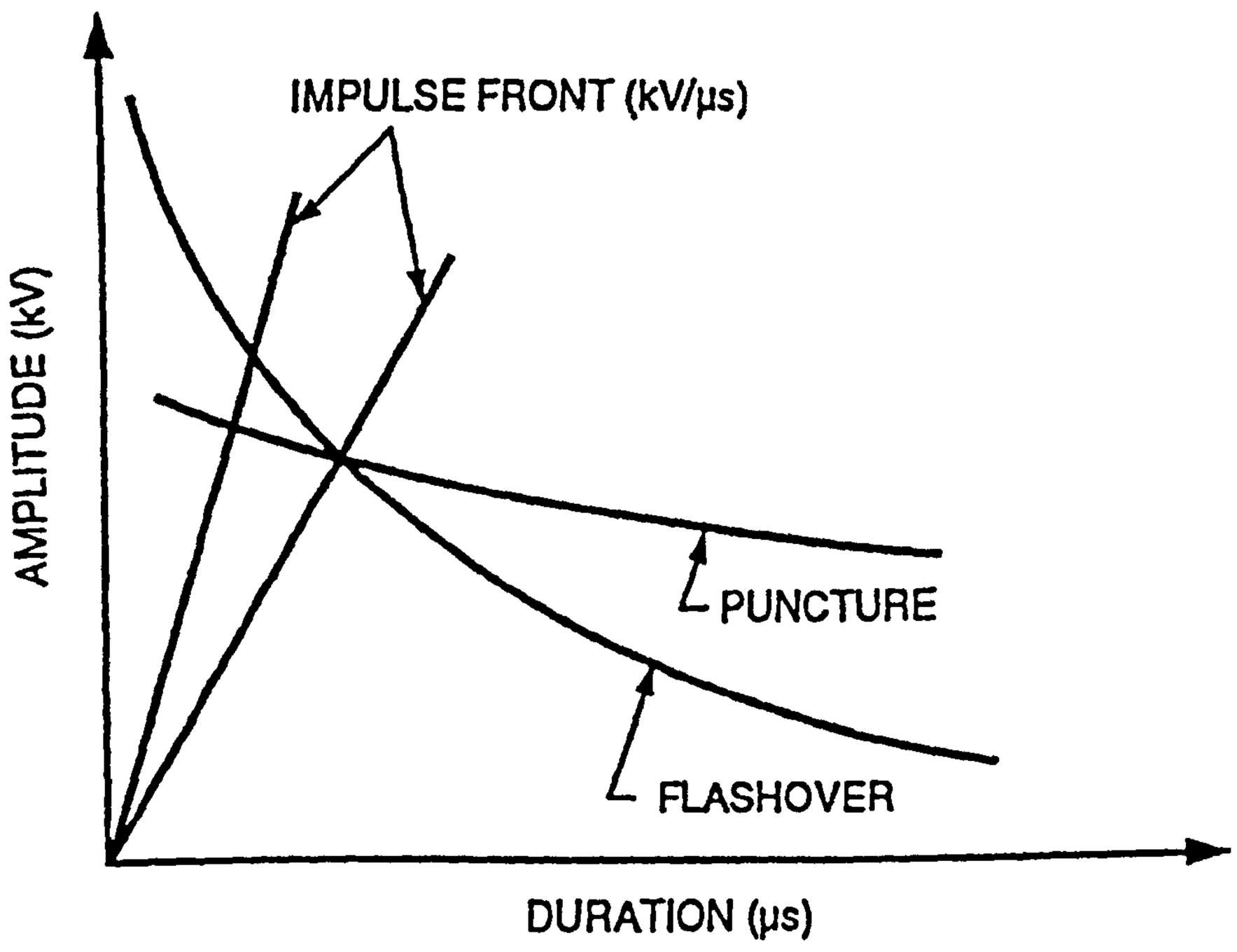

Fig (1.4) Relation between puncture and flashover of a suspension insulator

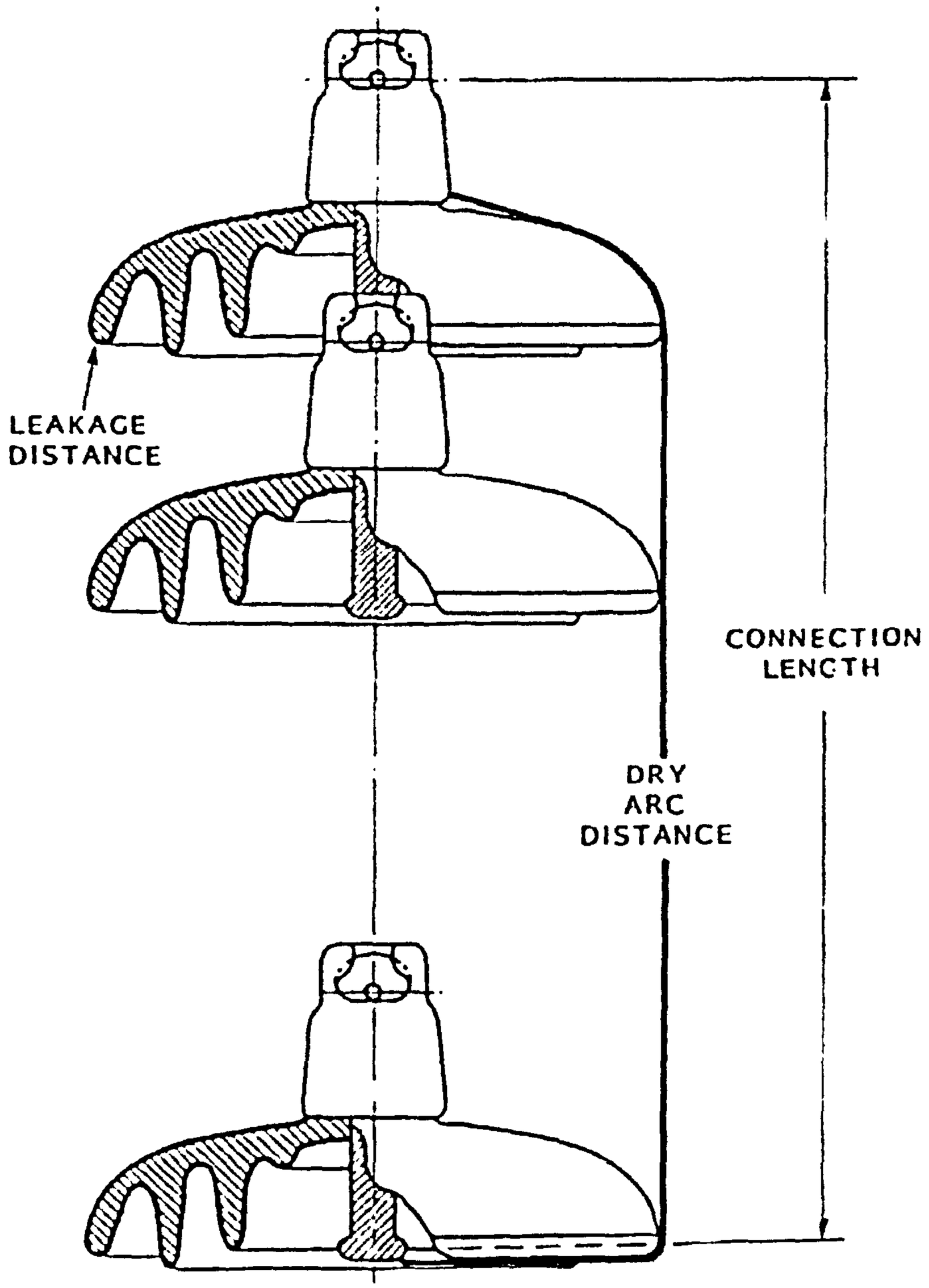

Fig (1.5) schematic of porcelain/glass insulator; illustrating arc and leakage distances.

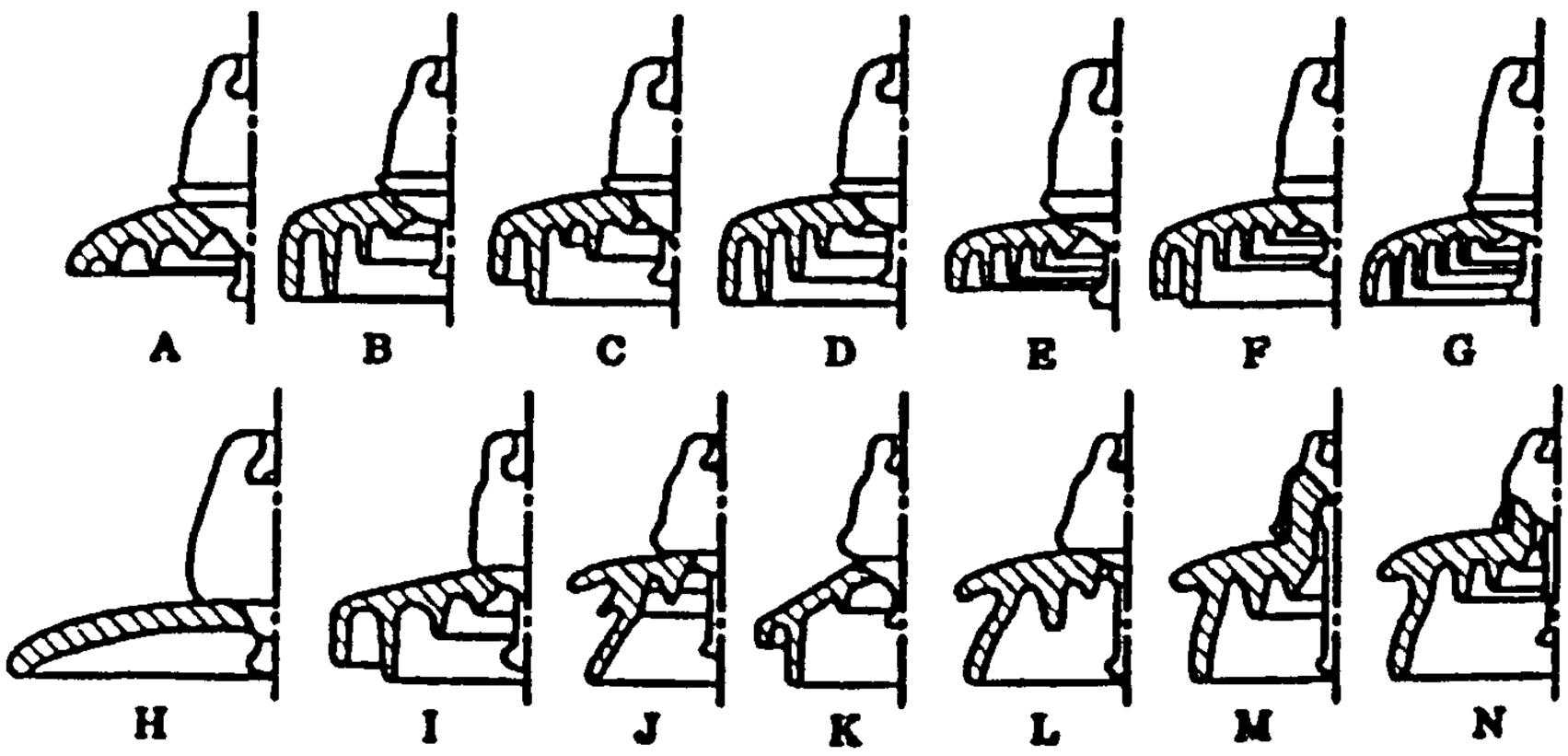

Fig (1.6) profiles of porcelain and glass insulators development.

Standard (A), fog type (B) and aerodynamic (H) are commonly used.

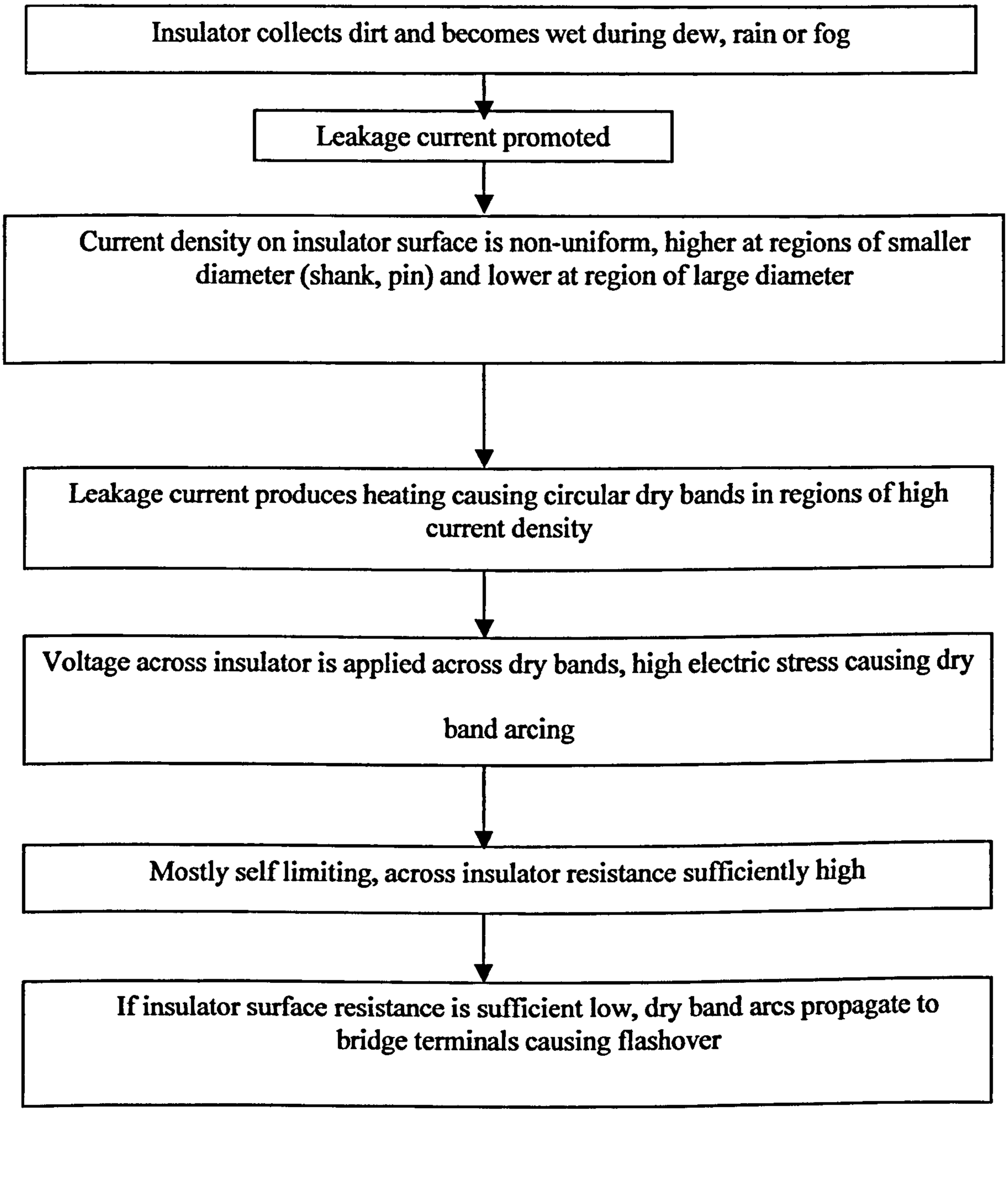

Fig (1.7): Schematic of events leading to contamination flashover

Type of force	Relative Magnitude
Gravity	1 PU (reference)
Voltage stress(E = 2 kV/cm DC)	10
Field Divergence ($E^2 = 0.2\ kV^2 / cm^3$)	0.0001
Wind (speed = 2 m/s)	1,000
Wind (speed = 5 m/s)	2,000
Wind (speed = 10 m/s)	3,000

Table (1.3) Relation comparison of magnitude of forces responsible for insulator contamination (particle size = 5 μm).

1.17 References

1- N. Dhahbi-Megriche and A. Boreal,' Flashover Dynamic Model of Polluted Insulators under AC Voltage', IEEE Trans. on Diel. and Elec. Insult. Vol.7 No.2 pp. 283-289 April 2000.

2- S. Shihab and L. Zhou,' Simulation of Contamination Performance of Outdoor High Voltage Insulators,' IEEE/KTH Stockholm Power Tech Conference, Stockholm, Sweden, pp.287-292, June 18-22, 1995.

3- A.Mekhaldi, M. Teguar, and A.Beroual,' Algorithm for Pollution Flashover Calculation,' Archives of Electrical Engineering. Vol.XLV No. 4, pp. 385-397 1996.

4- N.Dhahbi-Megriche and A.Beroual,' Dynamic Model of Discharge propagation on polluted surfaces under impulse voltages,' IEE Proceeding- Generation, Transmission and Distribution Vol. 147, No. 5. pp. 279-284, September 2000.

5- L. L. Alston and S. Zoledziowski,' Growth of discharge on polluted insulation,' ProC. IEE, Vol. 110 No. 7, PP. 1260-1266, 1993.

6- S. Shihab, V. Melik, L. Zhou, G. Melik, and N. Alame ,' On-line Pollution Leakage Current Monitoring System,' Proc. Of the 4th International Conference on Properties and Application of Dielectric Materials, Brisbane, Australia, Vol.2, pp. 538-541 1994.

7- S. Chakravorti and P. K. Mukherjee,' Power Frequency and Impulse Field Calculation around a HV Insulator with Uniform and Nonuniform Surface Pollution,' IEEE Trans. on Elec. Insult. Vol.28 No.1 pp. 43-53, February 1993.

8- IEC Publication 507,' Artificial pollution test on high-voltage insulators to be used on a AC system,' 1975.

9- P. S. Ghosh and N. Chatterjee,' Polluted Insulator Flashover Model for ac Voltage,' IEEE Trans. on Diel. and Elec. Insult. Vol. 2, No.1, pp. 128-136 February, 1995.

10- Ramiro Hernandez- Corona, Jose l. Fierro- Chavez and Jorge Gonzalez de la Vega,' The Mathematical Modeling of Experimental Data for The design of Anti-

Contamination Insulators,' IEEE International conference on electrical Insulation volume 2, pp. 334-337,1999.

11- R. Sundararajan and R. S. Gorur,' Dynamic Modelling of Flashover on Dielectric Surfaces,' Proc. Of 3rd International Conference on Properties and Application of Dielectric Materials, Tokyo, Japan, Vol. 2, pp. 949-952,1991.

12- Mohamed Afendi Mohamed Plah,' A Study on the Electrical Insulating Properties of the Epoxy Resin,' M.Sc. Strathclyde university 1990.

13- Reuben Hackam, "Outdoor HV Composite Polymeric Insulators", IEEE Transaction on Dielectric and Electrical Insulation", Vol. 6 No.5, pp. 557-594 October 1999.

14- J. S. T. Looms,' Insulators for High Voltage,' Peter Peregrinus Ltd, 1988.

15- Ravi S. Gorur, Edward A. Cherney, and Jeffrey T. Burnham,' Outdoor Insulators,'1999.

16- IEC 815,' Guide for the Selection of Insulators in respect of Polluted Conditions,' 1986.

17- Velazquez Blanco,'High voltage alternating current performance of insulators under several types and distributions of contaminants,' M.Sc., 1990.

18- S. M. Ghufran Ali and H. M. Ryan,' Insulation Co – ordination under polluted conditions,' the 7th BEAMA International Electrical Insulation Conference.

19- Dieter Kind and Hermann karner,' High-Voltage Insulation Technology,' 1985.

20- Ahmad ISM,' Voltage breakdown in polluted insulators,' Ph.D. Exeter 1989.

21- A. A. Hossam-Eldin and Mohie M Ali,' Performance of H.V. Insulators under Environmental Pollution in Arid Area,' IEEE International Conference on Conduction and Breakdown in Solid Dielectrics, pp. 414-417, June 22-25 Sweden 1998.

22- William H. Hayt,jr.,' Engineering electromagnetic,'.

23. E. Vlastos,' Pollution and Degradation of Outdoor Insulation,' Proc. of the 6th ISH 1989.

24. N. Dhahabi-Megriche and A. Beroual,' Evaluation of polluted insulators flashover voltage for different waveforms using an equivalent electrical network model,' IEE, High Voltage Engineering Symp. 22-27 August Vol. 4, pp. 337-380, 1999.

25- A. Ahmed and H. Singer,' New modelling of the boundary between wet and dry zones on the surface of polluted high voltage insulators IEE, High Voltage Engineering Symp. 22-27 August 1999.

26- A. Mekhaldi, D.Namane, S.Bouazabia and A. Beroual,' Flashover of discontinuous pollution layer on HV insulators,' IEEE Transaction on dielectric and electrical insulation Vol. 6 No. 6, pp. 900-906December 1999.

27- M. Farzaneh, S. Brettschneider and K. D. Srivastava, S. Y. Li ,' Impulse breakdown performance of the ice surface,' IEE, High Voltage Engineering Symp. 22-27 August Vol. 4, pp. 341-344,1999.

28- M.Teguar, A. Abimouloud, A. Mekhaldi and A. Boubakeur ,' Influence of discontinuous pollution width on the surface conduction. Frequency characteristics of leakage current,' IEEE Conference on Electrical insulation and dielectric phenomena pp. 211-214, 2000.

29- O. Elsässer and K. Feser ,' Flashover behavior of semiconducting Glazed insulators under positive switching impulse stress at different climatic conditions ,' IEEE Conference on Electrical insulation and dielectric phenomena Vol. 2, pp. 711-714 1999.

30- O. Elsässer and K. Feser ,' Flashover behavior of different insulatating under positive switching impulse voltage stress at different climatic conditions ,' IEEE international symp. on high-voltage engineering Vol. 4, 119-112, 1999.

31- Edgar P. Cssale and Stephen A. Sebo ,' polymer insulator fog chamber project data acquisition system development ,' IEEE Annual Report - Conference on Electrical insulation and dielectric phenomena pp. 4447-450,1996.

32- Stephen A. Sebo, Edgar P. Cssale, Jose R. Cedeňo, Wibawa Tjokrodiponto and Sheikh A. Akbar ,' Review of features of fog champer at ohio state university for polymer insulator evaluation ,' IEEE Annual Report - Conference on Electrical insulation and dielectric phenomena Vol. 2, pp. 443-446, 1996.

Chapter 2

Basic Processes Relating to Water Droplets on Insulator Surfaces

2.1 General

From chapter 1 it is evident that water pollution on the surface of polymeric insulators is an important cause of insulator failure. The natural hydrophobic state of polymer surfaces tends to form such surface water into discrete droplets. When, in addition, the surface is stressed by an applied electric field, such droplets will generate local changes in the distribution of the field and changes in surface properties of the polymer and so may affect conditions leading to flashover [1, 2, 3, 4].

In this chapter the important factors thought to be associated with such a process are identified.

2.2 Surface Factors

Surface tension

Due to an imbalance in molecular forces that occurs when two different materials (e.g., a liquid droplet on a solid surface) are brought into contact with each other forming an interface or boundary, a force is generated in each material in the region of the boundary. The force is due to the tendency for all materials to reduce their surface area in response to the imbalance in molecular forces that occurs at their surface of contact [5].

The force required to stretch a uniform field is proportional to the length of the film. The constant of proportionality, γ_s is known as the surface tension, and can be considered as the force exerted by a surface of unit length. Surface tension γ_s is also called the 'surface free energy per unit area' (J/m^2). The increase in γ_s during normal

aging of polymer is considered to be due to the formation of chemical functional groups on the surface which originate from additives. The surface tension for a solid can be expressed as

$$\gamma_s = \gamma_{sd} + \gamma_{sh} \tag{2.1}$$

and, for a liquid, as

$$\gamma_l = \gamma_{ld} + \gamma_{lh} \tag{2.2}$$

Where the suffixes *d* and *h* denote dispersive and non-dispersive forces respectively; and *l* and *s* denote liquid and solid, respectively [6].

Hydrophobicity and hydrophilicity

Hydrophobic Materials have the opposite response to water interaction to hydrophilic materials. Hydrophobic materials have little or no tendency to adsorb water which tends to "bead" on their surface (i.e., form discrete droplets) because they possess low surface tension and lack active groups in their surface chemistry for formation of hydrogen bonds with water molecules. Hydrophilic materials exhibit an affinity for water and such materials readily adsorb it. The surface chemistry allows these materials to be wetted, forming a water film or coating on their surface. Hydrophilic materials possess a high surface tension and have the ability to form hydrogen bonds with water molecules [5].

The coefficients γ_{sd} *and* γ_{sh} identified in equation (2.1) represent the hydrophobicity and hydrophilicity, respectively of the surface of the solid material. When a polymeric material is immersed in water, the interaction between the water and the surface results in a higher surface tension of the polymer (γ_s) and a consequent increase in hydrophilicity.

Contact angle

With reference to Fig (2.1), for a given droplet on a solid surface the contact angle, θ, is a measurement of the angle formed between the surface of a solid and the line tangent to the droplet radius from the point of contact with the solid.

The contact angle is related to the surface tension via Young's equation for a solid (see Fig (2.2)),

$$\gamma_s = \gamma_{sl} + \gamma_l \cos\theta \tag{2.3}$$

with

$$\gamma_l = \gamma_{ld} + \gamma_{lh} \tag{2.4}$$

where γ_{sl} is the surface tension of the solid-liquid interfacial surfaces [6]. Also according to [6 and 7], the relationship among γ_{sl}, γ_s *and* γ_l can be expressed as

$$\gamma_{sl} = \gamma_s + \gamma_l - \frac{4\gamma_{sd}\gamma_{ld}}{\gamma_{sd} + \gamma_{ld}} - \frac{4\gamma_{sh}\gamma_{lh}}{\gamma_{sh} + \gamma_{lh}} \tag{2.5}$$

From equations (2.3) and (2.5)

$$(1 + \cos\theta)\gamma_l = \frac{4\gamma_{sd}\gamma_{ld}}{\gamma_{sd} + \gamma_{ld}} - \frac{4\gamma_{sh}\gamma_{lh}}{\gamma_{sh} + \gamma_{lh}} \tag{2.6}$$

or, by combining equations (2.4) and (2.6)

$$(3 - \cos\theta)\gamma_l = 4\frac{\gamma_{ld}^2}{\gamma_{sd} + \gamma_{ld}} + 4\frac{\gamma_{lh}^2}{\gamma_{sh} + \gamma_{lh}} \tag{2.7}$$

Equation (2.7) indicates that for a given polymeric material and wetting environment the larger the γ_{sd} *and* γ_{sh}, the smaller would be the static contact angle [8]. Therefore, when the surface tension γ_s of the solid surface is increased, a smaller contact angle will be observed. That is, as a surface becomes more hydrophilic, a water drop would tend to spread across it.

For a virgin polymeric insulating material, $\gamma_{sd} > \gamma_{sh}$, dispersive forces dominate and the surface is hydrophobic. Therefore, γ_s is determined mainly by γ_{sd} on an un-aged polymeric surface [6]. During aging, γ_s changes with time due to, for example, interfacial interaction between the polymer and the moisture. Therefore the surface tension of the polymer increases because of the absorption of water and its adhesion to the surface. This causes a decrease of the contact angle as the surface becomes more hydrophilic. Other processes, such as the occurrence of suitably energetic electric surface discharges, may also be expected to affect γ_s by breaking molecular bonds in

the polymer at its surface and so allowing the formation of hydrogen bonds with water, as mentioned above.

2.3 Factors Associated with an Applied Electric Field

Under electrical stress, a water droplet on a polymer surface will experience forces arising from the presence of electrical charges or dipoles etc. It is useful to examine how these forces respond when the applied field varies with time. e.g. if it has a sinusoidal variation.

Coulomb force

As is very well known, Coulomb's law describes the electric force that one charged particle exerts on another [9]. This electric force between two charged particles is:

1) Directly proportional to the product of their charges.
2) Inversely proportional to the square of the distance between them.
3) Directly along the line joining them, and
4) Repulsive (attractive) for like (unlike) charges.

If q_1 and q_2 are two charged particles situated at points $P(x, y, z)$ and $S(x', y', z')$ as shown in Fig (2.3), the electric force acting on q_1 due to q_2 is

$$F_{12} = K\frac{q_1 q_2}{R_{12}^2}\overrightarrow{a_{12}} \tag{2.8}$$

Where F_{12} is the force experienced by q_1 due to q_2, K is the constant of proportionality, which depend upon the system of units used, R_{12} is the distance between points P and S, and $\overrightarrow{a_{12}}$ is the unit vector pointing in the direction from point S to point P. the distance vector from S to P is

$$\overrightarrow{R_{12}} = R_{12}\overrightarrow{a_{12}} = \vec{r_1} - \vec{r_2} \tag{2.9}$$

Where $\vec{r_1}$ and $\vec{r_2}$ are the position vector of points P and S, respectively.

In the International System of Units ("SI" system), the constant of proportionality is

$$K = \frac{1}{4\pi\varepsilon_0} \tag{2.10}$$

Where $\varepsilon_0 = 8.85x10^{-12} = 10^{-9}/36\pi$ farads /meter (F/m), is the permittivity of the free space (vacuum). Thus,

$$F_{12} = \frac{1}{4\pi\varepsilon_0}\frac{q_1 q_2}{R_{12}^2}\overrightarrow{a_{12}} \tag{2.11}$$

Or

$$F_{12} = \frac{1}{4\pi\varepsilon_0}\frac{q_1 q_2\left(\vec{r_1} - \vec{r_2}\right)}{\left|\vec{r_1} - \vec{r_2}\right|^3} \tag{2.12}$$

This coulombic force means that a charge, q, in the presence of an applied electric field, E, experiences a force, F, given by F = qE. If E varies as $E_0 \sin(\omega t)$ then clearly the force experienced by the charge will vary with the same frequency ω. It is also reasonable to assume that the force exerted on a collection of charges, such as might be associated with a charged water droplet, will also show the same fundamental frequency as that of the applied field, although some harmonics arising from the mechanical properties of the droplet might also be found.

Dielectrophoretic force

The force exerted by a non-uniform field on an electrically neutral body suspended in a fluid medium will now be examined.

In a static field, the net translational force on a neutral, small body at equilibrium is given by [10]:

$$F = (\mu \cdot \nabla) E \tag{2.13}$$

Where μ is the dipole moment vector (induced or permanent), ∇ is the vector operator "del", and E is the external electric field. For the case where the neutral dielectric body is homogeneously, linearly, and isotropically polarized:

$$\mu = \alpha V E \tag{2.14}$$

Where α is the polarizability, and V is the volume of the body. This gives us

$$F = \alpha V (E \cdot \nabla) E$$

$$= \frac{\alpha V}{2}\nabla |E|^2 \tag{2.15}$$

If we now consider the body to be a sphere of radius a, composed of an ideal (zero conductivity) dielectric of relative permittivity ε_2, suspended in an ideal dielectric

fluid medium of infinite extent and relative permittivity ε_1, then the field interior to the small spherical body is given by

$$E_{in} = \left(\frac{3\varepsilon_1}{\varepsilon_2 + 2\varepsilon_1} \right) E \tag{2.16}$$

The induced polarization per unit volume is

$$P = \varepsilon_0 (\varepsilon_2 - \varepsilon_1) E_{in} \tag{2.17}$$

and the induced dipole moment is given by

$$\mu = VP = \alpha VE$$

The polarization α per unit volume is therefore given from equations (2.16) and (2.17) as

$$\begin{aligned} \alpha &= \frac{P}{E} = \varepsilon_0 (\varepsilon_2 - \varepsilon_1) \frac{E_{in}}{E} \\ &= \frac{3\varepsilon_0 \varepsilon_1 (\varepsilon_2 - \varepsilon_1)}{\varepsilon_2 + 2\varepsilon_1} \end{aligned} \tag{2.18}$$

and from equation (2.15), the total dielectrophoretic force F acting on the small sphere of volume $V = \frac{4\pi a^3}{3}$, can be expressed as:

$$F = 2\pi a^3 \varepsilon_0 \varepsilon_1 \left(\frac{\varepsilon_2 - \varepsilon_1}{\varepsilon_2 + 2\varepsilon_1} \right) \nabla |E|^2$$

For the purposes of the present study, we will consider a spherical water droplet in air in which case the relative permittivity $\varepsilon_1 = 1$, $\varepsilon_2 = \varepsilon$ and $a = r$, the radius of the droplet,

The total dielectrophoretic force F is then

$$F = 2\pi r^3 \varepsilon_0 \left(\frac{\varepsilon - 1}{\varepsilon + 2} \right) \nabla |E|^2 \tag{2.19}$$

If the electric field arises from an applied voltage of the form $V = V_0 \sin \omega t$, equation (2.19) implies that the associated dielectrophoretic force will show an ω^2 dependence. From this it is reasonable to assume that a water droplet on an insulating surface would vibrate at twice the frequency of the applied field if the force on the droplet was mainly a dielectrophoretic one.

Electrostatic induction

Electrostatic induction is the phenomenon by which an uncharged object becomes charged when brought near (but not touching) a charged body. For an example if a positively charge body (A) is brought near an uncharged object (B), a separation of charges in produced in B. The positive charges on A simultaneously repel the positive charges and attract the negative charges on B as shown in Fig (2.4). The figure illustrates that the negative charges on B are closer to the positive charges on A than the positive charges on B. This implies that the force of attraction between the positive on A and the negative on B outweighs the force of repulsion between the positive region on A and the positive region on B, which results in object B being attracted to body A. This resultant force is called the electrostatic induction force. Electrostatic induction force will arise only if the external field is non uniform. This force is essentially linked to the presence of electrical charges and, as such, is coulombic in origin but will be directed to one of the electrodes irrespective of polarity. It should show twice the frequency of the applied electric field.

Electrical triple junctions

The point at which three media meet is called a triple junction. If electrical properties of the three media are different, considerable field enhancement may occur at this point. In our study the three media are water droplet, air and solid insulation. As mentioned above, solid insulation surface properties might change under the influence of an applied electric field, particularly if discharges occur, so it is important to examine how the behaviour of a water droplet may be affected by the distribution of the electric surface potential and the electric field strength around a triple junction point. This topic is examined in more detail in later chapters of this thesis in association with the experimental and theoretical work presented there.

2.4 Electrical Breakdown in Gases

The total average current in a gap between two parallel-plate electrodes before the occurrence of breakdown can be expressed as [see, for example, reference 11]

$$I = \frac{I_0 \exp(\alpha d)}{1 - \gamma\,[\exp(\alpha d) - 1]} \tag{2.20}$$

Where I_0 is the initial current at the cathode, α is the average number of ionizing collisions made by an electron per centimetre, γ is the secondary ionization coefficient, and d is the distance between the two electrodes. The coefficient γ represents a "positive feedback" mechanism which releases additional electrons into the discharge. As the distance between the two electrodes is increased, the denominator of the equation tends to zero and at some distance $d = d_s$.

$$1 - \gamma\,[\exp(\alpha d) - 1] = 0$$

For values $d > d_s$, I is approximately equal to I_0, and if the external source for the supply of I_0 is removed, I becomes zero. If $d = d_s$, $I \to \infty$ and the current will be limited only by the resistance of the power supply and the external circuit. This condition is called Townsend's breakdown criterion and can be written as

$$\gamma\,[\exp(\alpha d) - 1] = 1$$

Normally, *exp (α d)* is very large, and hence the above equation reduces to

$$\gamma\,\exp(\alpha d) = 1$$

for a given gap spacing and at a give pressure the value of the voltage V which gives the values α *and* γ satisfying the breakdown criterion is called the spark breakdown value V_s and the corresponding distance d_s is called the sparking distance. This equation can be re-arranged to give

$$\alpha d = \ln(1/\gamma) \qquad (2.21)$$

If the electric field is non-uniform, equation 2.21 may be expressed as an integral along a field line, s. That is,

$$\int_s \alpha(s)\,ds = \ln(1/\gamma) = k$$

where α is now expressed as a function of distance along the field line of interest. Close to breakdown, the feedback term $(1/\gamma)$ is very large ($\approx 10^8$) and k, known as the streamer breakdown constant, is found to be typically 12 to 18 at breakdown, depending on the gas involved. When written in the form

$$\int_s \alpha(s)\,ds = k \qquad (2.22)$$

this equation is known as the streamer criterion for electrical breakdown of a gas in a non-uniform field [11]. Equation 2.22 could be used to examine the likelihood of electrical breakdown in the air surrounding a water droplet.

A water droplet plays a number of roles in the electrical breakdown of an air/insulator interface: -

- It is a stress enhancer because of its high permittivity.
- It deforms under the influence of the electric field, due to both coulomb and field – gradient forces, thereby increasing its stress enhancing feature.
- It can be a good conductor, especially when heavily contaminated, and so partly short out some of the insulating surface thereby increasing the field in the surrounding gas.

2.5 Summary

Considering the importance of the water droplet pollution problem, continuous and intensive laboratory studies and field investigations have been taking place worldwide for many years. The work involves not only experimental investigations but also mathematical modelling to understand the different aspects of the behaviour of the water droplet on the insulator surface. The effect of a water droplet on partial discharge activity, hydrophobicity, contact angle, surface tension, flashover and breakdown has been studied. The influence of water-droplets at the surface of HV insulators on the distribution of the potential and the electrical field along the surface has been investigated in many publications. Behaviour has been studied with both ac and dc applied voltage. Partial discharge measurements from water droplets have been used as a means to study pre-leakage current development on the insulating surface. Visual observation of droplets on an insulator surface under ac or dc stress has also been performed and the results examined in many papers and publications. These studies have used high speed-video camera techniques to study the vibration, scattering and the extending of water droplets and to record partial discharge activity, flashover and the breakdown. In the next chapter we review in detail prominent recent papers, in particular those which have examined the behaviour of a single water droplet on the surface of a polymeric insulator under a high electrical stress.

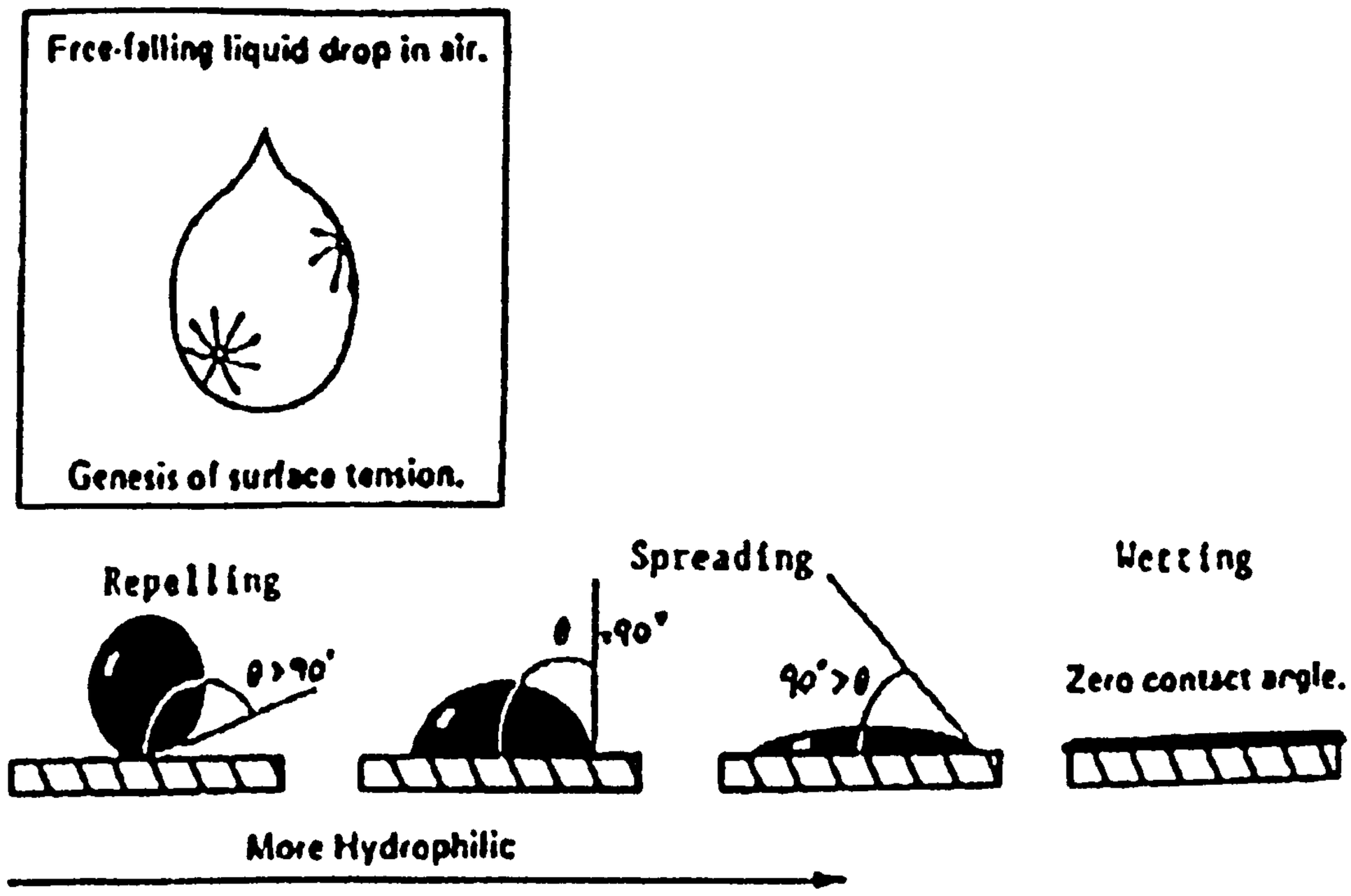

Fig (2.1) Wetting of solid surfaces: the contact angle θ decreases with increasing hydrophilicity.

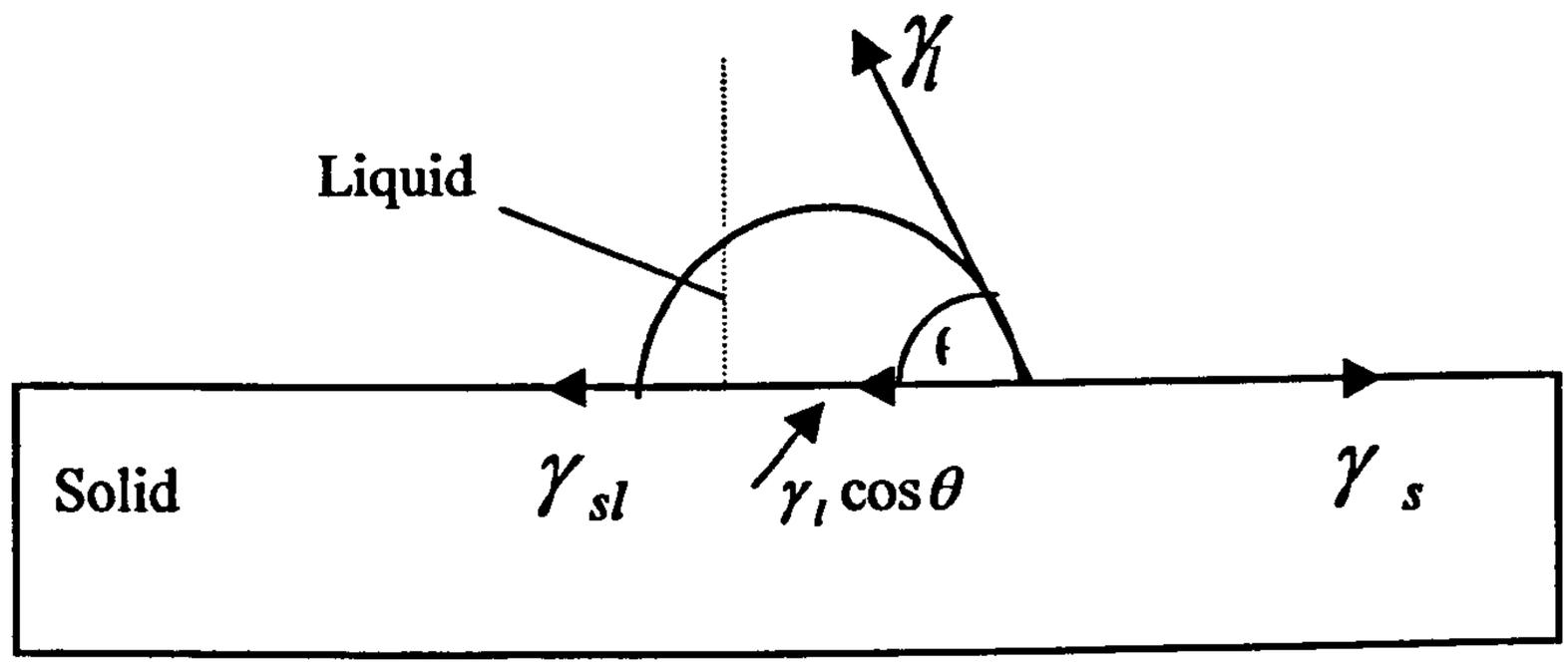

Fig (2.2) Illustrating Young's equation $\gamma_s = \gamma_{sl} + \gamma_l \cos\theta$ at the interface between a liquid droplet and a solid surface.

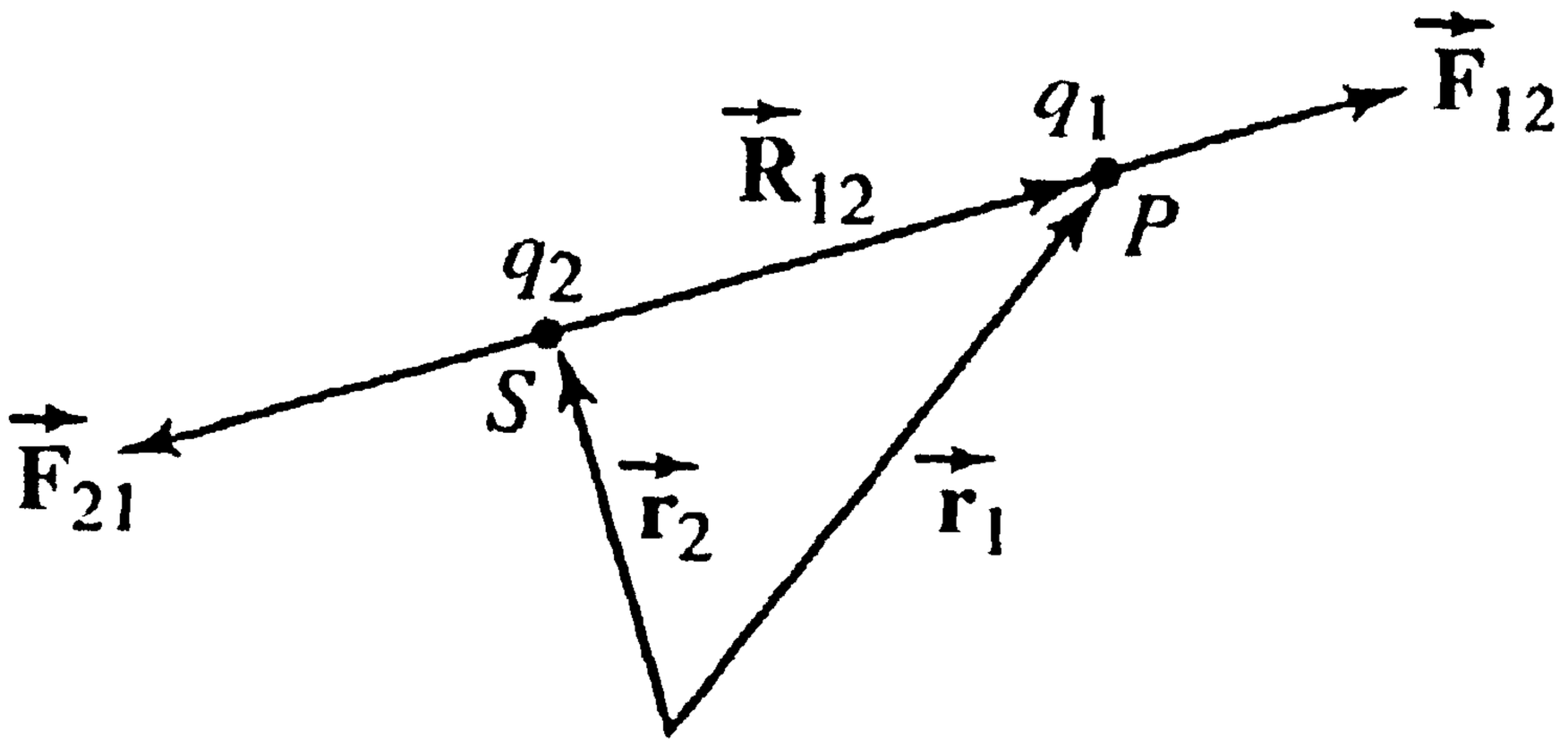

Fig (2.3) Electric force between two point charges

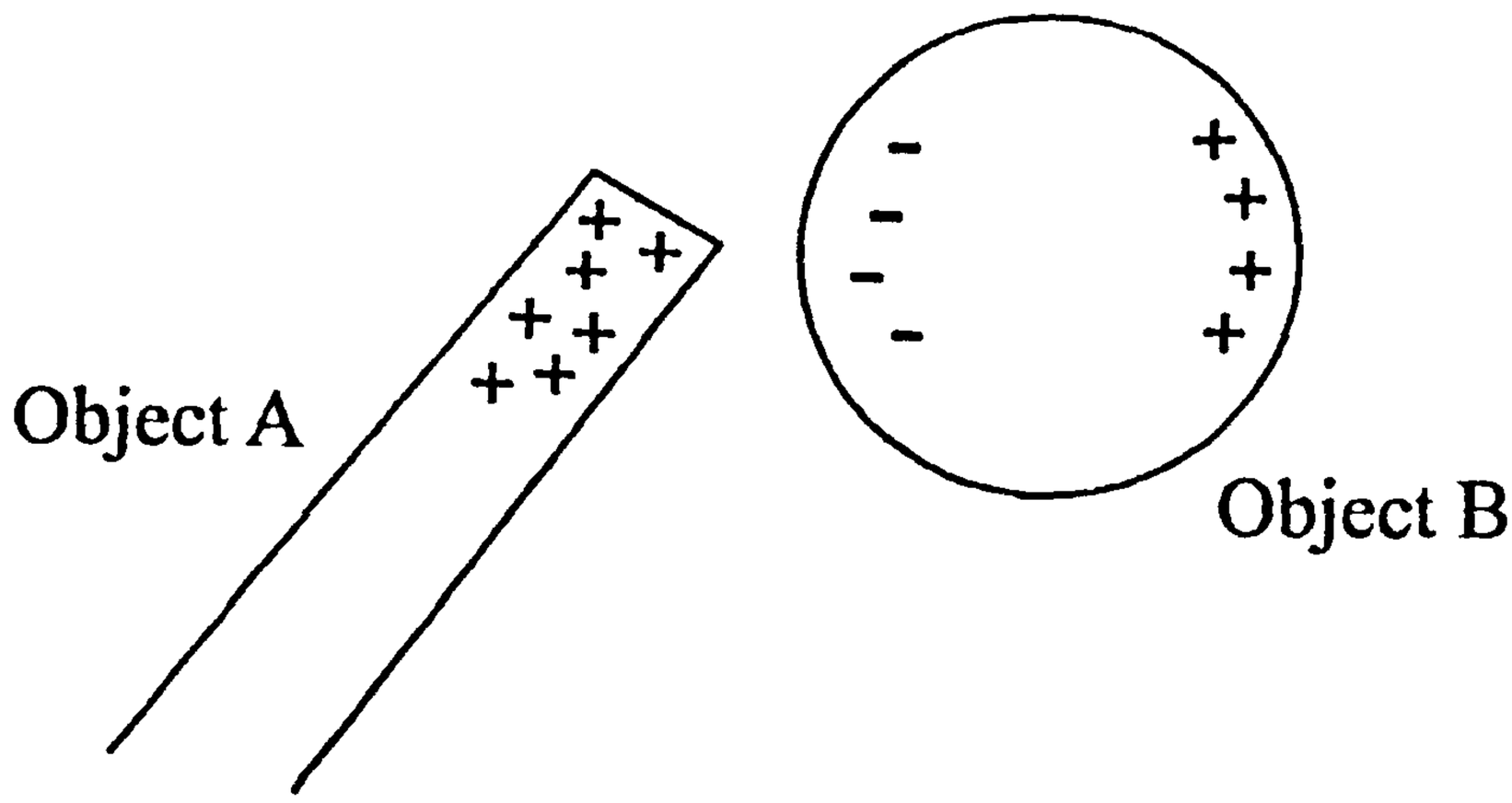

Fig (2.4) Charge separation in object B produced by electrostatic induction.

2.6 References

1- S. Keim and D. Koenig, " The Dynamic Behaviour of water Drops in an AC Field", Annual Report Conference on Electrical Insulation and Dielectric Phenomena pp. 613-616, 2001.

2- Heiko John, Roland Bärsch and Eckhard Wendt, " The Influence of Temperature on the Recovery of the Hydrophobicity on Silicone Rubber Surfaces", IEEE Conference on Electrical Insulation and Dielectric Phenomena Vol. 1 pp. 242 -245, 2000.

3- Y. Mizuno, and Others, " Behavior of Water Droplets on Silicone Rubber Sheet under AC Voltage Application", IEEE Conference on Electrical Insulation and Dielectric Phenomena Vol. 1 pp. 25-28, 1998.

4- A. Krivda and D. Birtwhistle, " Breakdown between Water Drops on Wet Polymer Surface", Annual Report Conference on Electrical Insulation and Dielectric Phenomena pp. 572-580, 2001.

5- http://www.osmonics.com/products/Page772.htm

6- Reuben Hackam, "Outdoor HV Composite Polymeric Insulators", IEEE Transaction on Dielectric and Electrical Insulation", Vol. 6 No.5, pp. 557-594 October 1999.

7- S. Wu, "Polymer Interface and Adhesion", Marcel Dekker Inc., NY, 1982.

8- H. Zhang and R. Hackam, "Electrical Surface Resistance Hydrophobicity and Diffusion phenomena in PVC", IEEE Transaction on Dielectric and Electrical Insulation, Vol. pp. 73-83 1999.

9- Ronald Pethig, " Dielectric and Electronic Properties of Biological Materials", 1979.

10- Bhag Singh Guru and Hüseyin R. Hiziroğlu, " Electromagnetic Field Theory Fundamentals", 1998.

11- M. S. Naidu and V. Kamaraju, " High Voltage Engineering", Second Edition 1996.

Chapter 3

Review of Recent Work on Water Droplets on Insulator Surfaces

3.1 General

As previously described in chapter 1, surface pollution of high voltage insulation is considered to be one of the most important factors leading to insulation failure. Also, as discussed in chapter 2, the specific feature of water droplets at the surface of HV insulators has a particularly significant effect on insulation performance, which can lead to flashover of the insulator.

In this chapter we review recent research on water droplets on polymer surfaces under high electrical ac stresses. The variety of test arrangements that have been adopted is described and their features discussed. Observations of partial discharge activity near the surface of droplets, droplet vibration and spreading, and surface flashover are compared.

In previous investigations of the effect of water droplets on electrically-stressed insulator surfaces, a very wide range of factors has been examined. Table 3.1, adapted from reference [15], summarises the fundamental parameters that may be considered as most important.

For the present purposes, we confine our review to work concerning applied electric fields with sinusoidal waveforms at frequencies relevant to the "power" values of 50 to 60 Hz. We examine the work done on essentially single water droplets with volumes of the order of tens of μl, representative of typical naturally-occurring rain, condensation or spray. We consider the conductivity of the water in three broad ranges: deionised, rain (or tap), and salt solution – again, representative of naturally-occurring conditions. In practice, most HV insulators with droplet contamination are otherwise undamaged and so, for the present review, it is considered appropriate to limit

consideration to essentially flat, smooth polymeric surfaces that are nominally clean and have not been contaminated by, for example, prior aging through prolonged exposure to electrical discharges or chemical degradation leading to breakage of molecular bonds. We also consider droplets and polymer surfaces exposed to ambient air.

Within the above general constraints, a number of recent studies have been identified [1-16] that describe experimental systems designed to investigate water droplet behaviour on polymer surfaces under power-frequency ac stress. In the review of this work presented below, we attempt to identify the key parameters, and where the areas of general agreement, or otherwise, lie – even although there are distinct differences in the individual test arrangements adopted by the various investigators concerned. From this review, it is expected to gain information on those areas where further research may prove useful.

3.2 Experimental Systems

Before examining the observed behaviour of droplets in detail, it must be recognized that the studies referred to above do not all adopt the same experimental arrangements. For example, several different electrode and polymer geometries have been employed as well as different polymer materials. In order to assist comparisons between studies, it was considered necessary to first examine the electrode and sample geometries that have been used, and to consider whether the resultant variations in the form of the applied electric field were of significance.

3.2.1 Electrode Geometry

Three different general forms of electrode geometry have been used in previous studies. Their essential differences are illustrated in Fig (3.1). First, there is an "end" electrode geometry where a length of polymer is mounted between two electrodes located at its ends. This arrangement has been used to give either an essentially uniform or a distinctly non-uniform field along the sample surface [1-3, 5-6, 10 and 12]. A second geometry commonly used is where the two electrodes are "surface" mounted on the polymer sample [4, 8-9, 11, 14 and 16]. A third geometry has the two electrodes positioned below the insulating surface i.e. "embedded" in the polymer [4, 7, 13 and

15]. It is useful to consider each of these geometries in turn before making comparisons between the behaviour of droplets in each system.

End electrodes. Figs (3.2, 3.3, 3.4 and 3.5) illustrate the typical use that has been made of end–electrode geometry, as adopted in references [3], [5], [6], [10] and [12]. The significant feature of this geometry is that it can produce an applied electric field that is directed along (i.e. tangential to) the surface of the insulator under test and which can be essentially uniform along that surface, in the absence of a water droplet. In previous work, the distances that have been employed between such end electrodes have shown a range of values, but 20mm has been commonly used. In [1] a flat piece of silicon rubber (SiR) - cut from a silicone rubber suspension insulator – was centrally mounted between two uniform electric field electrodes such that the electric field was along its 20-mm surface. In [3], electrodes were located at both ends of an insulation sample of length 250mm. In [5] and [12] samples were arranged horizontally between plane electrodes 20mm apart. In [6] two nominally uniform arrangements were used with distances between electrodes of 18mm and 20mm.

A second, end-electrode geometry used in [6] comprised an end portion of an SiR insulator fixed between two end electrodes of dissimilar dimensions (see figure 3.3B). A similar non-uniform geometry was used in [10]. The electric fields generated by these arrangements were significantly non-uniform. Neither of these papers provides clear detail of the shape of electric field generated by these non-uniform geometries. However, it may be assumed that field components both tangential and normal to the polymer surface were present.

Surface mounted electrodes. Figs (3.4, 3.6, 3.7 and 3.8) illustrate typical arrangements using surface-mounted electrodes. Fig (3.6), see reference [8], shows a pair of parallel rod electrodes of approximately rectangular cross–section and 10-mm apart used to form what is described as a tangential electric field along the surface of the insulation. In work reported in [8], [11] and [16], surface electrodes with a hemispherical cross–section were used. The cross-sectional dimensions of these electrodes were not stated but their separation was fixed at 30 mm. In [14], see Fig

(3.8), two elongated carbon electrodes were surface mounted on a silicon rubber test sample and the separation between electrodes varied between 18 and 22 mm. However, the other dimensions of these two electrodes, which appear square in cross-section, were not stated. In all of the above, it is safe to assume – from symmetry - that the electric field at the surface of the polymer near its centre was predominately tangential to the surface and essentially uniform.

Embedded electrodes. Keim and Koenig have published several papers in which they employed embedded-electrode geometry [4, 7, 13 and 15]. Figs (3.9) (see [4], [7], and [15]) and Fig (3.10) (see [13]) illustrate the geometry used. Typically, parallel circular cross-section rod electrodes were embedded parallel to the insulator surface at a depth of 1mm below the surface. The rods were 15 mm in diameter, 100 mm in length with the distance between the centres of the two electrodes set at 35mm – i.e. a gap spacing of 20mm. Such an arrangement can be used to generate fields at the central region of a sample surface that have comparable tangential and normal components.

The various electrode configurations described above can all generate high electric fields at the surface of the test sample. Uniform-field end electrodes generate field lines that are essentially tangential to the sample surface. Surface-mounted electrodes do not generate such a uniform field but, from symmetry, will produce field lines that are approximately tangential to the surface of the sample near the mid-point between the electrodes. However, non-uniform end electrodes, surface-mounted electrodes and embedded electrodes will generate non-uniform fields which are not completely tangential to the sample surface – i.e. they will generate field components normal to the sample surface, directed into or out of the surface. Clearly, a uniform, tangential field is more easily analysed, but non-uniform fields are more representative of practical applications. It must also be recognized that any applied field will be altered considerably when a water droplet is introduced, particularly a highly conducting one. The significance to droplet behaviour arising from the differences in applied electric field that result from variations in electrode geometry are examined further in the next sections.

3.2.2 Applied Electric Field

With the variety of electrode geometries noted above, it is of interest to examine whether agreement can be found between the various investigations reported, for example: what agreement is there about the values of the applied electric field required to force a droplet to vibrate, to spread, or to cause flashover of the polymer surface?

With the range of geometries as described above, the most straight-forward measure of the applied electric field in each case is to calculate an average value (E_o) by dividing the applied voltage by the distance between the electrodes. Such an average field may be calculated corresponding to the onset of droplet vibration, the onset of partial discharges or the flashover of the test sample. Although it would not be reasonable to expect such a simple measure to show, for any particular process, a close agreement between the various test geometries, it is possible that it will show some trends as to the relative field levels for onset of the various processes. For example, for all the geometries studied, does the average field at the onset of detectable partial discharges generally lie below or exceed that for vibration?

As mentioned in chapter 2, a water droplet on a surface will act as a local stress enhancer and so the electric field in the vicinity of a water droplet may be considerably higher than the average field E_o. Many of the studies mentioned above do not give sufficient data to calculate such local enhancements. However, any enhanced field will be proportional to the average applied field. For example, when adhering to a plane surface, a hemispherical droplet that is conducting or has a high permittivity generates a stress enhancement at its surface given by

$$E_z = \beta E_0$$

Where β, the stress enhancement factor, equals 3 at the point where the surface of the droplet intersects its axis of symmetry [1]. Hence, in the absence of clear data on enhancement factors such as β, it is reasonable to examine whether it is helpful to base initial comparisons on average values of applied field and to interpret apparent discrepancies in terms of likely local enhancement factors.

Approximately uniform applied fields. As described in the previous section, both the uniform-field end electrodes and parallel-rod surface electrodes can be considered as generating approximately uniform fields that are essentially tangential to the surface at the centre of the insulator (prior to placement of a water droplet). Hence, in the present study a comparison was made of the levels of E_o reported in the literature for these geometries corresponding to

a) The onset of partial discharges (E_{op})

b) The onset of droplet vibration (E_{ov})

c) The onset of droplet spreading (E_{os})

d) Breakdown between electrodes (E_{ob})

The applied stress is expressed in RMS values unless stated otherwise. For simplicity, only data for single droplets are considered.

Employing both end and surface-mounted electrodes with a 20-mm gap spacing, single droplets with a volume of 20μl and conductivities, σ, of 300μS/m and 5.8S/m on silicon rubber (SiR) were investigated in [1] and [2]. The conductivities are representative of deionised and saturated salt solutions respectively. With ac, these authors report that single droplets "distorted" at 21kV peak (deionised) and 18kVp (salt solution). Breakdown was found to occur at 23kVp (deionised) and 20kVp (salt solution). We identify "distortion" with E_{ov} and/or E_{os} and breakdown with E_{ob} and convert these peak voltages into corresponding RMS values of average applied field. Table 3.2, below, presents the values calculated.

Discharge activity is reported when 7.7kV was applied across a 20-mm gap with a deionised or salt-solution droplet of about 1-mm radius on SiR [6]. This paper also records that, as voltage was raised, vibration was followed by spreading and then followed by breakdown. PTFE is compared with SiR in [8]. Here droplets of either 10 or 30μl were placed on the surface at the mid point of a 10-mm gap. The water was deionised with a conductivity of 50μS/m. The voltage applied was varied in frequency from 20 to 50Hz. For 10-μl droplets on both PTFE and SiR, vibration onset was detected at 5kV and 36Hz. For 30-μl droplets, vibration began at 6.5kV (22Hz) with SiR and 8.5kV (20Hz) with PTFE, with breakdown at 11kV and 13kV, respectively.

According to [9], [11] and [16], for a SiR gap of 30mm and a 30-µl droplet of conductivity 56mS/m (acid rain), partial discharges were found at 8kV followed by vibration at around 10 to 15 kV and breakdown in excess of that. In [10] it is reported that for a 30-µl droplet of tap water on an SiR surface, partial discharges are detected at an applied field of 5.5 kV/cm (= E_{op}). With SiR surfaces of 18 to 20-mm length and droplets of conductivity 100mS/m it is reported in [14] that a 30-µl droplets showed spreading and breakdown at 5.75kV/cm, with 10-µl droplets showing similar behaviour at 6.1kV/cm.

Evidently, detailed comparisons of these essentially uniform values of the average applied tangential field are limited by the various test conditions that differed considerably between studies. However, for most cases described above, it is appears from table 3.2 that applied fields in excess of around 3kV/cm are generally required to generate partial discharge activity and at fields in excess of 5kV/cm droplet vibration, movement and spreading can be expected, with higher still values of average field (typically in excess of 7kV/cm) leading to breakdown.

Non-uniform applied fields. In [6], the dynamic behaviour and deformation of a water droplet under ac voltage placed on the surface of the simulated energized end of a hydrophobic polymer insulator was examined. The experimental arrangement (see figure 3.3B) employed non-uniform field end electrodes separated by a distance of 18mm. Under de-energized conditions the water droplet was quite round due to the hydrophobicity of the SiR surface. The authors report that a water drop started to vibrate at an applied voltage of 5 kV, with spreading evident at about 15 kV followed by gross deformation and movement to an end electrode at about 20 kV, corresponding to average field strengths of 2.8, 8.3 and 11.1 kV/cm, respectively. For non-uniform field conditions it may be less appropriate to examine such average values of electric field. However, comparison with table 3.2 indicates that the non-uniform conditions in [6] do not lead to large differences in the average fields E_{op}, E_{ov} and E_{ob} compared to the values found for uniform-field conditions.

In [4], [7], [13], and [15] embedded electrodes were used. A typical arrangement is shown in Fig (3.8). In [7] it is reported that elongation of droplets and PD activity could be observed when the applied voltage was increased from 4kV, corresponding to an average field of 2kV/cm, to 8 kV, corresponding to 4kV/cm. during a test period of 30 minutes. In [13] and [15], vibration was reported at an applied voltage of 13kV, corresponding to an average field of 6.5kV/cm. These authors did not provide more details of the different field strengths at which they first detected the onset of vibration, spreading or PD activity. However, the above values are comparable with the ranges shown in Table (3.2) and it would appear that in terms of average onset fields, embedded electrodes may give generally similar results to the other geometries.

3.3. Polymer Sample

In previous studies, several different polymer materials and sample arrangements have been employed. The surface properties of the samples examined are clearly significant.

3.3.1. Sample Surface

The dimensions, surface geometry and surface preparation of the polymer samples used in the recent work were examined. In [1], 20-mm long, flat sheet of SiR was cut from a suspension insulator. No information was given about the initial surface of the SiR other than that it was "fully hydrophobic". In this study, the surface was purposely degraded in order to achieve substantial loss of hydrophobicity by sparking the surface at a current of about 10mA for 1 minute. The loss was not expressed in quantitative terms, however it was sufficient to allow a droplet to spread on simple contact with the unstressed surface. In [4], a cylindrical epoxy-resin sample was used, similar in shape to a post insulator. Micro-discharges at droplets were considered to trigger and influence electrochemical degradation of the insulator surface, with a resultant loss in hydrophobicity. Again, only qualitative information was given. In [5], 70-mm long samples were cut from 2-mm thick sheets of SiR. The surface was described as initially clean, but no further details were given. This surface was also

deliberately contaminated with a water slurry which generated a uniform deposit of both non-soluble material and salt at densities of 0.1mg/cm^2. This process was described as producing a uniform contamination of the hydrophobic surface without causing any other physical and/or chemical changes. These authors reported that both droplet vibration and PD activity were substantially reduced when the contamination was first introduced, and that this could be attributed to low hydrophobicity due to the surface contamination. However, after several days the surface hydrophobicity appeared to recover. In [6] both the surface of an end portion of an SiR insulator and an SiR sheet were tested. No specific details of surface conditions were given and it must be assumed that no special surface preparation was undertaken. In [7], an epoxy resin was examined which was identified as Araldite F, HT 907, DY 061 with quartz filler W 12 EST (data from Ciba Geigy). The surface was described as initially smooth, as produced in the manufacturing process. For some experiments, this surface was also deliberately roughened by treatment (presumably blasting) with glass balls at a pressure of 5bar and a distance of 15cm. Droplet vibration was observed only on the smooth surface whereas with the roughened surface droplets tended to split into several, separated fractions. The authors did not identify the mechanisms that might account for such behaviour. In [10], test samples comprised either a slab of acrylic coated with silicone rubber or a distribution-class silicone rubber insulator. No special surface preparation was reported prior to testing.

The hydrophobic insulating materials used in [8] were polytetrafluoroethylene (PTFE), and silicon rubber (SiR). The surface of the PTFE was stated to show less friction than that of SiR. With deionised water, the initial static contact angles for SiR and PTFE were measured as 108° and 93°, respectively, indicating that the SiR was more hydrophobic - a result that was essentially independent of droplet volumes from 5 to 50μl. These authors found that droplets vibrate in different modes on PTFE surfaces compared to SiR. This appears to be due, at least in part, to the different contact angles found with these materials, and it was concluded that disturbances in droplet shape depended not only on electrostatic forces but also on the hydrodynamics of the liquid motion. Silicone rubber with $Al(OH_3)$ filler was employed in [11] where, again,

droplet vibration was found with ac applied voltage. However, no particular surface property other than hydrophobicity was noted.

3.3.2 Surface tension and hydrophobicity

The effects of the forces that act on a water droplet on an electrically-stressed solid insulation sample have been studied. As described in chapter 2, these forces are: the surface tension of the water, the solid and the interface tension between liquid and solid. In equilibrium these forces are in balance, see Fig (3.11). However, from [1] and [5], it can be seen that this balance is altered when an electric field is applied along the surface of the insulator due to additional forces that deform the droplet. Although such behaviour has been well researched for dc fields, it has received limited attention for the quasi-free droplet subjected to ac stressing [1]. However, it is reasonable to assume that droplet deformation, in the form of either vibration or spreading, may take place whenever the additional forces exceed those due to surface tension. The field, E_c, at which a free spherical water droplet distorts is known to be proportional to $(\lambda/r)^{1/2}$, where λ is the surface tension of the water and r the undistorted radius of the droplet [17]. This has been calculated in [1] for distilled water in terms of peak values of applied ac field for a range of droplet radii. Table 3.3 shows the values they obtained and, in addition, expresses these in terms of RMS values of applied field and droplet volume in μl.

Comparing tables 3.3 and 3.2, it is reasonable to suggest that it is the magnitude of the above field E_c that may well indicate the onset of vibration and spreading of droplets, and so point to a link between these processes and surface tension. However, it must be noted that table 3.2 concerns quasi-free droplets – which are approximately hemi-ellipsoidal - on a polymer surface, whereas table 3.3 refers to free, spherical droplets.

Many industrial polymers in their usual, manufactured form have surfaces with the degree of hydrophobicity required for well-formed water droplets to develop. In the previous work reviewed here, this is true for a range of water types from deionised

through tap and rain and on to salt solutions and for droplet volumes from at least 5 to 50ml. As noted in chapter 2, such initial hydrophobicity can be reduced when surfaces are damaged by sparking or contaminated by some surface deposits. For example in [1] sparking was found to lower flashover voltage by 30% but recovery to the fully hydrophobic value could take only a few minutes. In most cases, flashover is reported to be triggered by gross distortion of droplets such that they extend over the surrounding insulator surface, indicating the surface there has become hydrophilic. This part of the surface is then effectively shorted-out electrically, and so the stress-enhancing effect of the droplet increases, leading to further distortion and spreading of water droplets.

3.4 Water droplet characteristics

Next, we examine what previous studies have revealed about the significance of the dielectric and geometric properties of the water droplet placed on an electrically-stressed polymer insulator surface.

3.4.1 Dielectric properties

Over the limited range of frequency applicable to power applications, the relative permittivity of water may be assumed constant at 81.

In [1] conductivity was varied over more than four orders of magnitude from a deionised value of 300μS/m to that of an NaCl saturated solution of 5.8S/m. In [3], the water resistivity, ρ, was taken as $1x10^6\Omega m$ (corresponding to a conductivity of 10mS/m, which is typical of tap or rain water). In [4] the conductivity of the water droplet used was 5mS/m (tap water) and 31.2 S/m (salt water). In [6] two types of droplet were used: distilled and salt water. However, no quantitative details were provided on the conductivity of these droplets. In [7], the water was described as either deionised, with a conductivity 1mS/m, or with NaCl added to give a conductivity 1S/m). In [8] the conductivity of the deionised water used was 50μS/m whereas in [10] tap water was used which had a conductivity of 60mS/m. Two conditions were used in

[11]: deionised water, with a conductivity 20μS/m and an artificial acid rain with a conductivity 56mS/m. In [13], distilled water was used.

These previous studies have, therefore, used water droplets with conductivities that represent deionised, tap, rain up to saturated salt-solutions and range over 4 to 5 orders of magnitude. Typical values of conductivity are summarized in table 3.4.

From [1] and [2], increasing conductivity to this degree appears to reduce the measured average field strengths for PD activity, vibration onset or breakdown by only around 10%. However, in [5] it was reported that, when deionised water was replaced by tap water, the vibration inception voltage for a 15-μl droplet on clean SiR was reduced by about 50%, from about 16 to 8kV. With a fixed conductivity (tap water), this voltage fell from approximately 8 to 4kV when the droplet volume was increased from 15μl to 200μl. It was considered that higher conductivities coupled with larger volumes would, with a fixed applied voltage, increase the electric field between droplet and electrodes and so the result was to bring about a lower inception voltage.

From the above, it may be argued - at least for droplet volumes of the order of 10 to 20μl – that onset (inception) fields are particularly sensitive to droplet conductivity. However, this sensitivity falls off considerably for greater droplet volumes.

3.4.2 Volume and shape

As indicated above, droplet volume and shape has been found to influence behaviour. A 20μl, sessile drop on a strongly hydrophobic SiR surface can have two stable shapes under ac stress [1]. Once highly distorted from its initial near-spherical shape, a droplet can remain permanently squat and elongated. This has clear implications with regard to the effect a droplet might have on enhancement of the electric field around it. This is discussed in [3], where a water droplet with volume

100μl and radius 3mm was studied. The droplet was considered to elongate over a horizontal surface, partly due to field intensification at its tip and partly due to gravity but it should be noted that the possibility of an increase in surface hydrophilicity was not considered. As a result of elongation, an initial spherical shape would become ellipsoidal, with the same volume. Two expressions were given in [3], one to compute the contact angle θ as shown in Fig (3.12) and the other to estimate the water droplet volume v:

$$\theta = \frac{\pi}{2} + \arcsin\left[\frac{z_0 - z_i}{r}\right] \tag{3.5}$$

$$v = ab\pi\left[(c - z_i) - \frac{c^3 - z^3{}_i}{3c^2}\right] \tag{3.6}$$

Where a, b and c are the ellipsoid semi-axes, z_i is the insulator surface level and z_o is at the center of the droplet. They calculated field enhancement on the insulator surface at the triple junctions and found a 60% increase for the ellipsoidal shape over the spherical one, although part of this was because the edges of the elongated droplet were closer to the end electrodes thus shortening the gap between droplet and electrode.

In [5], the effect of varying water droplet volume has been considered. It was found that for tap and salt water on an SiR surface the onset field for vibration fell by 50% as volume was increased from 15 to 200μl. For deionised water, the reduction was very pronounced as volume increased from 15 to 50μl. The authors suggested the fall was associated with changes in electric field but did not offer an explanation. It may be that the shape factors mentioned in [3] above are concerned.

The droplet shape considered in [4] is shown in Fig (3.11). These authors considered force balance at a droplet on a solid surface. The forces generated from the application of a tangential electric field are considered to affect this balance and so deform the droplet into a more irregular shape. This, it was suggested, results in areas on a droplet which produce local field enhancement that leads to more deformation. This "feed-back" process could trigger what were termed micro-discharges and

electrochemical degradation of the insulator surface. The relation between point on the applied waveform and droplet shape have been examined for 10 and 30μl droplets on SiR [8]. At the zero-crossings the droplet was found to have a raised center and to have a shape approximating to a prolate semi-ellipsoid. At the maxima the droplet was flattened into a prolate semi-ellipsoid. The movement of drops with volumes between 6 and 100μl was studied in [12]. If we denote the height of an unstressed droplet by H, then these authors report that the stressed droplet height could lie between $H \pm {}^{1}/_{3}H$. Fig (3.13) shows the characteristic shapes they recorded for a drop of 100μl.

Droplet volume can influence behaviour from a hydrodynamic viewpoint. It is shown in [17] that the natural mode of vibration of a free spherical droplet is inversely proportional to its radius. Hence it would be expected that free spherical droplets of different volumes subject to oscillating forces in an ac applied field would show resonance at different frequencies, and these resonance frequencies should move to lower values as droplet volume is increased. It is considered here that a similar effect may also occur with quasi-free, hemi-ellipsoid droplets adhering to an insulator surface. In [8], such surface droplets were considered to be characterized by an aspect ratio given by droplet width over droplet height – i.e. this ratio is unity for a hemisphere. These authors detected the peak values of aspect ratio for 10 and 30-μl droplets of deionised water on PTFE and SiR surfaces as the frequency of the applied field was raised from 0 to 100Hz at a constant applied stress. The unperturbed aspect ratio was between 2.5 and 3. Their results are summarized in table 3.5.

It is evident that the larger droplet resonates at lower frequencies than the smaller one. This is consistent with the suggestion made above. However, with the departure from spherical symmetry indicated by aspect ratios greater than one, it seems reasonable that essentially two resonances are found. If we assume the shapes of these droplets can be approximated by semi-ellipsoids, then these two resonances are probably associated with its major and minor axes.

3.5 Modes of droplet vibration

The main influence on vibration is obviously the frequency of the applied field. However, as pointed out in chapter 2, it is possible that a droplet could respond by oscillating at twice the applied frequency. Also, as described above, departure from a simple hemispherical shape can introduce resonant responses over a range of frequencies. As discussed in section 2.2, two of the possible forces which a free particle floating in air experiences from the application of electric field oscillating at angular frequency ω are the dielectrophoretic and Maxwell forces. Both of these lead to a possible frequency of vibration of $(\omega/2\pi)^2$.

Most researchers find that water droplets vibrate synchronously with the frequency of the applied stress used in their investigations. A typical pattern of vibration is shown in Fig (3.14), taken from [7]. It is perhaps worth noting that these authors confirm that water droplets do not vibrate before breakdown with a dc applied field. These authors discussed deformation and vibration of a water droplet in terms of a model shown in Fig (3.15). They considered positive and negative charges to form at the edges of a droplet as illustrated in Fig (3.15) as a result of electrostatic induction (see section 2.2). Such charges are subject to a coulomb force in the electric field direction proportional to the applied field. Consequently, the edges of the water droplet having induced charges are subject to tensile forces proportional to the instantaneous magnitude of applied field. Under both positive and negative polarities, the same magnitude and direction of forces is induced and so, with electrostatic induction, the water droplet is subject to a constant deformation in the direction of the applied field which does not affect the frequency of droplet vibration.

In most previous studies it has been found that droplets become distorted in shape shortly before breakdown. An important feature is that, once distorted from its initial shape, droplets remain permanently elongated - even if the applied field is not raised further (see, for example, [1] and [3] and [5]). As shown in table 3.5, elongated droplets show more than one frequency of vibration at resonance. Hence it would appear likely that droplets which initially vibrate at the applied frequency will show more complex vibration patterns when they start to elongate or spread as the applied field is raised. Figures 3.16 and 3.17 illustrate this type of behaviour.

In [9] and [11] it was reported that water droplets could charge negatively before starting to vibrate and then change from negative to positive polarity after the onset of vibration. This phenomenon was thought to be due to "intermittent" vibrations of the droplet that caused pronounced shape changes generating tips from which electrical discharges could be triggered resulting in loss of electrons from the droplet and, eventually, a positive charge on the droplet. In [13] the deformation and vibration modes of the water droplet depend on a number of factors: applied field, surface tension, drop volume and water conductivity. These factors were investigated experimentally and theoretically. Fig (3.18) shows several vibration modes observed in a 50 Hz applied field where it can be seen that the water droplet can be deformed in a variety ways: elongation and contraction, Figs (3.18 a and c), sideways oscillation, Figs (3.18 b and d).

It has been reported that droplet vibration is found to be more evident on smooth (i.e. as normally manufactured) surfaces [8]. On surfaces deliberately roughed by blasting with glass beads, droplets tended to split rather than vibrate. Single droplets were found less likely to spread over a solid surface than an array of droplets, where droplet volume could increase due to the combination of several droplets under the influence of the applied electric field.

In [12] a vertical, up-and-down oscillation was observed, in which characteristic structures on the surface of the liquid were observed depending on the volume of the drops. These characteristic structures repeated every half cycle of the applied waveform. Consequently, this vertical oscillation was found to be at twice the frequency of the applied field. The same authors found that when a frequency of 25Hz was applied to 100 µl drops, there was a horizontal wave-like movement along the surface of the liquid that moved periodically at a frequency equal to the applied frequency. This was also observed at 50 and 60Hz. At an applied frequency of 100Hz, drops with volumes of 50 and 100 µl tended to show reduced vertical movement and developed what could be described as surface waves but which did not show a clear pattern of oscillation.

It should also be noted that on the inclined surfaces encountered in practice, the shapes that arise due to droplet deformation will be influenced in an asymmetrical way by gravity and so even further modes of vibration may be expected. See Fig (3.19) taken from reference [15]. When the solid surface was inclined by at 10° to the horizontal, 20μl droplets developed higher amplitudes of oscillation than on a horizontal surface where they tended not to be very active [12]. However, for the combinations of 10 μl at 50° and 50 μl at 20° vibration amplitudes were found to be lower than with the horizontal arrangement. A 50-μl droplet on a surface inclined at 30° rolled down the surface before the applied field reached a level high enough to cause flashover. On the other hand, 20-μl droplets on a surface inclined at 30° elongated but did not roll.

3.6 Partial Discharge Activity

As previously described in chapters 1 and 2 suitably energetic discharges located around droplets may reduce surface hydrophobicity by, for example, emitting UV light and so by breaking molecular bonds in the polymer at its surface allowing the formation of hydrogen bonds with water. That is, the surface tension of the solid, γ_s, may be increased by exposure of the surface to discharges. For this reason, partial discharge activity generated by the presence of water droplets on highly-stressed solid insulating surfaces has been widely investigated.

3.6.1 Physical Location and Distribution on ac Cycle

In [6] a water droplet was placed on an SiR surface mid way between two end electrodes. These authors report detecting leakage currents from corona discharges from deformed water droplets just before the positive and negative peaks of the applied ac voltage. The magnitude of these discharges does not depend on the polarity of the peak. Larger and more frequent pulses were found with a salt-water droplet compared to a distilled-water droplet. This might be expected because the higher conductivity of the salt water leads to a higher field enhancement as explained in section 3.3.2.

PD activity has been examined for a tap water droplet on a flat SiR surface between end electrodes [10]. The droplet was placed in three locations: near the high voltage electrode, the ground electrode or in the middle of the sample as shown in Fig (3.5). PD signals were sampled at 1.2MHz that is, each 60Hz-cycle was divided into 100 phase windows each of which comprised 200 samples. Fig (3.20) illustrates the results they obtained. It was concluded that PD activity occurred near to the peak values of the applied voltage. This activity was mainly in the positive half-cycle from a droplet near the high voltage electrode, and mainly in the negative half-cycle from a droplet near the ground electrode. For a droplet located in the middle of the sample, similar PD activity took place during both half cycles again near the peak values of the applied waveform. These authors did not report the physical location of the partial discharges.

Figures 5 and 6 of reference [11] show discharge activity from a single, 30μl, deionised, water droplet located at the center of a flat SiR sample between surface mounted electrodes, one of which was grounded. This discharge activity is reported to be from corona discharges at sharp tips formed during intense vibration of the droplet. The figures show discharges in both the positive and negative half cycles located between the zero crossing and the peak of the cycle. There appears to be a slight emphasis on activity during the positive half cycle, but this could be explained, according to [10] if the droplet was located slightly nearer the high voltage electrode. From measurements of the surface potential distribution in the gap space it was concluded that the droplet was negatively charged prior to vibration but during vibration tiny droplets were scattered and the droplet lost its negative charges and eventually became positively charged.

In [14] it was reported that partial discharge activity occurred at the triple point at the edge of the water droplet, as shown in Fig (3.21). Here ε_r for water was taken as 80, ε_r for air as 1 and ε_r for SiR as 4 and so the triple point intensified the electric field and discharges occurred in the high stress region. These authors do not calculate the

intensification nor explain these discharges in terms of, for example, the conditions required for electrical breakdown in air.

The effect of multiple 0.3-ml, deionised or salt-water droplets on an epoxy resin surface was examined in [7] with 50Hz applied stress. Partial discharges were found to take place between droplets but these authors do not record their location in time relative to the applied waveform. Over a 30-minuite period they found that the rate of PD activity increased, rose to a maximum then decreased with activity higher for the salt-water droplets. No explanation is suggested. However, if it is assumed that the droplets spread during the experiment then the gaps between them would decrease, which would initially lead to an increase in the field strength between droplets. Eventually, the droplets would be in contact in which case the field between them would fall to zero. Since the PD activity is determined by the field, it would show the same behaviour. Another possibility might be associated with the observation in [11] that droplets become positively charged through discharge activity and if this occurred for all of the multiple droplets then this also could lead to a suppression of discharge activity over a period of time.

Fig (3.22), taken from reference [13], shows calculated values of the tangential component of the electric field in the presence of distilled water droplets of diameters from 2 to 6mm centrally-located on the surface of an epoxy-resin sample with embedded electrodes. These calculations show a sharp maximum in the electric field at the triple points with a field enhancement of approximately 15 times. The enhancement was higher the bigger the drop, as would be expected from section 3.3.2. The high value of surface field suggests discharges will be located at triple points, but it would be useful to calculate the three-dimensional electric above the insulator surface close to the droplet in order to investigate the likelihood of breakdown in the air above the surface.

In reference [10] partial discharges were measured using a PD detector. However no details were given. The discharges were shown to have magnitudes of typically up to 2000pC. Other investigators have used a simple resistor of the order of

100 ohms in series with the test gap to detect partial discharges. They record partial discharge currents of typically less than 0.5 mA. Because significant vibration accompanied by droplet deformation and increased partial discharge activity appears to be required before complete breakdown, it would appear that few, if any studies have been designed to employ sensitive PD detection techniques to this type of problem.

3.7 Test Sample Flashover

There is general agreement - see, for example, papers [1], [5], [8] and [9] – that complete flashover of test samples takes a place when water droplets spread towards the electrodes and increase the wetted area on the sample. Flashover with sessile droplets was triggered by gross distortion of the droplet [1] such that, according to these authors, it covered more of the surface and its stress-enhancing effect was increased by about 60%. Flashover took place by bridging of water droplets on contaminated silicone rubber [5]. Higher flashover voltages were found with water droplets of smaller volume and lower conductivity, as would be expected from surface-shorting behaviour as noted above. In [8] discharge inception from a droplet was studied and during a relatively violent vibration, instability may happen, and several small droplets could be ejected from the upper surface of the droplet. Complete breakdown happened via these droplets. In [9], where condensation took place under the influence of an applied field, droplets could coalesce and thereby increased the wet contact surface area. The resulting large droplets, together with the associated increased PD, could lead to a raised value of leakage current and eventually complete flashover.

3.8 Summary and Discussion

It is reasonable to conclude that water droplets on ac-stressed polymer surfaces contribute to electrical flashover of the polymer surface through a series of processes: partial discharges, vibration, droplet deformation (spreading, elongation, fragmentation). These processes appear to occur with most combinations of electrode geometry, polymer types and surface conditions, and water droplet characteristics and surface location. A combination of large droplet volume and high water conductivity

reduces the magnitude of the applied voltage required to generate onset of partial discharges, vibration, etc. The physical location of partial discharges has been reported to be at the triple point, or at the side of the droplet, or at its tip. Finding further details about the location is of some importance, because it will determine how efficiently these discharges can lead to reductions in the hydrophobicity of the polymer surface - with the effects this can have on droplet deformation and movement. It is not clear from previous work whether partial discharges near triple points are wholly on the surface or wholly in the air or a combination of both. It may be that location is influenced by whether the applied field has predominantly tangential or normal components relative to the polymer surface near the droplet. In the following chapter, these specific points are considered further, and suitable aims for a programme of research are examined which is intended to aim at shedding light on some of the issues.

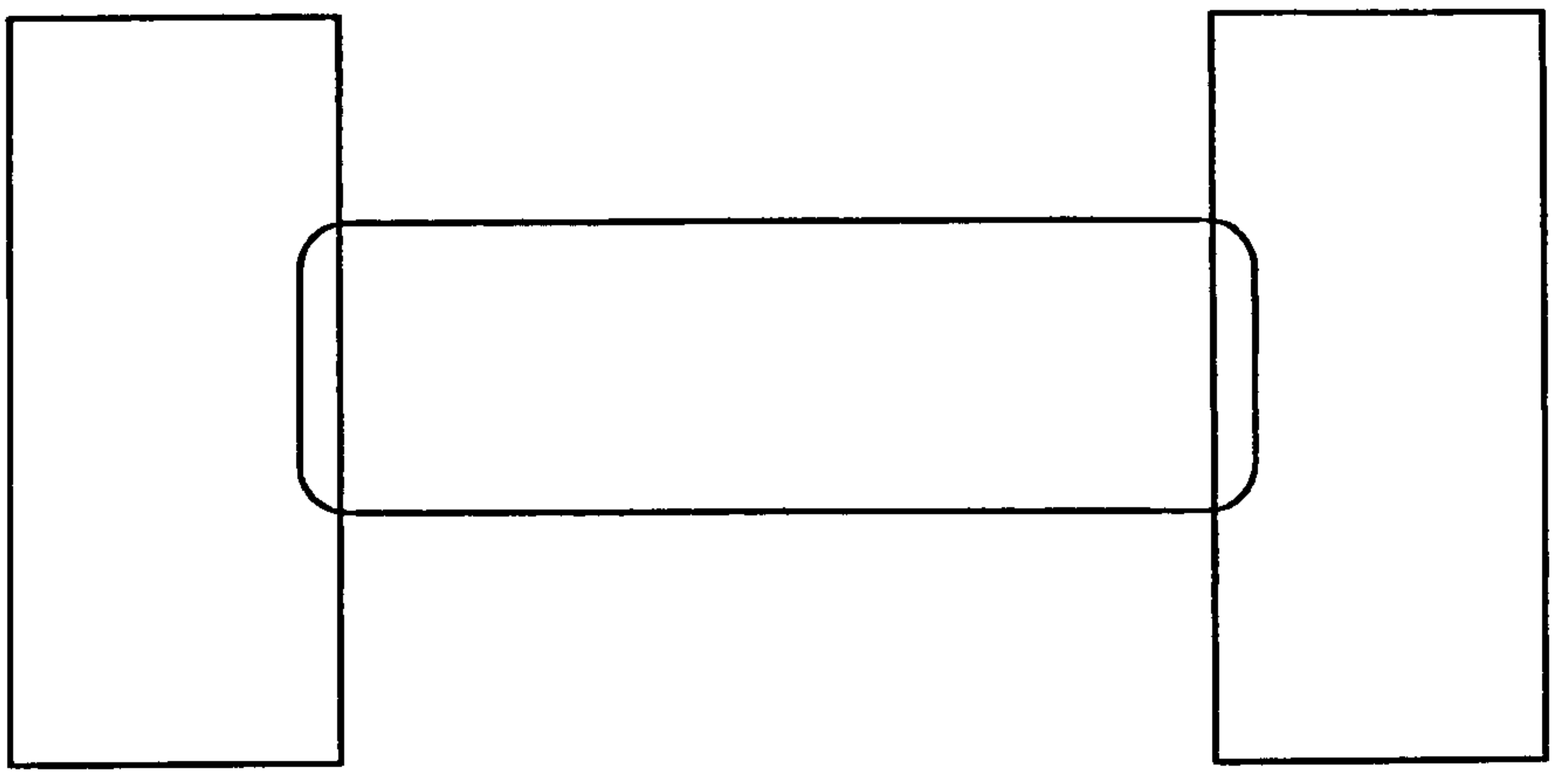

(a) End Electrodes

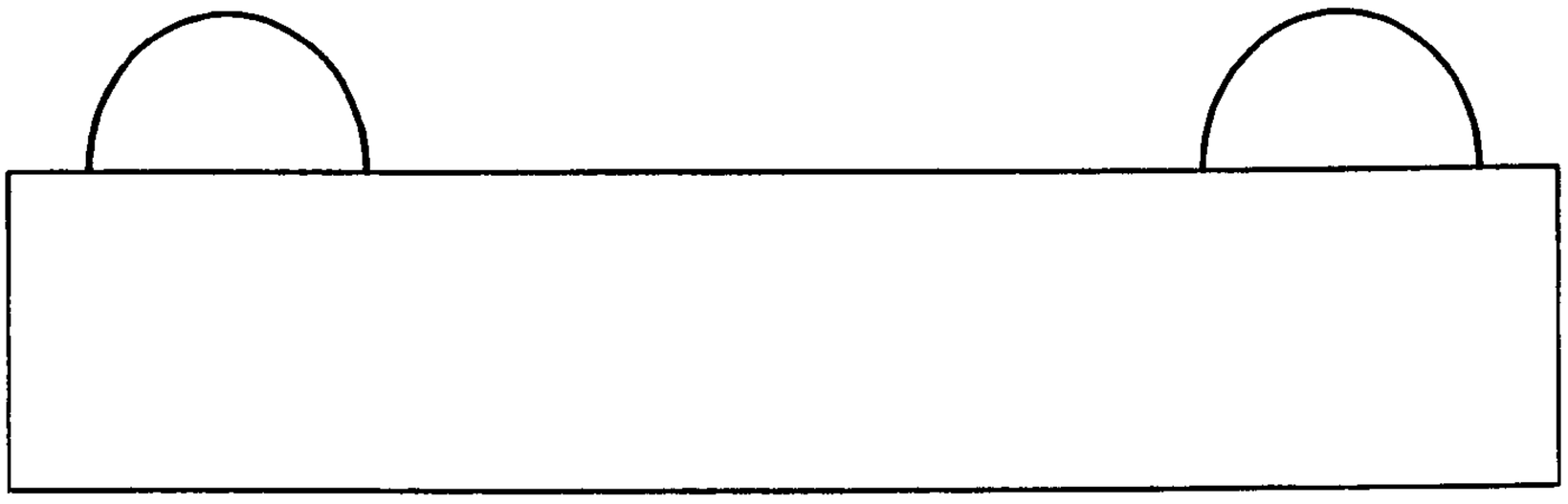

(b) Surface Electrodes

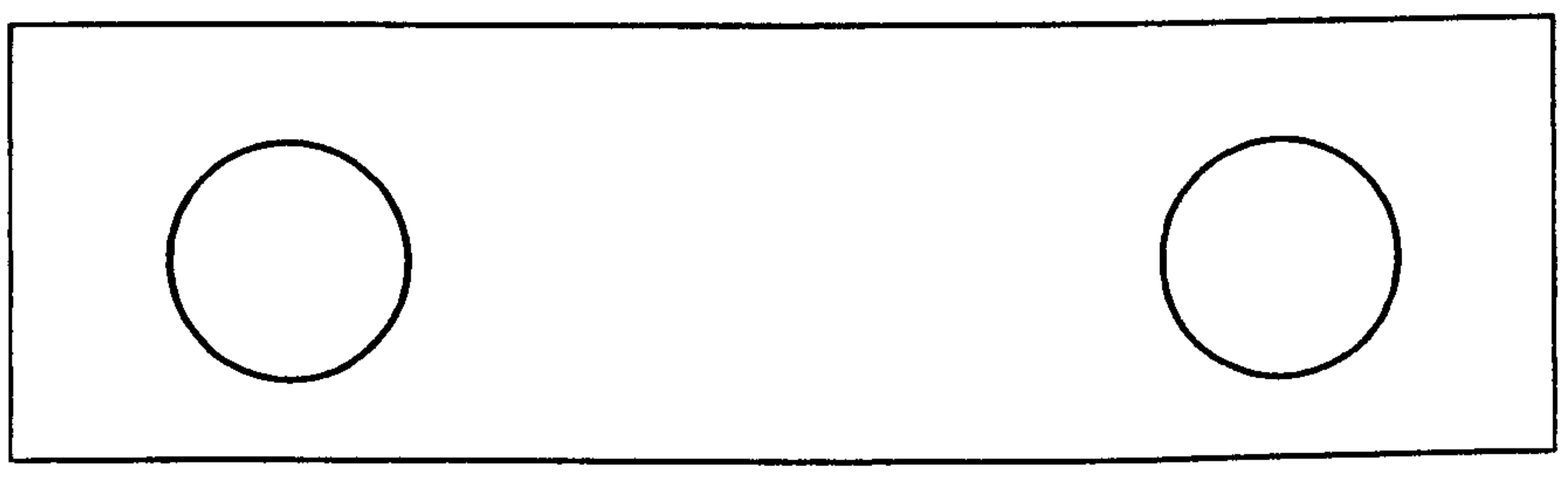

(c) Embedded Electrodes

Fig (3.1) General Types of electrodes Geometries

(a) End Electrodes, (b) Surface electrodes and (c) Embedded Electrodes

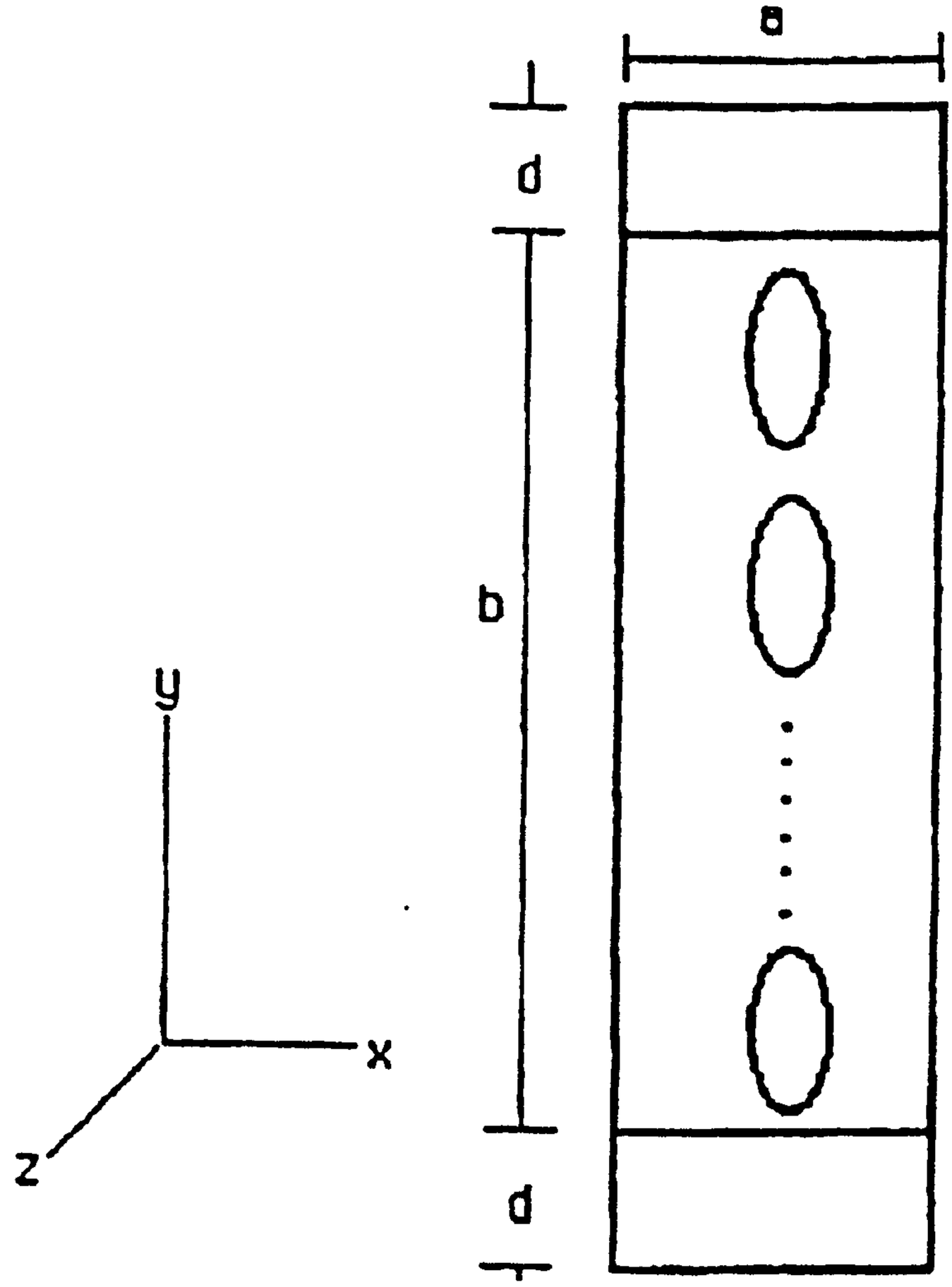

Fig (3.2) the insulator geometry modeled by H. El-Kishky [4] uniform field geometry with a = 20mm, b = 250mm and d = 50 mm

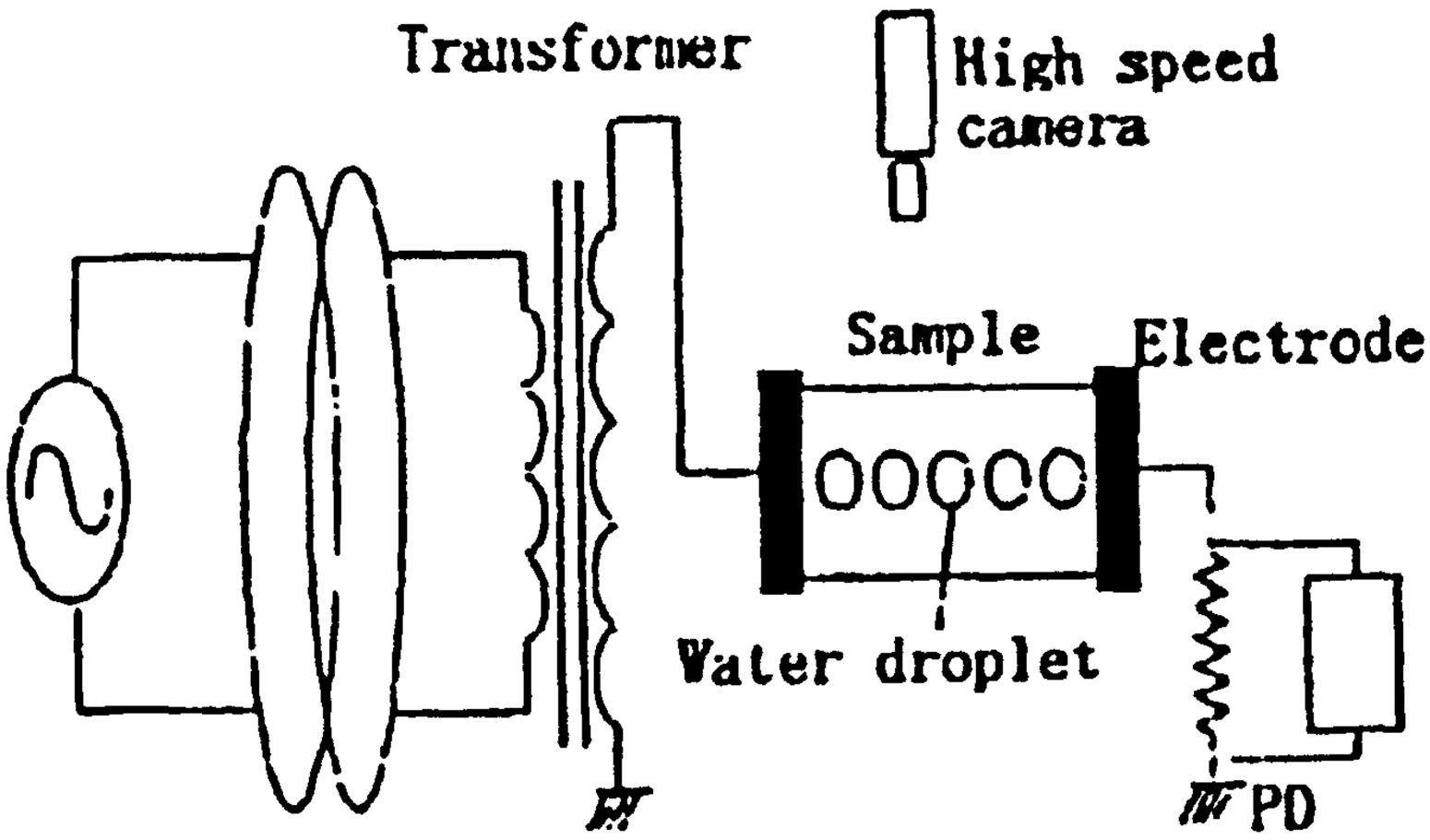

Fig (3.3) the experimental Procedure used Y. Mizuno [5, 12] approximately uniform-field geometry

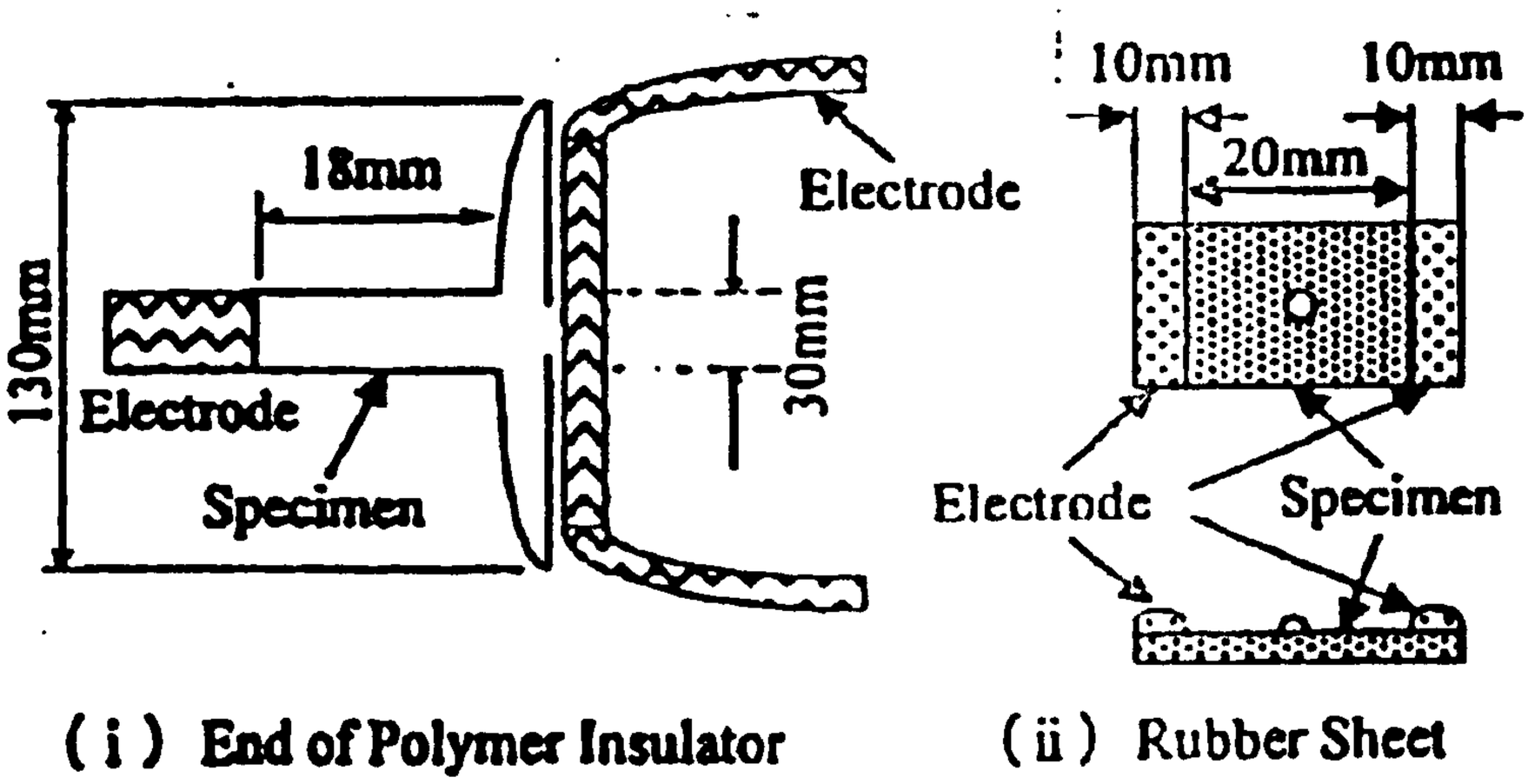

(i) End of Polymer Insulator **(ii) Rubber Sheet**

Fig (3.4) the test arrangement used by Koji Katada [7] non-uniform field geometry using specimen insulators (i) and approximately uniform electric field (ii) .

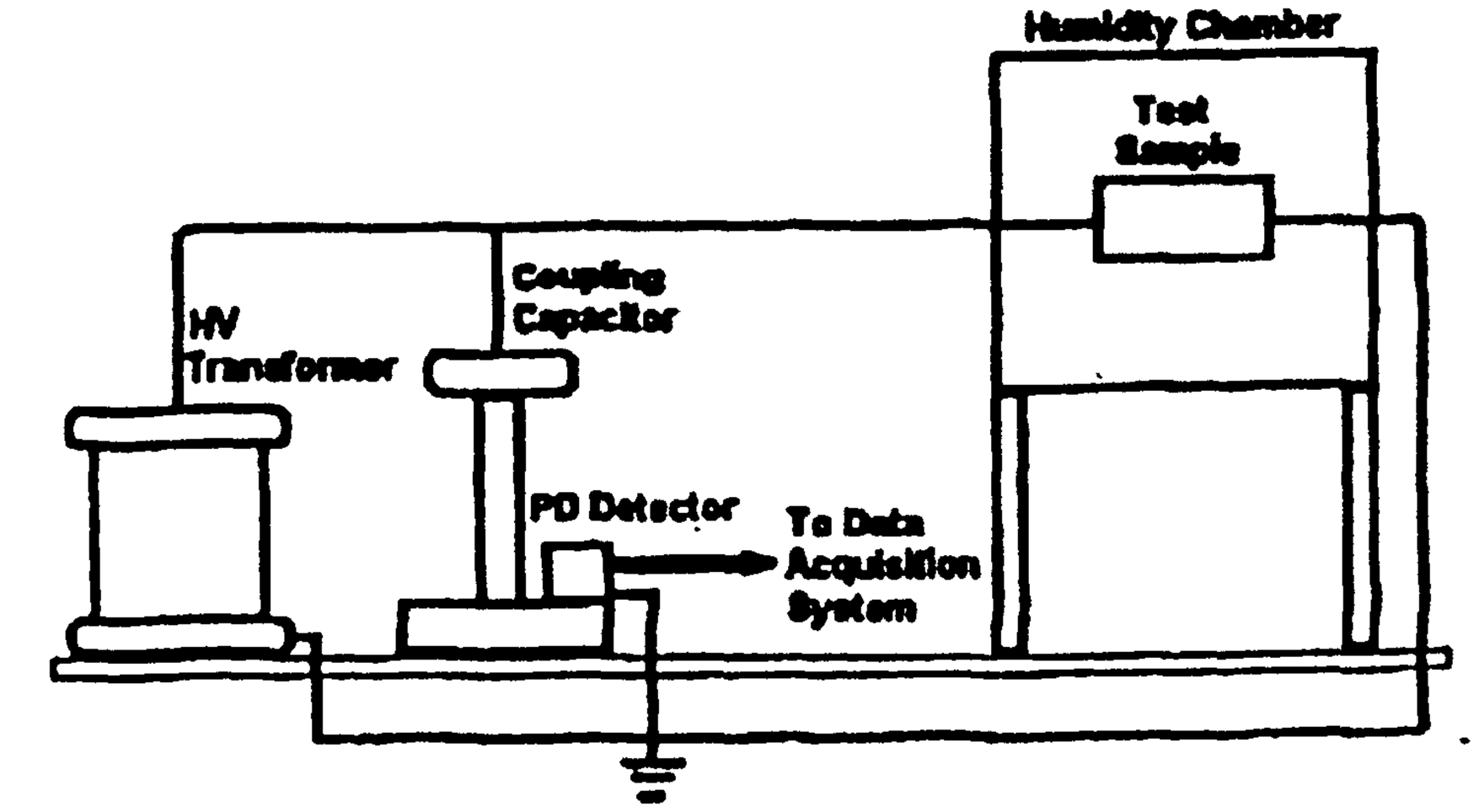

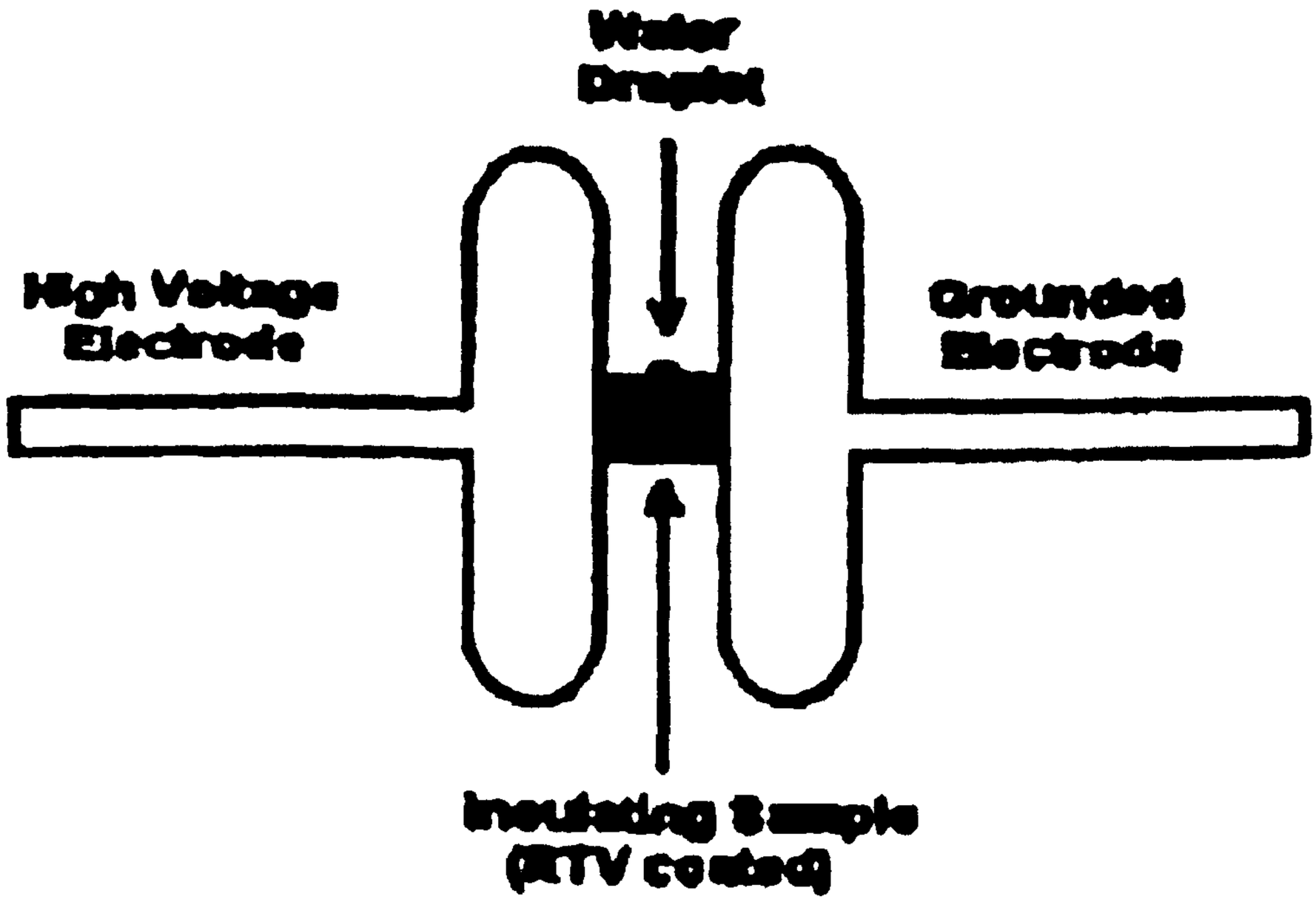

Fig (3.5) the test arrangement used by I. J. S. Lopes [10] (A) and schematic representation of the flat acrylic sample coated with silicone rubber uniform electric field geometry (B).

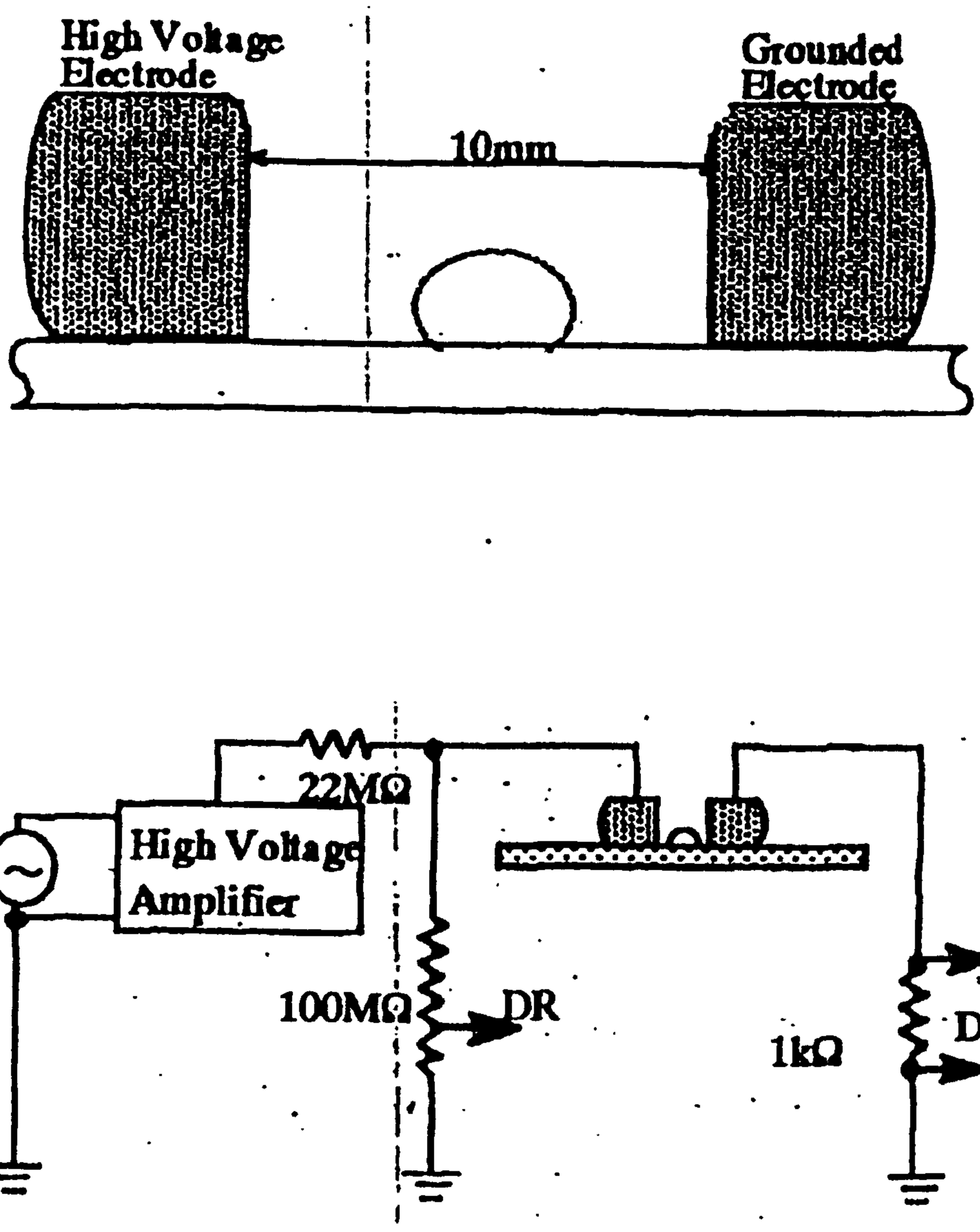

Fig (3.6) A Single Water Droplet between Parallel Rod Electrodes and Experimental Set-Up for Observing the Behaviour of Water Droplet used by Yoshio Higashiyama [8]. Electrodes geometry not uniform field geometry.

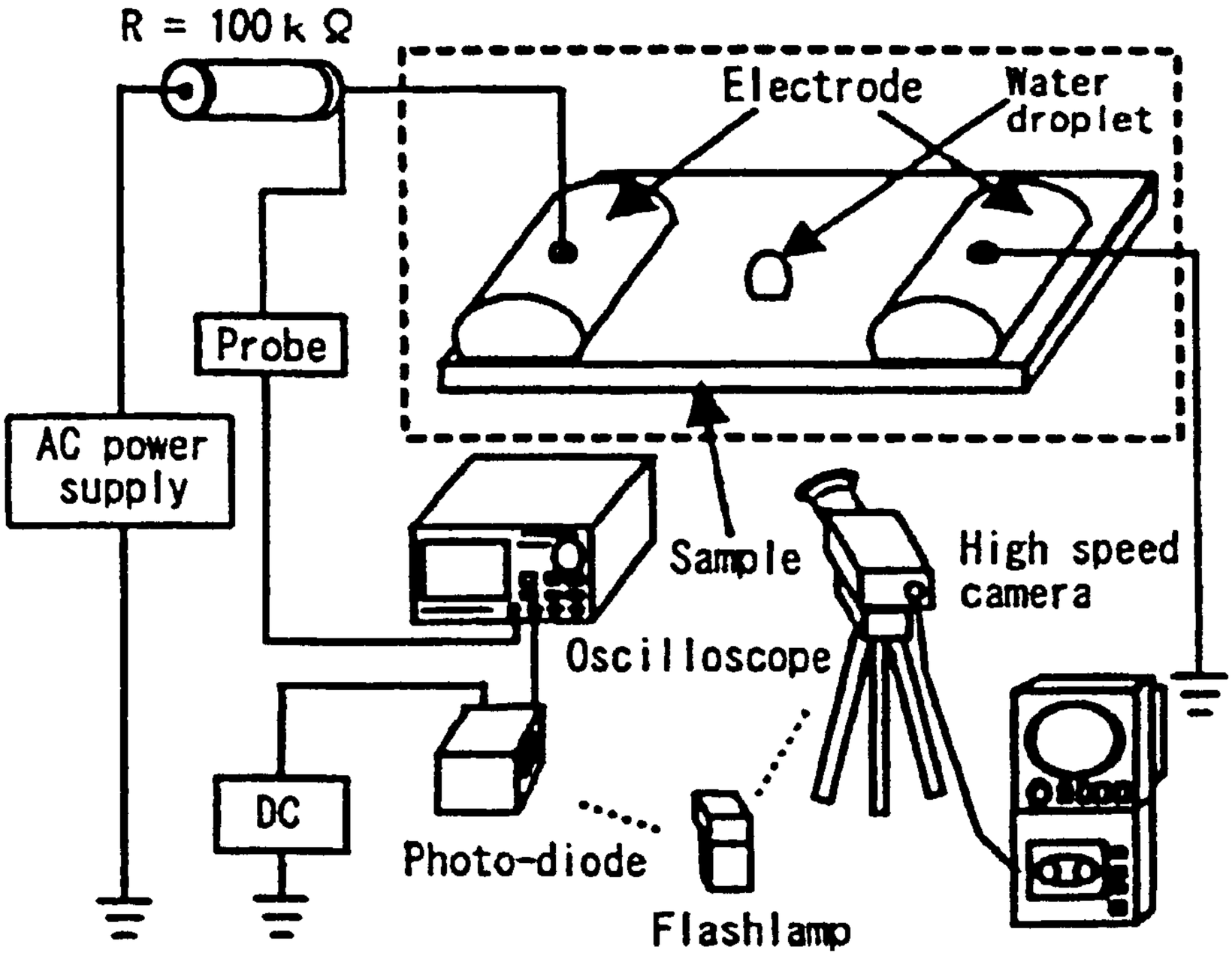

Fig (3.7) Experimental Set-Up for Observing the Behaviour of Water Droplet used by Norihiro Arise [8] and M. Otsubo [10]. Electrodes geometry not uniform field geometry.

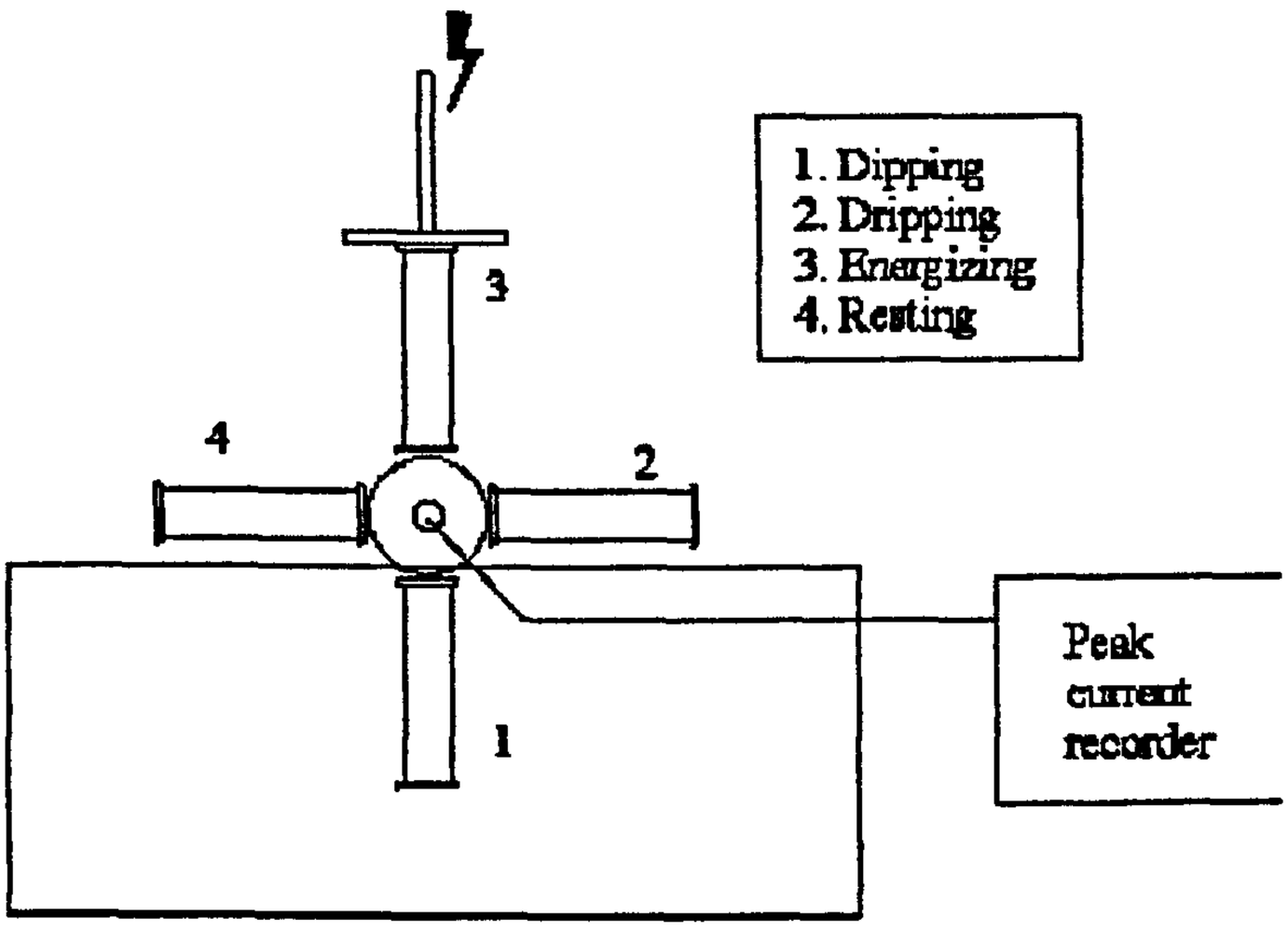

Fig (3.8) Measurement set-up for observation of a single water droplet in a 50-Hz electric field used by A. Krivinda [14] .

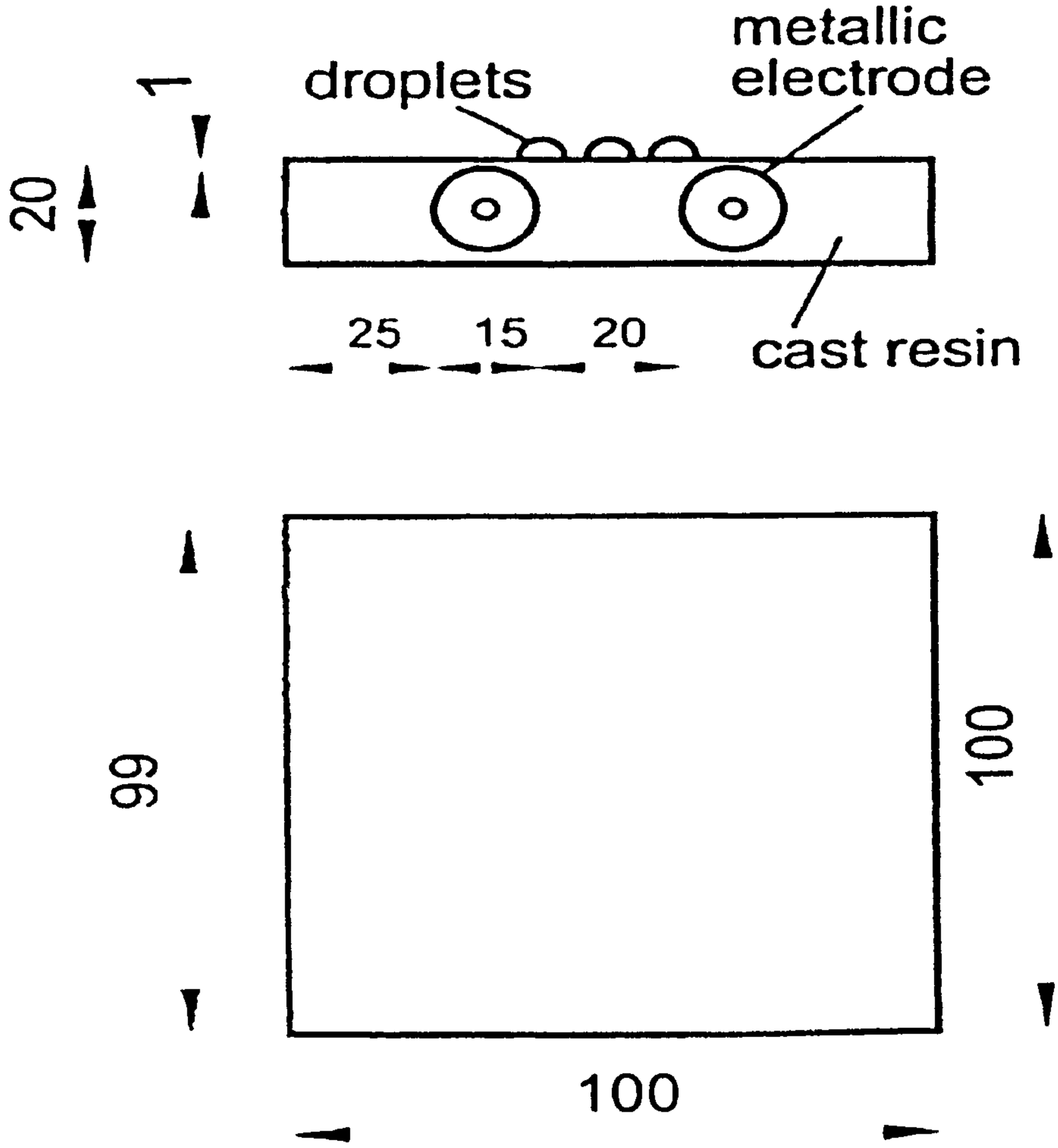

Fig (3.9) Test Object with Embedded Electrodes and droplets on the surface used by D. Koenig the electric field geometry approximately uniform [7]

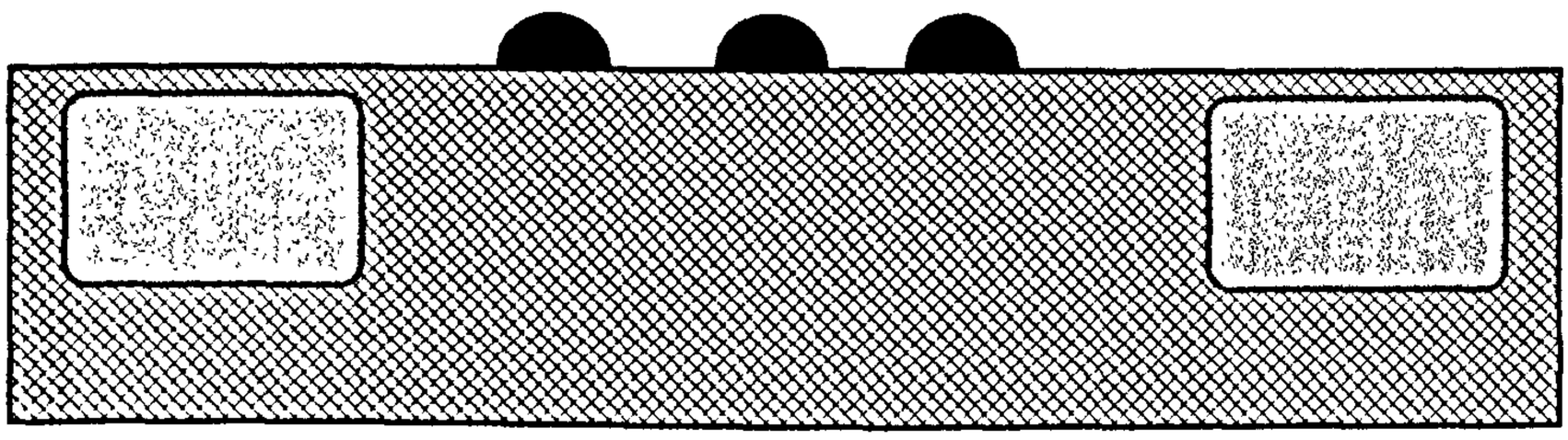

Fig (3.10) Teat Object with embedded electrodes and surface droplet as employed by D. Koenig [13]

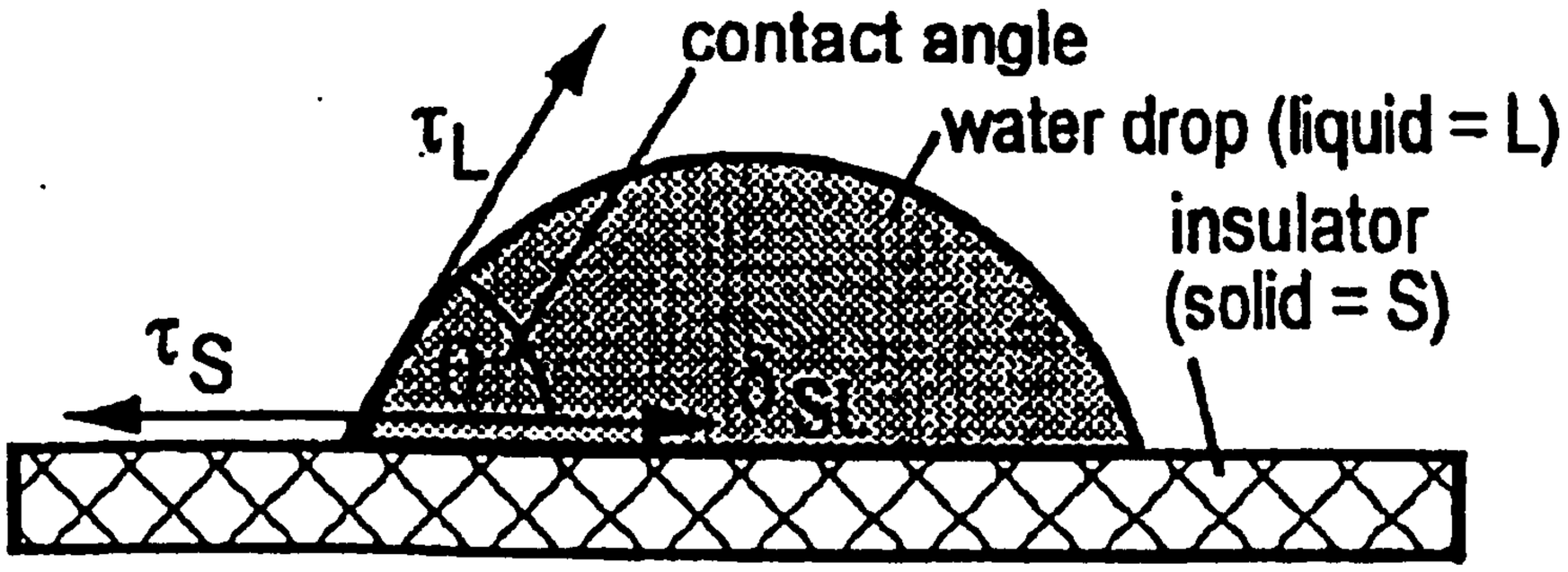

Fig (3.11) Force Balance at the interface Solid/ Liquid at a Water Droplet on a Solid Surface [4].

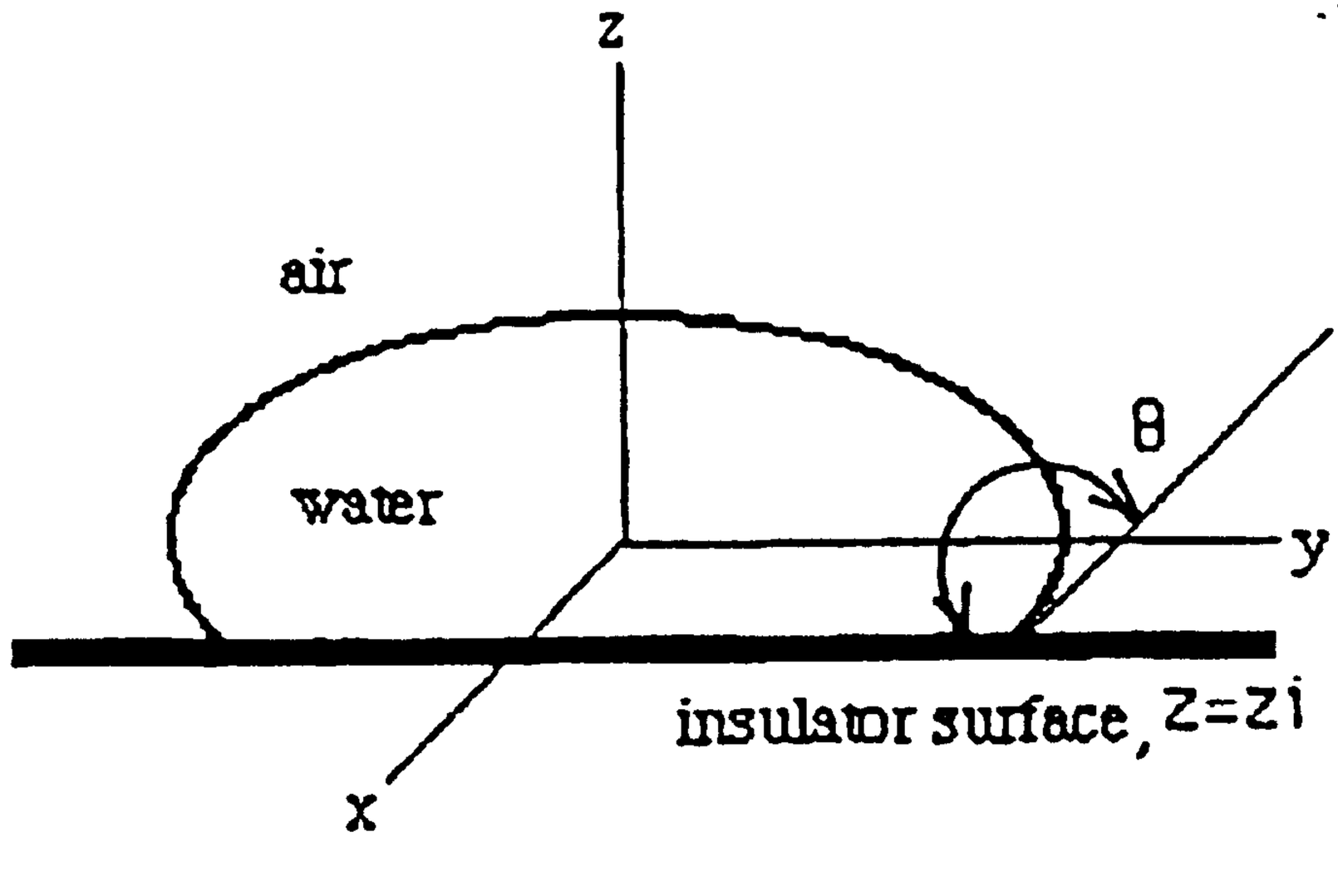

Fig (3.12) Cross Section (x = 0) Plane Water Droplet for calculating the contact angle and droplet volume [4].

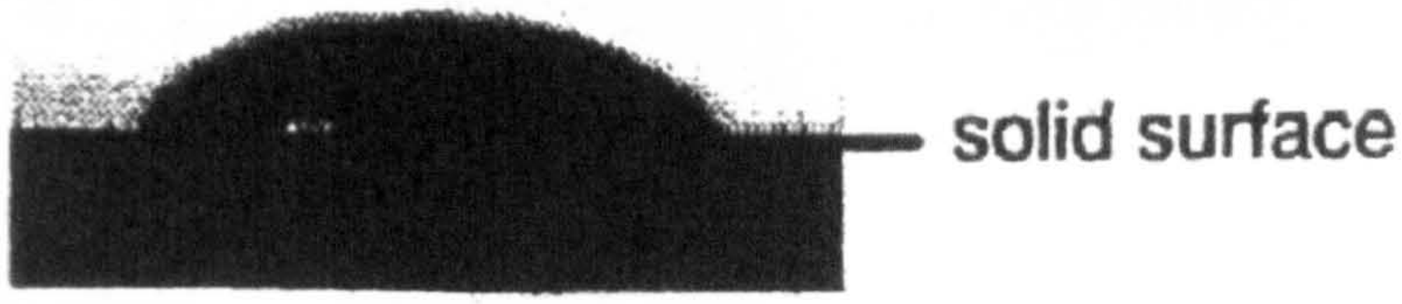

Drop of 100 µl, electrically unstressed, "natural" shape

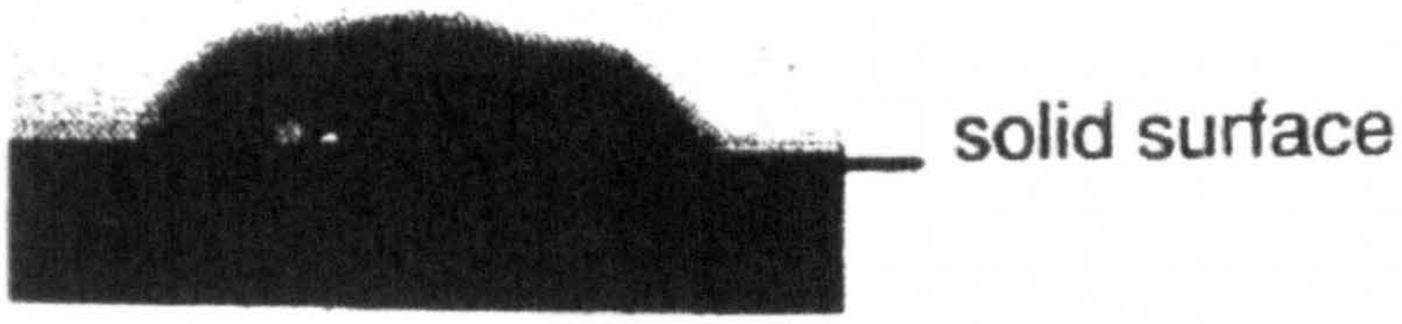

Drop of 100 µl with a transient structure on its surface, applied sinusoidal voltage $\hat{u}$ = 13 kV and f = 50 Hz

Fig (3.13) water droplet unstressed and stressed [15]

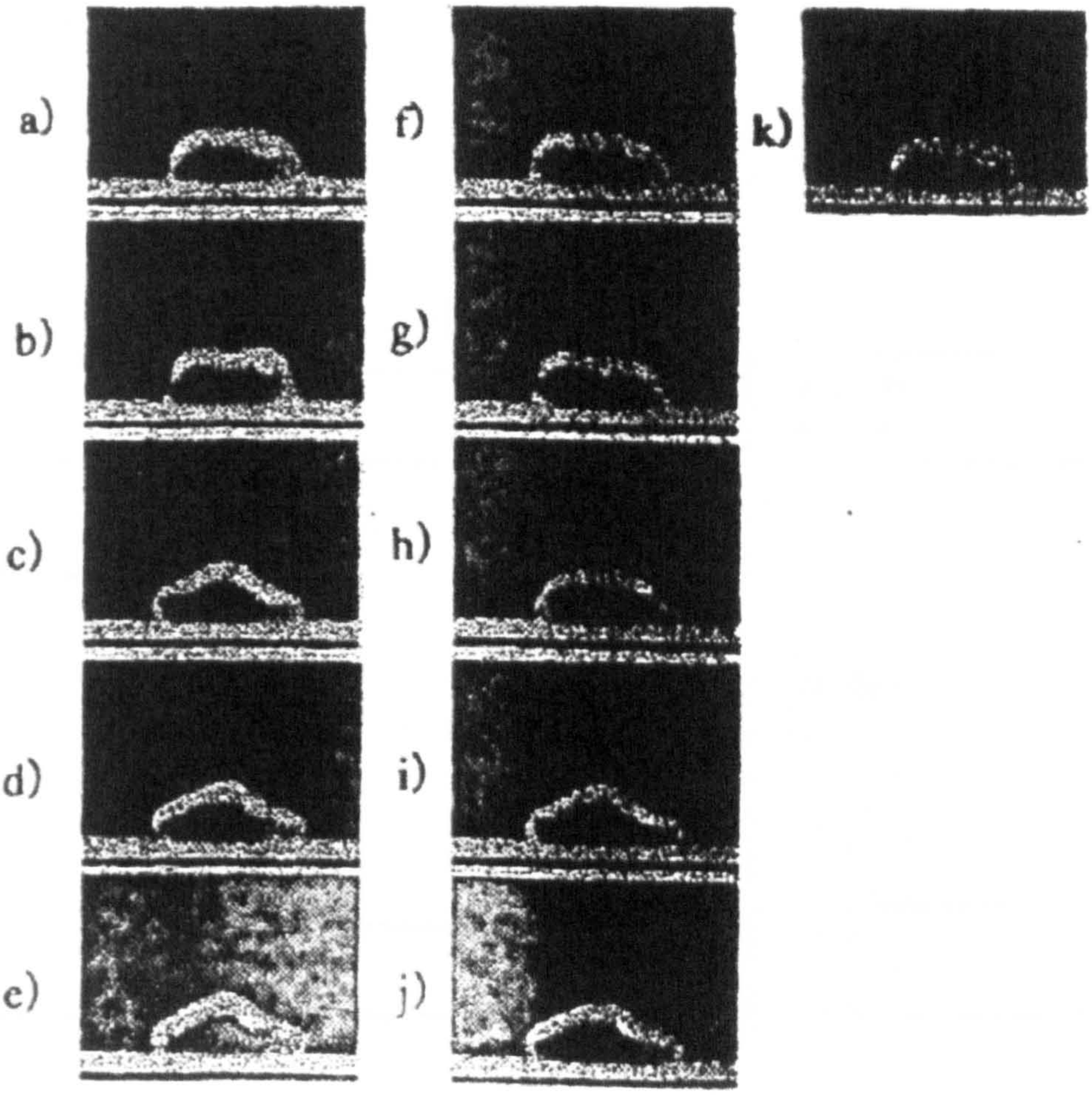

Fig (3.14) Sequential Frames during 1 Cycle of AC Voltage [7].

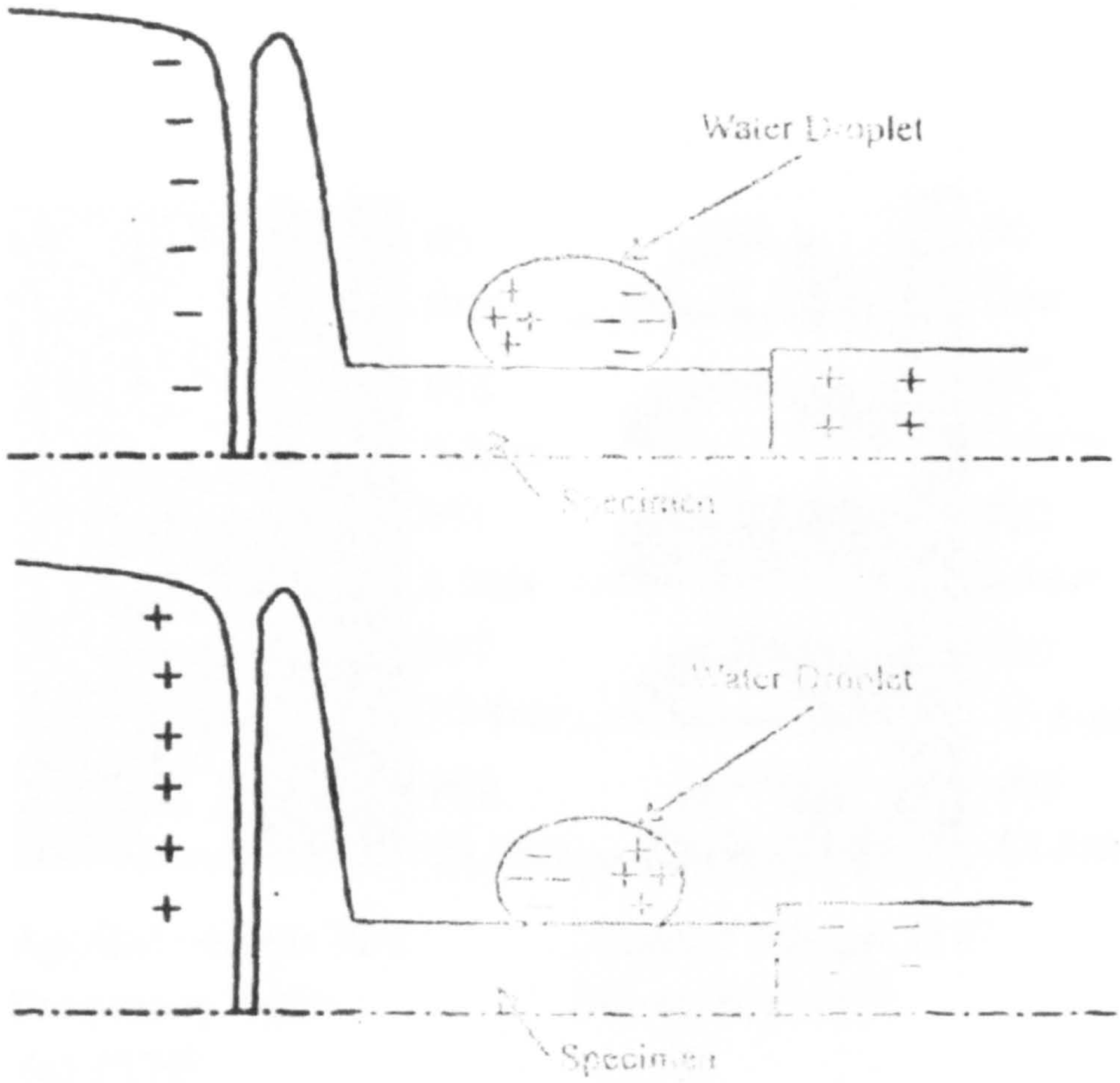

Fig (3.15) Deformation of Water Droplet due to Electrostatic Induction and Coulomb's Force [7]

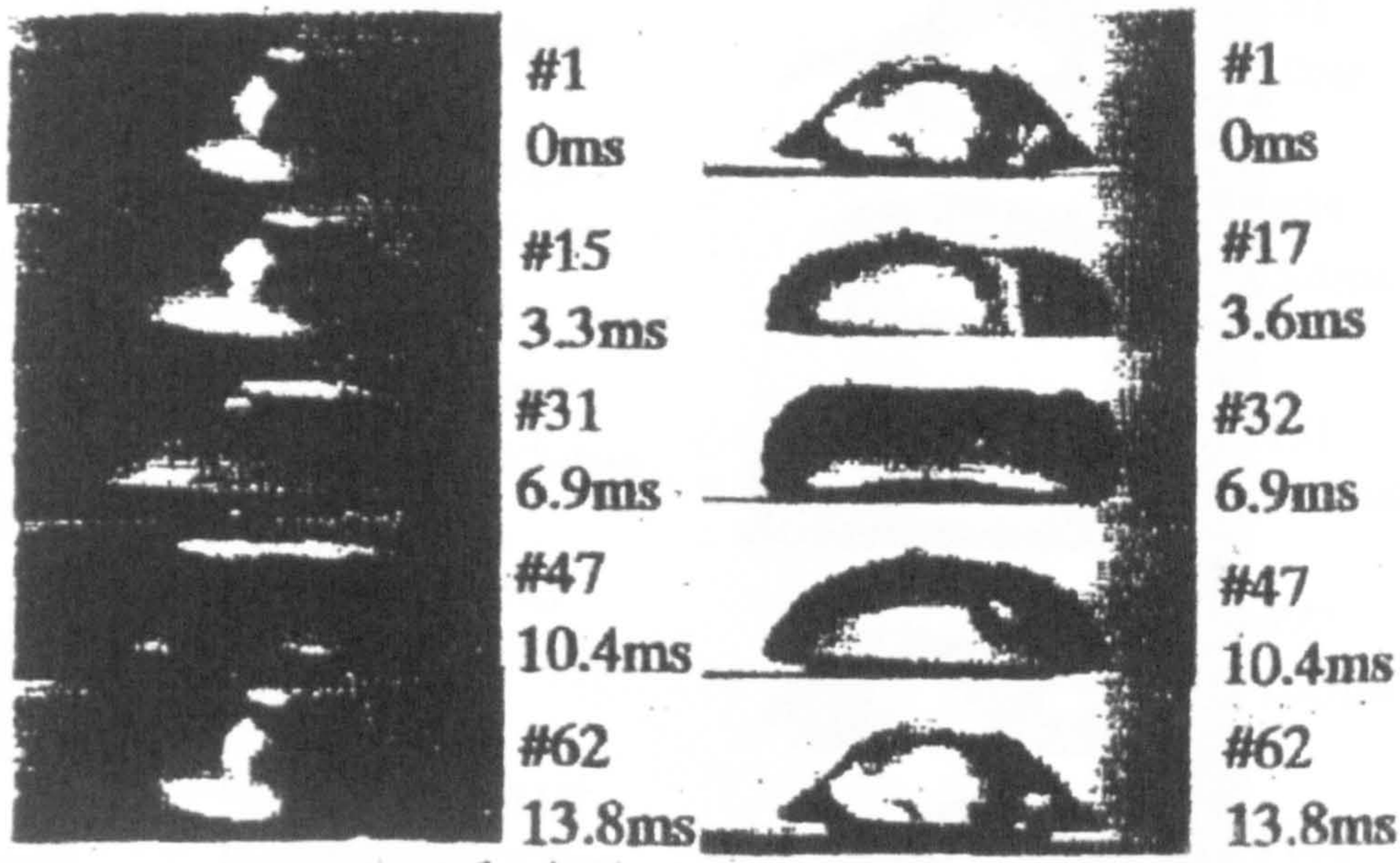

Fig (3.16) Vibration of Water Droplet with a volume 10μl [8]

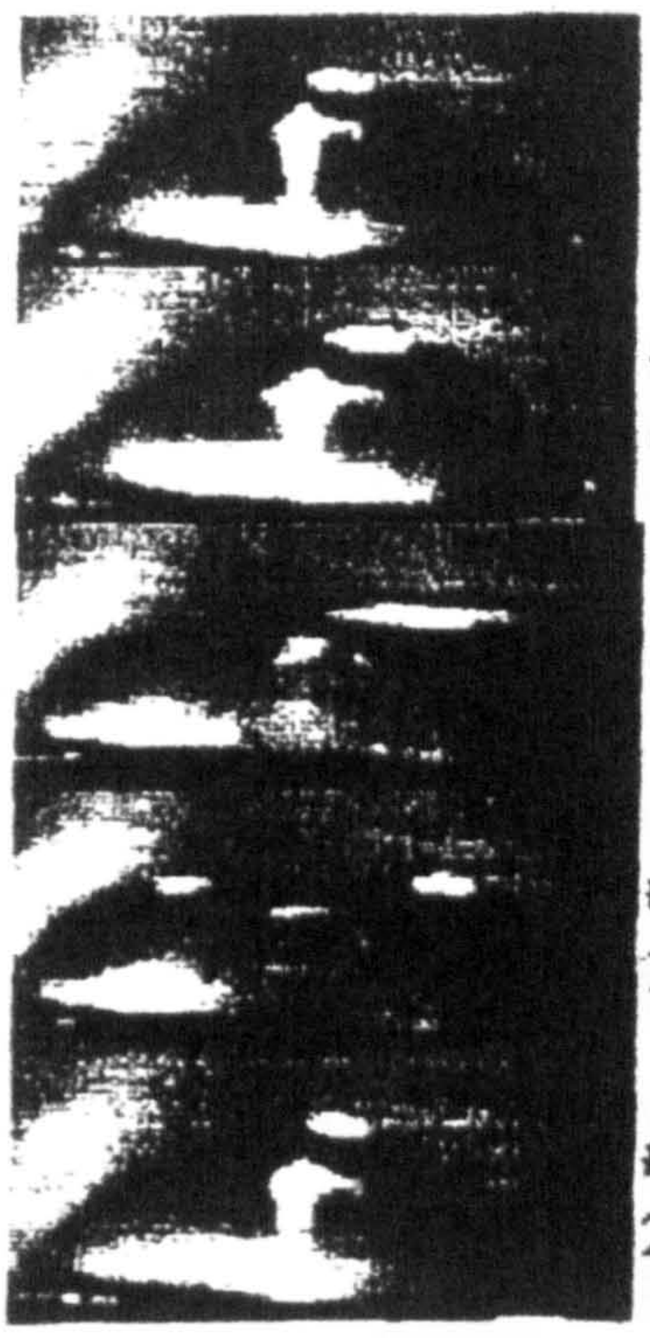

Applied voltage 8.5kV

Frequency 20Hz

(a) PTFE

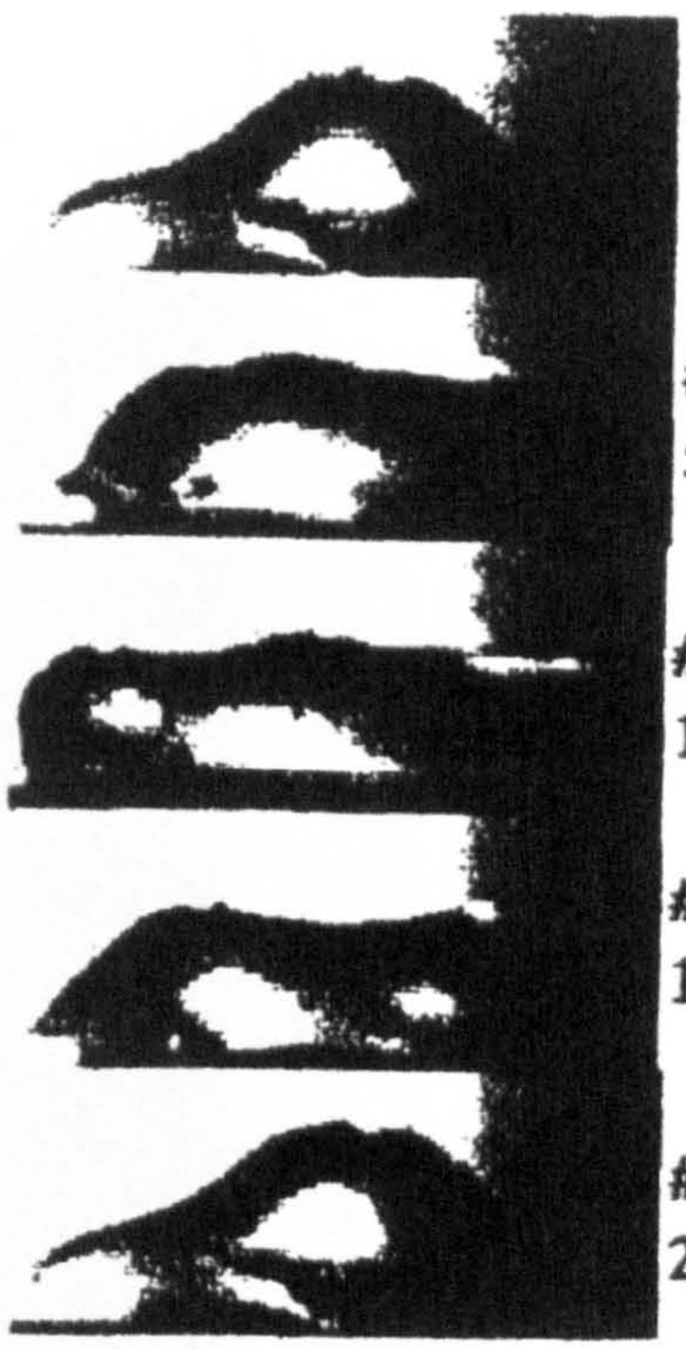

Applied voltage 6.5kV

Frequency 22Hz

(b) SR

Fig (3.17) Vibration of Water Droplet with a volume 30μl [8]

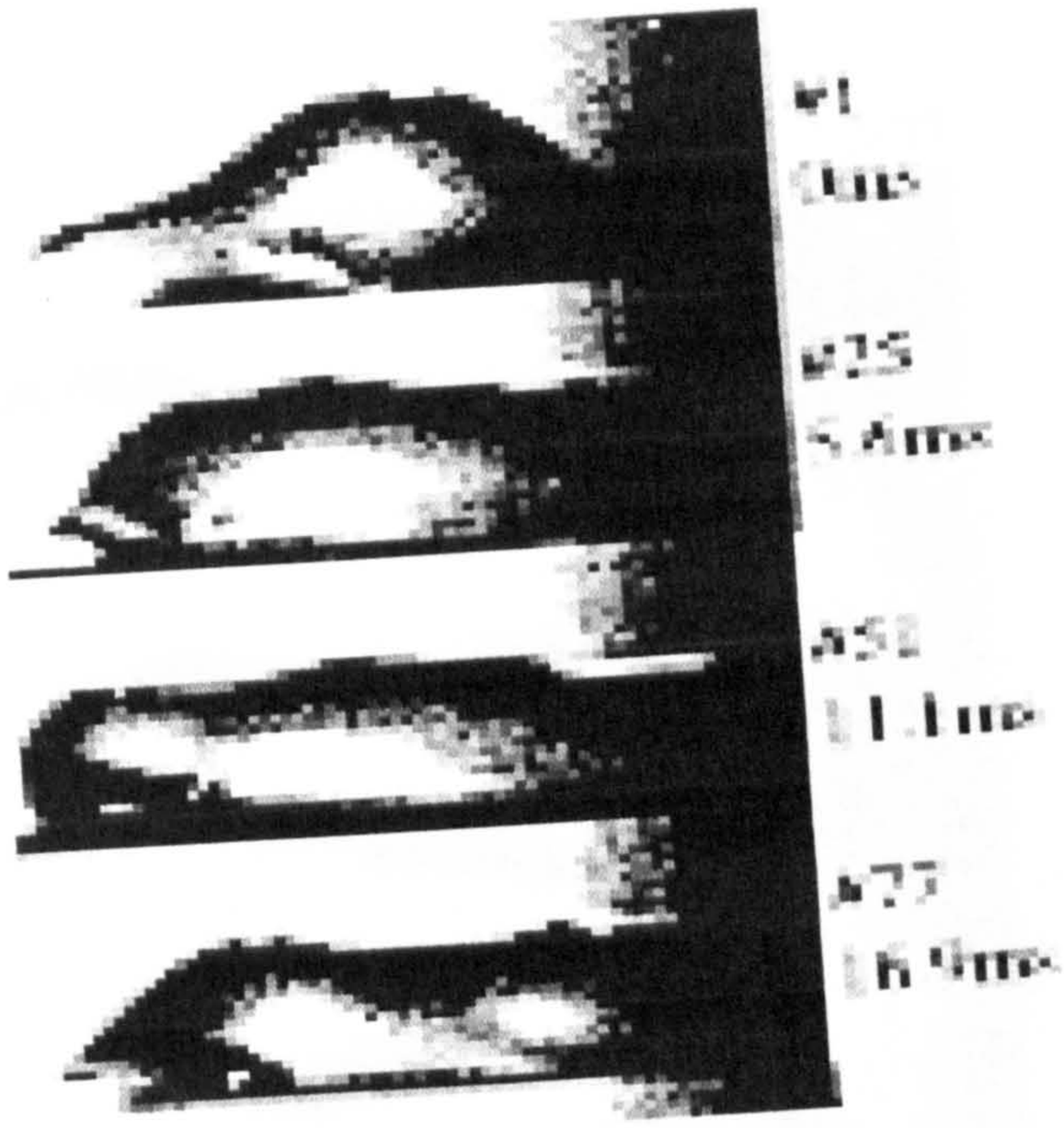

Fig (3.18) Four cases of droplet deformation in a 50-Hz field [14].

Fig (3.19) Deformation of droplet in 50-Hz field on inclined plane [14].

Fig(6.2) Partial Discharge with water droplet over the sample

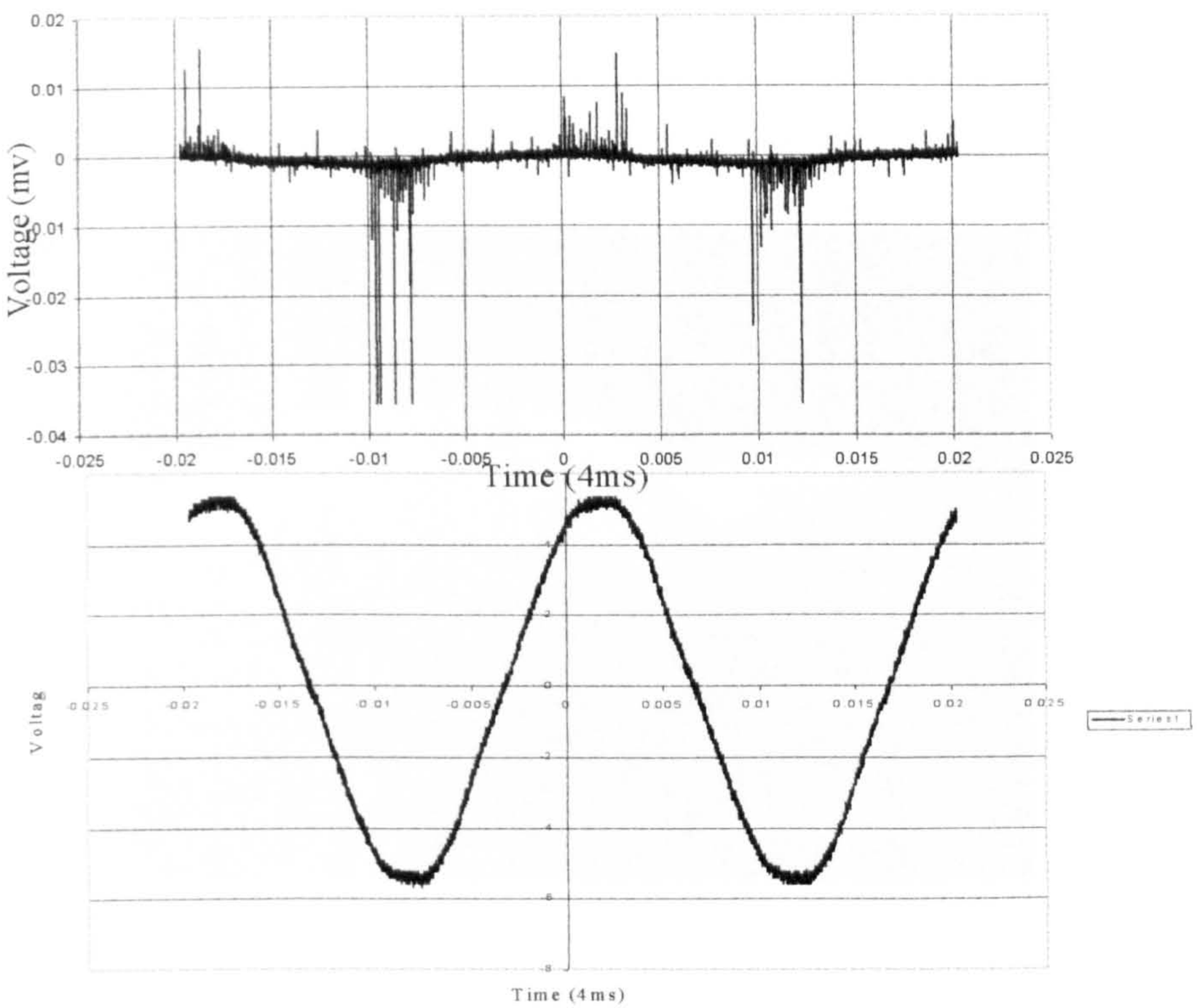

Figure (3.20) Phase resolved Partial Discharge pattern from a dropletmid way between the high-voltage electrodes.

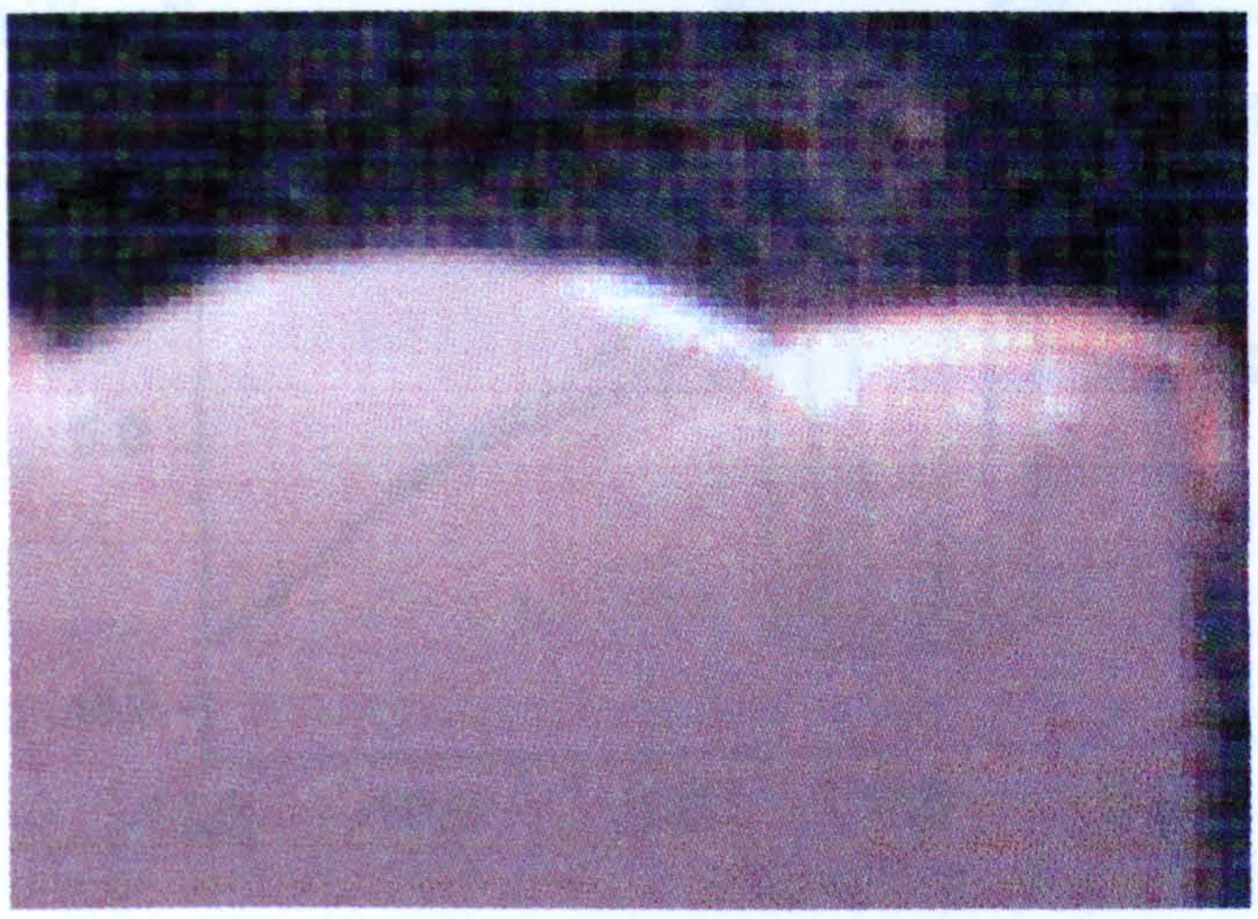

Figure (3.21) Partial discharge at a solid/liquid/gas interface [14].

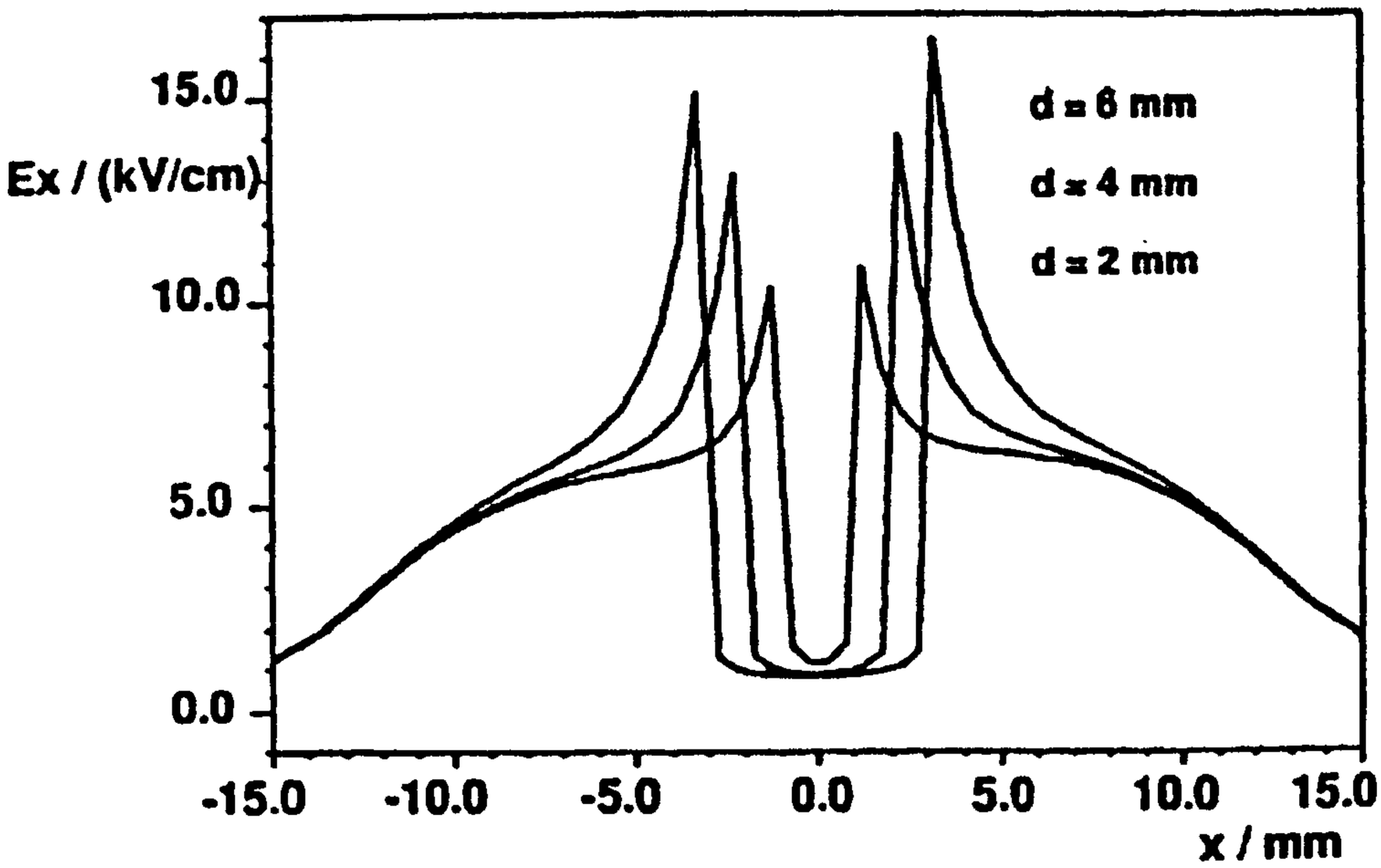

Fig (3.22) Field Strength component E_x on the Epoxy Resin surface in x – direction for three water drops with different diameters.

Basic parameters	Possible variations
Electrical field High voltage	Ac, dc, impulse Amplitude Frequency Waveform Periodic, non-periodic
Liquid	Chemical Dielectric properties Volume of droplet Number and separation of droplets Position in field
Solid	Material type Hydrophobicity Ageing Surface cleanliness Surface Roughness Orientation: horizontal/inclined Flat or curved
Gas	Chemical composition Ambient conditions: temperature, humidity, pressure.

Table 3.1 Parameters likely to influence droplet behaviou

References	P. D. E_{op}	Vibration E_{ov}	Spreading E_{os}	Breakdown E_{ob}
[1], [2]			6.4 to 7.4	7.02 to 8.13
[6]	3.85			
[8]		5.0 to 8.5		11 to 13
[9], [11], [16]	2.67	3 to 5	> 5	>5
[10]	5.5			
[14]			5.75	5.75 to 6.1

Table 3.2 Values of E_{ov} through to E_{ob} calculated from the data presented in references [1], [2], [6], [8], [9], [10], [11], [14] and [16].

Droplet radius (mm)	1	2	3	4	5
Droplet volume (μl)	4.2	33.6	113	269	525
E_c (kVp/cm)	13	8	7	6	5
E_c (kVrms/cm)	9.2	5.6	4.9	4.2	3.5

Table 3.3. Calculated values of electric field to cause gross distortion of a free, spherical droplet (from[1]).

Water type	Deionised	Tap or Rain	Salt solution
Characteristic Conductivity (S/m)	20μ to 1m	5m to 60m	1 to 30

Table 3.4. Typical conductivities used in previous studies

Material	Frequency (Hz)	
	10μl	30μl
PTFE	33, 50	22-25, 35
SiR	30-40	10, 22-25

Table 3.5. Frequency of strong vibration for deionised water droplets with volumes of 10 and 30μl at constant magnitude of applied ac stress.

3.9 References:

1- D. A. Swift, "Ac Flashover Mechanism for Water Droplet on an Hydrophobic Insulator", 8th International Sym. on High Voltage Engineering, paper 44.09, 1993

2- D. A .Swift, "Flashover of an Insulator Surface in Air Due to Polluted Water Droplets", IEEE Proceeding of the 4th International Conference on Properties and Applications of Dielectric Materials July 3-8, pp. 550-553, 1994 Brisbane Australia.

3- H. EL-Kishky and R. S. Gour, " Electric Field Computation on an Insulating Surface with Discrete Water Droplets", IEEE Transaction on dielectrics and Electrical insulation Vol.3 No. 3. pp. 450- 456, June, 1996.

4- H. J. Kloes and D. Koenig, "Basic Investigations of performance of droplets on Electrically Stressed Polymer Surfaces", IEEE Annual report-Conference on Electrical Insulation and Dielectric Phenomena, Minneapolis, October 19-22 pp.374-377, 1997.

5- Y. Mizuno, and M. Iwatani, M. Nagata, K. Natio, K. Kondo and S. Ito," Behavior of Water Droplets on Silicone Rubber Sheet under ac Voltage Application," IEEE Annual report-Conference on Electrical Insulation and Dielectric Phenomena pp. 96-99, 1998.

6- Koji Katada, Yoshikazu Takada, Makoto Takano and Ryosuke Matsuoka," Corona Discharge Characteristics of Water Droplets on Hydrophobic Polymer Insulator Surface," IEEE Proceeding of the 6th International Conference on Properties and Applications of Dielectric Materials June 21-26, pp. 781-784, 1999.

7- S. Keim and D. Koenig," Study of the Behavior of Droplets on Polymer Surface under the Influence of an Applied Electric Field. Annual report-Conference on Electrical Insulation and Dielectric Phenomena, pp. 707-710, 1999.

8- Yoshio Higashiyama, Toshiyuki Yamada and Toshiyuki Sugimoto," Vibration of Water Droplet Located on a Hydrophobic Sheet under the Tangential Ac Field," IEEE Proceeding of the 6th International Conference on Properties and Applications of Dielectric Materials June 21-26, pp. 1825-1830, 1999.

9- Norihiro Arise, Hidehi Nishioka, Yaw Okraku, and Masahisa Otsubo, "Behavior of Water droplet on polymer Material and the Influence on Discharge Characteristics", IEEE Conference on Electrical Insulation and Dielectric Phenomena, pp.455-458, 1999.

10- I. J. S. Lopes, S. H. Jayaram and E. A. Cherney," A Study of Surface Discharge from Water Droplets on Silicone Rubber Insulator," Annual report-Conference on Electrical Insulation and Dielectric Phenomena, pp. 199-202, 2000.

11- M. Otsubo, N. Arise, T. Hashiguchi, Y. Okraku – Yirenkyi, C. Honda, and T. Yamashita," Charge Characteristics of Water Droplet and its Influence on the Discharge Characteristics," Proc. of 13th International Conference on Gas Discharge & Their Application, Vol.2, pp.912-915, 2000.

12- Y. Mizuno, M. Nagata, K. Natio, K. Kondo, S. Ito and Y. Koshino, "Water Droplet Behavior and Discharge Activity on Silicone Rubber Sheet Energized by AC Voltage", Annual report-Conference on Electrical Insulation and Dielectric Phenomena, pp. 624- 627, 2001.

13- S. Keim and D. Koenig, " The Dynamic Behaviour of water Drops in an AC Field", Annual report-Conference on Electrical Insulation and Dielectric Phenomena, pp. 613- 616, 2001.

14- Krivda and D. Birtwhistle, " Breakdown between Water Drops on Wet Polymer Surfaces", IEEE Conference on Electrical Insulation and Dielectric Phenomena, pp. 572- 580, 2001.

15- Sabine Keim and Dieter Koenig, " Recent Studies About Single Droplets on Insulating Surfaces Stressed by Electric Field", International Conference Advances in Processing Testing and Application of Dielectric Materials pp.92-95, 2001.

16- Yamashita-S; Hashiguchi-T; Anamil-N; Otsubo-M; Honda-C; Takenouchi-O; Hashimoto-Y; Nakamura-M "Behavior of water droplets and their charged distribution on polymer surface" 33rd Symposium on Electrical and Electronic Insulating Materials and Applications in Systems 2001.

16- G.M.Barrow, "Physical Chemistry – 5th Ed", ISBN 0-07-003905-4, McGraw Hill, 1988

Chapter 4

The Aim of the Present Work

4.1 General

As previously explained, pollution phenomena constitute a serious problem, which must be taken into account in the design, dimensioning and operation of HV insulating structures. The presence of quasi-free water droplets on high voltage insulation surfaces has long been recognized as an important area within this general problem – although the work on the relatively new polymeric insulators, which have strongly hydrophobic surfaces, has not yet been as extensive as that on the more established glass or ceramic insulators.

In the previous chapter, we reviewed recent research on the behaviour of water droplets on hydrophobic polymer surfaces under high electrical stress, and examined the role played by droplets in partial discharge activity and surface flashover, and in the changes in the hydrophobic and other properties of the polymer surface associated with such discharges. From this review, general areas of potential future research were identified. The purpose of the present chapter is to describe the specific research aims that were identified at the outset of the present programme.

4.2 Areas of Interest

It is evident that several factors influence the effect of even a single water droplet on the surface of a polymer insulator. Clearly, the formation of partial discharges around the periphery of a water drop depends to a large degree on the local geometry of the electric field around the drop and at the surface of the polymer. This local geometry is determined by a number of factors: the form of the applied field; the dimensions and shape of the droplet, including its instantaneous shape as it vibrates; the conductivity of the water; the tendency of the polymer surface to lose hydrophobicity with exposure to electrical discharges.

The applied electric field on the surface of the polymer is considerably enhanced locally on the surface close to the triple junction. Clearly, this increases the probability of initiating electrical discharges there. However, there is some recent strong visual evidence – particularly the work described in reference [14] of chapter 3 and published in 2001 - that partial discharges may not necessarily occur only on the surface itself but may be located above the surface in the air between it and the side of the water droplet. If these discharges do not affect the polymer surface in immediate contact with the droplet, then spreading of the droplet due to loss of surface hydrophobicity will be affected.

In the light of this, the decision made at the outset of the present programme is to undertake a programme of research into the behaviour of water droplets on polymer surfaces that is designed to allow the location of such discharges to be investigated.

Experimental studies of water droplets on polymer surfaces under high ac stress have not previously been undertaken at Strathclyde and so the initial requirements are to develop suitable techniques for preparation of polymeric test surfaces with specified water droplets, to design and construct suitable high-voltage experimental apparatus with which to generate the required behaviour and discharges, and to devise suitable electronic and optical apparatus with which to record and measure this droplet behaviour.

It is anticipated that this experimental programme will provide new information about discharge activity at the edge of water droplets and on how this might affect the insulator surface there. In particular it is considered that this study might shed light on how discharges lower the hydrophobicity of the polymer in the vicinity of the droplet, so leading to changes in its shape that affect the local electric field and, in turn, the discharges themselves. In this context, the question of discharge location is of clear interest

Previous researchers have used three types of electrode geometry: end, surface and embedded. The uniform-field end-electrode geometry produces an electric field

tangential to the polymer surface and the embedded electrode can be used to generate a strong component normal to the surface near the periphery of the droplet. These two geometries are selected on the assumption that the absence or presence of normal components of applied field is likely to influence droplet vibration and the location of partial discharges. Surface-mounted electrodes are not considered to add any useful additional features.

Clearly, it was necessary to have quantitative information on the applied field around water droplets, and so a further aim of the programme is to examine the use computer modelling to determine the potential and electric field distributions around the droplets. This can be used to determine how static or distorted droplet shapes affect the local field and to provide quantitative data with which to investigate the applicability of the steamer breakdown criterion to the question of onset of partial discharges.

4.3 Specific Objectives

The specific objectives can be summarised as:

1. To develop suitable means of preparing specified water droplets on polymer samples.
2. To construct an HV ac test system, capable of generating:
   (a) discharges at the edges of water droplets on a polymer surface in atmospheric air
   and
   (b) droplet vibration and spreading.
3. To devise apparatus capable of electrically detecting discharge activity at the edge of a sessile water droplet.
3. To develop suitable high-speed camera techniques with which to record vibration, spreading and discharge activity at water droplets on a polymer surface.
4. To determine suitable field modelling techniques with which to investigate the electric fields around a droplet.
5. To investigate the location of partial discharge activity at the edges of a droplet.

The whole programme is conducted within the context of how these processes are important in understanding how surface pollution of HV insulators influences their effective operation when exposed to a combination of hostile environmental conditions and high electrical stress.

Chapter 5

Experimental apparatus and procedure

5.1 General

From previous chapters, the factors that are important for water-drop behaviour on insulators surfaces stressed with ac fields have been identified. These factors are interdependent and the most significant are: magnitude and frequency of applied stress; insulator surface properties, in particular hydrophobicity; contact angle and triple junction point; drop volume and shape; water conductivity; partial discharge location. It was also seen that it might improve our understanding of the overall breakdown mechanisms if the onset of the formation of partial discharges and their location at the surface of sessile water droplets could be more clearly related to the applied field at these locations.

The design, and operation of experimental apparatus with which to examine such questions is described below, as is software that could be used to determine the electric potential distribution and electric field around droplets.

5.2 General Arrangement

Clearly, the proposed research requires the generation of high ac voltages and, following a Risk Assessment, it was concluded that it was essential to contain all the high voltage apparatus in a fully-interlocked safety cage. Figure (5.1) shows the general arrangement adopted in the laboratory.

5.3 The High Voltage System

From table 3.2, the HV system must be capable of generating an electric field that is continuously variable up to 20kV/cm at 50Hz. As the proposed research was to examine the behaviour of single droplets of typically a few tens of μl –i.e. around 2 mm in diameter, it was decided at an early stage to assume a polymer sample length of

10mm. Consequently, an HV supply was required to generate voltages between 0 and 20kV.

The maximum discharge currents reported in the literature were less than 0.5mA and so it was decided that an HV supply capable of supplying a few tens of mA would be appropriate for investigation of partial discharges. Also, this limited current was considered to offer safety advantages.

5.3.1 The HV supply

A 0 to 230V ac variable transformer (variac) was connected to the primary of a 230/20kV, 2.8KVA, 50Hz (Admiralty Pattern W. 193) transformer which had rated primary and secondary currents of 12.2A and 0.14A, respectively. The HV transformer thus had a ratio of approximately 87. The variac was mounted outside the safety cage. It could be controlled manually, or driven by stepper motor, so that the HV delivered to test samples could be adjusted to required value. With steps taken to limit the secondary current to 20mA (as described below) and with a transformer ratio of 87, the primary current would not exceed 1.8A. It was decided that further protection would be obtained by including a fast-blow fuse rated at 1.0A in the circuit formed by the primary winding of the transformer and the variac.

The HV transformer itself was not rated as partial discharge free but, before conducting any experimental work, the complete HV system was tested for inherent partial discharges and its performance in this regard was found to be satisfactory, as will be described in more detail below.

5.3.2 Current limiting resistor

To limit the current drawn on the secondary side to maximum of 20mA at 20kV, required a 1-MΩ resistor to be inserted in the secondary circuit of the HV transformer in series with any test sample. As mentioned above, it was expected that partial discharge activity in the test samples would generate currents less than 1mA. However, if flashover of the sample occurred, the sample would effectively be short-circuited. It was therefore necessary to construct a current limiting resistor rated for 20kV at 20mA.

Consequently, the resistor was required to dissipate 400W. The design finally adopted consisted of 46 wire-wound resistors connected in series, each having nominal resistance of 22kΩ, voltage rating of 500V and power dissipation of 9.0W. The limiting resistor thus matched the required specification with a nominal total resistance of 46x22kΩ = 1.012MΩ, a voltage rating of 46x500V = 23kV and a power dissipation rated at 46x9W = 414W.

5.3.3 High voltage probe

In order to measure the voltage across the test sample, a high voltage probe was connected between the HV side of the sample and ground. This had an input resistance of 1000MΩ, a voltage division ratio of 1000:1 ± 2% (into10MΩ), a working voltage of 50kV dc or 50kV ac peak, a frequency range up to 300Hz and an operating temperature of 0°C to +50°C. A digital multimeter (Type 3225, Black Star, UK) was used to measure the output of the probe. With this arrangement, the voltage applied to the sample could be measured to an accuracy of ± 2%.

5.4 Oscilloscope

A Tektronix TDS 3032, 300Mhz, two-channel digital oscilloscope was used to display the applied voltage waveform and simultaneously record any partial discharge activity that might be generated in the test sample (see below). This oscilloscope has input impedance of 10MΩ ± 1% in parallel with 13pF± 2pF. The data captured on the two channels could be stored electronically on disk.

5.5 Test Sample Arrangements

As noted in chapter 3, some particular polymers commonly used for HV insulators - such as silicone rubber, polytetrafluorethylene and epoxy resins - have been the subject of studies by previous workers. However, the essential requirement for the present study is a polymer that is a good insulator, has good surface hydrophobicity, is easily formed into suitable samples and is readily available. As a result, ot was decided to employ a well-characterised polyethylene (PE) as a suitable test material. Although PE is not commonly used for HV line insulators, it is used in a number of high-voltage

applications including the outer casing of surge diverters used on overhead lines and high-voltage power cables.

PE is produced in a wide variety of compositions. Because of its easy availability the form selected for use in this study was high-density Cestilene HD1000 as this has very high impact strength, good abrasive wear resistance and was available in sheet and rod forms produced with a high-quality surface finish. This HDPE has a natural translucent white colour, a continuous working temperature of 60°C and is not sensitive to ambient levels of chemical or UV light exposure. This latter characteristic is particularly desirable in the present study where stability to ambient levels should allow the effects of exposure to the raised the levels of UV associated with electrical discharges to be distinguished (see sections 1.6 and 2.2). The electrical resistivity this HDPE may be taken as $10^{13}\,\Omega$/m and it's permittivity as 2.35. To confirm its suitability, a water droplet was deposited a horizontal surface of this HDPE. This is shown in Fig (5.2) where it can be seen that the droplet took an approximately spherical shape with a contact angle close to 90°. This compares well with the droplet shapes discussed previously in chapter 3.

5.5.1 The insulation sample

Test samples were prepared in the departmental workshop by cutting 10-mm lengths of polymer from the 20-mm diameter rods supplied by the manufacturer. In some experiments, the outer cylindrical surface of these rods was used as the test surface. This surface was washed in tap water and allowed to dry in air but otherwise it was as supplied from the manufacturing process. In other experiments, a flat surface was machined along one side of the rod-shaped samples. This machined surface was then treated by being placed on polished glass plate that was heated to 80°C for a period of 30 minutes and then allowed to cool naturally to room temperature. This produced a flat, even finish to the machined surface.

These samples were used in conjunction with two different electrode geometries.

5.5.2 End - electrode geometry

See figure (5.3). This model provided was adopted to provide an essentially uniform-field in which to examine experimentally and theoretically the behaviour of water droplets such as the onset of vibration, spreading or partial discharge activity. The significant feature of this geometry is that it produces an applied electric field that is essentially directed along (i.e. tangential to) the surface of the insulation sample under test and uniformly distributed along the surface, in absence of a water droplet. As previously described in chapter 3 (see table 3.2), the values of the average applied surface electric field sufficient to promote the onset vibration, spreading or partial discharge activity all lie below 20kV/cm. With the 20kV supply described above, sample lengths of 1.0cm would generate this field. This length would also allow suitable water droplets of a few mm diameter to be located between the electrodes.

The electrodes and electrode supports. Two circular, 20-mm diameter, "uniform field" electrodes were machined from stainless steel. One electrode was connected via the current limiting resistor to the high voltage winding of the transformer. The other electrode was connected to ground through a small impedance that was used to detect discharges (see below). The electrodes were mounted between supports made from PVC and which were moveable, so that the samples of PE could be clamped between the two electrodes.

It was recognized that such an arrangement would itself be liable to produce partial discharges at the sample/air/electrode interfaces and preliminary tests to determine this activity would be required. However, it was anticipated that activity would most evident around water droplets and that activity there would be clearly distinguishable from other sources.

The complete electrode and support arrangement was mounted inside an aluminum case with a small viewing port. This was a precaution considered necessary to protect the high-speed digital camera employed (see below, section 5.6) from possible damage from the sudden flashover of the test sample that was to be expected during the experimental procedure.

5.5.3 Embedded – electrode geometry

From chapter 3 it may be inferred that partial discharge development around a water droplet or the onset and development of droplet vibration could well be influenced by a significant normal component of the applied electric field. The essential feature of the embedded-electrode geometry is that it can generate fields at the central region of the sample surface that can have comparable tangential and normal components. Hence, it was decided to employ this type of electrode geometry in some experiments. The geometry adopted is shown in Figure (5.4). Compared to the end-electrode arrangement, the embedded arrangement has the drawback that it is more time-consuming to prepare and replace fresh samples if, for example, a sample becomes damaged through exposure to discharges.

Following preliminary studies, a second embedded arrangement was developed which was easier to manufacture and to replace following exposure to discharges. This is shown in Figure (5.5). For this second embedded arrangement, rod electrodes of 10-mm diameter were inserted through "push-fit" holes drilled at each end of the sample at right angles to the sample axis. The electrodes were located at a depth of 2 mm below the test surface and were separated by a gap of 10mm.

A finite element program (Quickfield®) was used to model the shape of the electric fields generated in each of the above sample and electrode geometries.

5.6 Partial Discharge Detection

Two types of partial discharge detector were proposed to investigate the partial discharge activity electrically. A "non-contact" antenna system using UHF signals which was under development at Strathclyde. The essential features of this are summarized below and are fully described in reference [1].

5.6.1 Antenna type

This partial discharge detection system (known as a Monopole Transfer Function Model) consisted monopole probe acting as a receiving antenna. The antenna is connected by UHF cable (RG 58, 50Ω) to the input amplifier of the digital

oscilloscope (see section 5.4). In the frequency domain, the transfer function of the probe in this configuration can be expressed as [1]

$$H = \frac{V_L}{E_I} = \frac{h_e Z_L}{Z + Z_L}$$

where E_I is the incident electric field normal to the ground plane and V_L is the output voltage into the load impedance, Z_L. The probe's effective height h_e and impedance Z are both frequency dependent functions of its dimensions. The monopole used in these experiments was constructed from a readily-available SMA connector with a centre pin of radius r = 0.65mm. The probe length h = 25mm was selected to avoid any resonances below 2GHz. Using these dimensions, Z and h_e can be obtained from values for the corresponding dipole [2] because the ground plane of the monopole forms a plane of symmetry between the probe and its image. The effective half-length of the dipole then becomes the effective height of the monopole, while the monopole's impedance is half that of the corresponding dipole.

5.6.2 Series resistor type

As shown in Fig (5.6), this very simple partial discharge detection arrangement consisted of a resistor connected between the low-voltage electrode and ground. A value of 90 Ω was adopted. The signal developed across this resistor was fed via a short length of coaxial cable of the same impedance and detected using the digital oscilloscope. To protect the oscilloscope against overvoltage surges that might be generated by inadvertent breakdown of a test sample, a Siemens gas discharge tube type A81 C90x with voltage 90V and peak current 20 kA was connected in parallel with the detection resistor. It was considered that this simple detection system would be appropriate to monitor the occurrence and location on the ac cycle of the established partial discharge activity expected during the time when a water droplet was showing visible signs of vibration and spreading.

5.7 High-speed Camera

A high-speed digital camera was used to investigate the behaviour of water droplets on the surface of stressed insulation samples. This was expected to record the

mechanical vibration of droplets, the location of partial discharge development at droplet edges and the eventual surface flashover. As described in chapter 3, droplet vibration would be expected to be at the frequency of the applied voltage or, possibly, at double this frequency. At 100Hz, one cycle takes 10ms. If it is assumed that droplet vibration can be reasonably observed by recording at least 10 frames during this 10ms period, a frame rate of at least 1,000 frames per second would be required. To distinguish clearly between 50Hz and 100Hz a frame rate of 3 or 4 times this would be desirable.

The camera used was a Photron Fastcam Super 10k series, which can take up to 20,000 frames per second [4]. This camera was interfaced to a 750 MHz PC via a standard SCSI interface (see below). Frames were downloaded for real-time viewing and capture and sequences of frames were stored on compact disc. The main camera features used in the present study are described below.

Trigger signal Two modes of the trigger signal were available: **TTL** in which the camera accepted a TTL-compatible signal to start or end a recording and which could be used to trigger the camera from an external source (for example, in the present study it was expected that suitable signals could be generated from the PD detection systems); **Manual** in which case, the start of recording was directly activated by the individual conducting the experiment.

SCSI Card System This is the widely–used Small Computer System Interface. This interface utilizes standard protocol commands to provide a data path for digital video downloads between camera and PC. The SCSI Card used in the present study was an ISA SCSI Adaptor (Adaptec 1510).

The Video Output

The video output is designed to drive a 75 Ω coaxial cable connected to a video monitor.

The sample illumination System

The system adopted consisted of two 12-V AC spot lights, each rated at 50 W. This was found to provide a satisfactory degree of illumination with which to record frames. It could be focused onto the sample until the movement of the water droplet could be detected and recorded clearly. The system allowed control the angle of the light incident on a water droplet placed on the PE sample. With the camera on the same plane as the sample, it was found that optimum illumination was obtained by placing the light source directly above the camera with its beam directed at the droplet and set at an angle of between 55° and 60° to the plane of the sample

Preparation of camera prior to recording

At power on, the camera performed a self-check routine and then automatically entered live mode. This mode was used to initially adjust the focus and lighting system for best results.

Before recording, one of the three available trigger modes was selected. namely, start mode, centre mode or end mode. In start mode, the camera is ready to record images until every frame in memory has been filled and then stops the recording automatically, when the memory is full. In center mode, the camera records an equal number of frames before and after the trigger signal input. The frames numbered before and after the trigger were equally placed in the memory of the camera. By triggering on partial discharge activity, this mode was frequently used to observe the behaviour of the droplets before and after the action of such discharges. With end mode, the camera stops recording the instant the trigger signal is received. The video stored in the memory will contain images covering events up the time when the trigger signal was received. This mode was used to capture activity prior to the occurrence of surface discharges.

The frame rate must be selected as noted above. A further constraint was that the dimensions of the image recorded reduces with increase in the selected frame rate. It was found that with frame rates over 5000 frame/second up to 20000 frame/second the size of images displayed on the video monitor was relatively small and weakly illuminated, although the number of frames stored in the memory was high. At frames rates below 1000 frames/second, the video image was bigger and well-illuminated.

However, the smaller number of frames then recorded in memory were normally insufficient to allow convenient use of trigger center mode. After considerable experimentation, it was determined that the optimum frame rate for most of the experiments intended in the present project would be around 3000 frame/second. With this, the number of frames recorded in the memory was 8,736. At this frame rate, the available combination of picture size, illumination requirements and number of frames recorded in memory was particularly suited to the present study.

It was proposed that the frequency of water vibration could be determined from the number of frames required for the water droplet to undergo a vibration and return back to its original shape. In the present work, the frequency of the applied voltage was 50Hz, which corresponds to a cycle lasting approximately 20 ms. For 3,000 frames/ second the time for one frame is ~0.33 ms – that is, the number of frames in one cycle equals 6 or 7. It was assumed that if a water droplet required 6 or 7 frames to vibrate before returning back to its original shape, the frequency of vibration would be equal to the frequency of the applied voltage. However, if the number of frames equaled 3 or 4, then the frequency of vibration might be closer to 100Hz . From tests conducted at 500, 1,000, 2,000 and 5,000 frames/second it was concluded that 3,000 frames/second was the best frame rate with which to record the vibration of the water droplets.

5.8 Water Droplet Properties

Three general "grades" of water were used in the experimental work: Deionized, Tap and Salt. The conductivities were as shown below.

Water Type	Conductivity
Deionised	300μS/cm
Tap	100μS/cm
Salt	to ~ 10 S/m

Each "grade" was assumed to have a relative permittivity of 81. The conductivities of were chosen to compare with those employed in the previous studies decribed in chapter 3. From chapter 3 it is worth noting again that it was reported that

conductivity itself had little or no effect on droplet contact angle, with a horizontal plane PE sample. However, it was to be expected that the above range of conductivities should show a significant effect on vibration, spreading, partial discharge activity and surface flashover. In nearly all experiments, the water droplet volume was 10μl measured using a precision syringe with a rated accuracy of ± 0.5μl. Static contact angle is not sensitive to volumes in this range [5]. The droplet was normally placed manually at the center point between the two electrodes. It was estimated that this could be done to an accuracy of ± 0.5mm.

5.9 Typical Experimental Run

After setting up the PE sample and placing the water droplet, the safety cage was closed. The sample was then illuminated and the camera checked for focus, frame rate setting and image brightness. The applied AC voltage was then slowly increased either manually or by stepper motor. The oscilloscope monitored for evidence of partial discharge activity. Depending on the particular objective of the run, the appropriate camera trigger mode was selected. Manual triggering was generally used to record droplet behaviour prior to the onset of partial discharges. When recording behaviour in the presence of partial discharges, start or center triggering was generally used. If the voltage was raised to bring about surface flashover, then end mode was found to be most appropriate. The images held in the camera memory were then downloaded to the PC and viewed for content. In some experiments, simultaneous partial discharge pulse records were stored on the digital oscilloscope. A run lasted typically less than 30 minutes. It was considered that the water droplet was not significantly exposed to environmental variations during such a short period and would not undergo significant evaporation. After completion of the run, the voltage was removed and the sample inspected for visible surface changes.

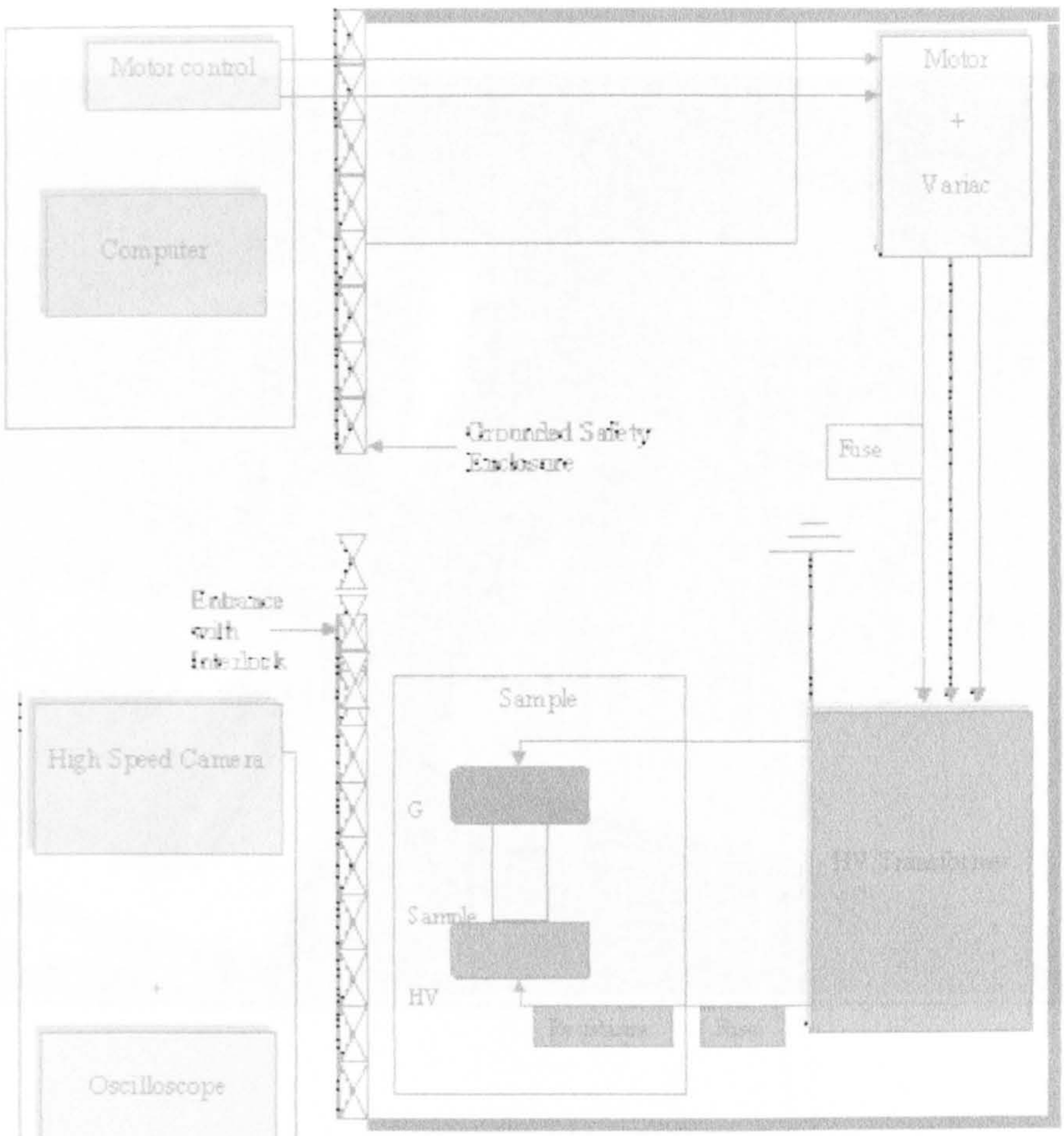

Figure 5.1A Illustrating the general plan of the laboratory and the location of the HV equipment within the safety cage.

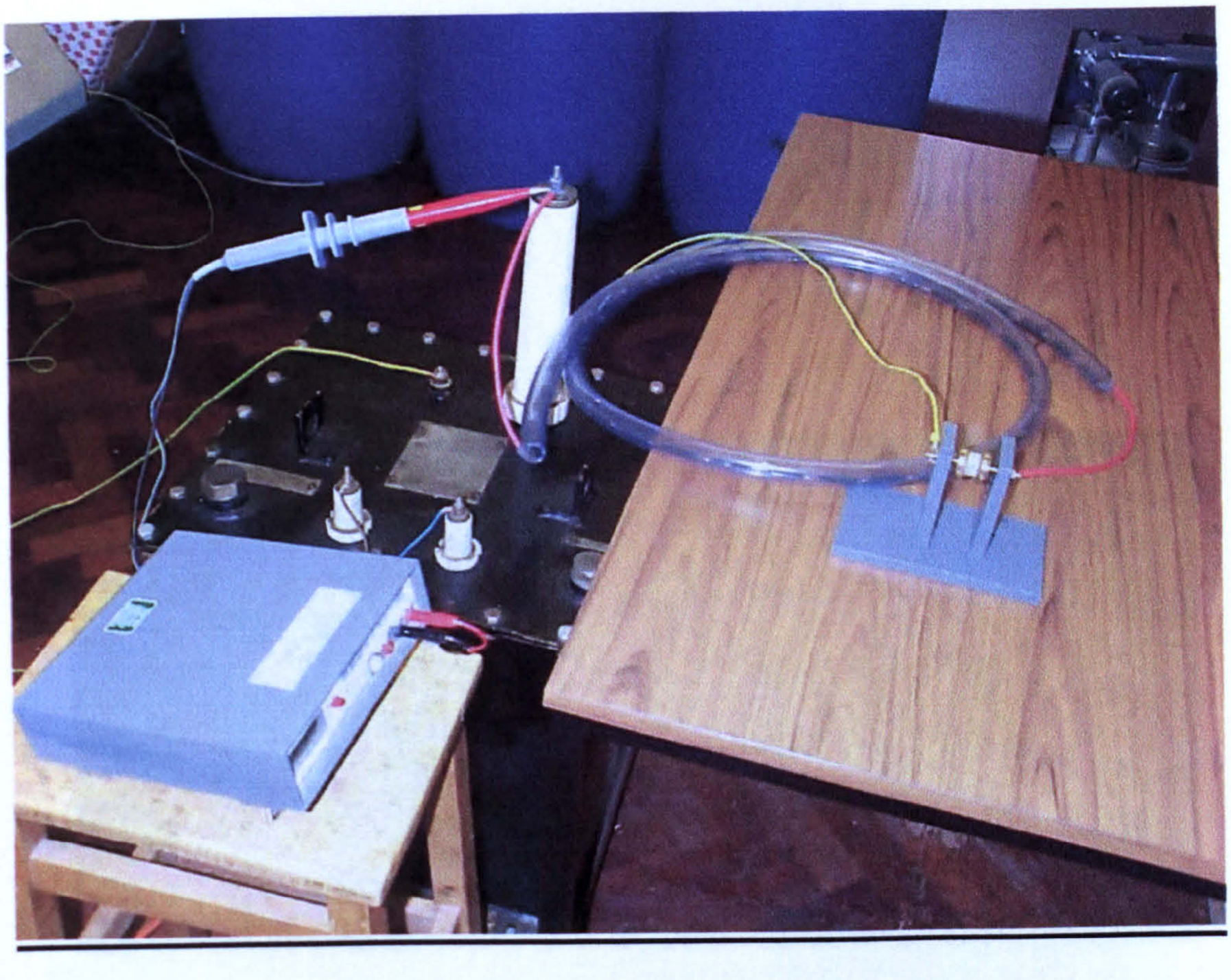

Figure 5.1B Illustrating the HV transformer, AC measuring probe and associated circuitry.

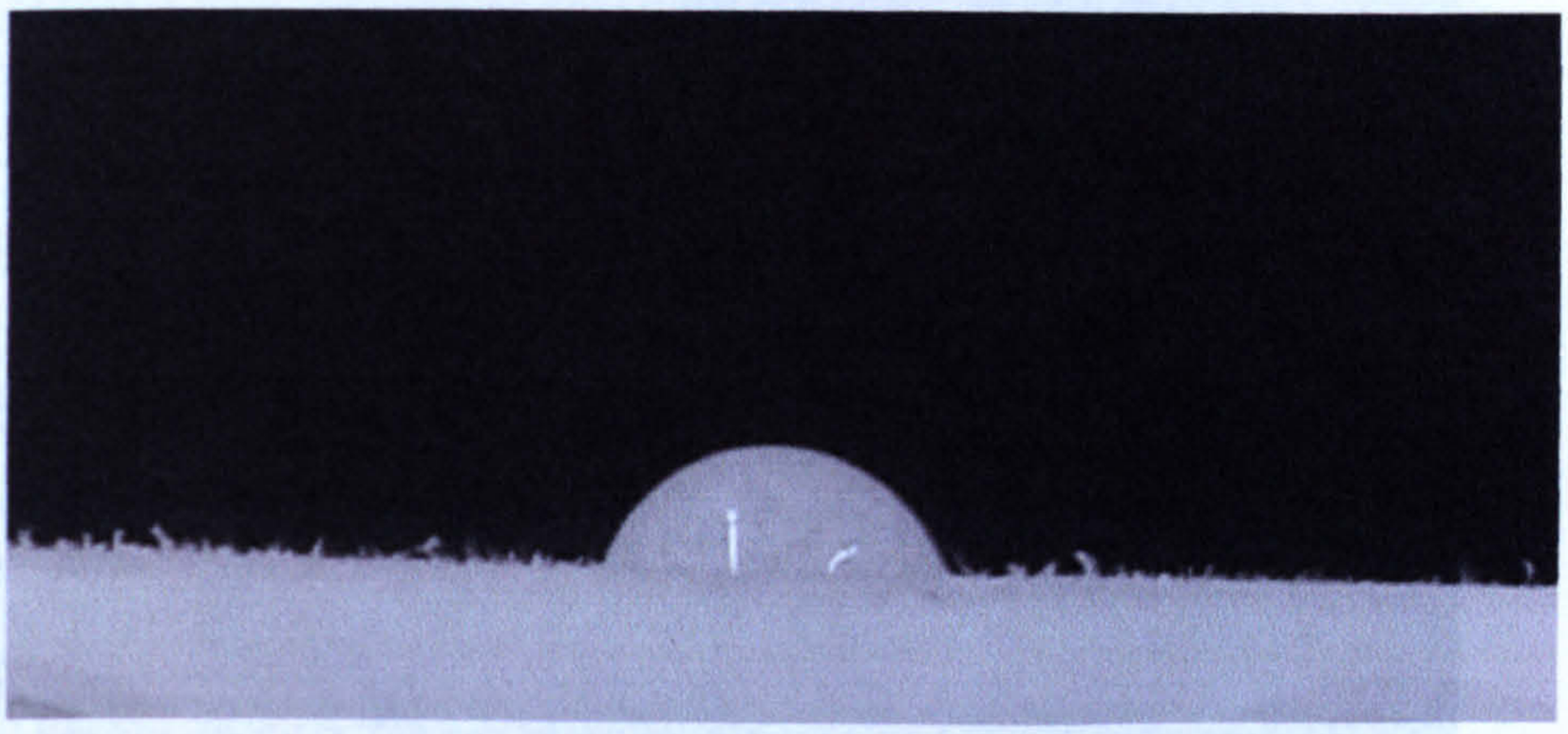

Figure 5.2. Approximately spherical droplet formed on a horizontal surface.

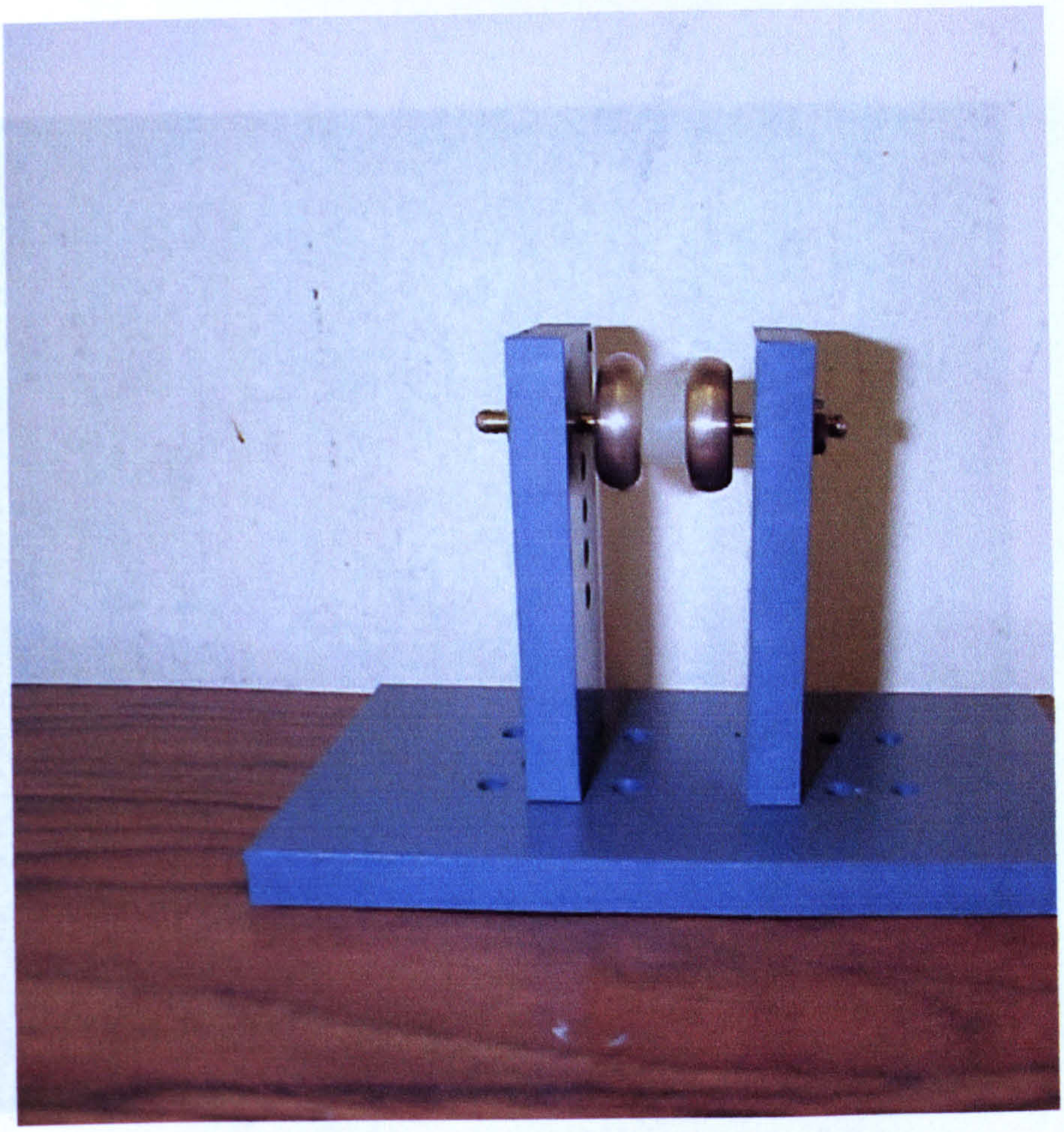

Figure 5.3. End electrode geometry

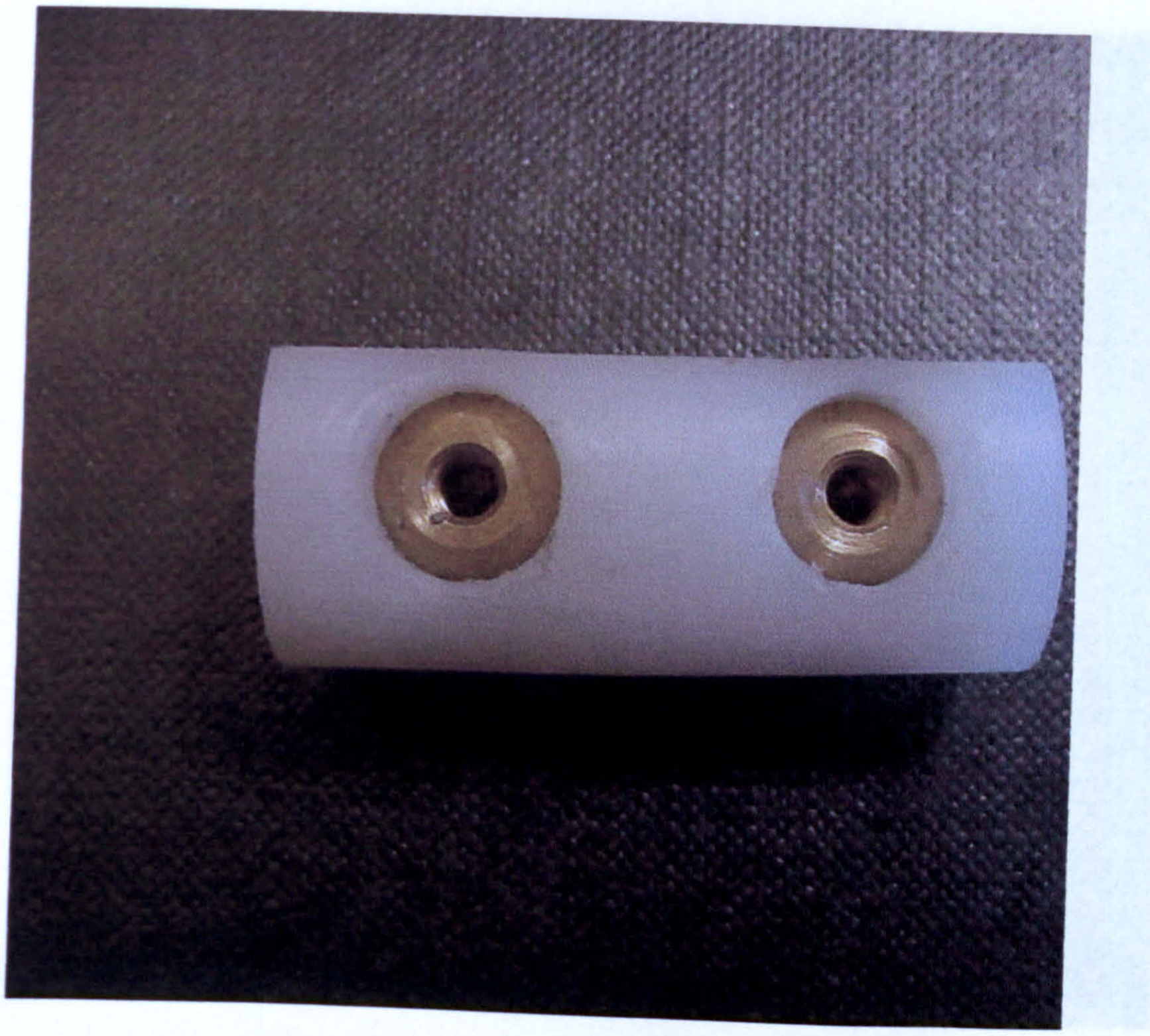

Figure 5.4. Embedded electrode – geometry 1

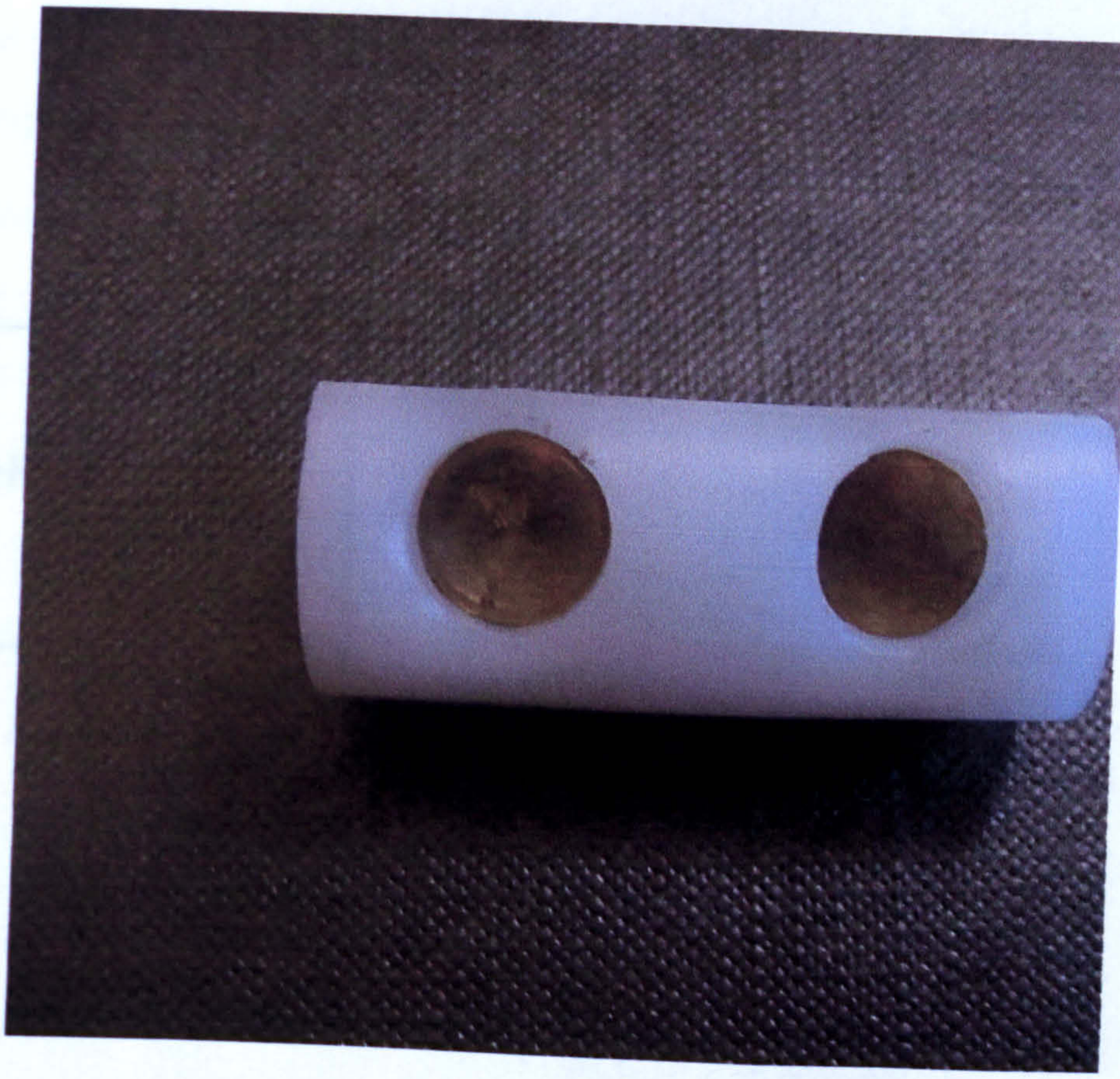

Figure 5.5 Embedded electrode - geometry 2

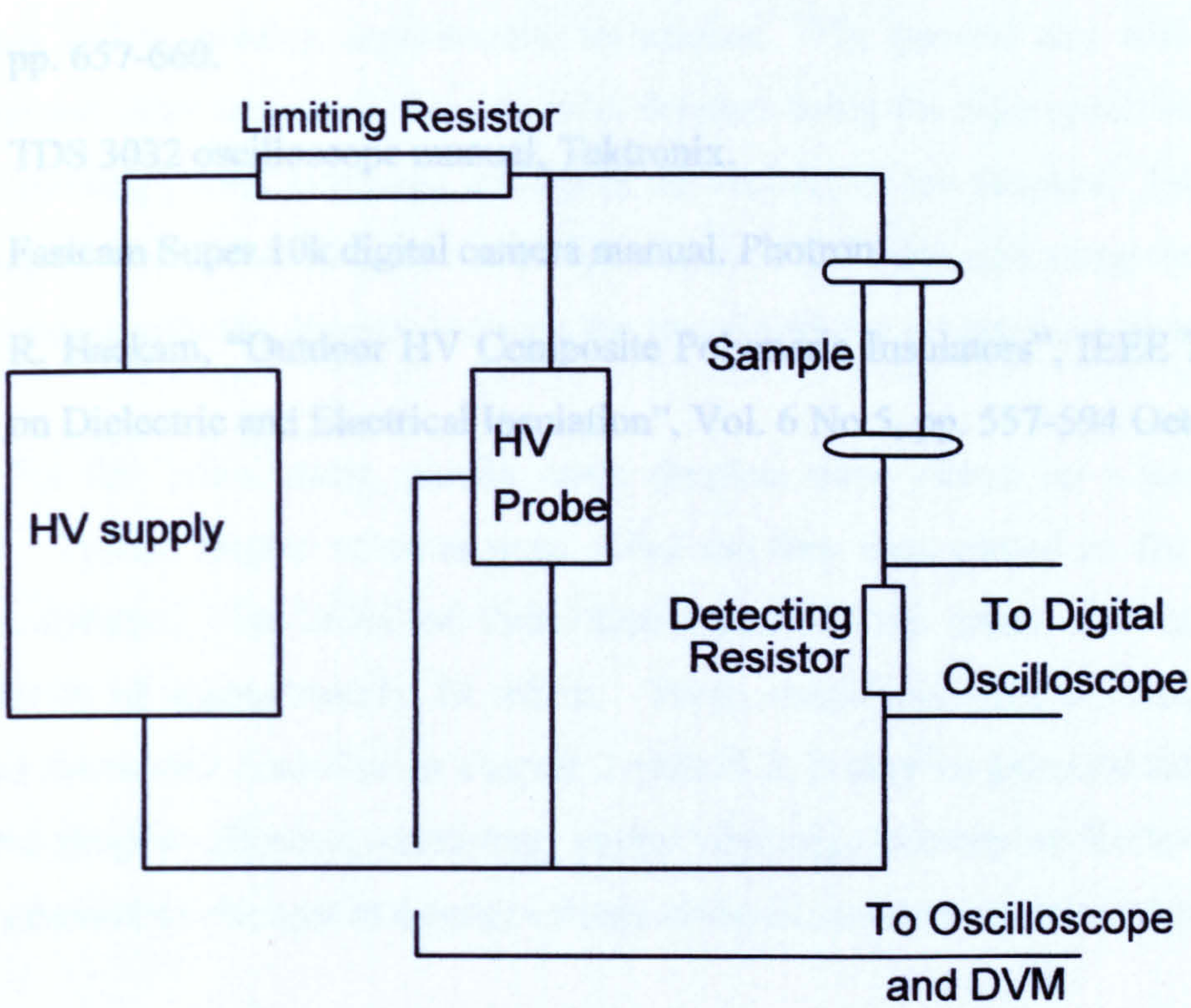

Figure 5.6. Resistor PD detection arrangement.

5.9 References

1- M. D. Judd,' Transient Calibration of Electric Field Sensors,' IEE, 1999.

2- C W Harrison, " The radian effective half-length of cylindrical antennas less than 1.3 wavelengths long" IEEE Trans. Antennas Propagation 1963 AP-11, (6), pp. 657-660.

3- TDS 3032 oscilloscope manual, Tektronix.

4- Fastcam Super 10k digital camera manual. Photron.

5- R. Hackam, "Outdoor HV Composite Polymeric Insulators", IEEE Transaction on Dielectric and Electrical Insulation", Vol. 6 No.5, pp. 557-594 October 1999.

Chapter 6

Initial Experimental Studies

6.1 General

Initial studies were undertaken in order to test the operation of the experimental apparatus and to develop experimental techniques. The general aim was to observe vibration and other motion of discrete water droplets using the high-speed video camera whilst detecting partial discharge activity in the vicinity of the droplets. End-electrode geometry was employed to generate a high electrical field directed along the surface of the PE sample with the distance between the two electrodes set between 10 and 20 mm.

For this initial study, sessile water droplets were placed on a horizontal PE surface. Typical droplet volumes were ~10μl and they were placed on the PE surface using a syringe. For most of these initial studies, tap water was used with a conductivity of approximately 10 mS/m. These conditions were considered typical since, as previously described in chapter 3 table 3.3, it may be assumed that the onset fields for droplet vibration, spreading, partial discharge activity or flashover are not highly sensitive to changes in droplet volume or the dielectric properties of the water.

6.2 Experimental Procedure

In a typical experimental run, the applied voltage was raised slowly and until PD activity was detected electrically via the series resistance detector. This PD activity was then recorded using the digital oscilloscope. The applied voltage was then increased gradually until partial discharge activity was observed visually. The video camera was used to record the location of these discharges and the vibration and other movement of water drops. Sequences of images, up to a maximum speed of 3000 frames per second, were then saved to PC as jpeg files, as described in chapter 5. In most experimental runs, the applied stress was then raised slowly until: (a), substantial, visible discharge activity took place, and / or, (b), flashover took place across the gap between the electrodes, destroying the sample. For most test condition studied, this sequence of

observations could be repeated two or three times before a flashover destroyed the sample.

6.3 Partial Discharge Activity

Most of the partial discharge observations were made with droplets of tap water located in the centre of the PE test sample. A 10-mm gap was used so that fields up to 20kV/cm were possible. These experiments to detect partial discharge activity were repeated using at least 10 samples in order to examine repeatability.

As outlined above, the PD activity was observed in two ways: electrically and by using the video camera.

6.3.1 Electrical Detection of Partial Discharges

Figures (6.1) to (6.4) show the typical partial discharge activity detected electrically with a 100-Ω resistor in series with the test gap and observing the voltage pulses generated across it with the digital oscilloscope, as described in chapter 5.

When no water droplet was present on the sample surface, the onset of PD activity in the test samples was detected at 9.5 ± 0.3 kV (i.e. an average applied field of E_0 = 9.5 kV/cm). A typical record is shown in figure (6.1). This PD activity was found to occur during both positive and negative half cycles close to the peak value of the applied voltage. The PD activity had a maximum magnitude at the negative half cycle of ~4 to 5μV. At an applied voltage of around 9.5kV, sustained PD activity did not generate any visual damage to the test sample nor lead to full breakdown, at least in the short term, that is over a few hours.

When the water droplet was located at the centre of the test sample mid way between the two electrodes, the onset of PD activity was detected at an applied voltage of 6.0 ± 0.3 kV (i.e. E_0 = 6kV/cm), ~ 3.5 kV below the level found with no droplet

present. Figure (6.2) shows a typical record. Compared to the case with no drop present, discharge activity appears to be more frequent and to have significantly increased in amplitude to a maximum of ~35 μV during the negative half cycle. With the droplet present, partial discharges over the negative half cycle appear greater (approximately double) than during the positive half cycle. It was found that these PD signals were suitable for use as a triggering signal for the high-speed digital camera as described in chapter 5.

At this comparatively low level of applied stress (E_0= 6kV/cm) no vibration or motion of the droplet was observed, as might be expected from table 3.2.

Figure (6.3) shows the level of PD activity with the droplet present when the voltage was increased to 7 kV (i.e. E_0= 7kV/cm). The magnitude of the PD activity was not observed to increase and showed a maximum of ~36μV around the peak of the negative half cycle. At this increased level of applied field the water droplet was observed to vibrate and subsequently, over a period of several minutes, to spread over the surface of the insulation sample as noted in chapter 3 (see, for example, Lopes 2000, Higashiyama 1999). Again, the PD activity recorded during the negative half cycle is higher in magnitude.

From the above, it appears that the values of applied field found in the present investigation - corresponding to the onset of partial discharges, vibration and spreading - are generally comparable with the values reported in previous studies and shown in table 3.2 in chapter 3.

There is particular agreement between the present observations and those reported in reference 5 of chapter 3 where the test geometry was similar to the present study. In that case, when the water droplet in the middle of the sample, partial discharge activity was reported to occur over both half cycles close to the peak value of the applied voltage. However, that study did not find partial discharges over the negative half cycle to be stronger than over the positive half cycle. It is difficult to explain this difference – it is unlikely that all droplets in our study were consistently off-

centre – but this point was not investigated further at this stage because the main purpose in detecting partial discharges in the present study was to provide a suitable trigger signal for the camera.

Figure (6.4) shows the frequency of PD activity increased when the applied voltage was raised to 8.5 kV (i.e. E_0= 8.5kV/cm) although the magnitude remained around the same level as in the previous two cases. At 8.5kV/cm, it was observed that vibration of the water droplet lead within seconds to spreading over the sample until contact was made with one or both electrodes. This resulted in immediate breakdown of the test sample with physical damage to its surface. .

For the remainder of this initial study, it was considered appropriate to increase the sample length to 20mm - and to correspondingly raise the applied voltage - in order to allow more extensive droplet motion prior to sample flashover.

As a check for the significance of water conductivity, the conductivity of a 10-µl droplet was varied from tap value (~10mS/m) to saturated solution (~5.8S/m) using common salt (NaCl). It was found that, for the lower conductivities, discharge activity and droplet motion were not sensitive to small variations in conductivity. However, figure (6.6) shows discharge activity with a 10-µl, saturated-solution droplet on the insulation surface at an applied voltage of 9kV, 50Hz (E_o = 4.5 kV/cm). With this high conductivity, the partial discharge activity was found to be significantly higher than that observed with tap water, or water containing a small amount of added salt. Also, with a saturated-solution droplet, breakdown occurred in a few seconds, and the sample was damaged, at an applied voltage of 14kV (E_o = 7.5 kV/cm). This applied field is lower than the 8.5kV/cm noted above for tap water in connection with Fig (6.4). One explanation of these observations might be that the lower applied fields with a saturated-solution droplet are at least in part due to an increased stress-enhancement factor (β) with the higher conductivity water, as previously described in chapter 3.

During these tests, many samples were permanently damaged and so had to be discarded. It was evident during these initial studies that visual damage caused by

breakdown of the test samples increased with the applied field. Also, as previously described in chapters 2 and 3, it was probable that some surface degradation was caused by partial discharge activity and the associated emission of ultra-violet radiation affecting the insulator surface.

6.3.2 Observation of Droplet Motion

The electro-mechanical activity undergone by water droplets on the insulation surface was recorded using the high-speed digital video camera operating at up to 3000 frames per second. As noted above, the onset of droplet vibration was found to occur at an applied field of ~7kV/cm and figures (6.5) and (6.6) show the behaviour observed for a 10-μl sessile water droplet in a 10-mm insulation surface mounted between end electrodes at an applied voltage of 7kV, 50 Hz.

From the video camera records, it can be seen that a typical vibration cycle took approximately 6 or 7 frames at 3000 frames per second. This corresponds to a cycle lasting approximately 20ms. This is, the frequency of droplet vibration was also 50Hz, the same as the applied stress. This measurement strongly suggests that the mechanism of vibration is in accordance with equation (3.9) rather than with equations (3.8) or (3.10). That is, the vibrations observed here result from electrostatic forces on the droplet.

Figures (6.5) and (6.6) also show discharge activity during vibration. The discharges appear to be located in the gas away from the surface of the insulator and not close to the triple junctions.

6.4 Initial Conclusions

From this initial study it was evident that the experimental system that had been designed and constructed and the experimental techniques that had been developed were generally appropriate to the overall programme of work which had been outlined in chapter 5.

For the present conditions, it was also concluded that as applied AC stress is increased, partial discharge activity precedes the onset of droplet vibration. It was also concluded that electrostatic forces are responsible for the initial vibration of the droplet and that lateral spreading of the droplet in the direction of the applied field follows the onset of vibration. The effect of water conductivity on partial discharge activity and droplet vibration was not significant except at very high concentrations of salt near the saturated-solution level.

The observation of partial discharge activity in the gas away from the triple junction as shown in figures (6.5) and (6.6), was interpreted as suggesting that the path of these discharges might be governed by gas-breakdown rather than surface-breakdown processes. That is, that the electric field configuration in the gas surrounding the droplet may allow the streamer breakdown criterion to be satisfied even although surface flashover conditions are not met. This is considered to have implications for the interaction between partial discharges and the insulator surface and, therefore, to the ultimate performance of insulators under such contaminated conditions. It was decided to investigate this question further.

A paper based on this work was published in the XIV International Conference on Gas Discharges and their Applications in Liverpool University, 1 – 6 September 2002, under the title "Electrical Breakdown at Sessile Water Droplets on Insulating Surfaces Subject to High AC Stress". A copy of this paper is appended to this thesis.

Fig (6.1) Partial Discharge no Water Droplet

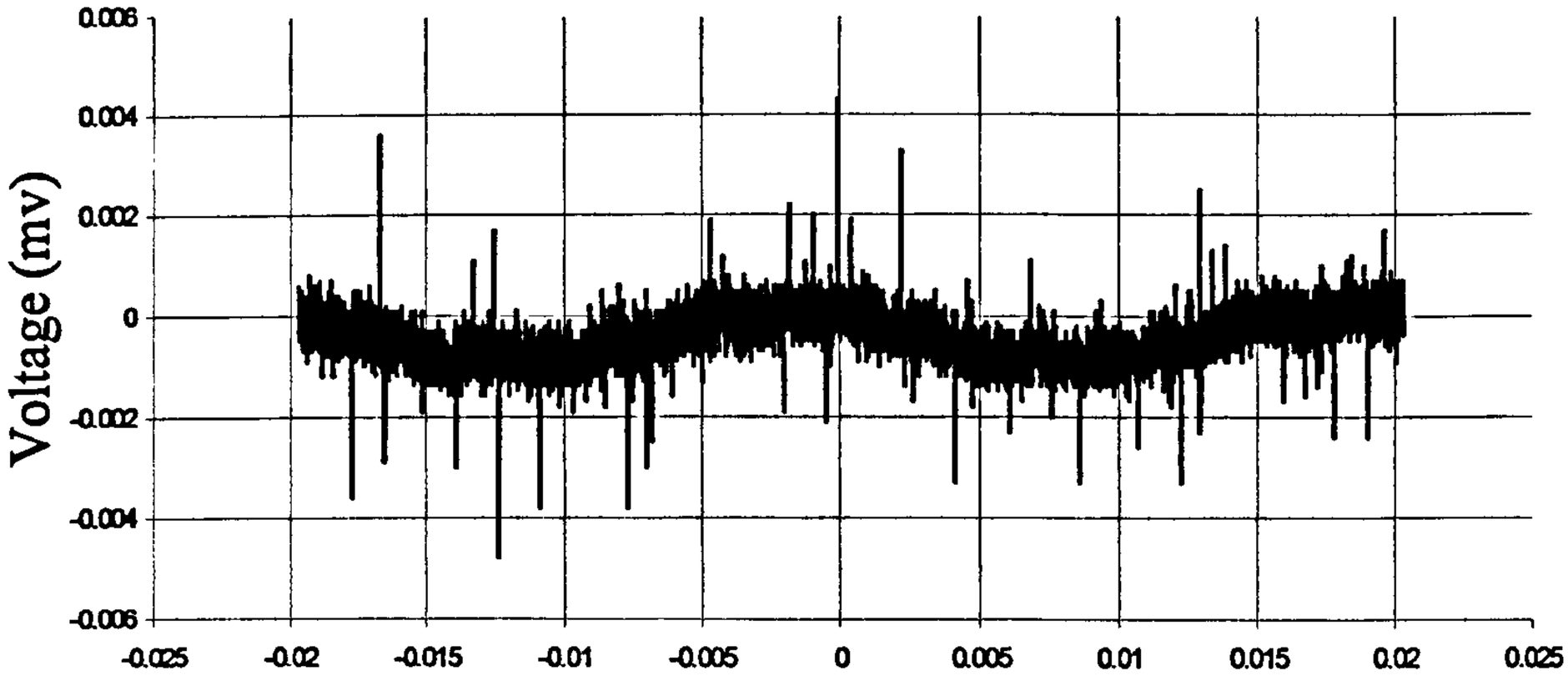

Applied voltage wave form

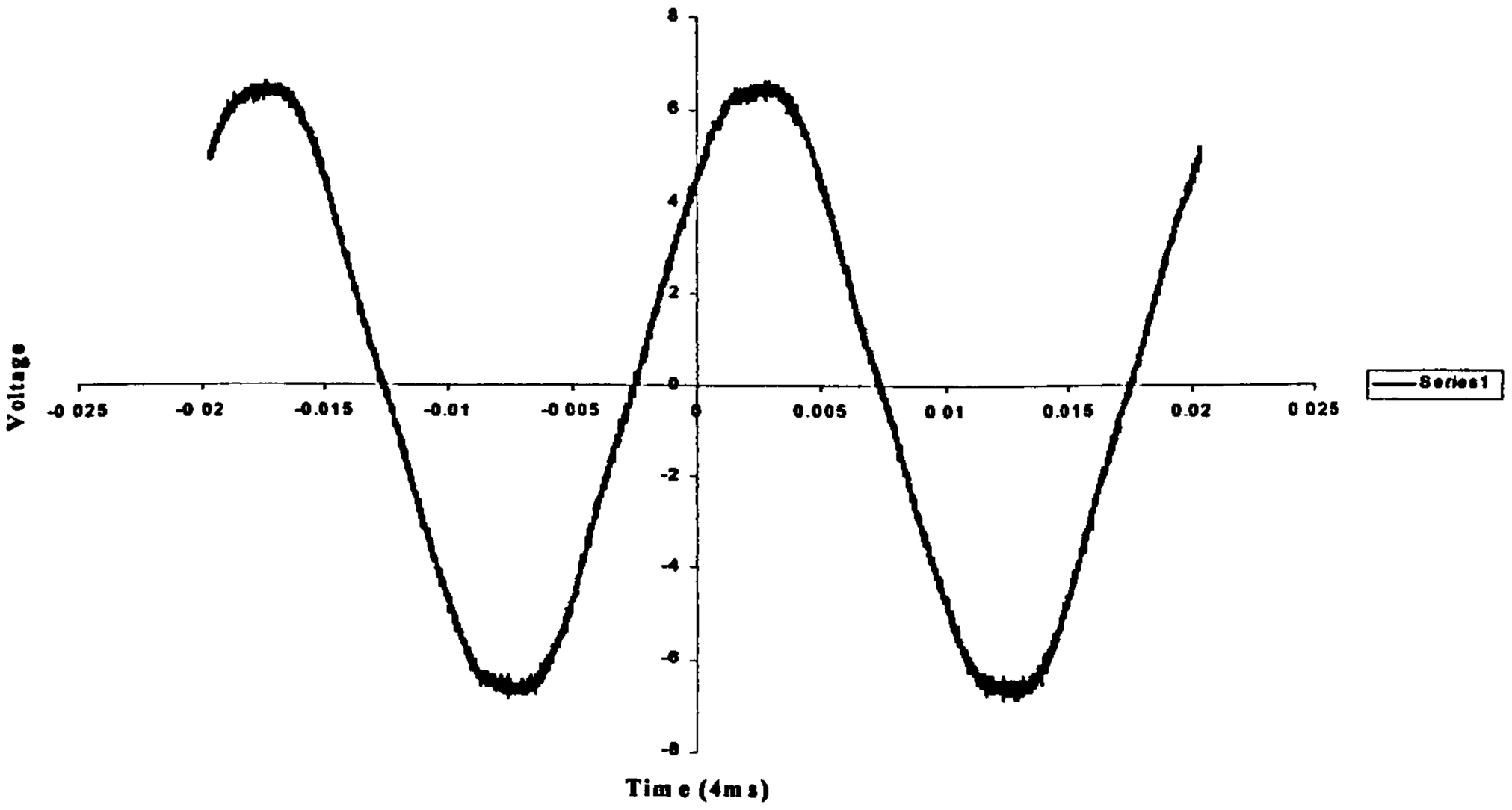

Fig(6.2) Partial Discharge with water droplet over the sample

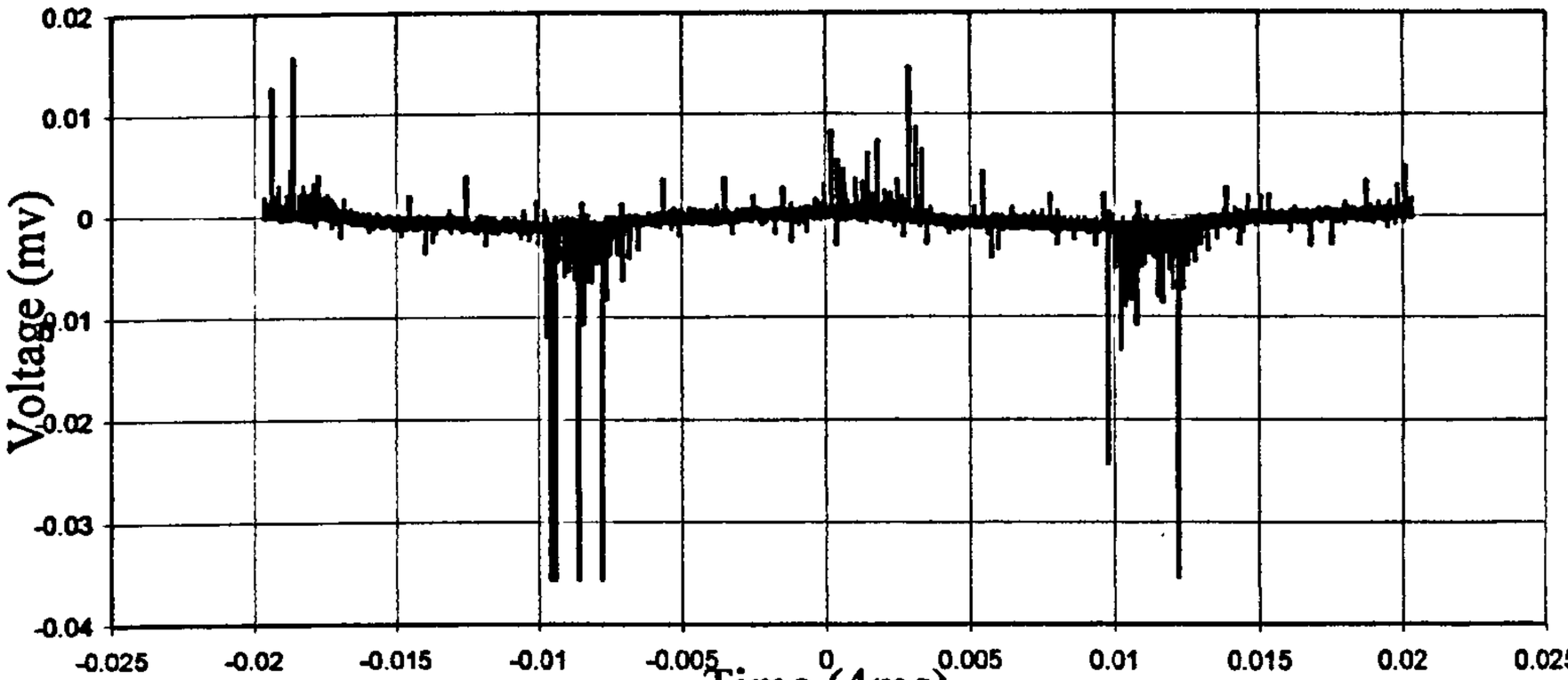

Applied voltage wave form

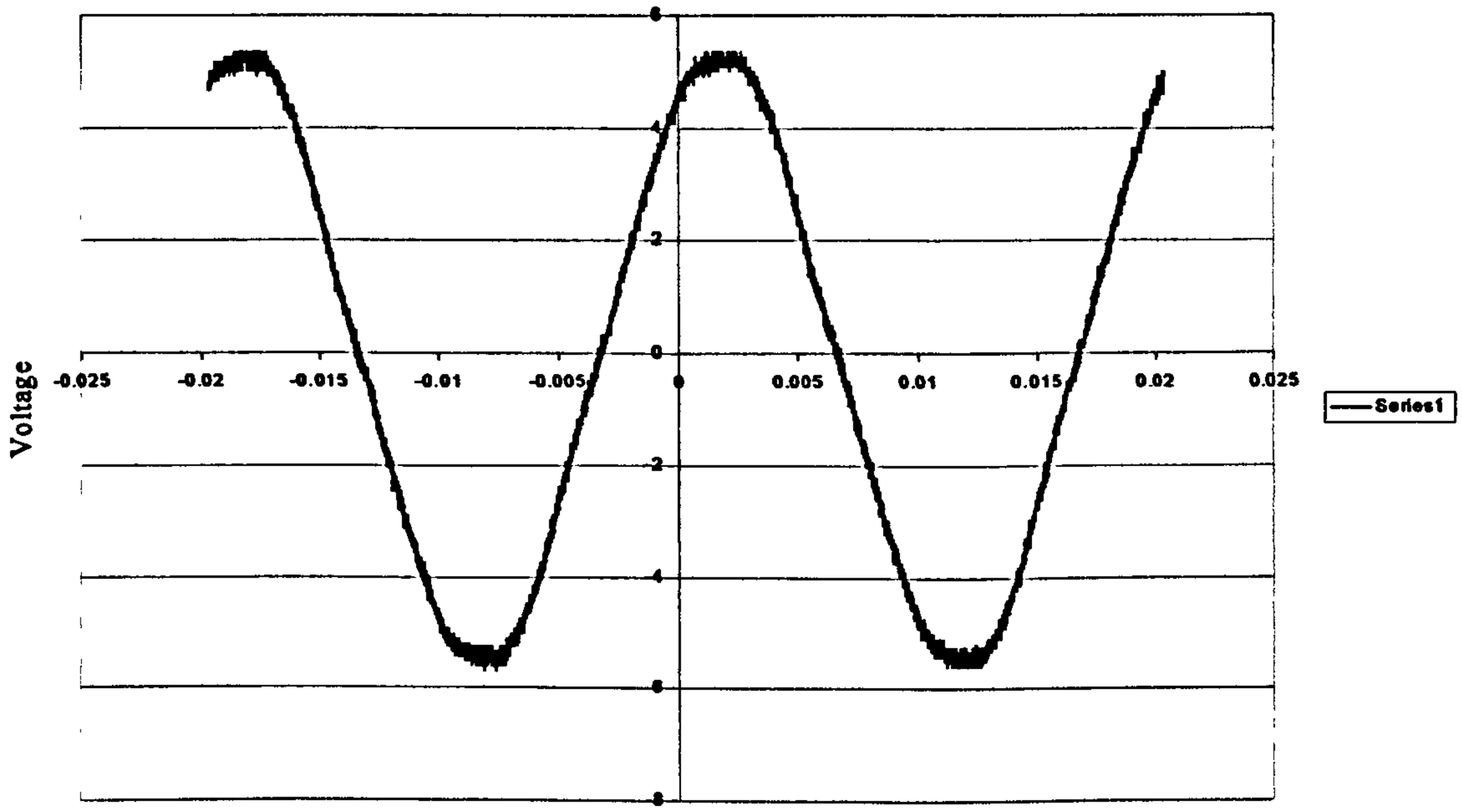

Fig (6.3)The Partial Discharge with the Water Droplet scattered over the sample

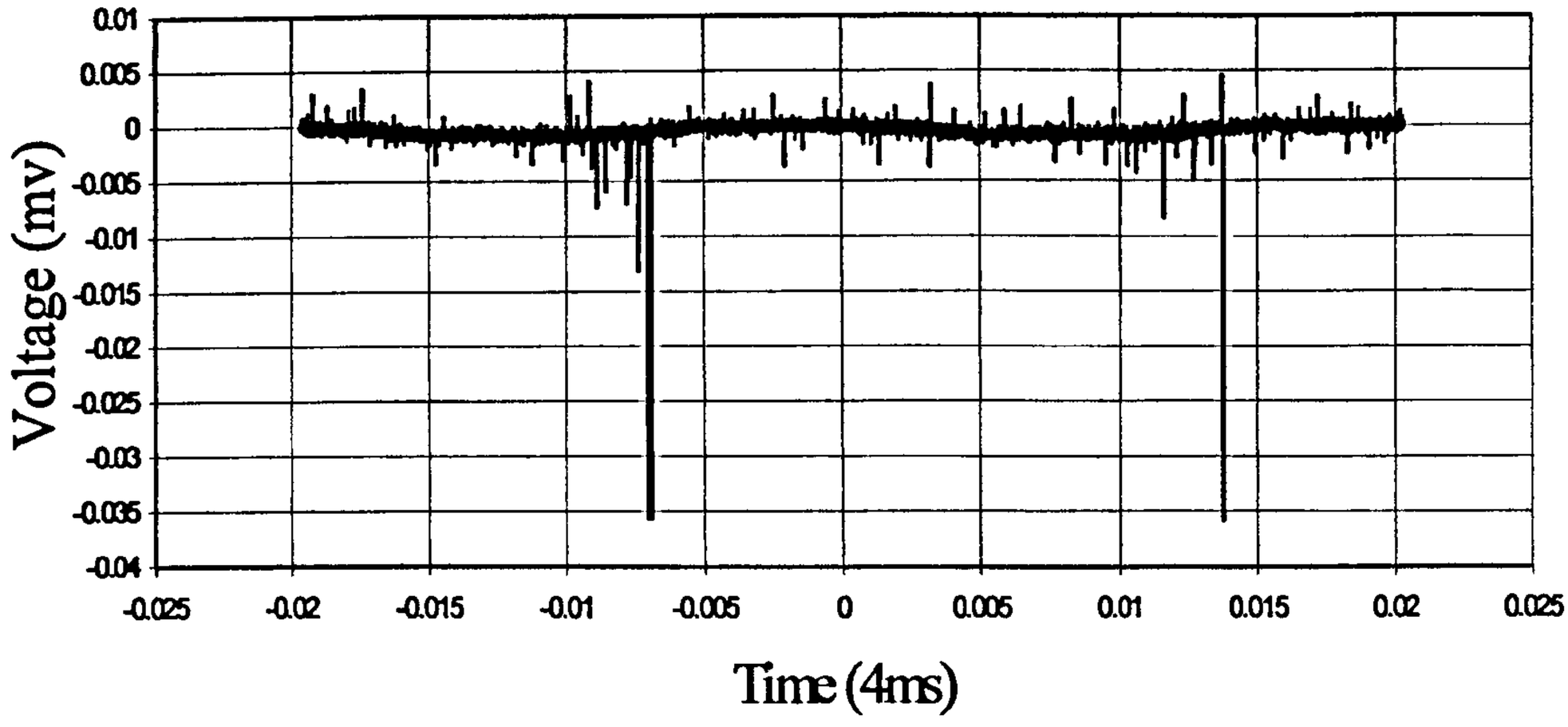

Fig (6.4) Break Down when the Water Droplet expanded

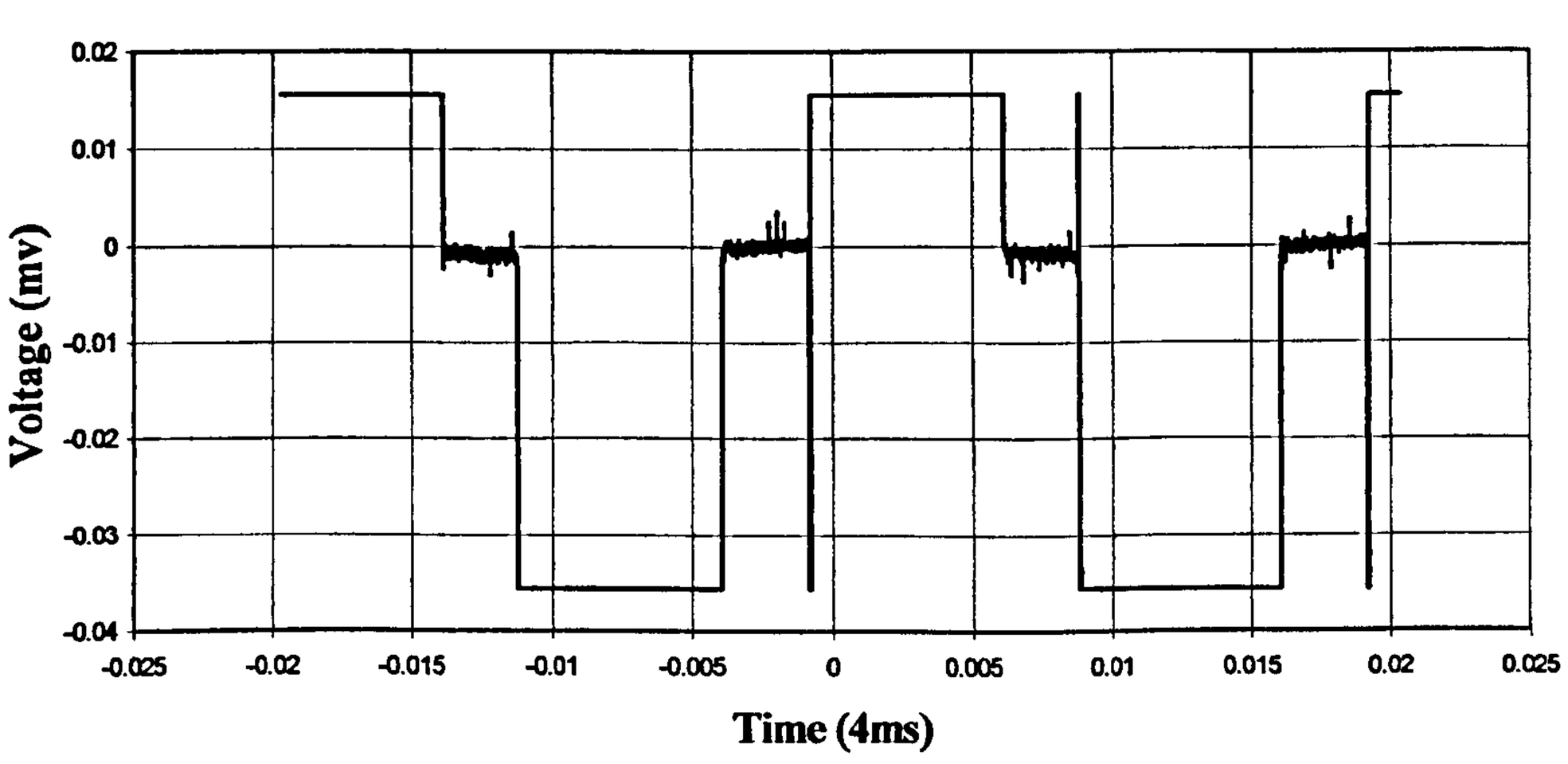

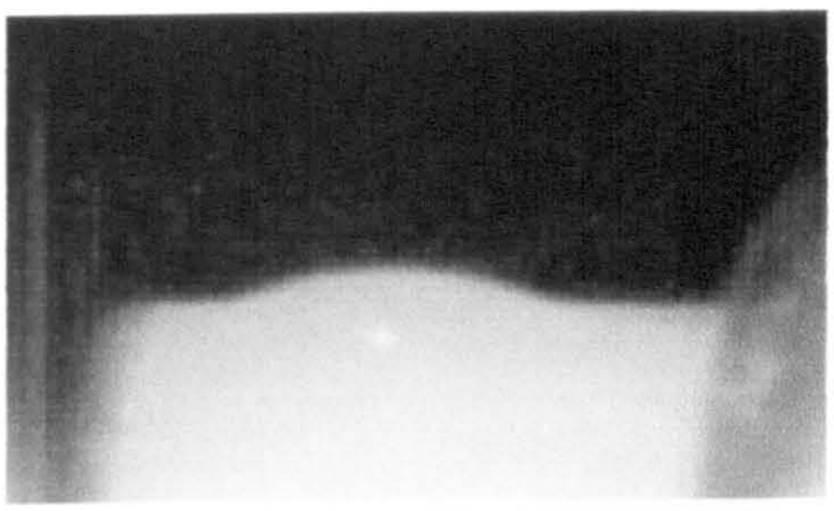

1

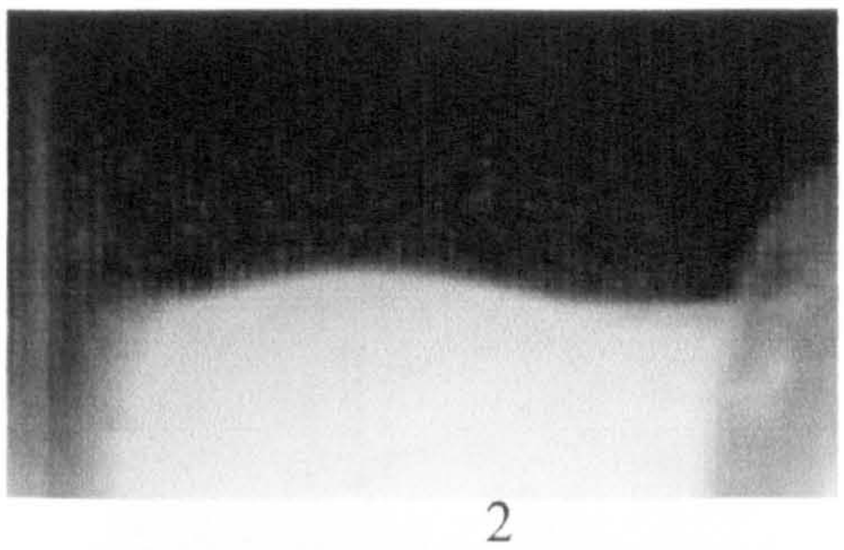

2

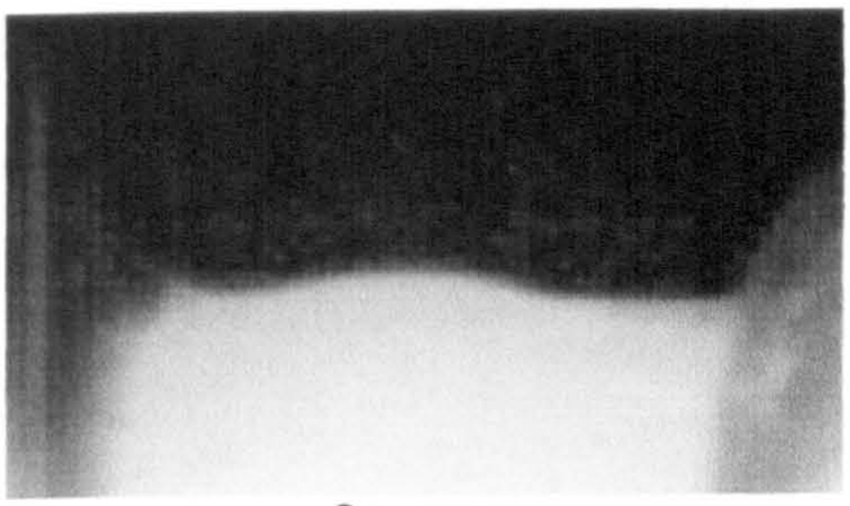

3

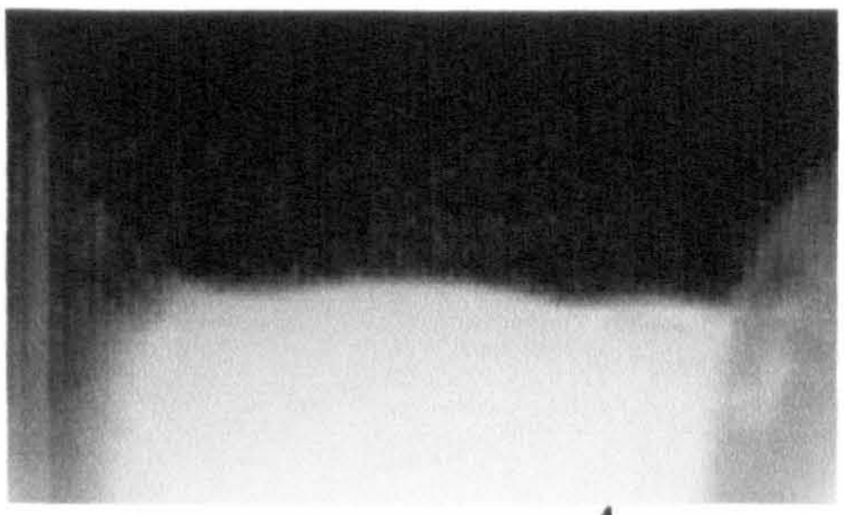

4

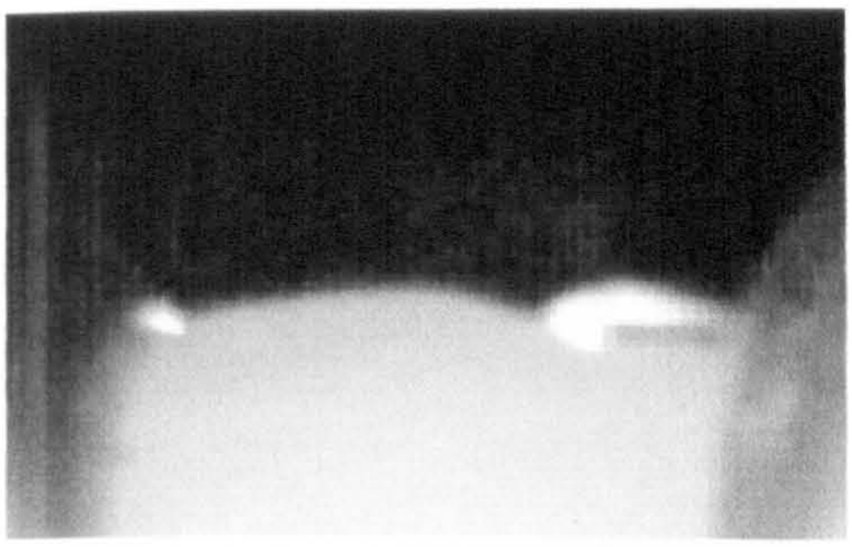

5

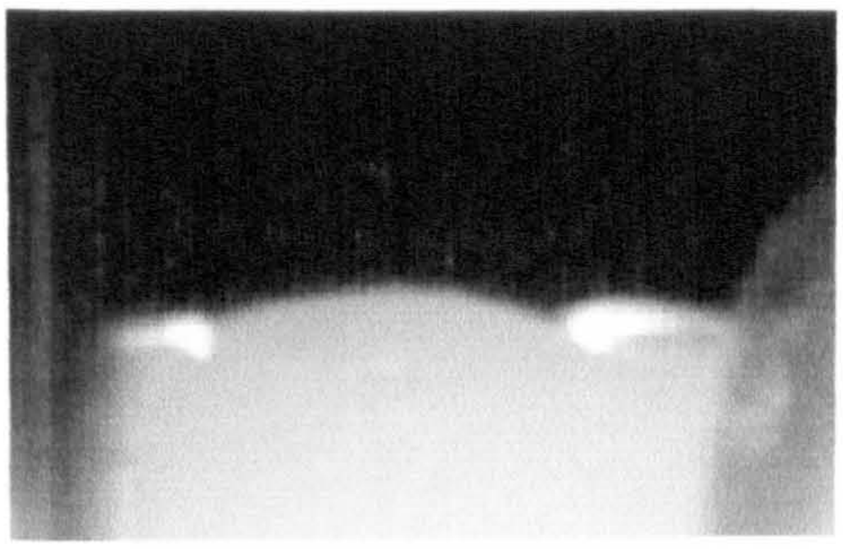

6

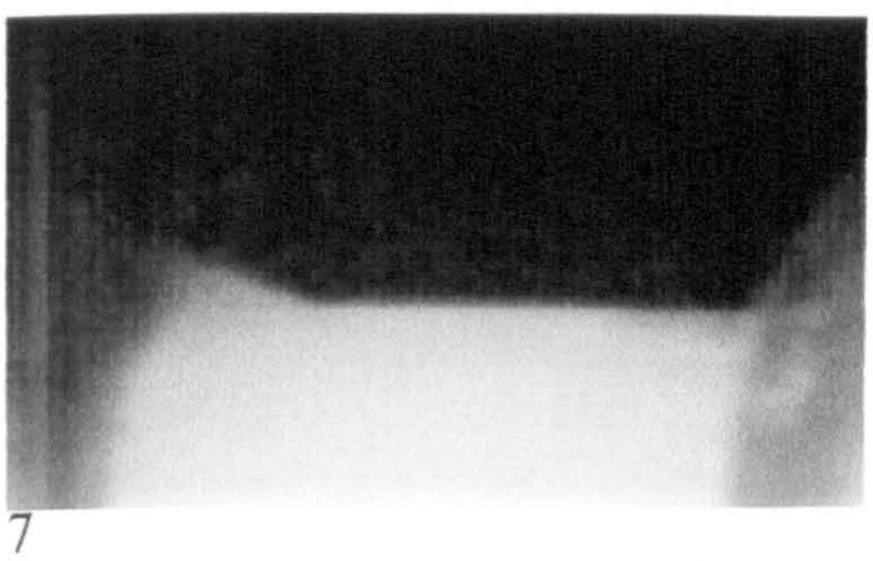

7

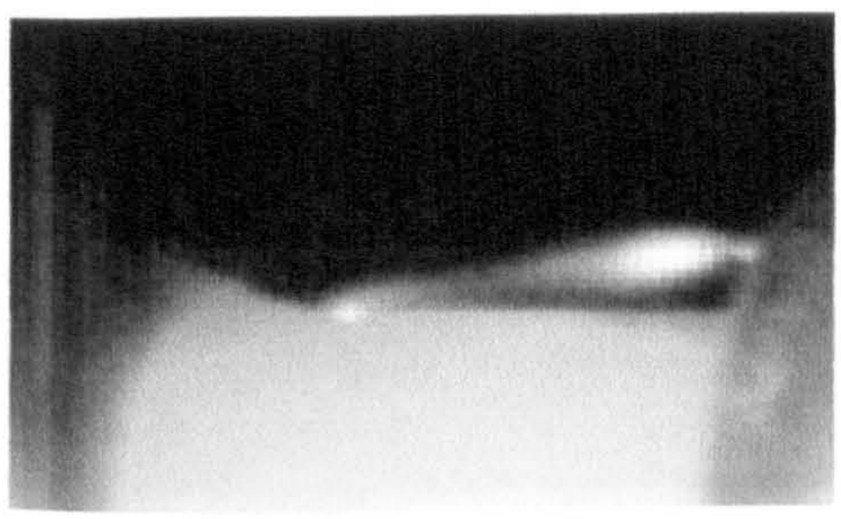

8

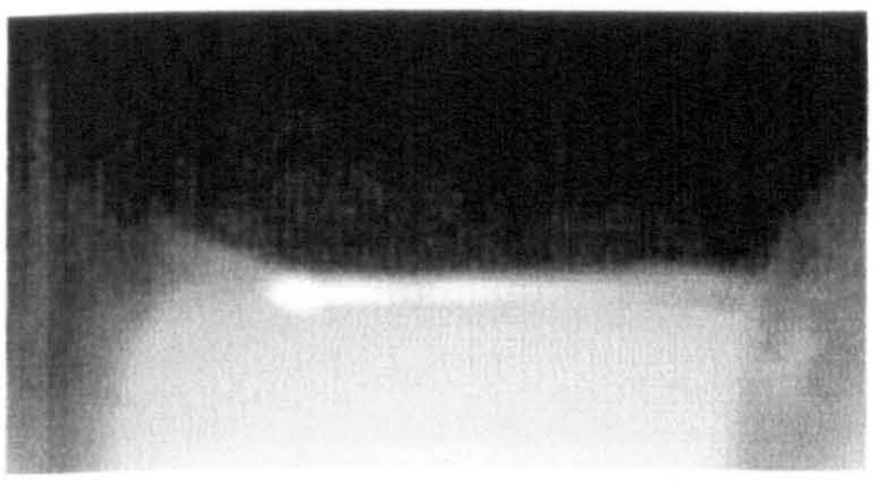

9

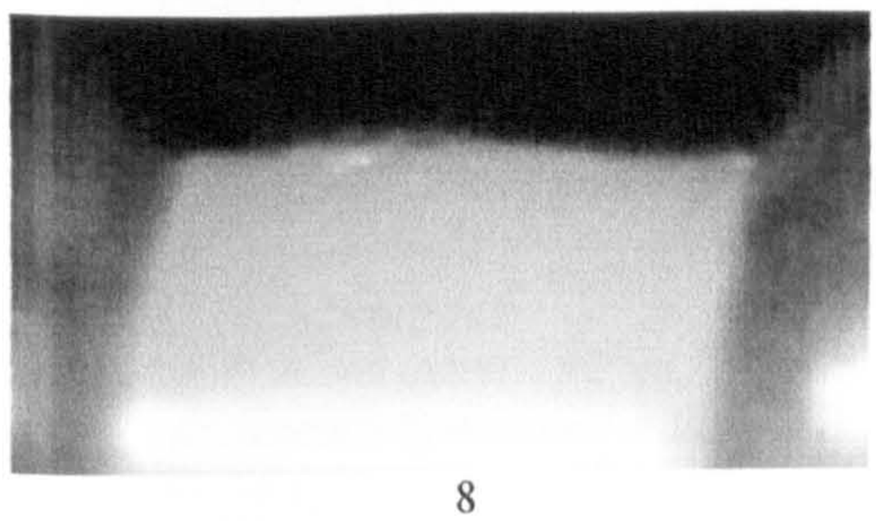

10

Figure (6.5) Droplet on insulation surface average applied stresses 7kV/cm (RMS).

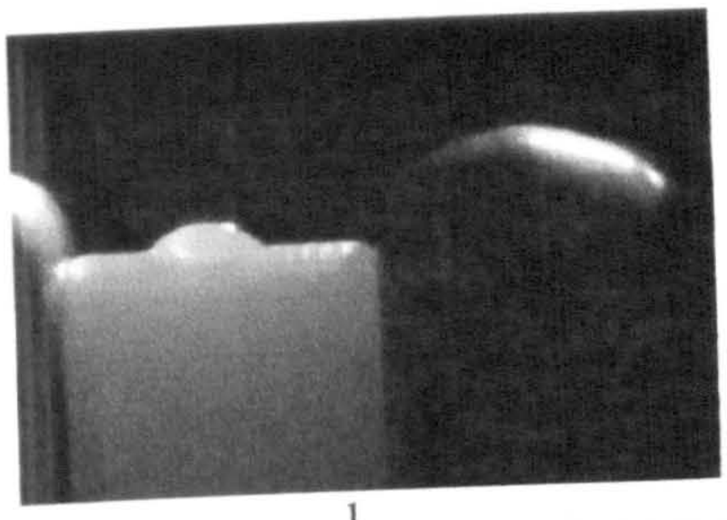

1

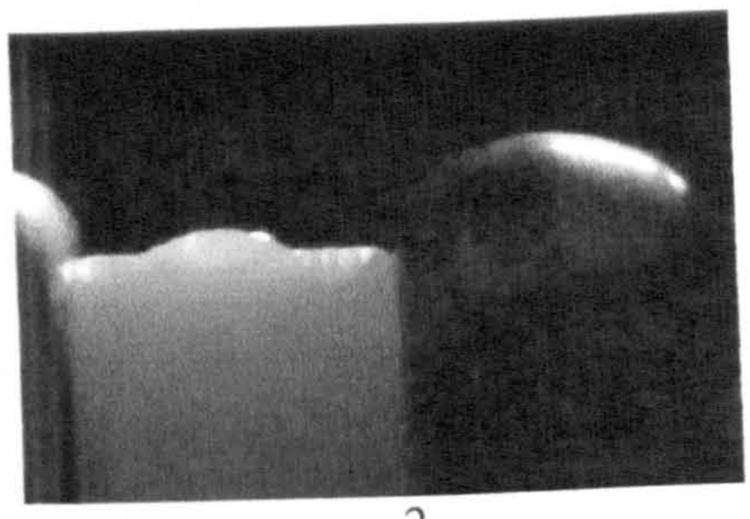

2

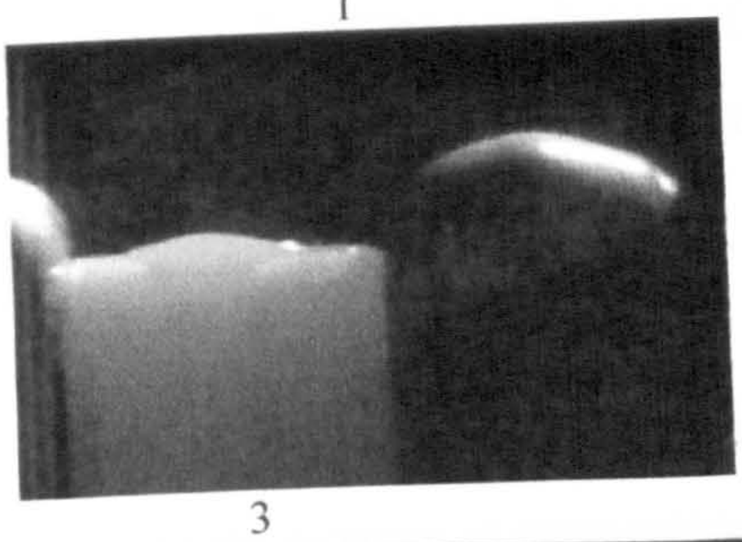

3

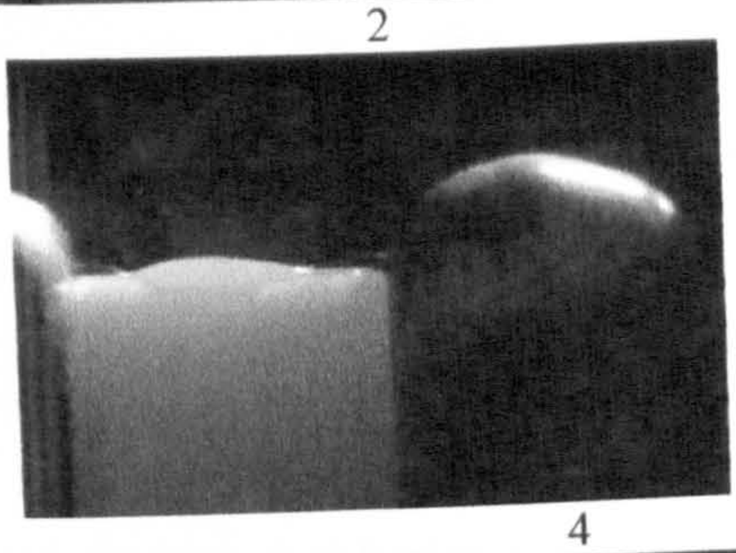

4

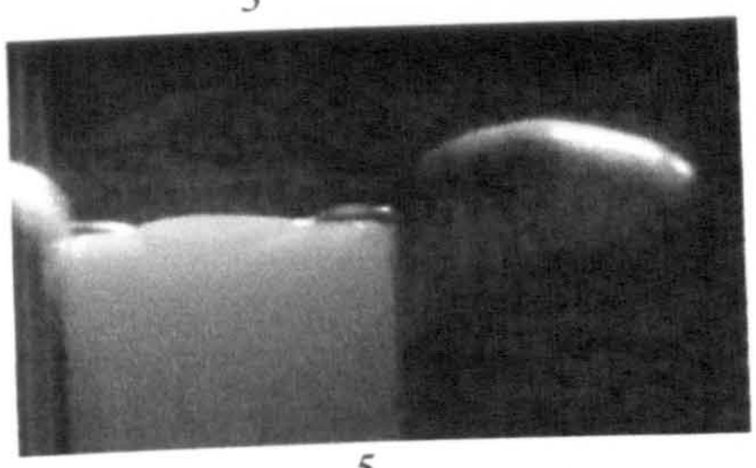

5

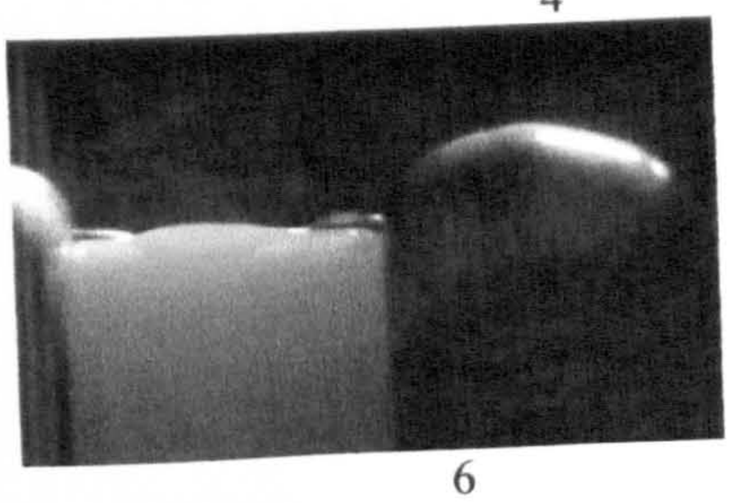

6

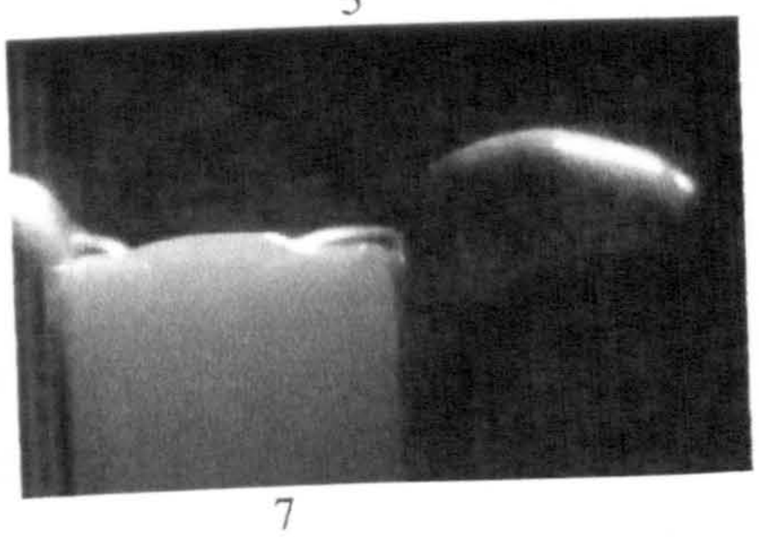

7

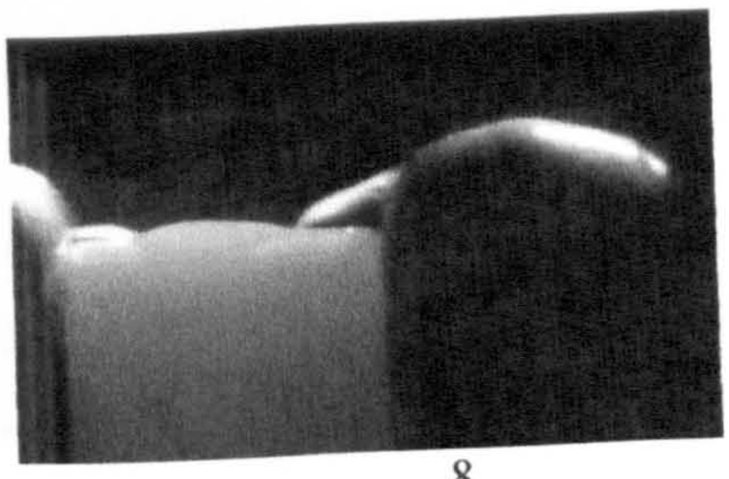

8

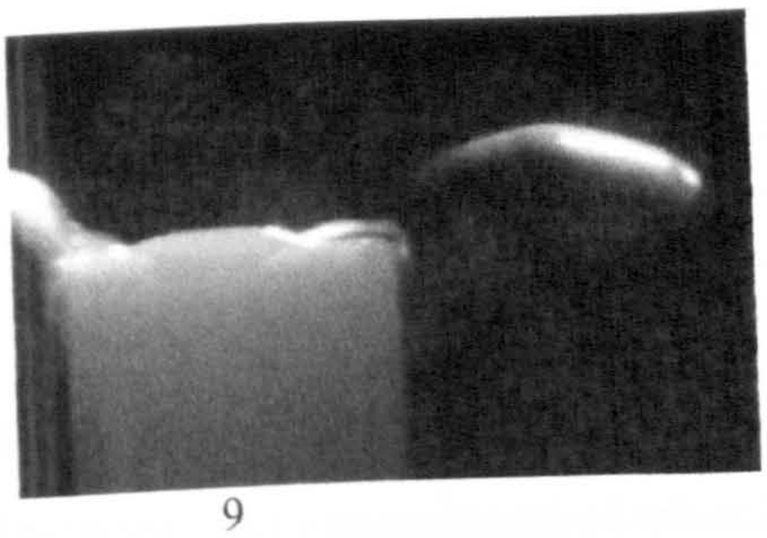

9

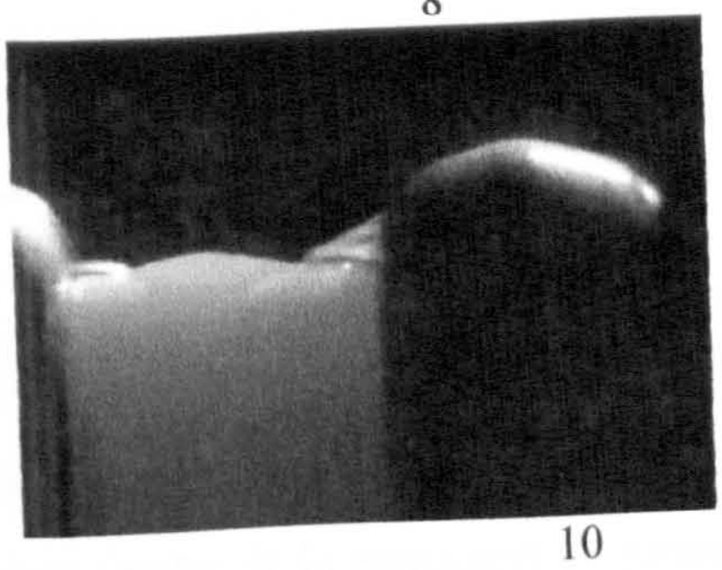

10

Figure (6.6) Salt droplet on insulation surface average applied stresses 7kV/cm (RMS).

Chapter 7

Development of Electric Field Models

7.1 General

In this chapter, the development of electric field modeling of test sample geometry and material properties is described. Modeling was done using a Finite Element Method (FEM) software (QuickField® version 4.2). This is a 2D/3D-rotational symmetry, PC-oriented interactive environment for electromagnetic, thermal and stress analysis. Standard analysis types include:

- Electrostatics.
- Linear and non-linear magnetostatics.
- Time-harmonic magnetics (involving eddy current analysis)
- Linear and non-linear heat transfer and diffusion.
- Linear stress analysis.
- Coupled problems.

With this program the system to be analyzed can be specified in terms of its geometry, material properties, field sources and boundaries. A variable element mesh size can be specified to focus on regions where the highest accuracy is required whilst keeping computation time acceptable. Computed solutions can then be analyzed both visually and quantitatively using a range of post-solution processing facilities.

7.2 Computation of Electromagnetic fields

This FEM program does not allow analysis of transient conditions or electrical problems simultaneously involving both electrostatic and current flow (i.e., both conductance and capacitance at once). For the present study, it is required to determine how electrical breakdown is affected by the electric field at a water droplet on an insulator surface in air under electrical stress at 50Hz. Given the fast nature of gas or surface breakdown (typically ~μs) compared with period of the applied field (20ms), it

is reasonable to assume quasi-static conditions for modeling and that an electrostatic computation will accurately determine the electric field for the purposes of evaluating electrical breakdown criteria.

7.2.1 Electrostatic analysis

Electrostatic computation combined with post-solution analysis can be used to calculate potential distribution, electric field, capacitance, gradient of electric field intensity, electric induction, total electric charge in a particular volume, total electrostatic force acting on bodies contained in a particular volume and total torque of electrostatic force acting on bodies contained in a particular volume. This analysis is based on finite-element solutions to Poisson's equation with the following conditions:

- **Material properties**: Orthotropic materials with constant permittivity.

  In this study the materials were air, polymer and water as a droplet. Under quasi-static conditions these materials may be assumed to satisfy these conditions.

- **Loading sources**: Specified voltages at defined contours and specified electric charge densities within defined volumes.

  The test geometry is consistent with these requirements.

- **Boundary conditions**. Prescribed potential values, prescribed values for normal derivatives (surface charge), and prescribed constraints for potential boundaries with given total charges.

  In the present study, the region of computation was contained within a suitably remote boundary that was specified to adopt local values of the field at the boundary surface. It was assumed that such an outer boundary would not distort the calculated values of electric field in the inner regions close to the droplet.

7.2.2 Current flow analysis

The FEM package could also be used to calculate current density and power loss (joule heating) at a constant frequency of applied voltage. For this, the following conditions applied:

- Material properties: Orthotropic materials with constant resistively.
    - The resistivity of the water droplets was known and suitably high values were assumed for air and polymer.
- Loading sources: Voltage, and electric charge density.
- Boundary conditions. As described above in electrostatic analysis.

7.3 Use of QuickField:-

Before using this FEM package to analyze the present test geometries, it was used to examine several arrangements previously described in the literature. The results were found to show good agreement with this previous work and it was concluded that the computation conditions described above were satisfactory (see section 7.4). Having established acceptable field-modeling techniques, computation with the present material conditions and test geometry were undertaken. In using the FEM package to analyze a problem, the typical sequence of phases gone through in the present study is described below and depicted in the flow chart as shown in Fig (7.1).

7.3.1 Problem Description

A database was built for each problem to be solved with QuickField. The core of the database is the problem description, which is stored in file with the extension .pbm. The problem description contains the basics of the problem: its type (e.g. electrostatic), co-ordinate type (e.g. Cartesian), precision class, etc., and also references to all other files, which constitute the problem database. These files are the **model file** (with standard extension .mod) which contains the geometrical data and the **physical data files** (with extension .dms, .dhe, .des, .dcf, .dht, or. dsa - depending on the subject and type of problem) which contain the data concerning material properties. A single problem may require several files of physical data. Usually, the first file contains

specific data related to the problem, as the other files are libraries of standard material properties and boundary conditions, which are common for a whole class of problem.

When solving a problem QuickField creates a **results file** with the extension .res. The data held in this file can then be repeatedly analyzed in different ways without the requirement to re-solve the finite element problem on each occasion. This is termed post-processing.

7.3.2 Choosing Length Units

QuickField allows the specification of polar or Cartesian coordinates and a wide range of units of length (e.g. μm to km) when creating the geometrical data for the model file.

7.3.3 Creating a model

Model development consists of three stages:

- Geometric description.
- Definition of material properties, field sources and boundary conditions;
- FEM mesh generation.

Model geometry is defined by specifying the co-ordinates of vertices (points) and contours (edges) connecting vertices. This procedure is used to form the closed boundaries of all different sub-regions having specific physical properties. Following this, these regions can be labeled (e.g. air, water, electrode, insulator, etc.) and their physical properties defined. In addition sources can be specified (e.g. a region of specified potential) and boundary conditions set (e.g. equipotential or floating surfaces).

There are two options available for creating the FEM mesh:

- A **fully-automated** method which generates the FEM mesh in all regions with mesh sizes linked to each region's typical geometrical dimensions. This method has the drawback that it can generate very fine mesh dimensions over

large regions containing one small feature, and so lead to very long computational times.

- A **manual** method that allows the user to specify the typical mesh dimension at selected locations by setting the value at specific vertices. This feature allows the system to be modeled in fine detail around selected regions of greatest interest and to adopt a coarser mesh elsewhere. This option reduced computational time and proved particularly useful in our applications.

7.3.4 Solving the Problem

Following a complete specification of the model and data files, it is possible to then solve a problem to obtain data on, for example, equipotential and field distributions in the form of a results file. This file can then be further analyzed using the postprocessor features that provide various forms of presentation and analysis, e.g.:

- Colour-graded equipotential and/or field distributions,
- Individual equipotential and/or field values at selected points,
- Integration operations that can be applied over selected contours to calculate: capacitance between bodies, electric charge within a volume, electrostatic force acting on a particular body, torque due to electrostatic forces.
- Graphical plots of parameter distributions along selected contours,
- Numerical data on parameter distributions over selected regions in the form of Tables.

In order to analyze potential or field, for example, it is possible to select a particular existing geometrical contour within a particular region of interest, or even insert a new contour. For example, in this study an existing contour might be along the edge of a water droplet or along the surface of the insulator. The facility to introduce a new contour proved useful to investigate the electric field distribution in the air along a selected field line extending from the edge of a water drop, and hence to the question of electrical discharge development in this location (see Chapter 9).

7.4 Model Development

As mentioned above, several known electric field geometries were modeled using the above FEM program before applying it to the present work. To illustrate this, we choose two cases from those examined that show details of use in specific situations. These cases are based on material taken from relatively recent papers that consider the effects of a pollution layer and a water droplet on the potential and electric field distributions over an insulator surface [1, 2, 3, 4].

In the first case a cylindrical dielectric insulator with a layer of surface pollution is mounted between a pair of uniform-field, end electrodes, as shown in Fig (7.2). The upper electrode is at high-voltage and the lower is grounded. The upper section of the layer is wet (i.e. conducting) and the lower section is dry (i.e. insulating). The system is axially-symmetric and located within a boundary specified to take up local values of potential. With a voltage applied, the typical resultant potential distribution, electric field and current density calculated using the FEM program are shown in figures (7.3), (7.4) and (7.5) respectively. These results were compared with those described in references [1] and [2] and were found to be in good agreement.

The second case from the literature (see reference [3] and [4]) comprised surface-mounted rod electrodes of hemispherical cross-section mounted 30-mm apart on a flat, hydrophilic insulation sample, as shown in Fig (7.6). To compare with references [3] and [4], the FEM model included a water droplet with a contact angle greater than 90^{o} located at the center point between the two electrodes. The colour-graded potential distribution, electric field and current density computed using the above FEM program are illustrated in figures (7.7), (7.8) and (7.9), respectively. As expected, figure 7.8 shows an enhancement of the electric field at the triple junction where the water droplet touches the insulator surface. The distribution of this field was closely matched that shown in references [3] and [4] and numerical values at individual locations were in close agreement.

Such agreement in the two cases above was interpreted as confirmation that our general application of the FEM software was appropriate, and, in particular, that the selection of boundary conditions, mesh density, material parameters and other model factors was also appropriate.

7.5 Theoretical Procedure

This section describes an initial application of the post-solution processing facilities available from the FEM software to model and examine a water droplet on a PE surface between end-electrodes.

7.5.1 The Geometry of the Model

Similar to section 7.4, an end-electrode model was adopted in order to study theoretically a water droplet located on a pollution layer on an insulation sample. Using this model, the effect of varying the permittivity and conductivity of the wet pollution layer on the electric field strength and leakage current density was examined. By applying the post-processing features of the software to selected geometrical contours, it was possible, in theory, to investigate the electro-mechanical forces on the droplet.

This general arrangement is illustrated in Figs (7.10a) and (7.10b). One electrode is specified to be at a potential of 20kV and the other grounded. For simplicity in selecting a contour, the droplet profile was assumed to be an arc of a circle (this may in fact not be an unreasonable approximation for a sessile droplet on a PE surface, as found in chapter 9 and illustrated in figure 9.8 b). The water droplet conductivity was taken as 100 μS/cm and that of the air and polymer as $1 x 10^{-15}$ S/cm and $1.2 x 10^{-13}$ S/cm, respectively. The relative permittivity of the water droplet was taken as 81 and that of the polymer as 2.35. The droplet diameter was arbitrarily set at 2.0 mm.

Two types of FEM analysis were undertaken:

(1) Electrostatic analysis to calculate potential and field;

(2) Current flow analysis to calculate leakage current density.

7.5.2 Electrostatic Analysis

Three cases were considered. **Case A.** The permittivity of the pollution layer was set to be the same as the PE insulation sample (i.e. 2.35), so there was effectively no pollution layer. **Case B.** The relative permittivity of the pollution layer was set equal to 40 (approximately mid-way between PE and Water). **Case C.** The relative permittivity of the pollution layer was set equal to 81 (Water). These values of relative permittivity – ranging from a completely dry surface to a completely wetted one - represent the full extent likely to be encountered in the present investigation.

The general distributions of the electrostatic potential and field for case A are shown in figures (7.11) and (7.12), respectively. Post-processing facilities were used to examine in more detail the electric field along the surface of the polymer, including the triple junction at the water droplet. This was done by selecting the contour passing along the surface of the pollution layer on which the droplet was located between the electrodes. The results are presented in figures (7.13 A, B and C). The average electric field (E_o) in each case is 20kV/cm. As expected - see chapter 3 and references [2] and [3] in particular, the surface electric field reaches a maximum ($E_{s\ max}$) at the triple junctions at each side of the water droplet and a minimum value ($E_{s\ min}$) at the centre of the water droplet.

For a dry PE surface, figure (7.13 A) shows that the presence of the water droplet "shorting out" part of the inter-electrode gap raises the surface field near the electrodes from the average value of 20kV/cm to ~20.9kV/cm. At the edge of the droplet, the field reaches a maximum value ($E_{s\ max}$) of ~22.5kV/cm, that is about 12.5% above the average value. Table (7.1) shows computed values of the surface field for the

three cases A, B and C. This shows that as the relative permittivity of the surface layer increases from 2.35 (case A) to 81 (case C) the percentage increase in $E_{s\ max}$ over the average field falls from 12.5% to 5.5%. Increases of this order would have a considerable effect on gas breakdown in the vicinity of the droplet edge. In the light of this, it was concluded that care should be taken to ensure that the surfaces of test samples should be dry prior to stressing.

By selecting contours on each side of the droplet, the electro-mechanical forces, $\mathbf{F}_m$, on the droplet were calculated in the high-voltage electrode direction (HVED) and in the ground electrode direction (GED). Results for the three cases A, B and C are shown in table (7.2). The calculated ratios of HVED/GED are all slightly greater than one, which indicates that the calculated electro-mechanical force in the HVED consistently exceeds that in the GED. Symmetry dictates that the two forces should be equal and, following further inspection of the FEM mesh diagrams, it was concluded that slight imbalances in the automatic mesh generation on either side of the droplet were the most likely cause for calculating an apparent force imbalance.

Assuming the HVED and GED forces should in fact be equal, it is reasonable to take an average value of the computed $\mathbf{F}_m$ for each case of layer permittivity. In table (7.3) the average value of $\mathbf{F}_m$ for cases A, B and C is presented and it can be seen that this tends to increase with increasing permittivity: compared to a dry PE surface (case A), case B shows a 3.1% increase and the fully wetted surface (case C) shows a 5.2% increase. However, these increases are not large which suggests that the force on a droplet will not be particularly sensitive to small changes in nominally-dry surface conditions. Therefore, prior to any experimental investigation of droplet behaviour, no special control of surface conditions appears to be required other than straight-forward cleaning and drying.

7.5.3 Current Flow Analysis

As an example of current flow analysis we examined the effect of the water droplet and the pollution layer on the leakage current (I_c) between the electrodes. The

surface-mounted electrode geometry described above in section 7.4 was examined with the resistivity of the PE taken as $10^{13}\Omega$m and that of the water droplet as $10^{5}\Omega$m.

Initially, the case when the layer resistivity was equal to that of the PE was computed – i.e. when the pollution layer should have no effect. Figure (7.9) illustrates the distribution found. It is interesting to note that droplet effectively forms a conducting bridge across the PE such that the current density through the PE immediately below the droplet is therefore reduced substantially. Figure (7.14A) shows the variation in current density along the pollution layer. Typically, this current density in the layer is of the order of $2\text{x}10^{-7}$ A/m^2. The droplet causes an increase in layer current density at its periphery where current is seen to flow from the bulk of the PE to the droplet. However, where the droplet bridges the layer a substantial decrease in layer current density is shown. The computed maximum and minimum values of the current density in the layer are shown in table (7.4). Similar calculations were made for the cases where the resistivity of the layer taken as $10^{10}\Omega$m and $10^{5}\Omega$m, the latter representing a fully-wetted layer. These results are presented in figures (14B) and (14C), and also summarised in table (7.4). It is evident that highest current density in the pollution layer occurs when the resistivity of the layer equals that of the water, as would be expected, and for this case the current density is of the order of A/m^2. This is approximately seven orders of magnitude greater than for the "dry" layer, and suggests that with a fully-wetted layer surface breakdown would be highly probable.

Note: a preliminary version of the work described above was presented at the 36th Universities Power Engineering Conference (UPEC 2001) 12-14 September 2001, Swansea, UK in a paper entitled "A Study of Water Droplet Behaviour on Insulator Surfaces under High Electrical Stress".

7.6 Conclusions

The application of the Quickfield® FEM software to the present study is appropriate subject to suitable selection of boundary conditions, mesh density, material parameters and other model factors.

The permittivity of a surface layer on a PE sample influences the field there, and so might be expected to have a considerable effect on gas breakdown in the vicinity of the droplet edge. In the light of this, care should be taken to ensure that the surfaces of test samples should be consistent prior to stressing, e.g. appropriately dry.

The electro-mechanical forces on a droplet are not particularly sensitive to small changes in nominally-dry surface conditions. Therefore, from this point of view, no special control of surface conditions appears to be required other than straight-forward cleaning and drying.

For a dry sample, leakage current density near the surface is of the order of 2×10^{-7} A/m^2. The presence of a water droplet causes an increase in current density around its periphery where current flows from the bulk of the PE to the droplet. However, where the droplet bridges the PE a substantial decrease in leakage current through the PE occurs. With a fully-wetted surface, the relatively high level of leakage current through the surface layer suggests that surface breakdown would be highly probable.

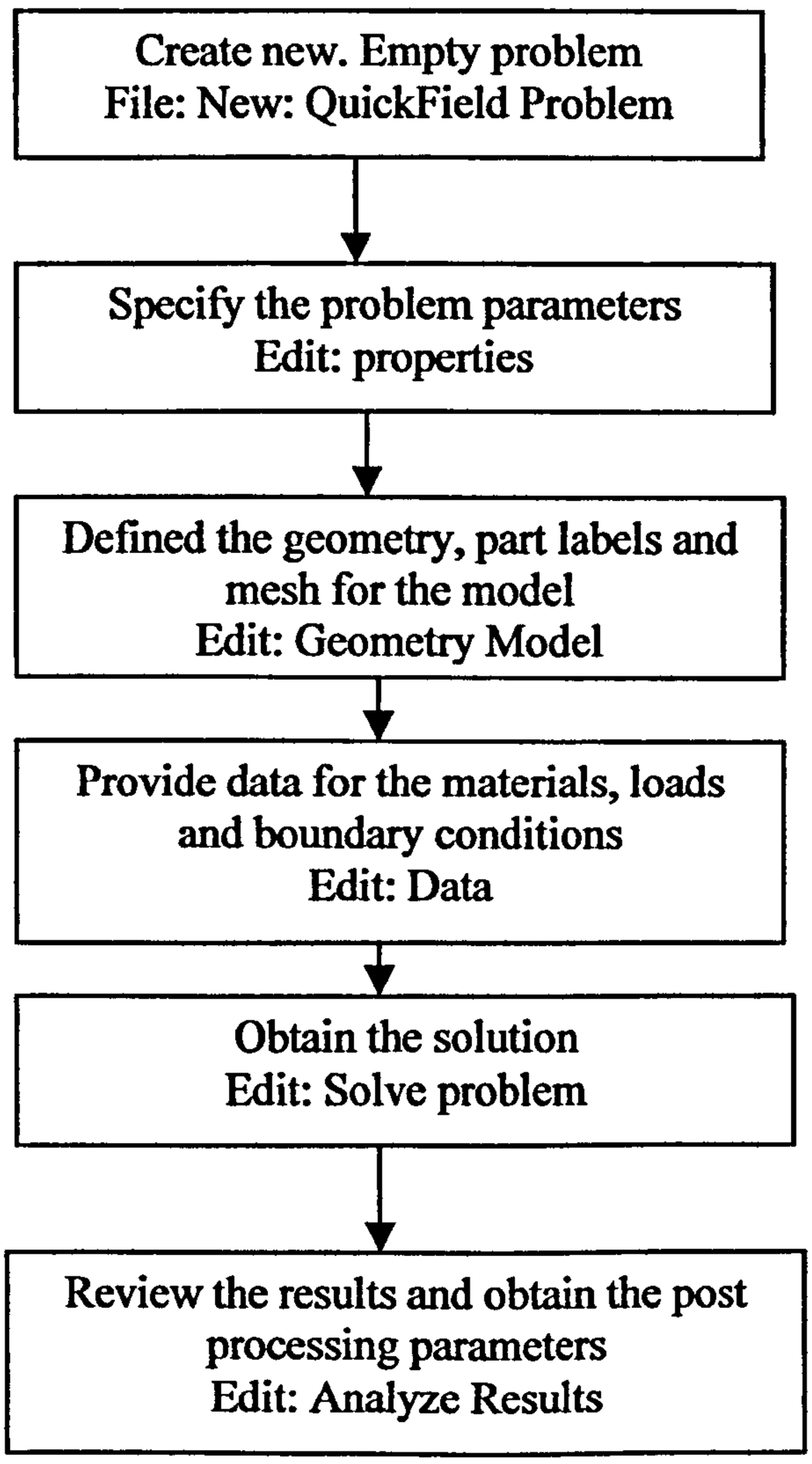

Fig (7.1) QuickField Flow Chart

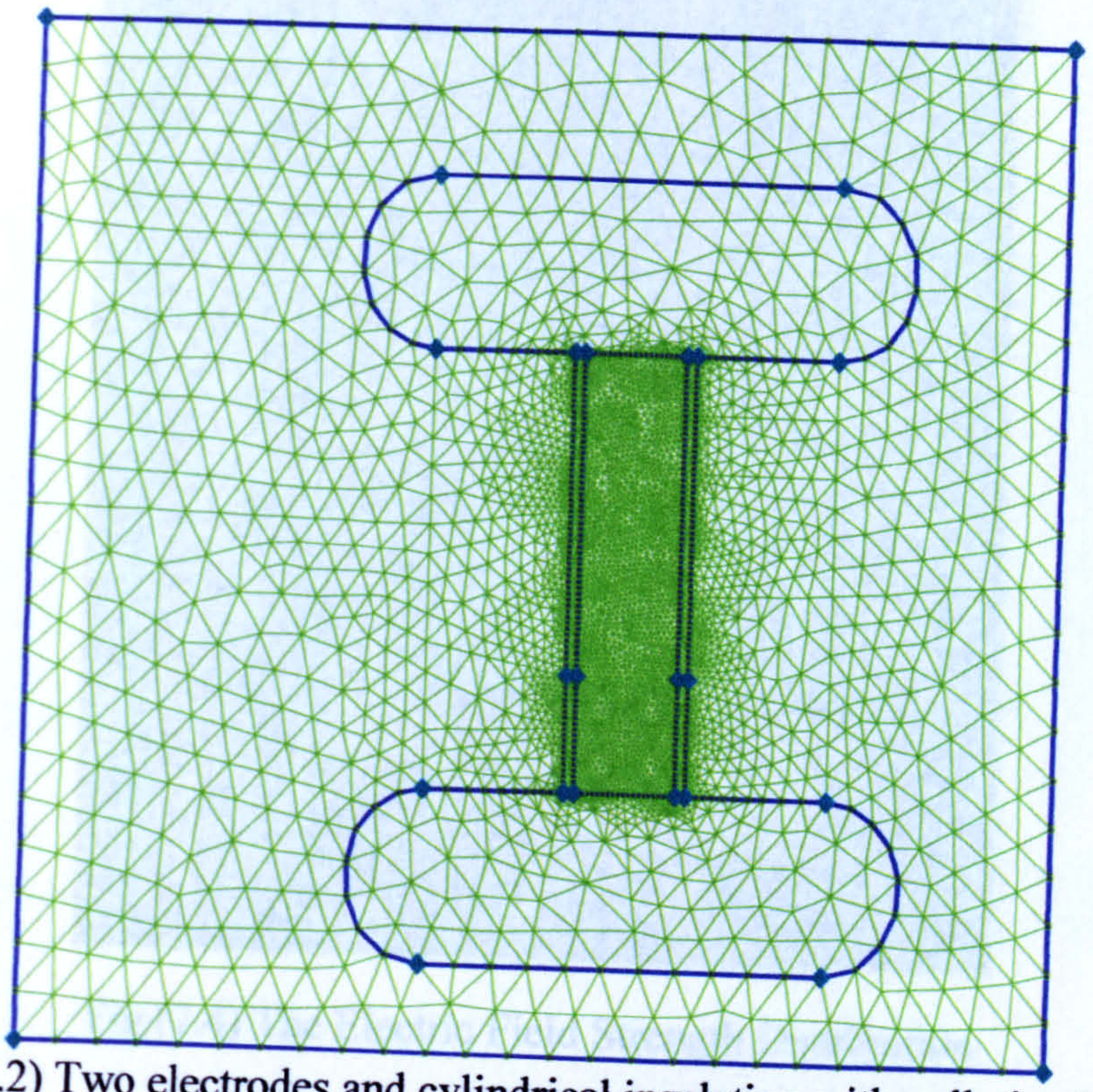

Fig (7.2) Two electrodes and cylindrical insulation with pollution layer

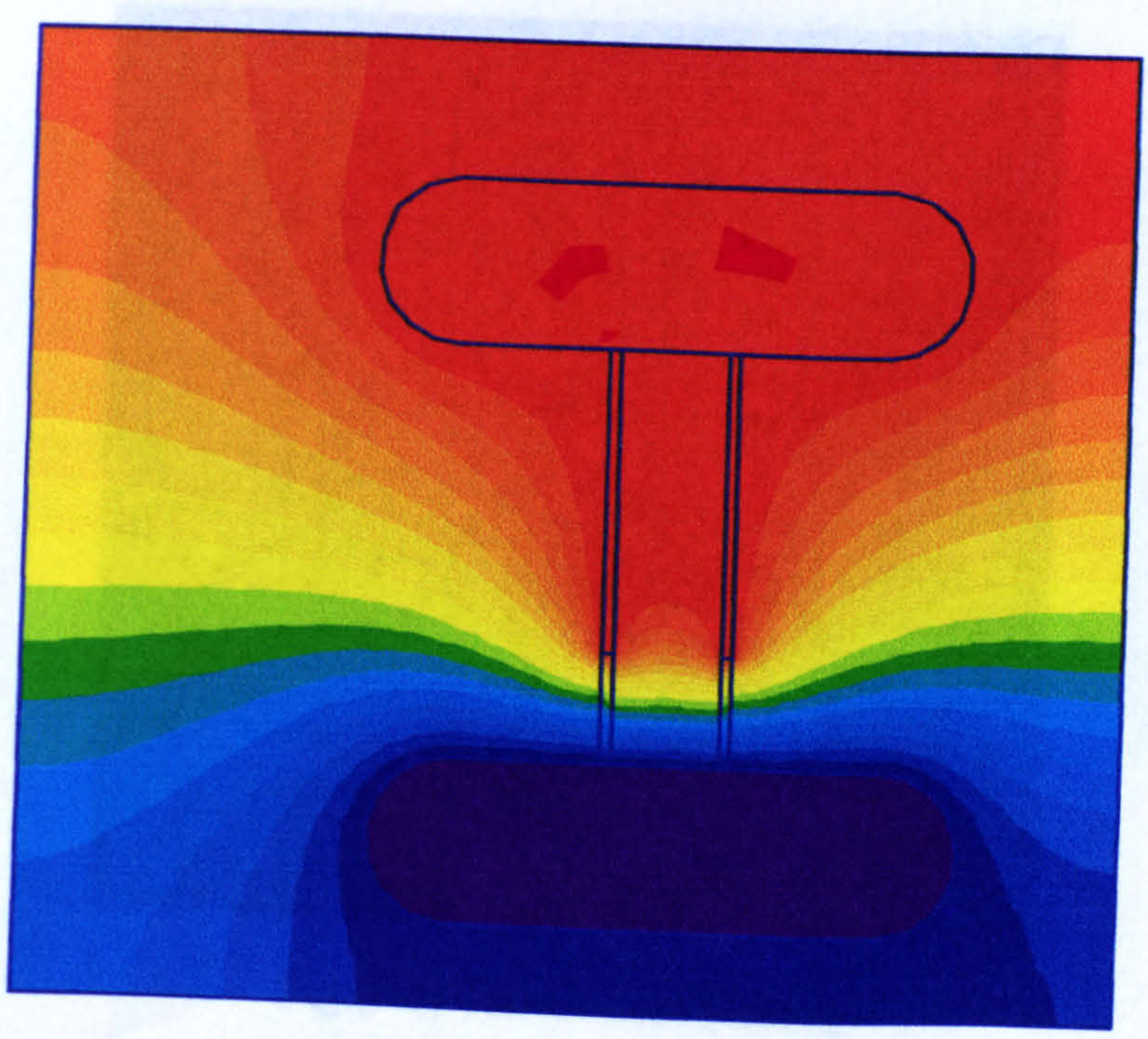

Fig (7.3) The Equipotentials Distribution

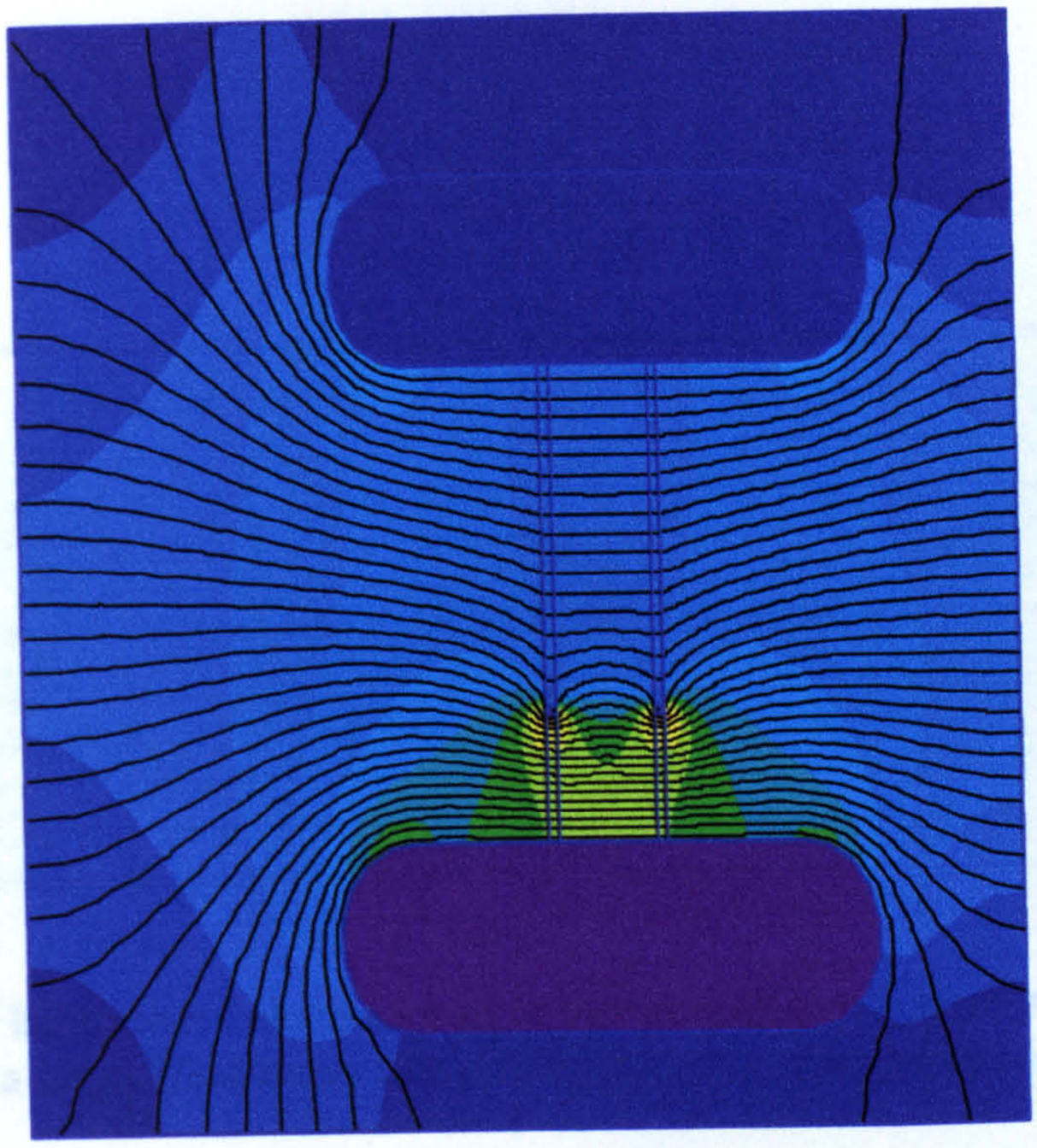

Fig (7.4) The Electric Field Strength Distribution

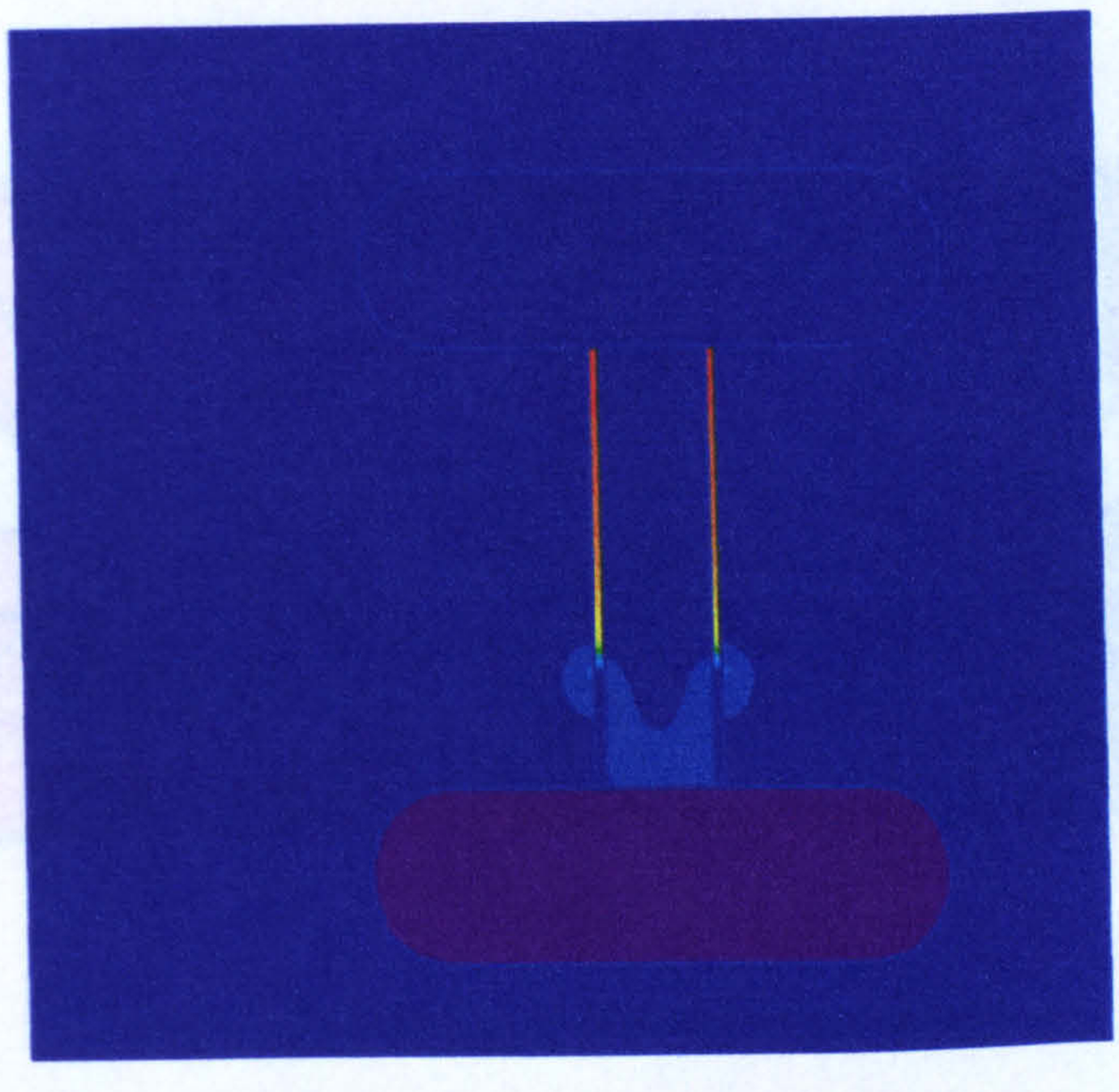

Fig (7.5) The Current Density

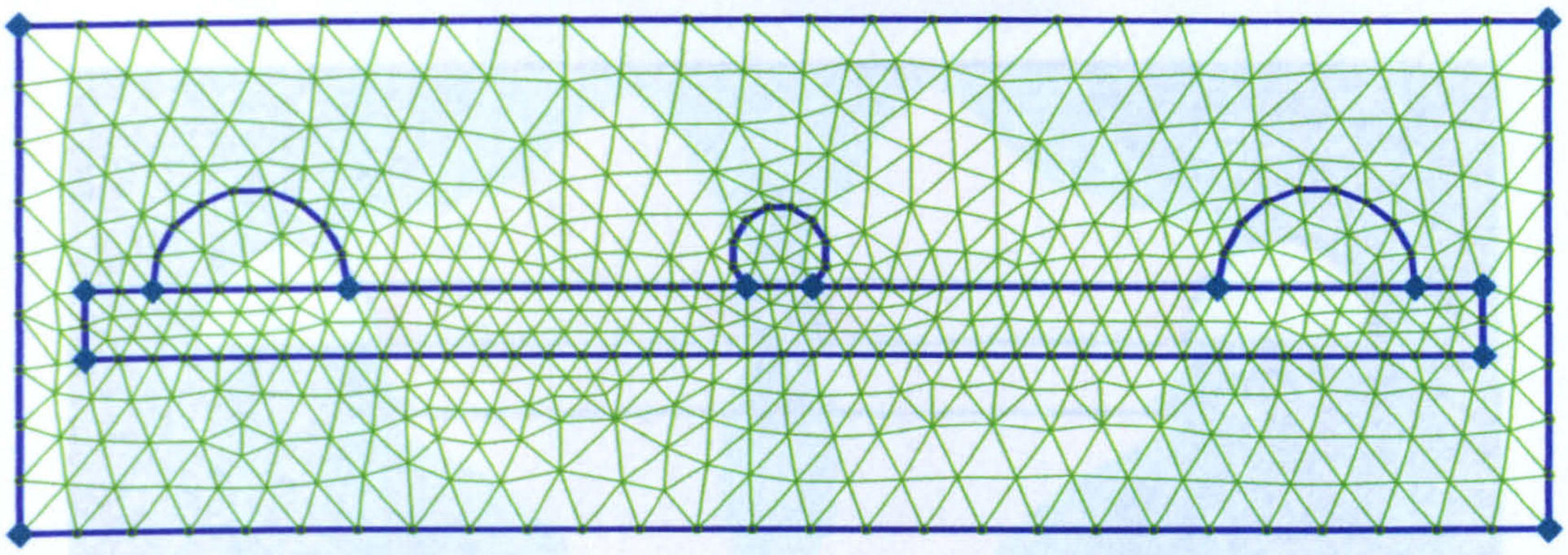

Fig (7.6) Two hemisphere electrodes over the insulation sample and water droplet
Note: a large FEM mesh size shown here for illustrative purposes.

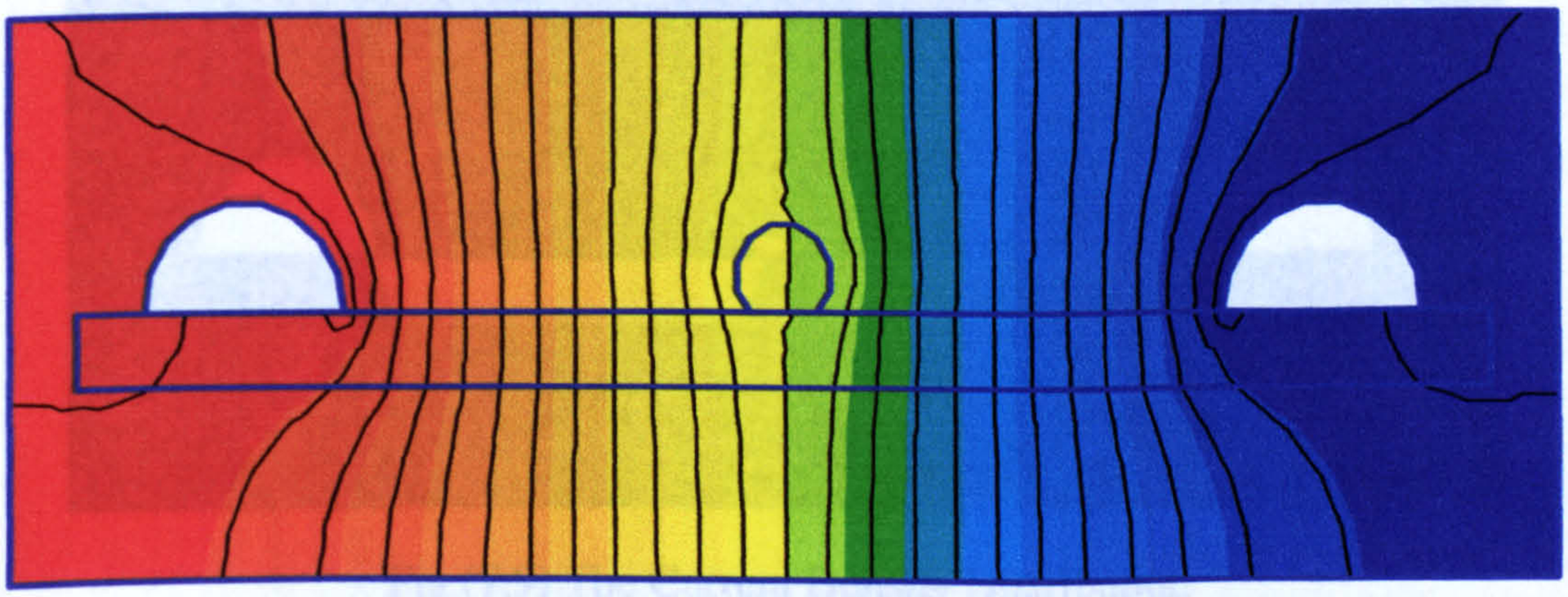

Fig (7.7) The Equipotential Distribution

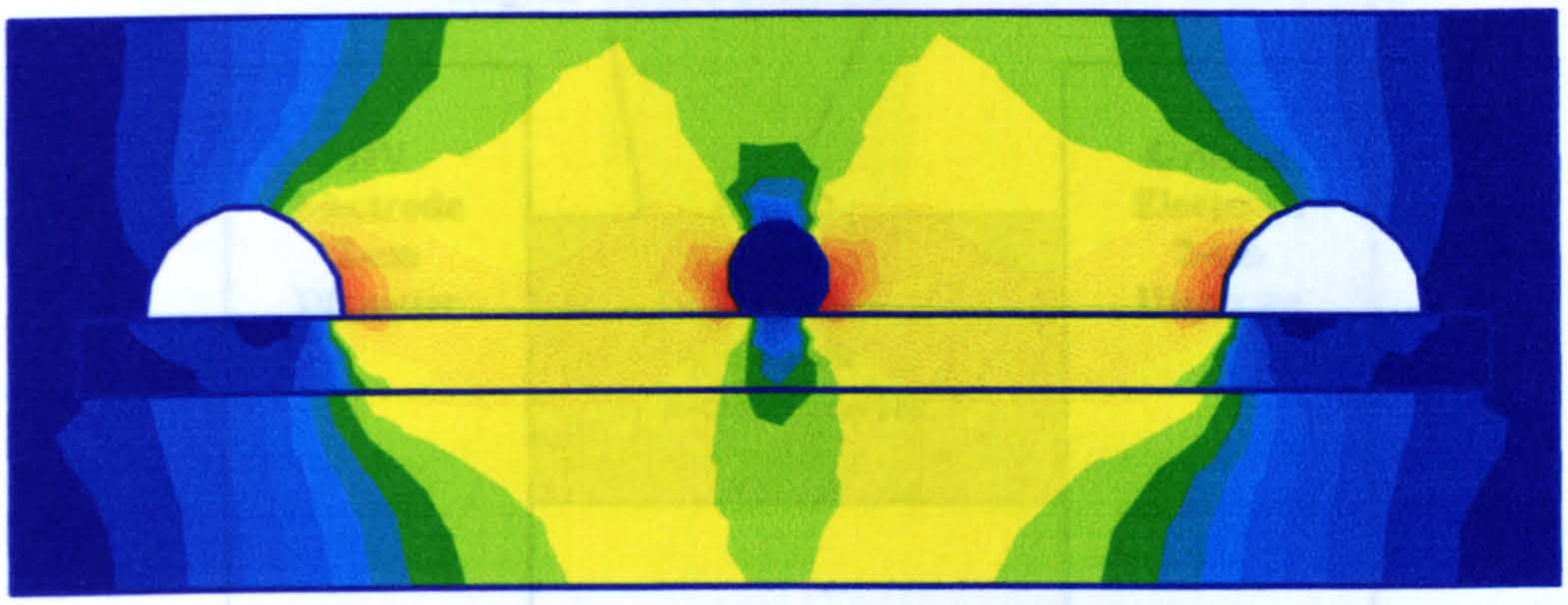

Fig (7.8) The Electric Field Strength Distribution

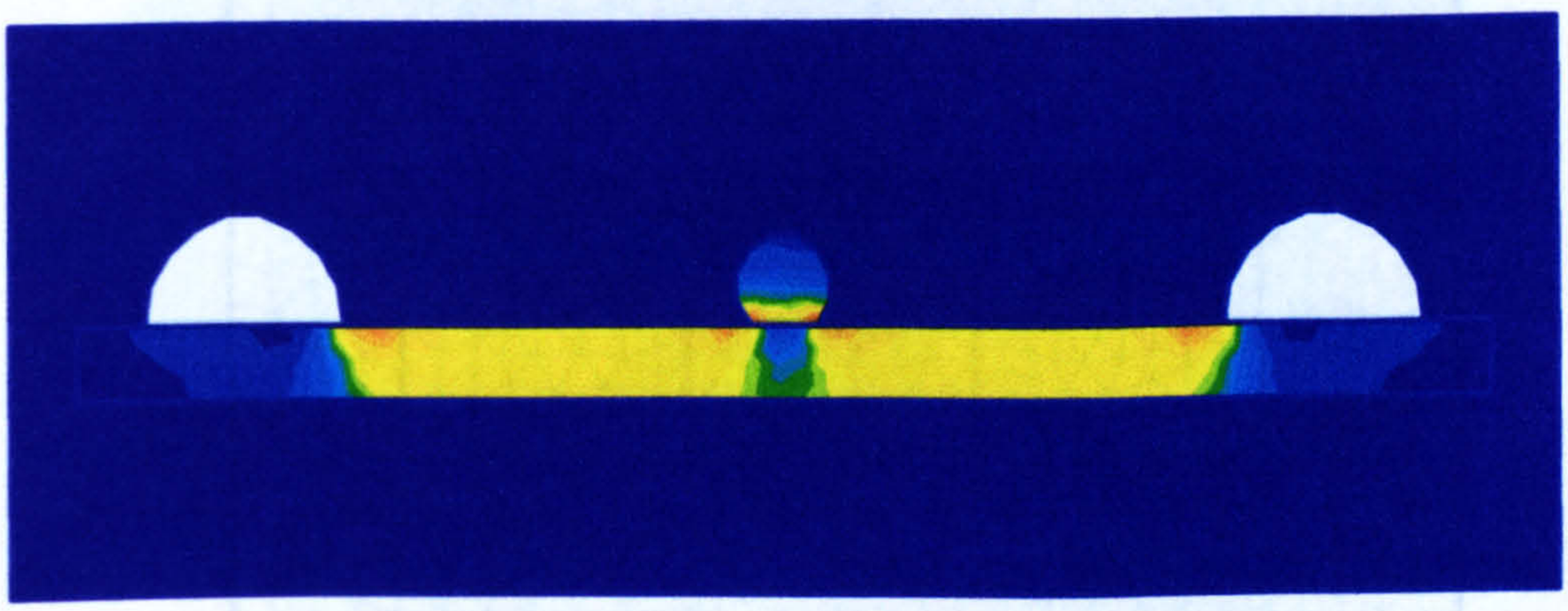

Fig (7.9) The Current Density Distribution

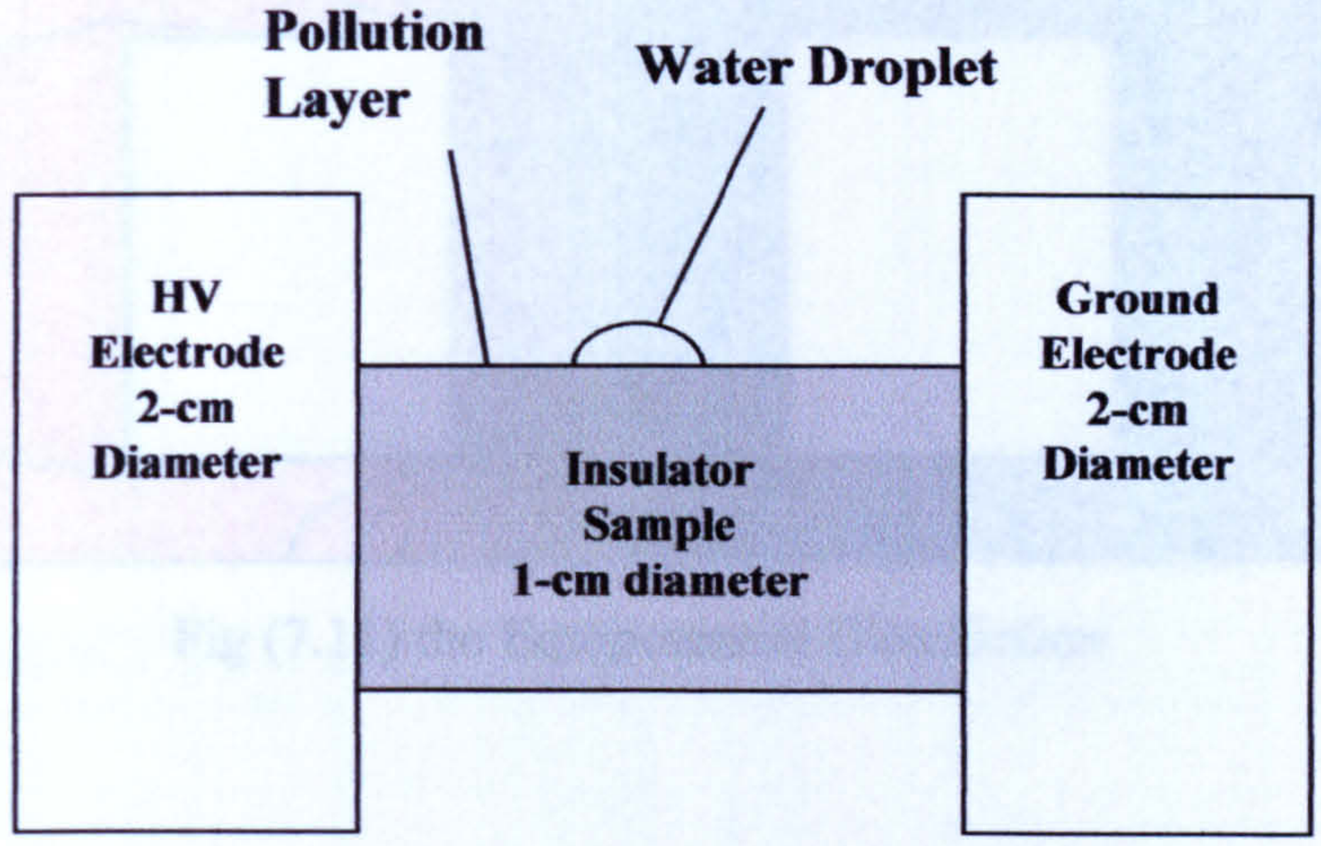

Figure (7.10 a) The Geometry for Initial Model

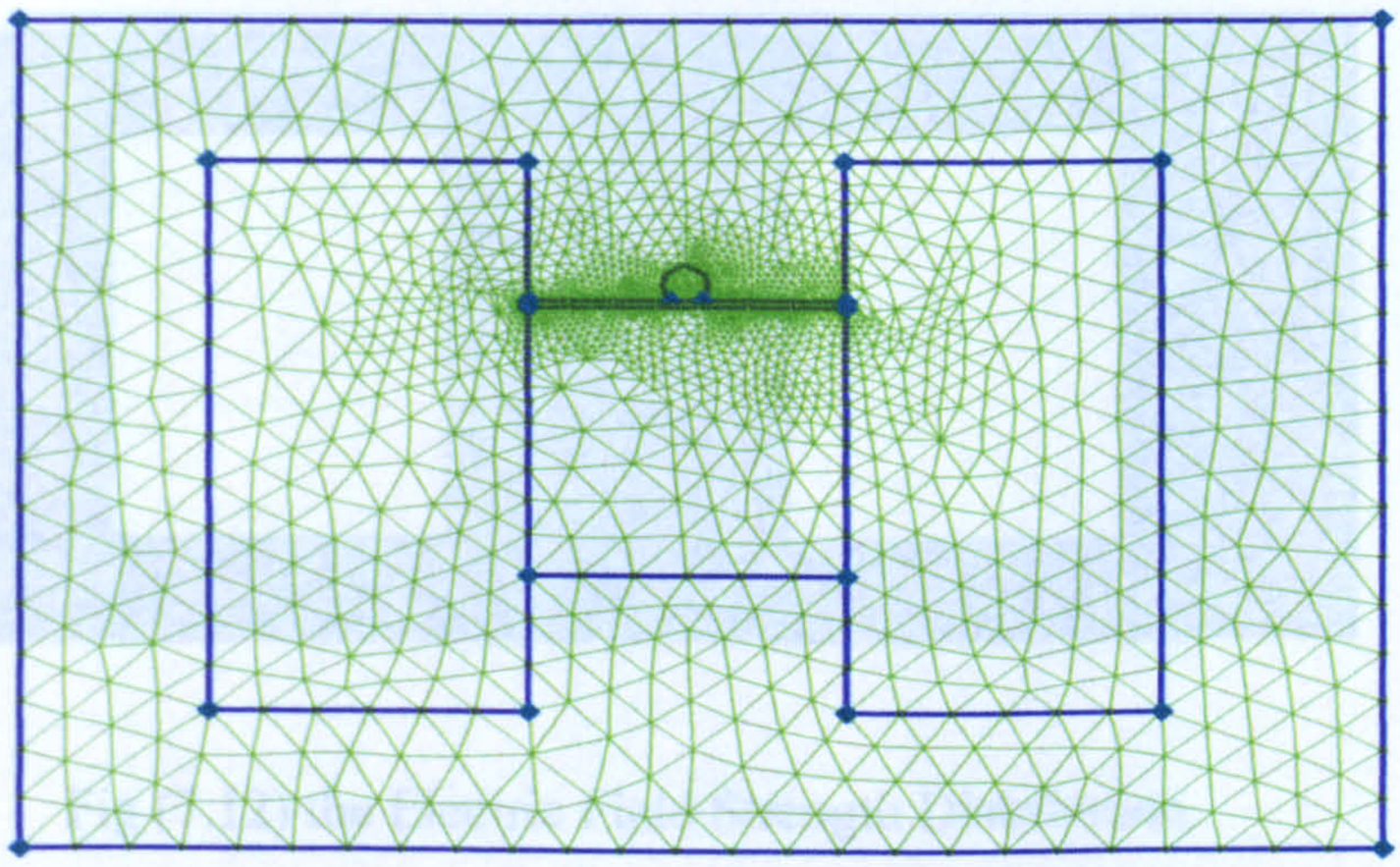

Fig (7.10 b) The mesh Geometry adopted for the FEM calculations showing the variations in mesh size.

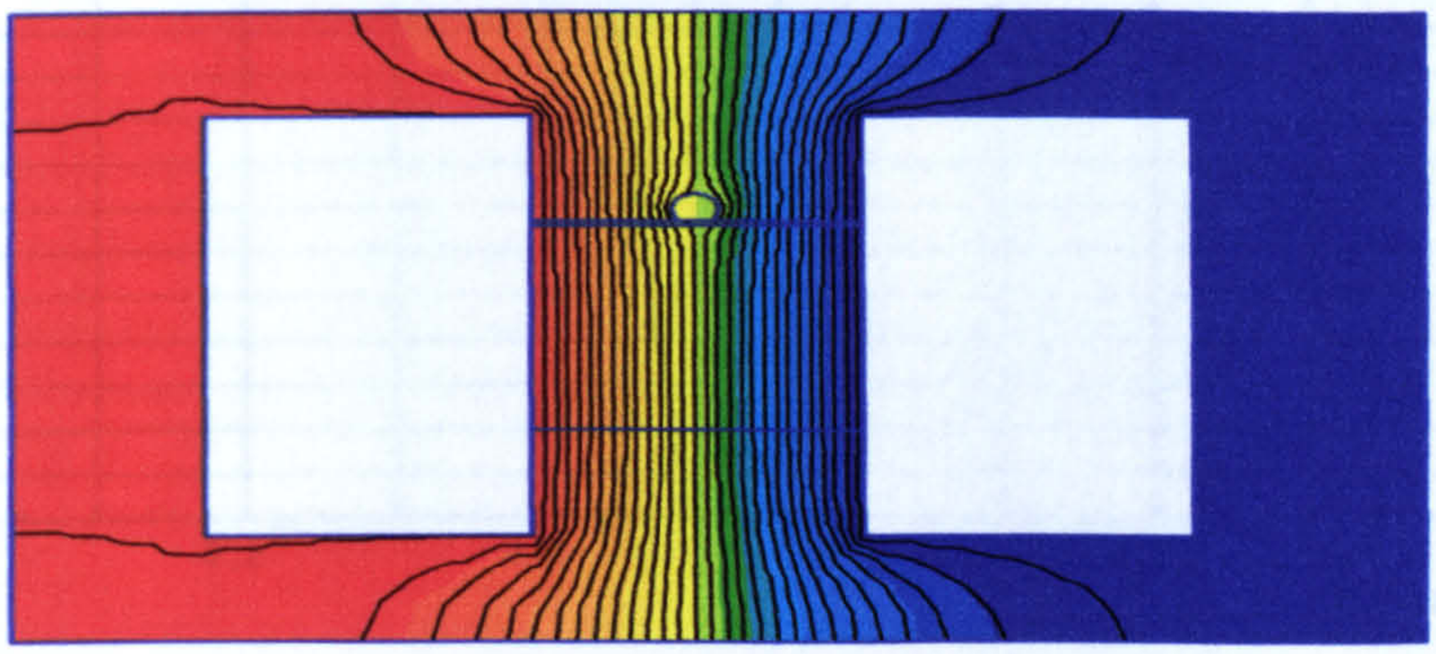

Fig (7.11) the Equipotential Distribution

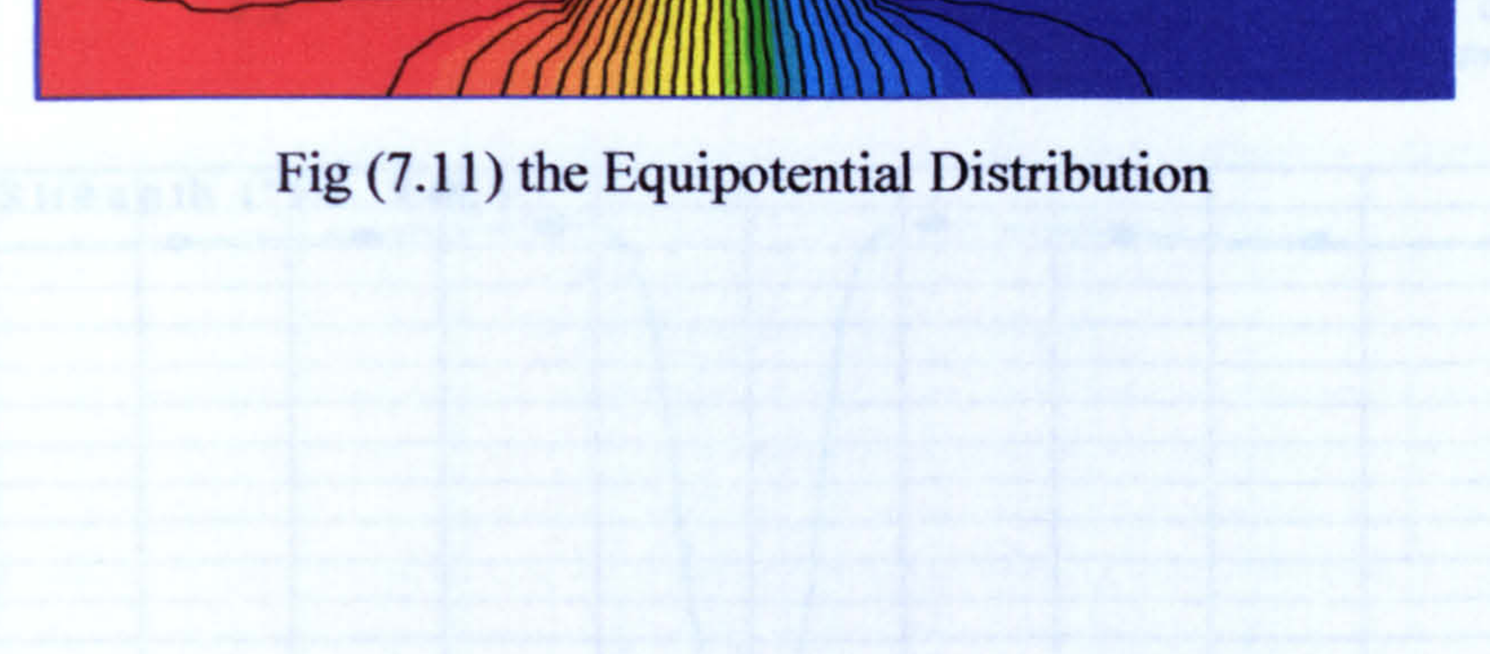

Fig (7.12) the Electric Field Strength Distribution.

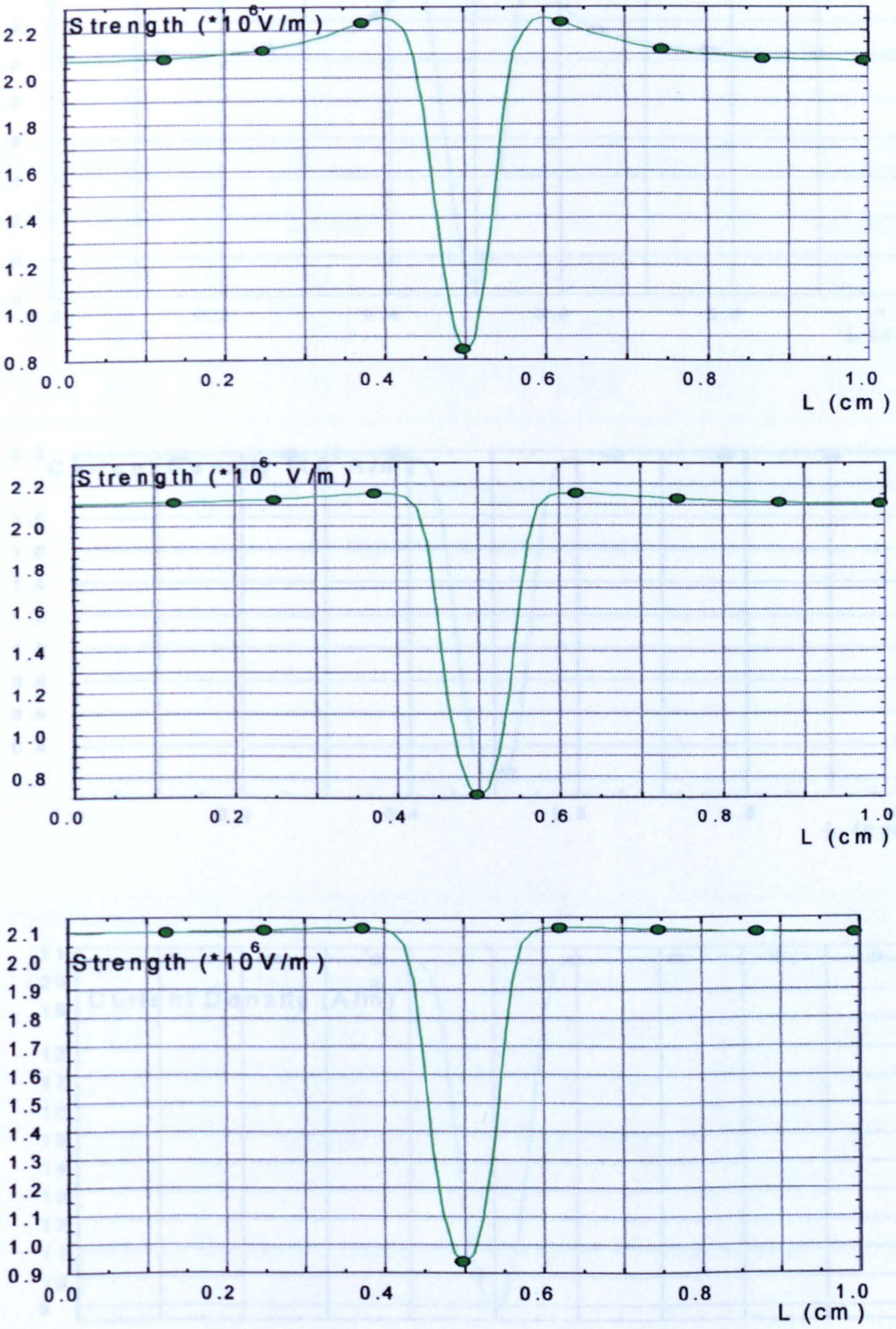

Fig (7.13 A, B and C) the electric field strength along the surface of the insulation sample.

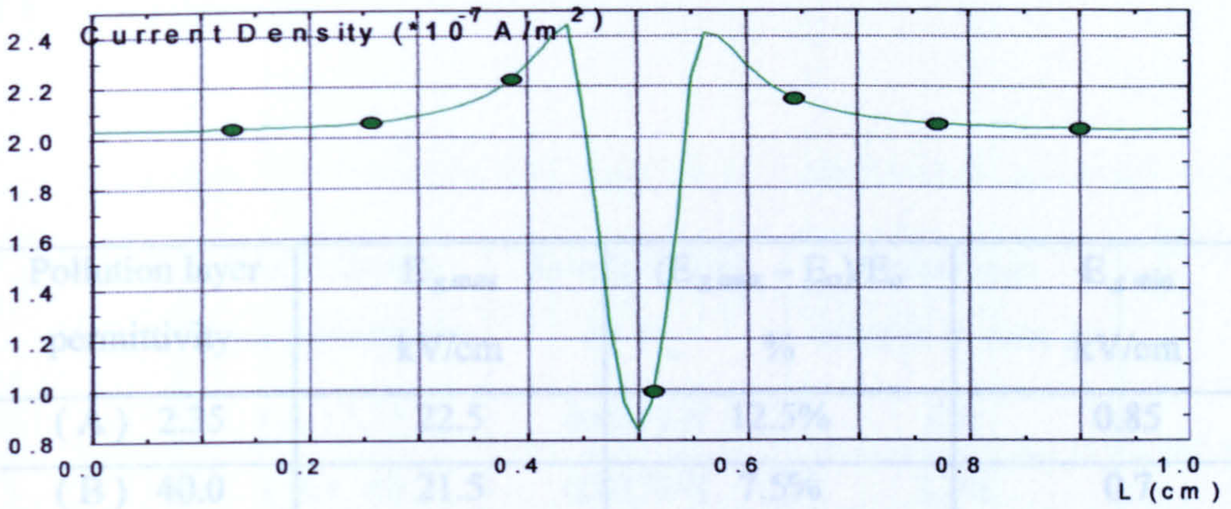

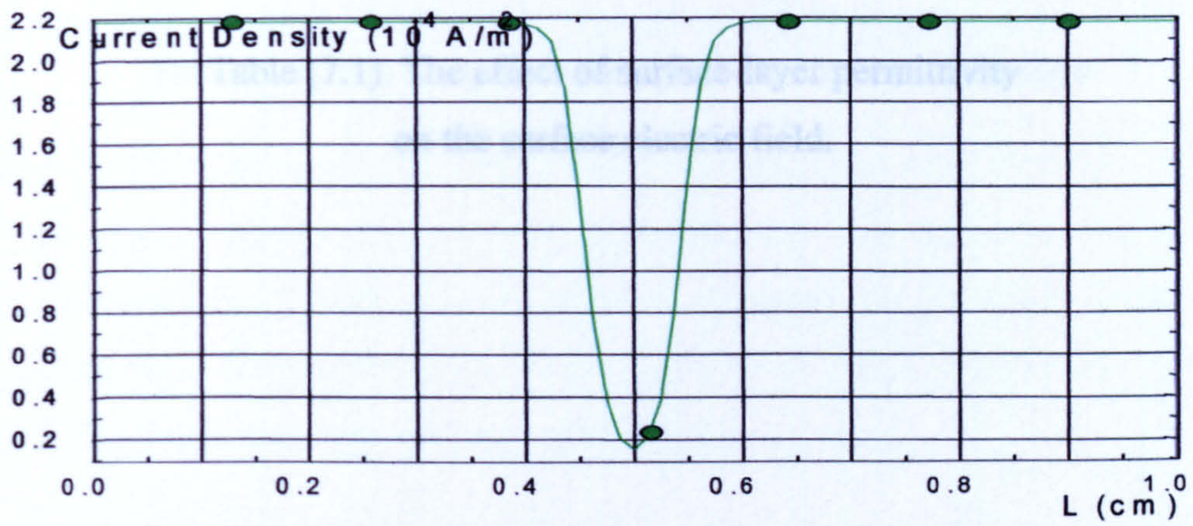

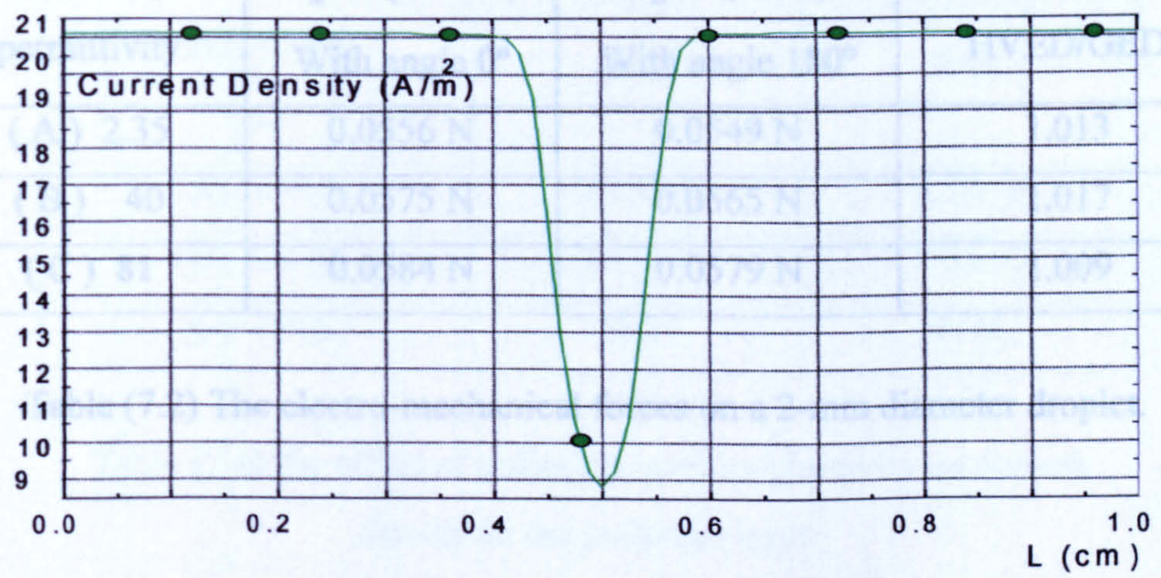

Fig (7.14 A, B and C) the current density along the surface of the insulation sample.

Pollution layer permittivity	$E_{S\,max}$ kV/cm	$(E_{S\,max} - E_o)/E_o$ %	$E_{S\,min}$ kV/cm
(A) 2.35	22.5	12.5%	0.85
(B) 40.0	21.5	7.5%	0.7
(C) 81.0	21.1	5.5%	0.95

Table (7.1). The effect of surface-layer permittivity on the surface electric field.

Pollution layer permittivity	F_m in (HVED) With angle 0°	F_m in (GED) With angle 180°	Ratio HVED/GED
(A) 2.35	0.0556 N	0.0549 N	1.013
(B) 40	0.0575 N	0.0565 N	1.017
(C) 81	0.0584 N	0.0579 N	1.009

Table (7.2) The electro-mechanical forces on a 2-mm diameter droplet.

Wet Pollution layer permittivity	Average value of F_m	Percentage relative to case A
(A) 2.35	0.0553 N	0%
(B) 40	0.0570 N	3.1%
(C) 81	0.0582 N	5.2%

Table (7.3) The computed average electro-mechanical force on a 2-mm diameter droplet..

Pollution layer conductivity Ωm	I_c Maximum A/m^2	I_c Minimum A/m^2
(A) 1e+13	2.45e-7	8.59e-8
(B) 1e+10	2.18e-4	1.53e-5
(C) 1e+5	21.11	8.78

Table (7.4) the effect of pollution layer conductivity on current density in the pollution layer.

7.7 References:-

1- Mukherjee-PK, Ahmed-A and Singer-H, " Electric field distortion caused by asymmetric pollution on insulator surfaces,'' IEEE-Transactions-on-Dielectrics-and-Electrical-Insulation. vol.6, no.2; April 1999; p.175-80.

2- Ahmed-A and Singer-H, " New modelling of the boundary between wet and dry zones on the surface of polluted high-voltage insulators,'' Eleventh International Symposium on High Voltage Engineering (Conf. Publ. No.467). IEE, London, UK; 1999; 5 vol. (xx+368+437+375+384+448) pp. p.35-8 vol.2.

3- Arise-N, Nishioka-H, Okraku-Yienkyi-Y, Otsubo-M, and Honda-C, "Behavior of water droplet on polymer material and the influence on discharge characteristics," 1999 Annual Report Conference on Electrical Insulation and Dielectric Phenomena (Cat. No.99CH36319). IEEE, Piscataway, NJ, USA; 1999; 2 vol. xvii+xiii+833 pp. p.455-8 vol.2.

4- Yamashita-S, Hashiguchi-T, Anamil-N, Otsubo-M, Honda-C, Takenouchi-O, Hashimoto-Y, and Nakamura-M, "Behavior of water droplets and their charged distribution on polymer surface," Proceedings of 2001 International Symposium on Electrical Insulating Materials (ISEIM 2001). 2001 Asian Conference on Electrical Insulating Diagnosis (ACEID 2001). 33rd Symposium on Electrical and Electronic Insulating Materials and Applications in Systems (IEEE Cat. No.01TH8544). Inst. Electr. Eng. Japan, Tokyo, Japan; 2001; xix+901 pp. p.59-62

Chapter 8

Droplet Behaviour at Applied Stress Close to Gap Breakdown

8.1 General

As described in chapter 6, the initial study employed uniform-field, end-electrode geometry to study the behaviour of a water droplet on a 1-cm long, level PE surface and, as described, flashover of the test sample confined these studies to average stresses less than 10kV/cm. After some further experiments with this end-electrode geometry, it was found that at higher stresses this geometry was prone to surface discharge development from the electrodes in the form of what appeared to be surface tracking. Following development of the FEM field modelling techniques described in chapter 7, which allowed quantitative analysis of non-uniform fields, it was decided to examine the use of a non-uniform field, embedded-electrode test arrangement that would have an increased surface path along the PE between the metal electrodes. A design was developed (described below) which allowed average stresses up to 20kV/cm (i.e. 2.0MV/m) to be applied without evidence of surface tracking - at least in the short term over which droplet vibration and PD observations were made. An additional consideration was that embedded-electrode geometry could be used to introduce a significant component of applied electric field normal to the PE surface and so influence – in theory – the development of discharges at the droplet edge. As a further means of varying the field around the edge droplets, it was decided to alter the static contact angle between droplet and insulator surface. This could be done either by varying the droplet by volume and/or by other physical properties (e.g. water conductivity) or simply by inclining the plane of the insulator from the horizontal. Partial discharge activity at the droplet was investigated using a combination of the high-speed video camera, operating at up to 3,000 frames per second, and the electrically-coupled partial discharge detection system described in chapter 5. A key objective was to examine whether the location of partial discharges was primarily along the PE surface or in the air close to the droplet

8.2 Experimental Procedure

The test geometry finally adopted for this part of the study is shown in Fig (8.1). This consisted of a 30-mm long, 20-mm diameter cylinder of solid PE with a flat surface prepared along one side, as described in chapter 5. Two, 10-mm diameter rod electrodes were embedded at right angles through the PE cylinder with their surfaces placed 2mm below the flat surface of the PE cylinder. The axes of the rod were located 20mm apart, leaving a 10-mm gap between them. It was found that voltages up to 20kV could be applied between the electrodes without causing short-term surface flashover across the PE.

During a test run, a single droplet of tap water with resistivity of approximately 10^6 Ωm (conductivity 10mS/m) was placed centrally on the flat surface. For field modelling purposes, relative permittivities of 81 for water and 2.35 for PE were assumed. The conductivity of PE was taken as $1.2 x 10^{-13}$ S/cm. Figure (8.1c) shows the general form computed for the electric field. It can be seen that near the centre of the PE plane surface the electric field has a significant tangential component.

The applied voltage was raised slowly until partial discharge activity was detected by observing the associated voltage pulses, generated across a 100-Ω resistor connected between the low-voltage electrode and ground, on the digital oscilloscope. Vibration and movement of the droplet was recorded using the high-speed video camera operating at up to 3,000 frames per second. In some experiments, the camera was triggered from the voltage pulses generated by the partial discharges.

8.3 Contact Angle on an Inclined Surface

As described in chapter 2, static contact angle is the angle contained by the tangent to the water droplet, at its point of contact with the planar surface on which it is placed, and the plane itself. This angle gives a measure of the hydrophobicity of the

surface when the surface is horizontal. In this part of the study, contact angle was varied by tilting the insulator plane from the horizontal - without, of course, altering surface hydrophobicity. This increased the contact angle at the lowest point of contact between the droplet and the plane surface and decreased it at the highest point - as shown in Fig (8.1b). For ease of reference here, the larger contact angle (at the lower point of contact) is designated "A" and the smaller angle (at the higher point) "B". For example, with the 60° angle of inclination shown in Fig (8.1b), the angle A is ~ 95° and the angle B is ~ 20°. It is clear that the geometry and magnitude of the electric field at the edge of a droplet will be strongly influenced by these different angles.

To determine sensitivity to conductivity, angles A and B were measured to an estimated accuracy of ± 5° for 10-μl droplets of de-ionised, tap and "salt" water (tap water containing 1% saturated sodium chloride solution). The results are shown in Figs (8.2) and (8.3). Deionised water consistently shows the highest values of A and B. For a level surface ($\theta = 0$) the angles A and B are equal (~ 65 ± 5°) and are independent of conductivity. As θ rises to 30°, A increases to 70° (salt), 75° (tap) and 80° (deionised), whereas B shows a decrease to 25° (tap), 35° (salt) and 40° (deionised). As θ rises further from 30° to 40°, the upward trend in A and the downward trend in B continue, except for one case (salt) where A falls to ~ 60°. Beyond $\theta = 40°$, all water types show a downward trend in A with an upward trend in B, although A always exceeds B – as would be expected. A decrease in A might occur with increase in θ if the lower edge of a droplet were to slip down the PE surface to form an increased contact area between droplet and PE. However, it should be noted that no droplet slippage was observed during these tests, although slippage was evident in later studies in which an ac stress was applied (see section 8.4 below). The increase in B at higher values of θ suggests that the surface of the droplet may be developing a double curvature, but this is not clear.

After several further experiments it was concluded that a 10-μl droplet of tap water at an inclination angle of 20° would prove a particularly suitable combination with which to examine behaviour under AC stress. This combination gives A ~ 75° and B ~ 40°, ensuring different electric field conditions at each side of the droplet, whilst

avoiding the high values of θ at which droplet slippage might be occurring. These tests also confirmed that droplets remained static for at least one hour when no electrical stress was applied, showing no tendency to move down the insulator surface.

8.4 Drop Movement Caused by High AC Stress

Fig (8.4) presents frames recorded with the digital camera. The first frame shows a 10-μl, tap-water droplet with the PE surface inclined at 20° the horizontal. With zero applied voltage the droplet remained static. With the upper electrode grounded and a 50-Hz voltage applied to the lower electrode, the onset of vibration was observed at 8.6 kV (E_0= 2.9kV/cm). With the camera operating at 3,000 frames per second, sequences of frames were recorded that show the droplet vibrating at 50Hz at the onset voltage. Fig (8.4, 2 to 6) are selected from these at 5ms intervals over a period of 20ms – i.e. covering one complete cycle. These frames show that at the onset voltage the droplet does not slip down the surface. However, it does become distorted, with wave-like undulations appearing on its surface. Fig (8.4, 7 to 12) shows a set of 5 records obtained with the applied voltage raised to 11.85 kV (E_0= 3.95kV/cm). These frames cover a period of about one minute and show the lower edge of the droplet slipping down the PE surface while the upper edge remains fixed. Similarly, frames (13 to 18), obtained at an applied voltage of 14.8 kV (E_0= 4.95kV/cm), show that the complete droplet eventually flows down the surface to accumulate at the lower end of the PE. In the complete video sequence, vibration and spreading of the water droplet over the whole sample can be observed.

Figure (8.5, frames 1 to 15)) were recorded after the water droplet accumulated at the lower end of the PE sample and the applied stress was raised to 17.2 kV (i.e. E_0= 5.75kV/cm). These 16 frames are 2ms apart in time and so extend over 1.4 cycles. Breakdown and arc formation can be seen twice during a cycle and appear around the voltage maxima. At this high voltage, the insulation sample was permanently damaged as soon as arc breakdown occurred, with visible evidence of extensive tracking along its surface (see Fig (8.6)).

For comparison purposes, the behaviour of a salt-water droplet was examined (i.e tap water containing 1% saturated sodium chloride solution). The volume of the droplet was 10μl, as in the previous case, but the water conductivity was ~10 S/cm. Typical video camera records are shown in Fig (8.7). Frames 1-6 show activity over a half cycle at an applied voltage of 8.5kV. The droplet is static with no evidence of movement down the PE surface. In frame 3, a discharge is visible at the upper edge of the droplet. This discharge is evidently not along the PE surface, but is more consistent with one extending along a field line from the conducting surface of the droplet into the surrounding air. At an applied voltage of 12.5 kV, frames 7 to 18 of Fig (8.7) show the typical discharge activity recorded after a droplet has moved down the surface of a PE sample. These frames record arc discharges forming twice over a complete cycle. For each stage of droplet behaviour, the values of applied voltage for tap and salt water are similar. The values of average applied field found here are comparable with those reported in previous studies (see chapter 3 table 3.2).

The consistent pattern found in the present work is that water droplets first vibrate, then, as voltage is raised, edge discharges become visible with the video camera and finally, as the voltage is further increased, droplets move to the lower end of the PE surface. Following this, flashover is usually observed to follow, with permanent damage to the sample.

8.5 Partial Discharge Activity

To examine PD activity in more detail, 10-μl, tap-water droplets were located in the middle of the flat portion of the insulation sample and then partial discharges observed in two ways: (1) electrically and (2) visually - using the video camera.

8.5.1 Electrically detected partial discharges

Horizontal Surface. Figure (8.8) shows the electrically-detected PD activity generated by the system in the absence of a water droplet. The inception voltage for

such activity was found to be 8.25kV (E_0= 2.75kV/cm) and discharges were observed on both half cycles close to the peak of the applied voltage waveform as previously described in chapter 6. Over a period of several hours, the presence of discharges of this magnitude did not appear to damage the dry PE sample nor lead to breakdown when sustained for longer periods.

When a 10-μl, tap-water droplet was placed midway between the electrodes on the flat section of a horizontal PE sample, it was observed that surface partial discharge activity at the edges of the droplet was initiated when the applied voltage was raised to 11.7kV(i.e. E_0= 3.9kV/cm). Figure (8.9) shows a typical record under these conditions. The magnitude of this PD activity is of the order of 10 to 20 times greater than that observed without a droplet present. The amplitude of the PDs in the negative half cycle were observed to be higher than those in the positive half cycle, although the droplet was placed centrally on the sample surface. Optical observation showed that the sessile droplet was static and did not vibrate.

When the applied voltage was increased to 14.25 kV (i.e. E_0= 4.75kV/cm), the water droplet was observed to vibrate but without spreading. With the voltage raised to 16.8 kV (i.e. E_0= 5.6kV/cm), the droplet was observed to vibrate vigorously and then spread over the surface of the insulator. The measured PD activity at 16.8 kV is shown in figure (8.10). The peak magnitude was typically 25 times above the level observed without a water droplet. As before, PD activity was more pronounced during the negative half cycle. Under these conditions, the motion of the water droplet along the surface of the supporting insulator eventually lead to total breakdown along its surface.

The above observation that water droplets on a horizontal surface spread at an E_0 of the order of 6kV/cm is consistent with previous studies - see chapter 3 table (3.2) - and with the preliminary experiments described in chapter 6.

Inclined Surface. For the sample inclined at an angle of 20° to the horizontal, the partial discharges measured are shown in Figures (8.11) to (8.14).

Figure (8.11) shows the PD activity generated by the system when no water droplet was present on the surface of the sample. The inception voltage was 8.3 kV (i.e. E_0= 2.76 kV/cm) and discharges were observed on both half cycles close to the peak of the applied voltage waveform. As would be expected, this is nearly identical with the activity found for horizontal samples and, as in that case, the discharges do not appear to damage the sample nor lead to breakdown if allowed to continue for a period of time.

When a water droplet was placed midway between the two electrodes it was observed that partial discharge activity at the edges of the droplet was initiated when the applied voltage was raised to 9.6kV(i.e. E_0= 3.2kV/cm). This is significantly lower than the value of E_0= 3.9kV/cm found with the horizontal surface. Figure (8.12) shows the typical PD record obtained under these conditions. Again, the magnitude of PDs in the negative half cycle appears to be larger than in the positive half cycle. The magnitude of this negative PD is some 15 times greater than that observed without the presence of the droplet. As with the horizontal case, optical observation showed that the sessile droplet was static and did not vibrate.

In Fig (8.13), When the applied voltage was increased to 11.95 kV (i.e. E_0= 3.78kV/cm), the water droplet was observed to vibrate but without spreading. Analysis of video records showed that the vibration frequency was 50 Hz. With the voltage raised to 14.67 kV (i.e. E_0= 4.89kV/cm), the droplet was observed to vibrate vigorously and then spread down the surface of the insulator. Over a period of a few minutes, the water was observed to accumulate at the lower electrode.

The measured PD activity at 17.2 kV (i.e. E_0= 5.4kV/cm) is shown in figure (8.14). The peak magnitude was typically 10 times above the level observed without a water droplet. As before, PD activity is more pronounced during the negative half cycle. Under these conditions, the motion of the water droplet along the surface of the supporting insulator eventually leads to total breakdown along its surface.

From these observations it can be seen that drop vibration and spreading takes place at lower applied fields on the inclined surface. It is considered that this may be because the shape of the electric field around the droplet changes when the surface is inclined. This question will be examined further in the next chapter.

8.5.2 Visual observation of partial discharges

Horizontal surface. Fig (8.15) shows discharges recorded at the edge of a 10-μl, tap water droplet deposited at the centre of a horizontal PE surface. Frames 1 to 3 were obtained at an applied voltage of 14.25 kV (E_0= 4.75kV/cm) and show partial discharge activity at the edges of the water droplet. For frames 3 to 8, the applied voltage was increased to 16.8 kV (E_0= 5.6kV/cm). Here the water droplet vibrated and expanded, and the visible partial discharge activity increased. Frames 9 to 12 were recorded with the applied voltage was increased to 17.2 kV (E_0= 5.7kV/cm). Here, the partial discharge activity at the edges of the water droplet was very clearly observed and of higher visible intensity than that observed in frames 1 to 8. The surface of the PE was damaged following the occurrence of these stronger discharges increased, as shown before in fig (8.6). In the complete video sequence, droplets were observed to vibrate and eventually spread over the whole sample. A wave-like vibration mode developed along the spread-out droplet before complete electrical breakdown took place. Using the methods described previously in section (6.3.2), the frequency of these vibrations was found to be 50 Hz.

It is interesting to note that the location of these discharges is not along the PE surface but is in the air at the side of the droplet and, in this respect at least, appears to be similar to the observations reported recently (2001) by Krivda and D. Birtwhistle (see chapter 3, reference [14]).

Inclined surface. Partial discharge activity was also examined using the video camera with samples inclined at 20° to the horizontal plane. Similar to the conditions described in sections 8.4 and 8.5 above. Typical results are shown in fig (8.5). As might be expected, water droplets spread faster, probably through gravity, and move

quickly to the lower electrode. This activity is immediately followed by complete flashover and the breakdown across the sample with significant damage to surface. In all cases of an inclined sample, the onset of partial discharge activity, vibration and spreading was observed using the video camera and was found to be at a lower applied stress than with horizontal samples. As noted above in section 8.5.1, this effect may be due to the change in shape of the inclined droplet and with the associated change in the shape of the electric field surrounding a droplet.

A preliminary account of this work was published in the 37th international Universities Power Engineering Conference 9th – 11th September 2002, School of Engineering and Advanced Technology, Staffordshire University in a paper entitled: "Sessile Water Droplets on Insulating Surfaces Subject to High AC Stress: Effect of Contact Angle".

8.6 Discussion

The above experimental study initially identified that a 10-µl droplet of tap water on a PE surface inclined at an angle of 20° was a particularly suitable combination with which to examine behaviour under AC stress. This combination produces different electric field conditions at each side of the droplet but avoids droplet slippage when no field is applied - in fact droplets remained stationary for at least one hour with no stress applied.

Following the application of ac stress, 50-Hz vibration of the water droplet was first observed and then followed, with increased applied stress, by spreading and movement over the insulation surface with the droplet eventually moving down the inclined surface to accumulate at the lower electrode. After this, surface flashover and breakdown were observed which permanently damaged the insulation surface.

Before spreading of the droplet, partial discharge activity was detected both electrically and optically at the edges of water droplets. The optical results show the discharges are not confined to the PE surface but are located in the air near the locus of contact between the droplet and the surface. This effect is evident with the inclined

surface and is presumably associated with the different upper and lower contact angles between drop and surface and the associated changes in the local electric field. It is considered that this observation should be more closely examined because the location of the discharge and its influence on surface hydrophobicity is likely to affect the process of droplet spreading and movement. This idea is examined in the following chapter.

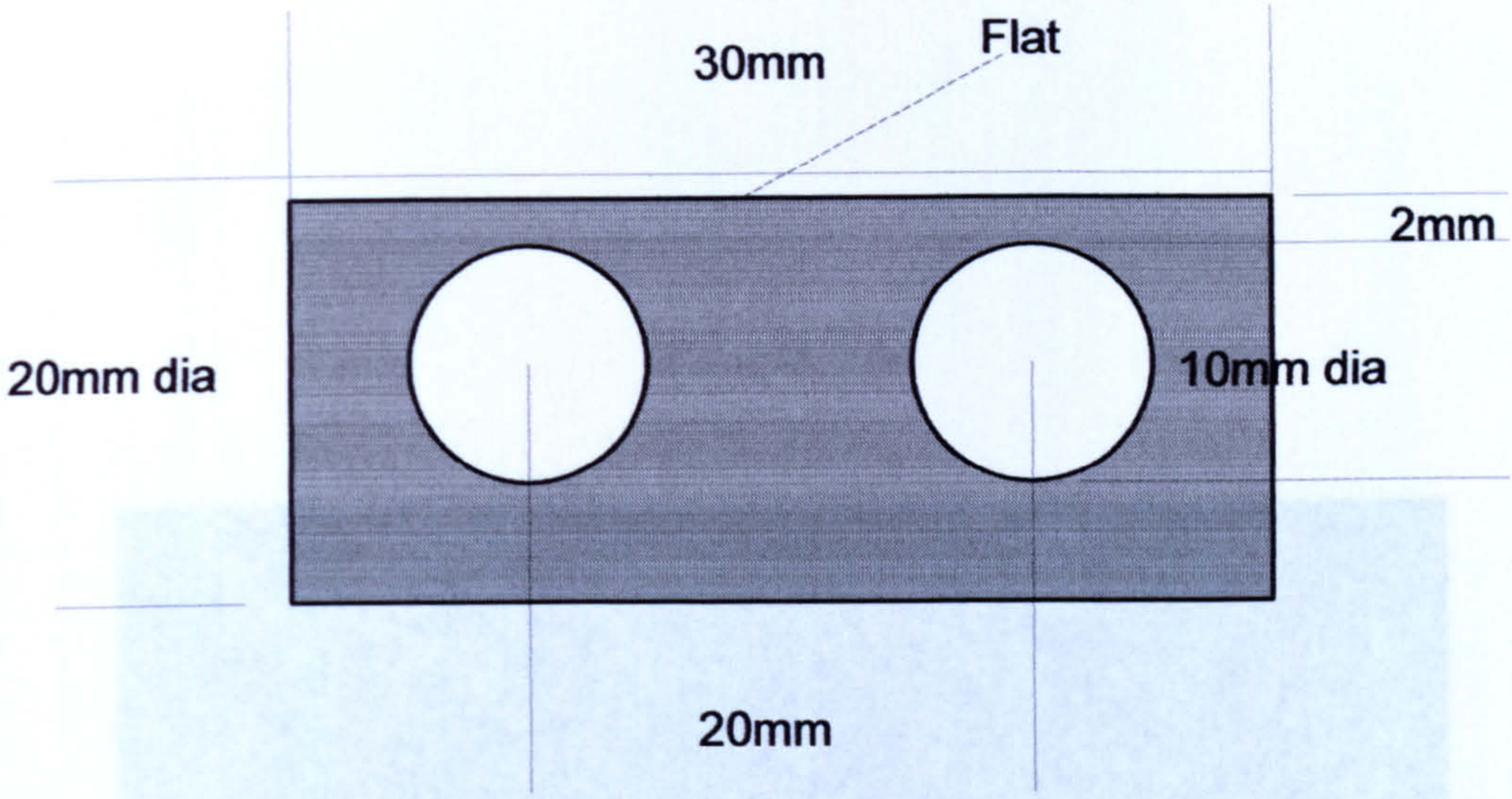

(a)

(b)

Fig (8.1 a and b) (a) Embedded-electrode geometry
(b) A 10μl water droplet on the embedded- electrode sample inclined at an angle 60°. Note difference between upper and lower contact angles.

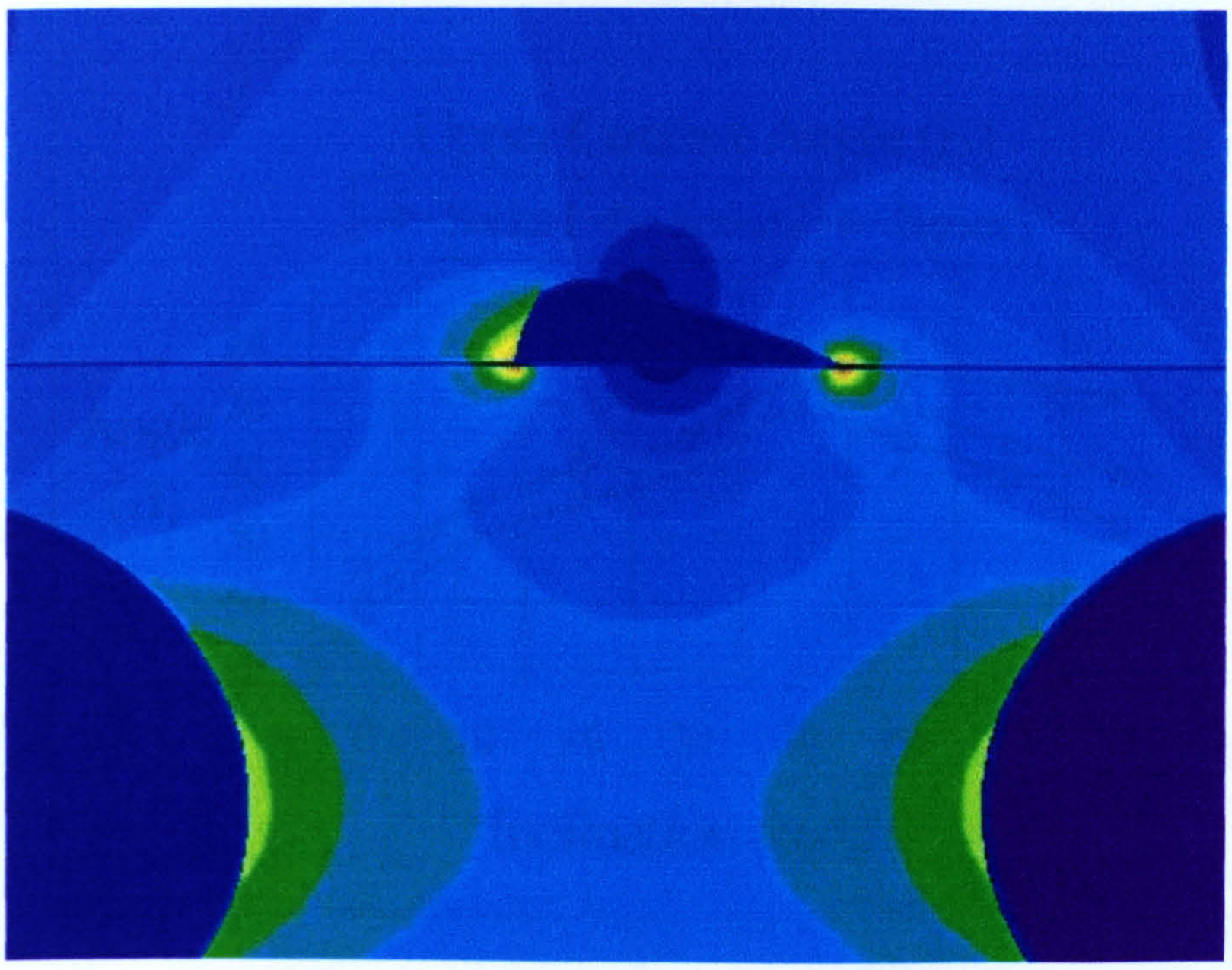

Figure (8.1c). The computed equipotential distribution for the embedded-geometry. It can be seen that the surface the electric field has a significant tangential component.

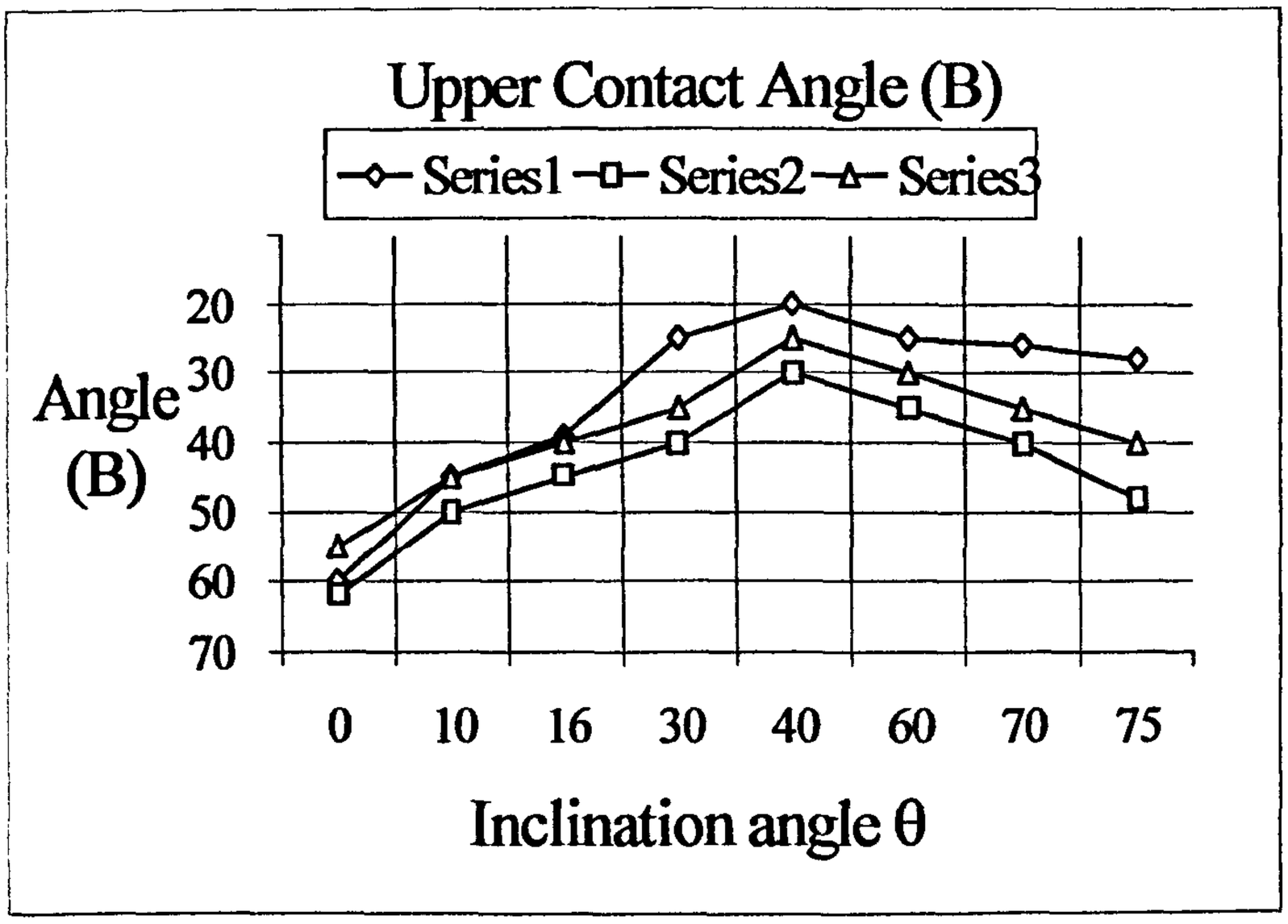

Fig (8.2) Upper Contact Angle B.
◊-Tap water, Δ -Salt water, □-Deionized water.

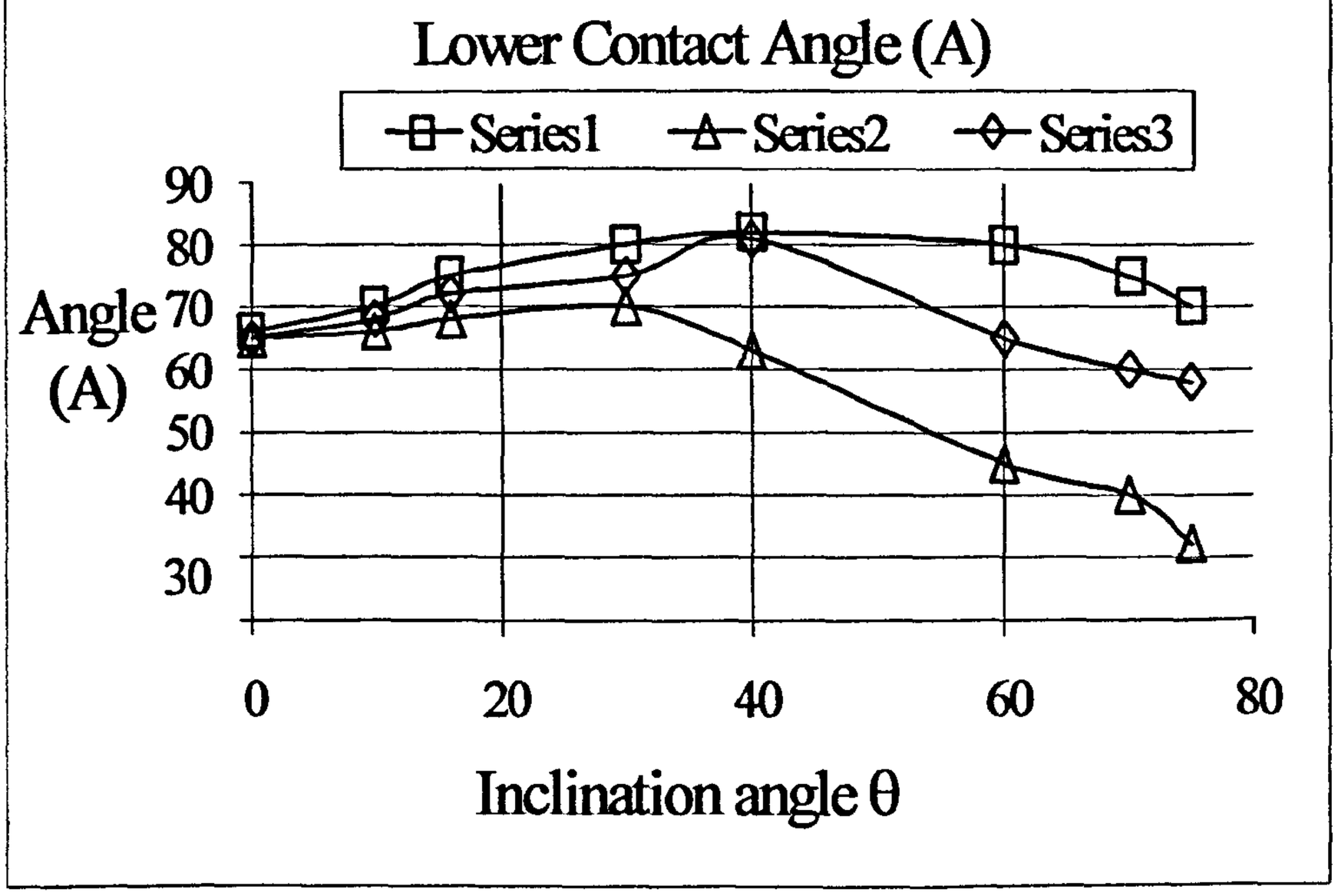

Fig (8.3) Lower Contact Angle A.
◊-Tap water, Δ -Salt water, □-Deionized water.

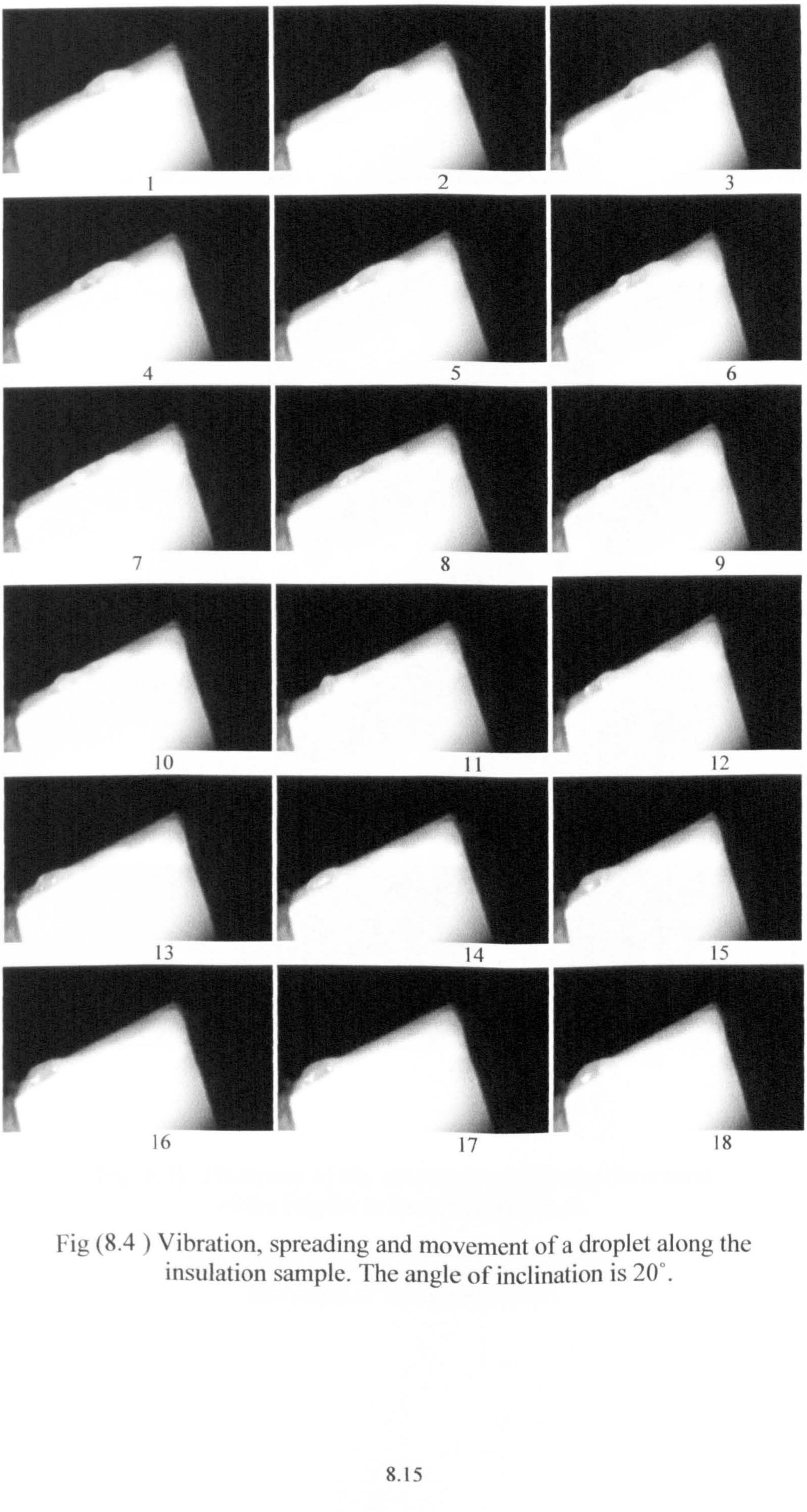

Fig (8.4) Vibration, spreading and movement of a droplet along the insulation sample. The angle of inclination is 20°.

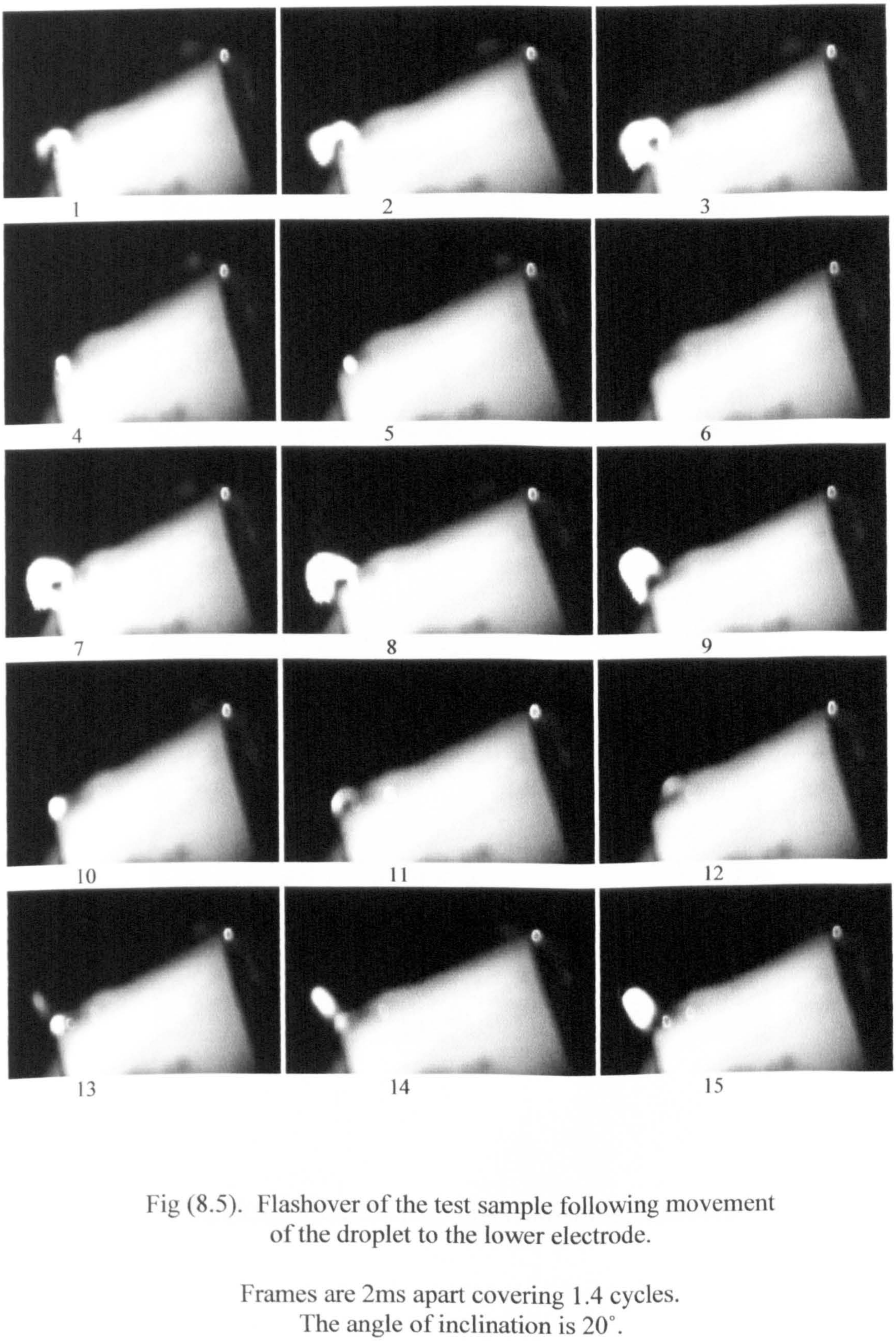

Fig (8.5). Flashover of the test sample following movement of the droplet to the lower electrode.

Frames are 2ms apart covering 1.4 cycles.
The angle of inclination is 20°.

Fig (8.6) Typical damage to a sample after flashover.

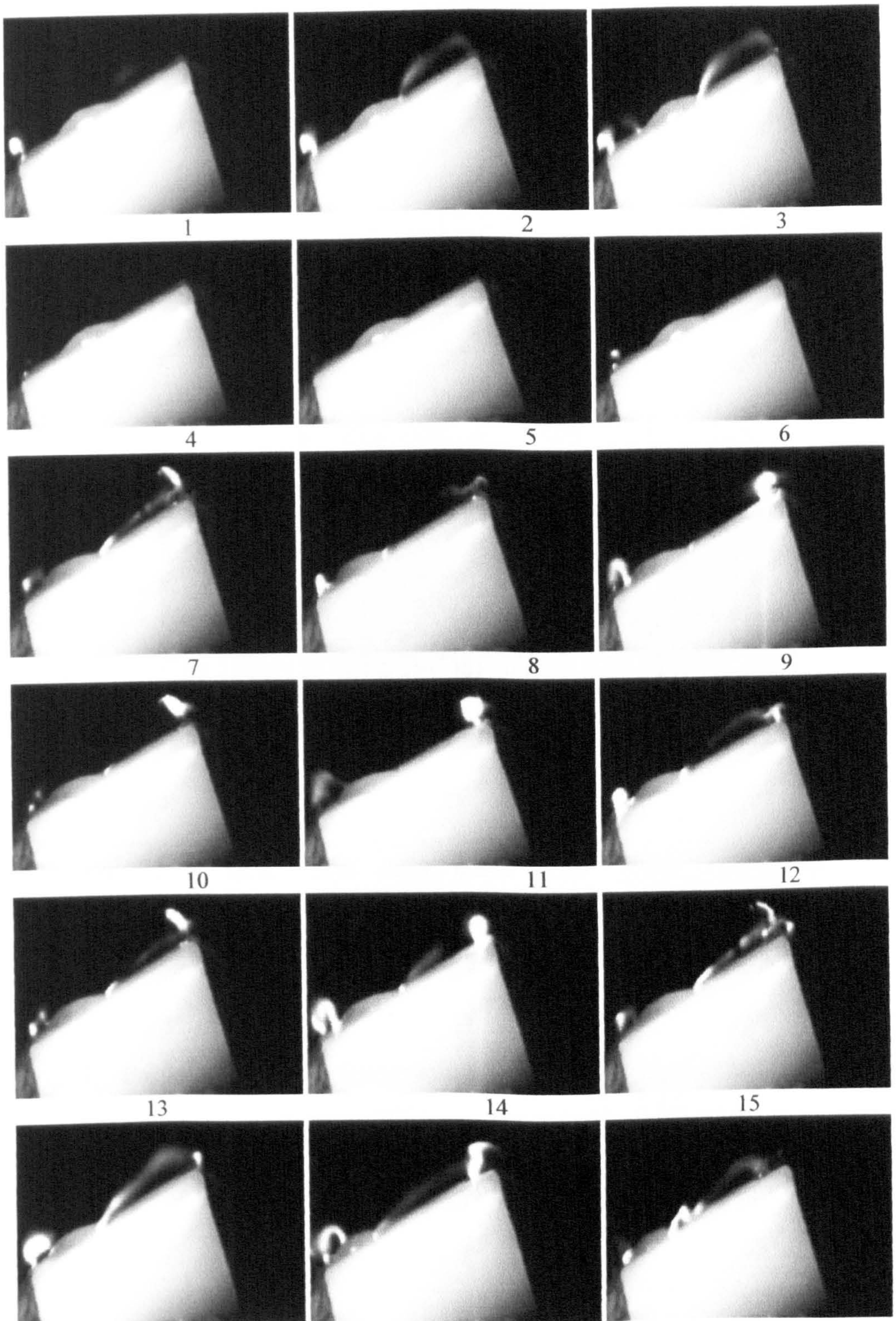

Fig (8.7) Movement of the salt water droplet along the insulation sample.
The angle of inclination is 20°.

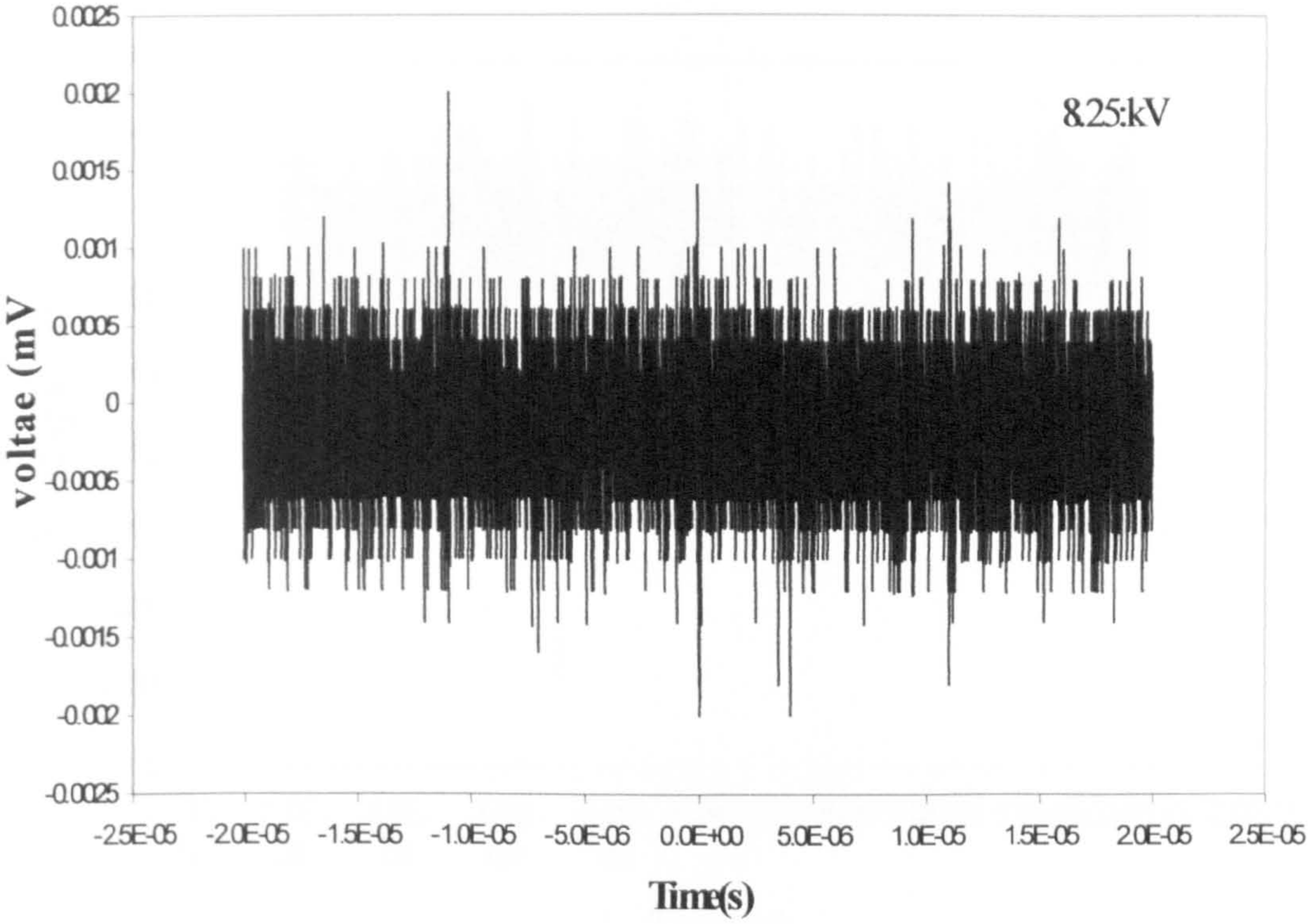

Fig (8.8) Partial discharge activity with no water droplet present. Level surface

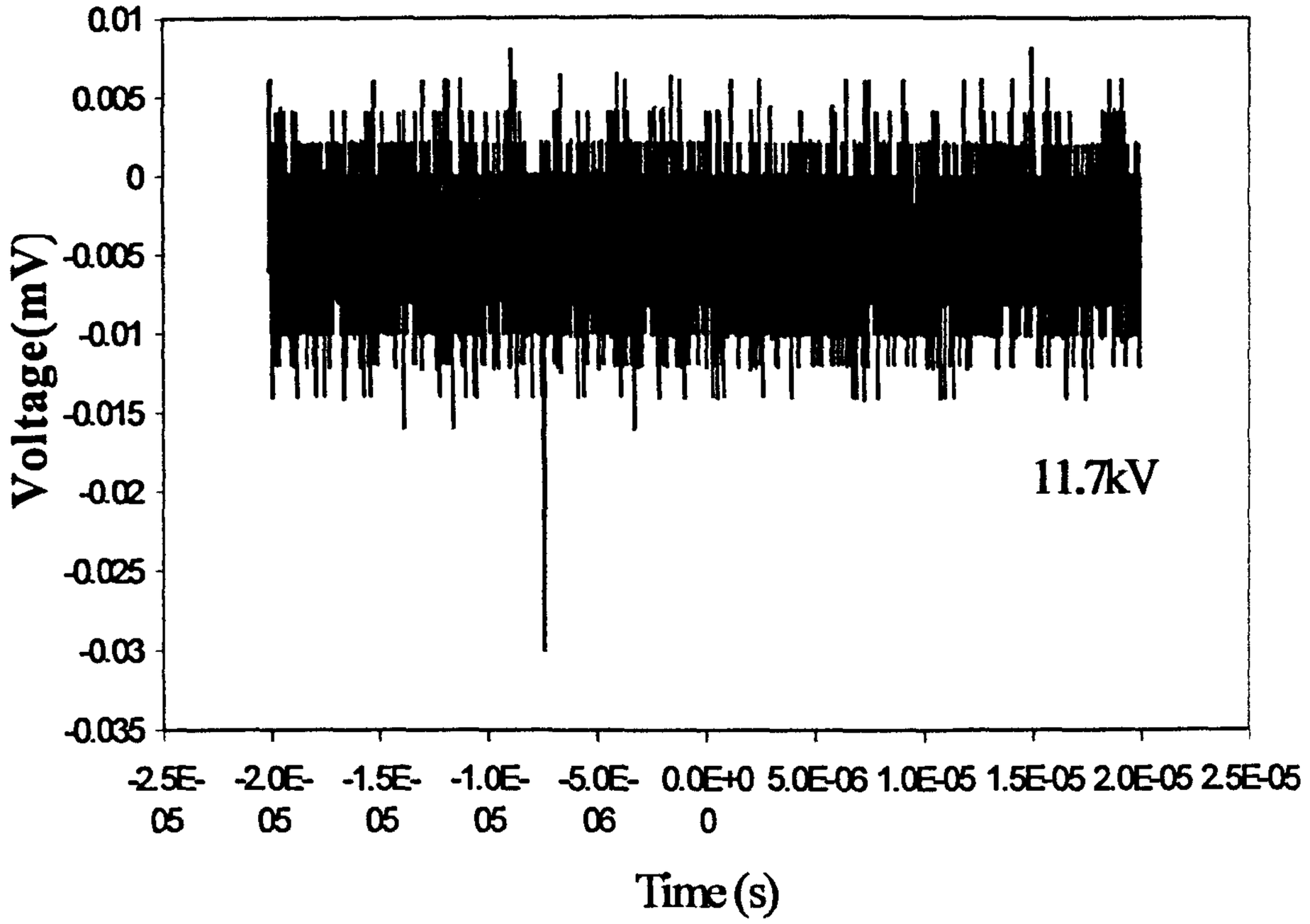

Fig (8.9) Partial discharge activity at the edges of a water droplet in the absence of droplet vibration. Level surface

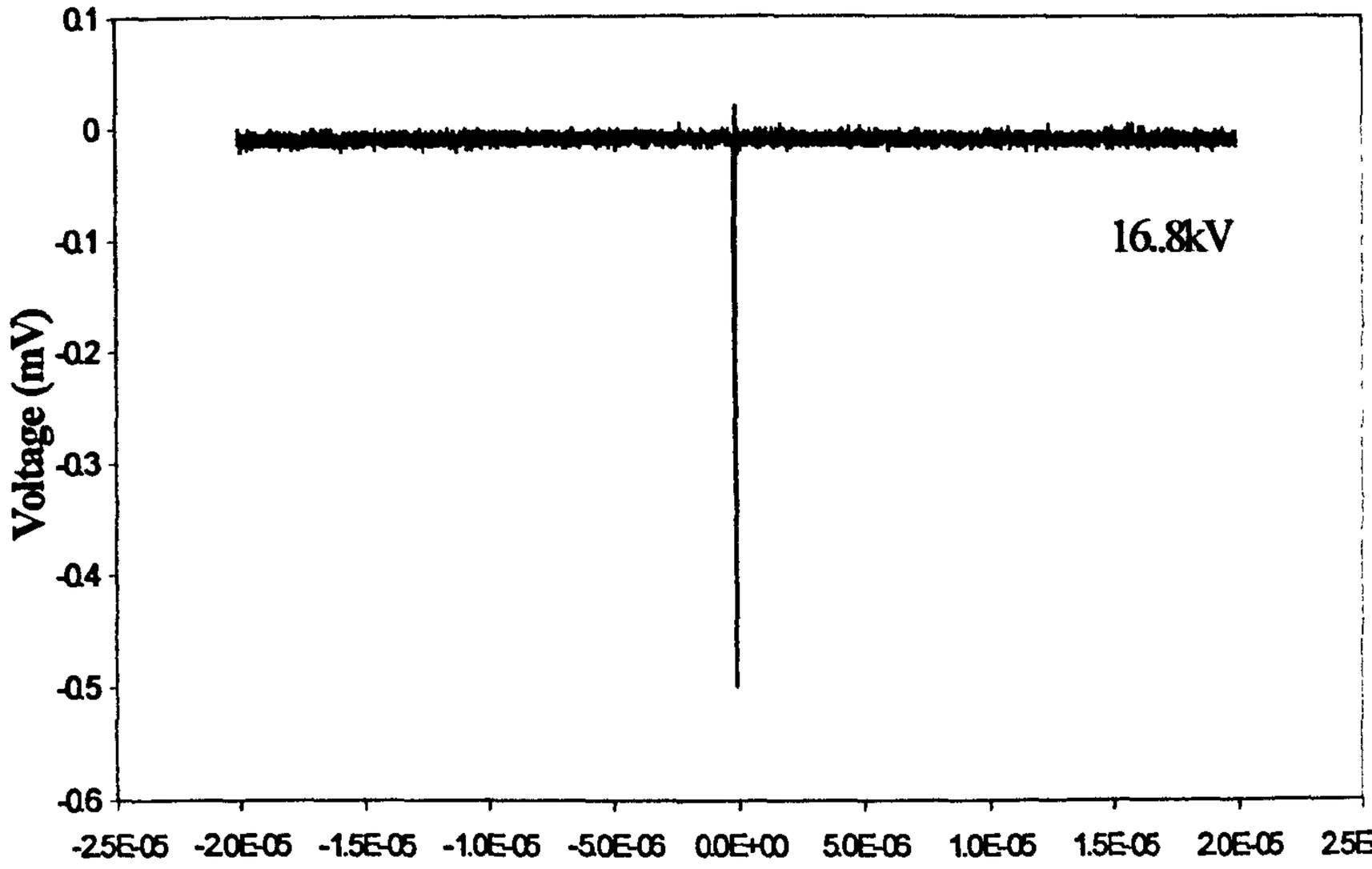

Fig (8.10) Partial discharge activity as the droplet spread over the surface. Level surface

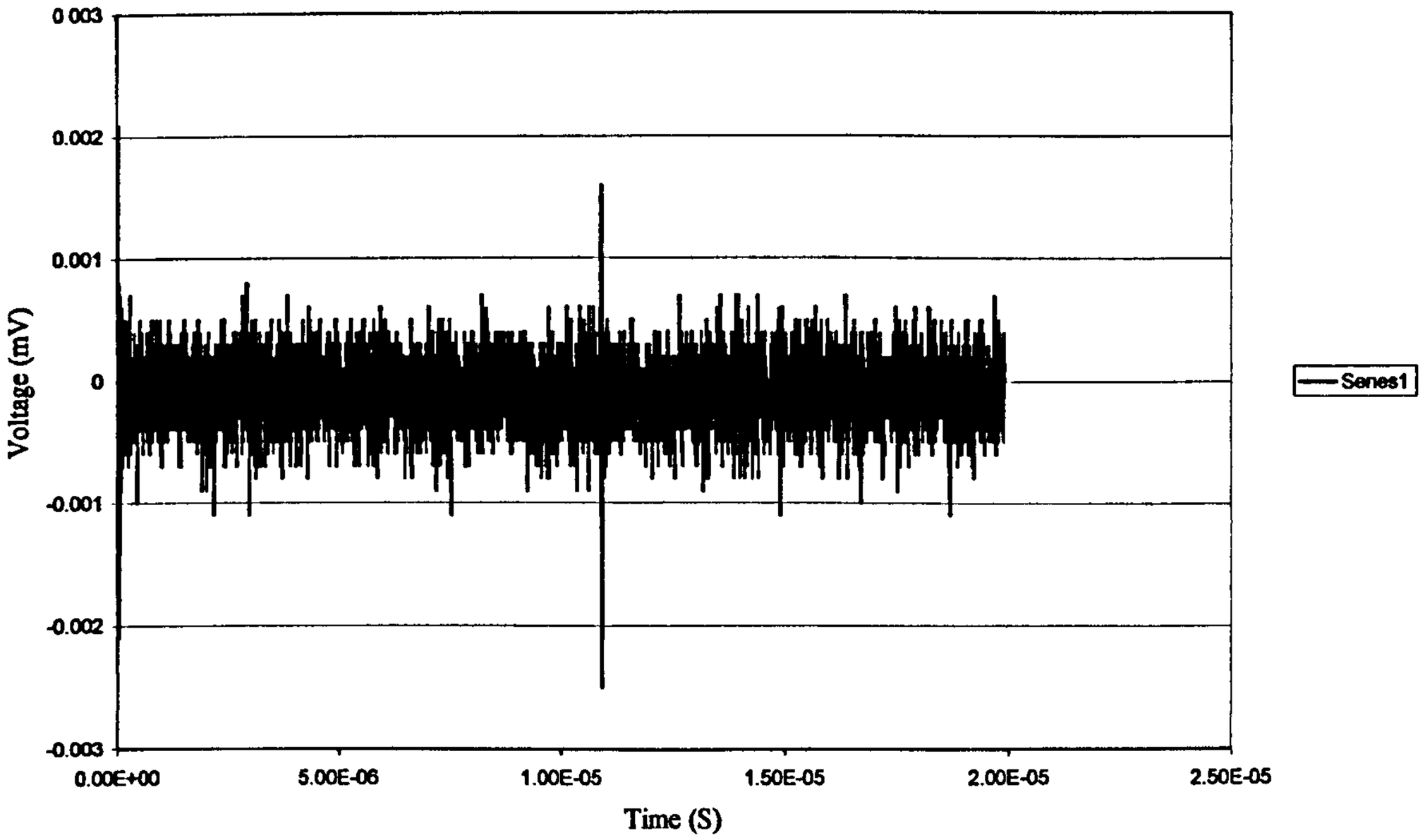

Fig (8.11) Partial discharge activity with no water droplet present. Surface inclined at 20°.

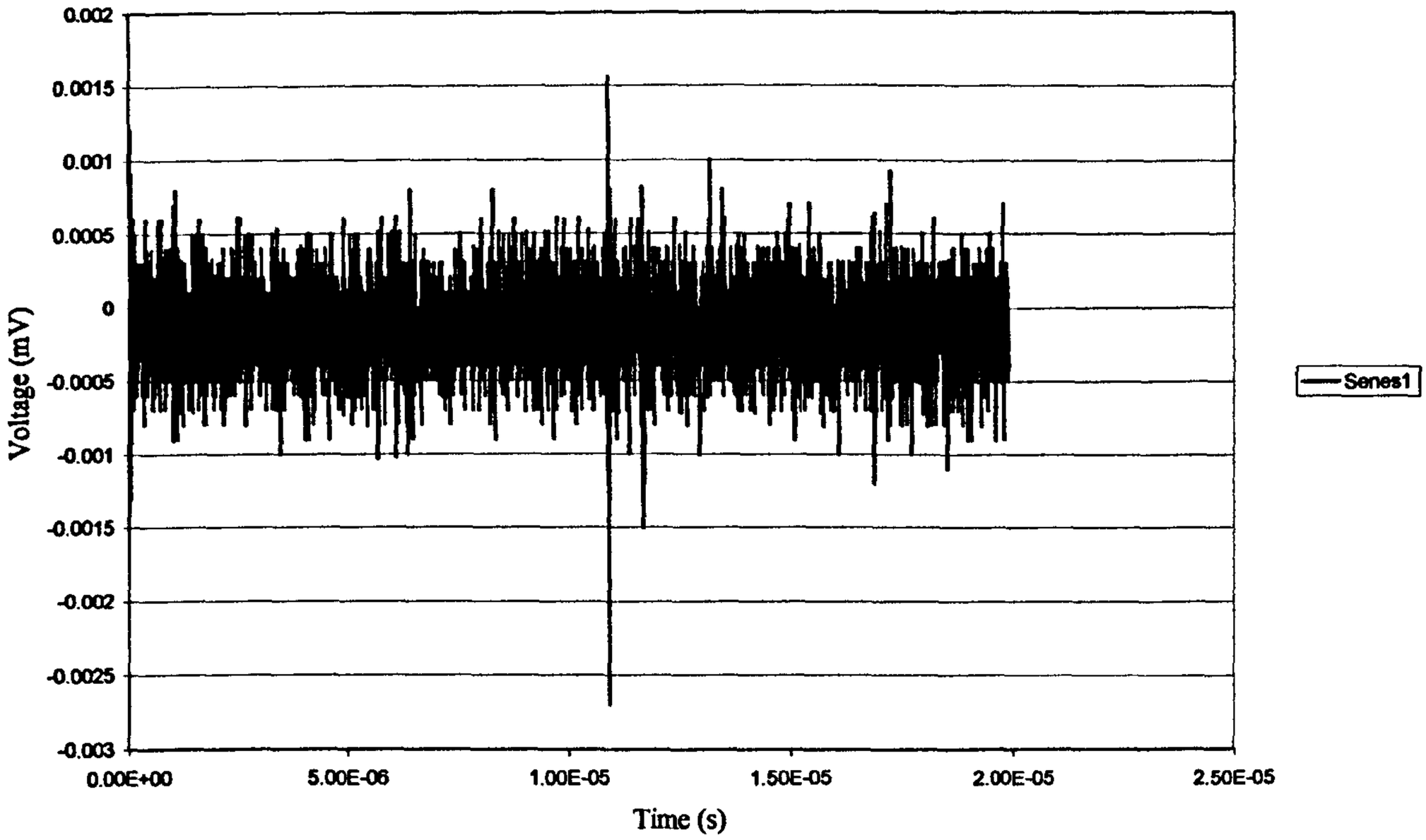

Fig (8.12) Partial discharge activity at the edges of a water droplet in the absence of droplet vibration. Surface inclined at 20

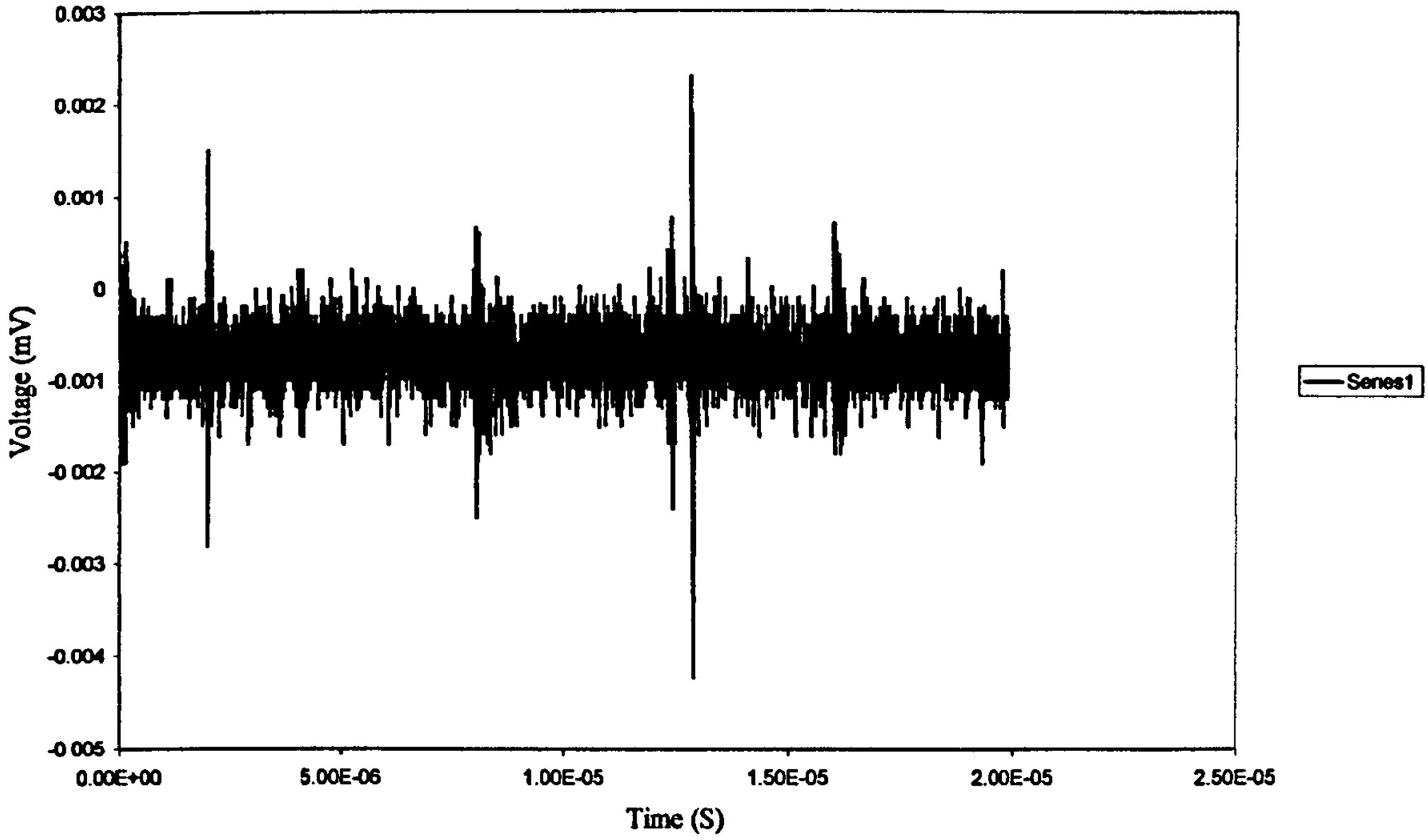

Fig (8.13) Partial discharge activity at the edges of a water droplet in the presence of droplet vibration. Surface inclined at 20

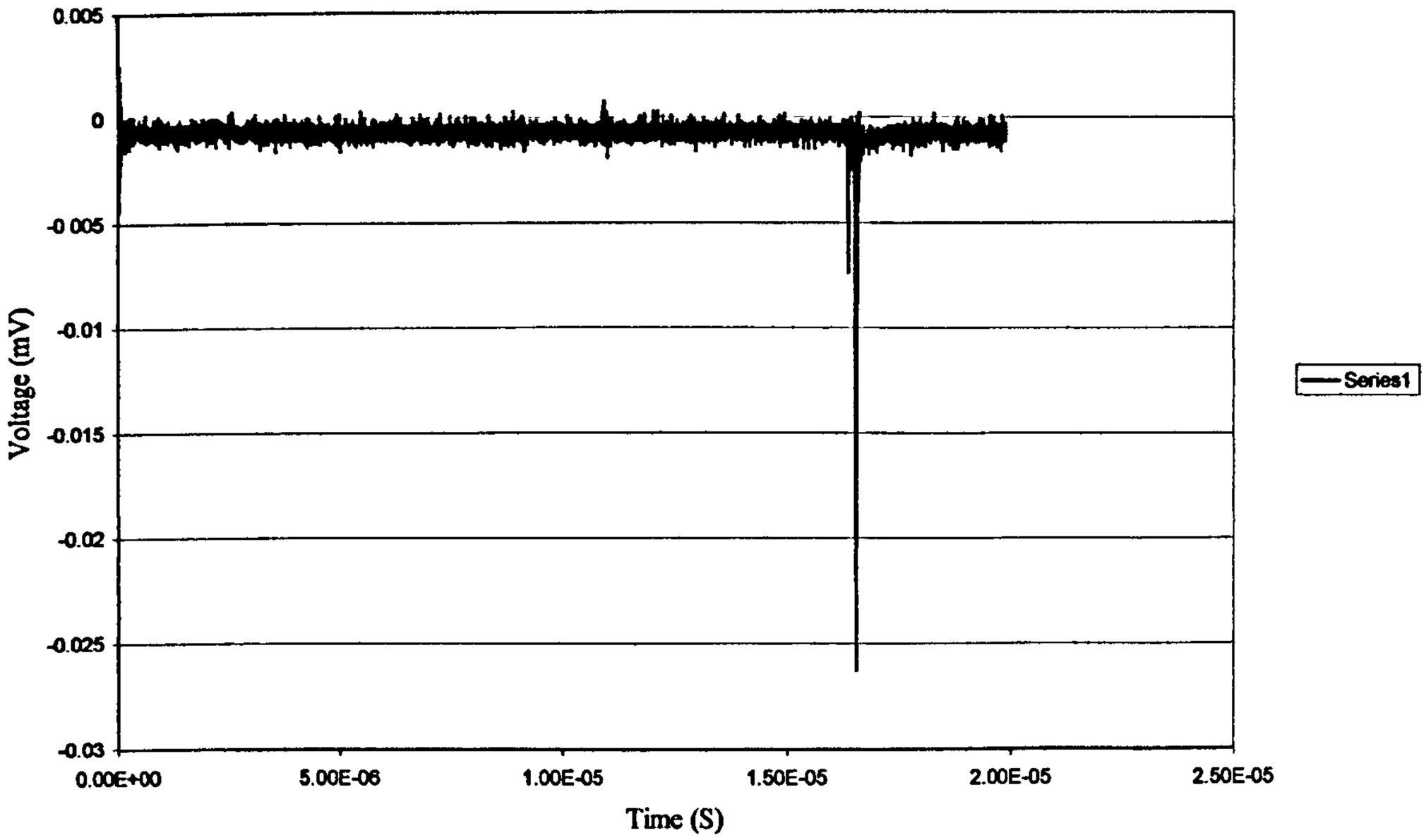

Fig (8.14) Partial discharge activity as the droplet spread over the surface and accumulated at the lower electrode. Surface inclined at 20°.

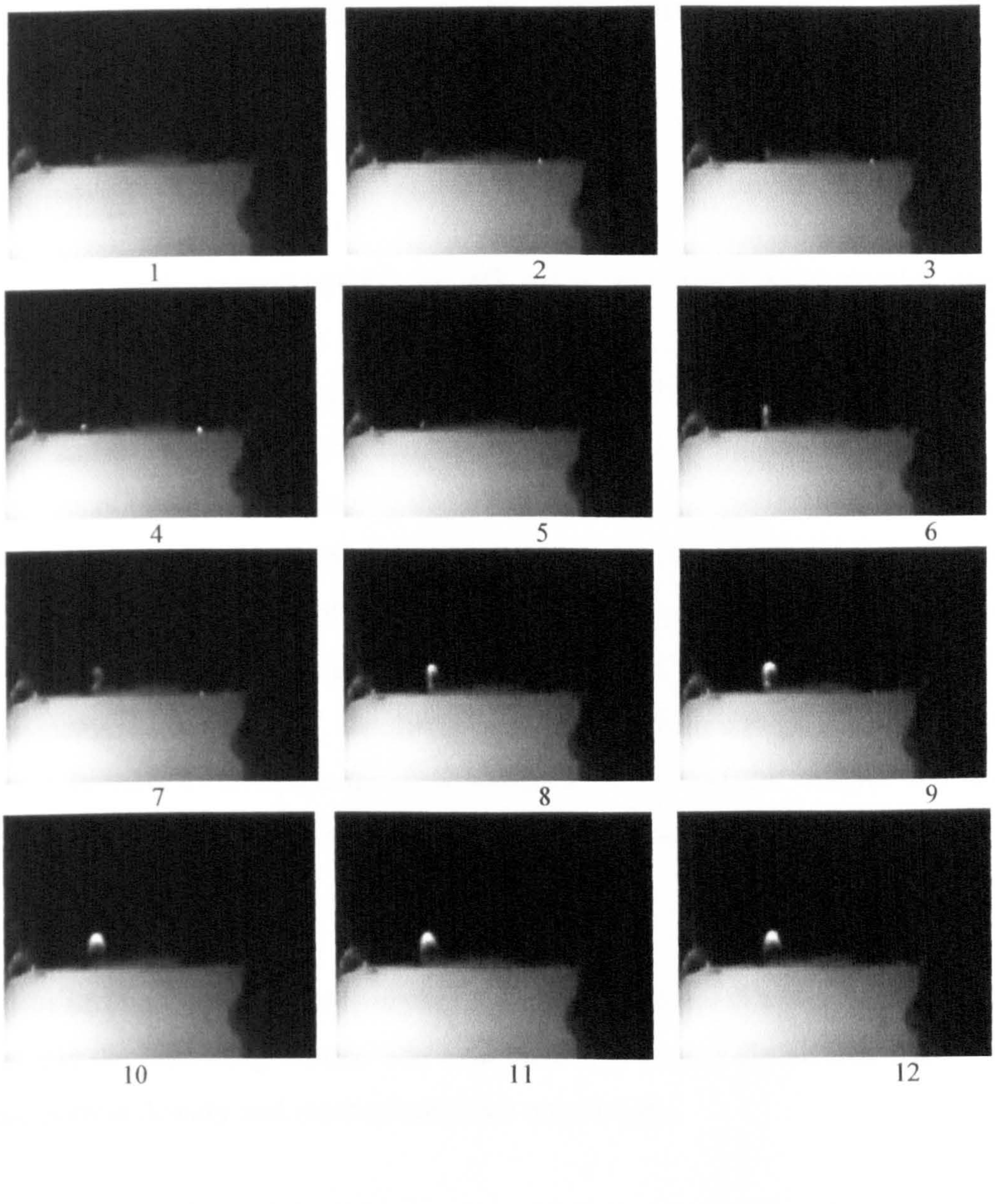

Fig (8.15) Partial discharges at the edge of a droplet spreading over a horizontal insulator surface.

Chapter 9

Physical Interpretation of Discharges at the Edge of Water Droplets

9.1 General

In the present chapter we will examine a single water droplet placed on the insulation sample, using the second embedded – electrode model described previously. In particular we investigate the electric field at the edge of such droplets, both the surface field along the insulation and the field in the air surrounding the droplet. Quantitative information on these fields allows an examination of the discharge processes concerned with partial discharge formation around the edges of a droplet. In order to emphasise the effect of the electric field at the droplet edge, the particular case where the insulation surface is inclined at an angle of 60° to the horizontal is examined. In this study, further use of the finite-element QuickField® package described in chapter 7 is used to compute the field distribution around the droplet and use this information to examine quantitatively the conditions that can lead to electrical breakdown.

In addition, the effect of varying the permittivities and conductivities the water droplet and the insulating sample was examined in terms of the electric field strength, leakage current density and mechanical force on a droplet.

Unless stated otherwise, the calculations described below assume the conductivities of water, air and polymer sample to be 100 μS/cm (typical of rain water), 1e-15 S/cm and 1e-13 S/cm, respectively, and the relative permittivities of water and polymer to be 81 and 2.35, respectively.

9.2 The Geometry Model

The embedded–electrode geometry used for this part of the work is illustrated in Fig (9.1).

Fig (9.2) shows the shape adopted by a droplet placed on an initially horizontal surface which is then inclined at an angle of 60°. The following procedure was developed to obtain data on the profile of the droplet suitable for use with the field modelling software. Fig (9.2) was read into image manipulation program (Microsoft Photo Editor). It was then reduced to a 2-bit format as shown in Fig (9.3). This image was then processed to find the edge contours. The resulting image is shown in Fig (9.4). From this line image, it was possible to express the profile of the droplet in terms of a set of coordinates these are shown in Table (9.1). Using a spreadsheet, these coordinates were then transformed into data points which could be input to quick field. These coordinates are also included in Table (9.1).

Using the geometrical data given in Table (9.1), the profile of the droplet on the inclined, embedded-electrode system was input to the FEM software. Before generating the FEM mesh, the dimensions of the mesh were manually set at very small values compared with the droplet dimensions close to the droplet and at larger values well away from the areas of potential interest. The mesh pattern then generated is shown in Fig (9.5). This pattern was found to form a suitable compromise between accuracy and computation time.

9.3 Electrostatic Analysis

Electrostatic analysis was primarily used to calculate the equipotential and electric field strength distributions around the droplet. In addition, it was also considered useful to use the results to examine the mechanical forces on the droplet.

Electric field. Fig (9.6) shows a false colour image of the equipotential distribution calculated. A closer view of the equipotentials around the droplet is presented in Fig (9.7). These figures give a qualitative presentation of the FEM output, but this was of course also available in detailed numerical format to allow quantitative examination.

On Fig (9.7) two points are marked A and B. These are on the surface of the PE and at either side of the droplet. Numerical values of the electric field strength along the insulator surface between the locations A and B obtained from the FEM computation are shown in the graph of Fig (9.8). With a water relative permittivity of 81 this computation reveals maxima at the triple junctions, as would be expected, with the higher peak associated with the higher contact angle (lower edge of the droplet). This higher peak is about 20 times the average field. It should be noted that the peak of the electric field extends only a short distance from the edge of the droplet, about 0.1mm at 50% maximum – the droplet extending about 3.5mm over the PE surface. A relatively shallow minimum in the surface field is shown over the droplet/PE interface.

Figs (9.9) and (9.10) show the results obtained for similar calculations where the relative permittivity of the droplet was lowered to 40 and 2.35 (i.e. the same as the PE). These results, summarized in Table (9.3), show how the peak values of the high-field regions decrease and the minimum correspondingly increases with this large decrease in droplet permittivity. Further calculations shown in Fig (9.11) show how the maximum field changes as the droplet relative permittivity is varied from 10 to 80. However, for the present purposes it may be concluded from these results that relatively minor variations in droplet permittivity – such as would be associated with changes in dissolved content between deionised, tap and salt solution – would not result in significant changes in the field distribution.

Table (9.5) and Fig (9.12) show results obtained when the relative permittivity of the insulation was varied from 1.5 to 6 for a fixed droplet value of 81. From table (9.5) we can notice that the peak value of the electric field decreases by about 7% and

the minimum increases by about 3% when the relative permittivity of the insulating sample increases from 1.5 to 4. It was concluded from these results that small variations around the assumed value of 2.35 for the relative permittivity of PE would not cause a significant change in the electric field distribution around a droplet.

Mechanical Force. The post-processing facility incorporated in the QuickField® software was used to compare the mechanical forces acting on each side of the droplet resulting of the applied field. QuickField® computes the average force per unit area over a selected contour. Two contours were selected starting at the apex of the droplet and extending down to the PE surface at each side of the droplet. With reference to the slope of the insulation, these are designated the "lower" and "upper" sides of the droplet and the respective forces as Fl and Fu. The calculations showed that Fl and Fu fell by about 3% when the droplet relative permittivity was varied from 81 to 40 – i.e. the forces were not sensitive to relatively minor variations in permittivity. However, because the shape of the inclined droplet is no longer symmetrical it would be expected that Fl and Fu would differ, unlike the case with a horizontal droplet. Table (9.2) shows that the computed ratio of Fl/Fu is 1.30±0.1 for droplet relative permittivities of 81, 40 and 2.35. That is, Fl exceeds Fu and there is a net force, due to the applied field, acting down the slope but the ratio is not sensitive to these changes in droplet relative permittivity. The effect of varying the insulation sample permittivity was also examined. The computed results are shown in table (9.4). The ratio of Fl to Fu decreases from 1.31 to 1.28 as sample relative permittivity increases from 1.5 to 4. This is a similar ratio to that shown in Table (9.2) and it may be concluded that the Fl/Fu ratio is also insensitive to such changes in sample relative permittivity.

An overall conclusion drawn from the above electrostatic analysis, was that computations using the geometry and physical data described above would provide meaningful and reliable data on the electric field surrounding a droplet which could reasonably be compared with the fields encountered during the other similar studies described in chapter 3, even though minor variations in physical parameters might be present.

9.4 Current Flow Analysis

In the present study, current flow analysis was not as extensively used as electrostic analysis. However, by using Quickfield in current flow analysis mode it was possible to examine the effect of variations in the resistivity of the water droplet and the insulating sample on the electric field around the droplet and on the leakage current through the water droplet passing between the embedded electrodes. Unless stated otherwise, the calculations described below assume the conductivities of water, air and polymer to be 100 μS/cm (typical of rain water), 1e-11 S/cm and 1e-13 S/cm, respectively. Expressed in the form preferred by the FEM software, these correspond to the resistivities 1e6 Ωm, 1e11 Ωm and 1e13 Ωm, respectively. The geometry examined is that of the inclined droplet as illustrated in Figs (9.1) to (9.7). We again refer to the locations A and B marked on Fig (9.7).

Figs (9.15), (9.16) and (9.17) show computed values of the electric field along the sample surface from A to B for droplet resistivities of 1e6, 1e11 and 1e13 Ωm, respectively. As with the electrostatic analysis, the field shows two maxima at the triple junctions and minimum near the center of the droplet, with the greater maximum at the lower edge of the droplet. Table (9.7) shows how this maximum decreases and the minimum increases as the water resistivity increases. Fig (9.18) shows computed values of this maximum electric field up to very high values of droplet resistivity. The leakage current passing through the droplet showed maximum density at the triple junction edges, and minimum density at the central region of the droplet. The maximum and minimum values computed at water droplet resistivities of 1e+6; 1e+11 and 1e+13 Ωm are shown in Table (9.8). As would be expected, high current density occurs when the resistivity of the water droplet is low. Also we can found the current density decreases when the resistivity of the water droplet increases. Maximum and minimum values of computed electric field strength and current density are shown in Tables (9.9) and (9.10), respectively, for insulation resistivities of 1e6, 1e11 and 1e13 Ωm with constant

water droplet resistivity of 1e+6 Ωm. These tables show that the field increases with sample resistivity but the current density decreases.

The effects on the electric field around the droplet due to variations in droplet and sample resistivities revealed by current flow analysis could be further explored, and it is suggested that this might be a useful area of further study. However, for present purposes, it was considered that enough information about the electric field distribution had been revealed by the electrostatic analysis to allow a quantitative examination of the physical conditions for electrical discharge formation in the location of the droplet, and this is described in the next section.

9.5 Gas Breakdown at the edge of the inclined droplet

With the droplet inclined at 60°, as shown in Figs (9.2) to (9.7), it was found that at an applied voltage of 9.5kV (E_0 = 3.2kV/cm) the water droplet started to vibrate and the onset of partial discharges could be detected electrically. Discharges were observed to be located in the air, particularly at the lower edge of the droplet, and these were not confined to the polymer surface. From visual observations, one end of the discharges appeared to terminate on the droplet surface a distance (d) above the triple point. It was estimated that d lay typically between 1.5 and 2mm. This observation appeared to be similar to that reported recently by Krivda and Birtwhistle (reference 14, chapter 3). To investigate this, the electric field around the droplet on an insulating surface inclined at 60° was computed and the results used to examine how electrical breakdown of the air surrounding the droplet might occur through a Townsend or streamer process (see section 2.4).

Fig (9.13) shows the configuration examined. First, the surface electric field (E_s) was calculated as a function of distance along a path away from the droplet along the polymer surface starting at the triple junction. This field was then compared with the electric field (E_l) as a function of distance along a path away from the droplet along a field line starting at a point on the droplet surface a distance of d = 1.8mm above the triple junction. To form this second path, the line was tracked away from the droplet

surface, always keeping at right angles to the equipotentials, and terminated on the polymer surface. These two paths are shown on Fig (9.13). To compare the fields, the ratio of E_l to E_s was calculated as a function of distance away from the droplet. The result is shown in Fig (9.14), which shows that equal distances away from the droplet surface the field strength in the air (E_l) can exceed that along the surface (E_s). This result indicates that the Townsend or streamer criterion for electrical breakdown of the air may be satisfied along a path in the air above the triple junction in preference to a path on the polymer surface.

In order to investigate this possibility further, it was considered useful to evaluate equation (2.22) along the selected field line to determine whether the conditions for streamer breakdown in air were satisfied at the level of applied voltage at which discharges had been observed. To do this, the integral $\int \overline{\alpha}\, ds$ given in equation (2.22) was replaced by an approximation in the form of a summation $\sum \overline{\alpha} \Delta s$. Where Δs is a small increment of distance along the path s.

The value of the effective ionisation coefficient for atmospheric air is known as a function of applied electric field. In this case, the applied field at which discharges were observed was 3.2 kV RMS - i.e. an applied voltage of 9.5kV RMS, as noted above. To calculate the ionisation coefficient, it is appropriate to use the instantaneous peak value of the applied voltage, that is $9.5/\sqrt{2} = 6.5$ kV. This is because gas breakdown is a process that is associated with the peaks of the applied stress and is takes place on a μs time scale during which the applied voltage is effectively constant at the peak value.

To evaluate $\sum \overline{\alpha} \Delta s$, a spreadsheet was constructed of the form shown in Table (9.6). In this, column 1 is distance, s, along the field line starting at d = 1.8mm above the triple junction. Column 2 is the incremental step, Δs, along the line. Column 3 shows the computed value of the applied field at each point s and column 4 the corresponding value of the ionisation coefficient at s. Columns 5 and 6 evaluate $\sum \overline{\alpha} \Delta s$ as a function of distance along the field line. From the discussion presented in

chapter 2, it may be concluded that gas breakdown along the field line can take place provided $\sum \overline{\alpha} \Delta s$ exceeds 18.

When the spreadsheet calculation was performed for an applied voltage of 6.5kV, at which discharges had been observed, it was found that the final column showed a value of $\sum \overline{\alpha} \Delta s$ well in excess of 18. When the calculation was repeated with a reduced applied voltage of 6kV, the results shown in Table (9.6) were obtained. This shows that $\sum \overline{\alpha} \Delta s$ exceeds 18 at s = 3.67mm, close to the termination of the field line at the polymer surface. That is, it is possible for electron avalanches propagating along the field line to grow large enough to trigger streamer formation and therefore an electrical discharge.

9.6 Discussion

Although an applied voltage of 6kV peak is nearly 8% below the peak voltage at which discharges were observed experimentally, it is reasonable to suggest that discharges may be occurring that are below the detection threshold of the present experimental system. In any case, it can be concluded that the above calculations demonstrate that it is possible to satisfy the conditions required for electrical breakdown of the air along a field line from the edge of a droplet and which starts a distance above the triple junction and off the polymer surface. Such a possibility may account for the present observation of discharges in the air at the edge of a droplet and the similar experimental observations reported by Krivda and Birtwhistle. Of possible significance is that in the model described here it is considered that these discharges terminate on the polymer surface at some distance away from the triple junction. If, as discussed in chapter 3, such discharges are responsible for changes in the hydrophobicity of the polymer and therefore the spreading of the droplet, then the existence of a gap between the edge of the droplet and the point of discharge termination may have considerable influence on the mechanism of droplet spreading.

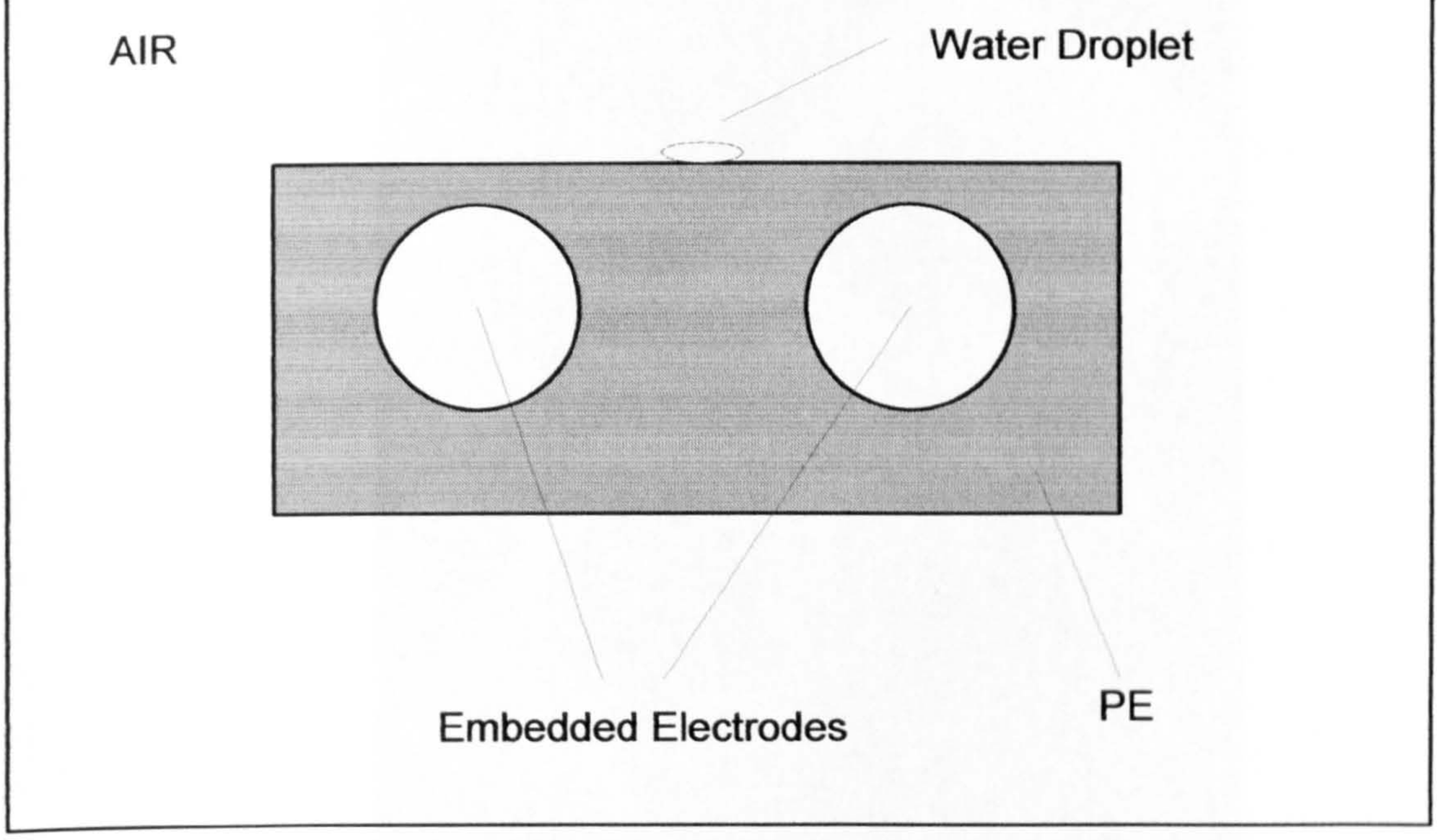

Fig (9.1). The geometry adopted.

Fig (9.2) Droplet located on sample inclined at 60

Fig (9.3) Close-up version of figure (9.2) processed in 2-bit form.

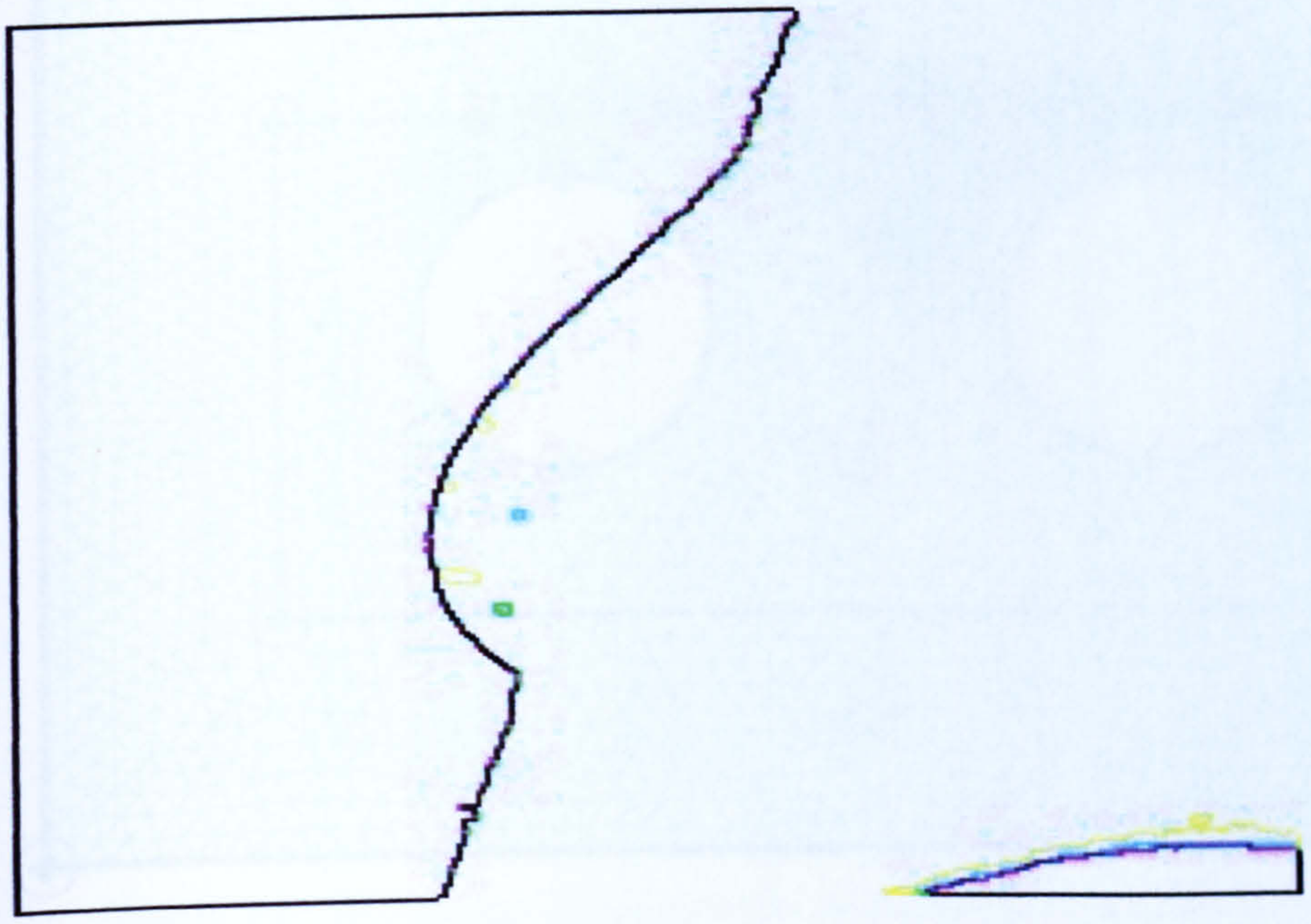

Fig (9.4) Edge Contour version of figure (9.3)

Fig (9.5) FEM Geometrical Model

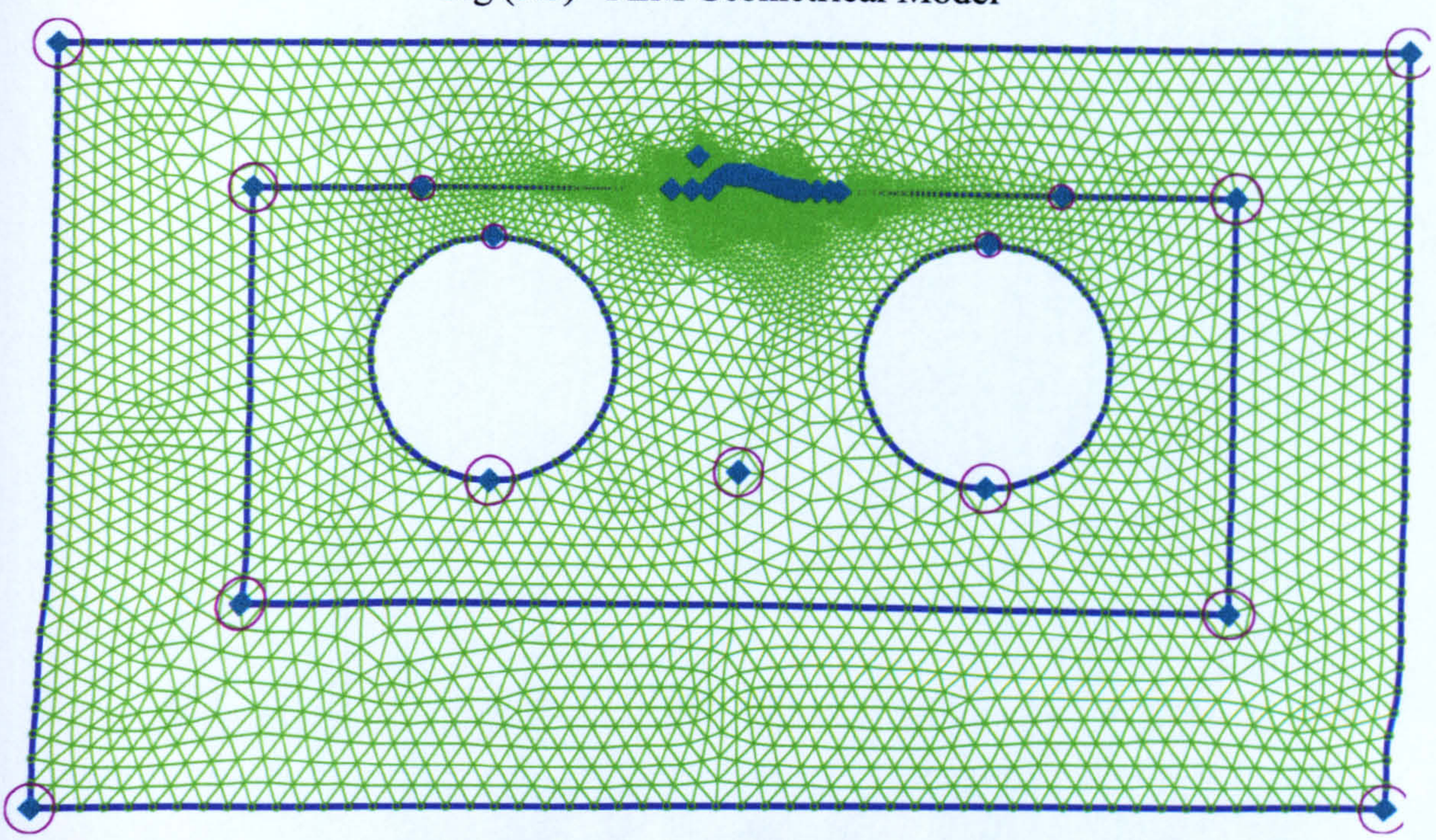

PE sample with embedded electrodes.
The droplet shape is for a surface inclined at 60° to the horizontal

A greatly reduced mesh size is set around the water droplet.

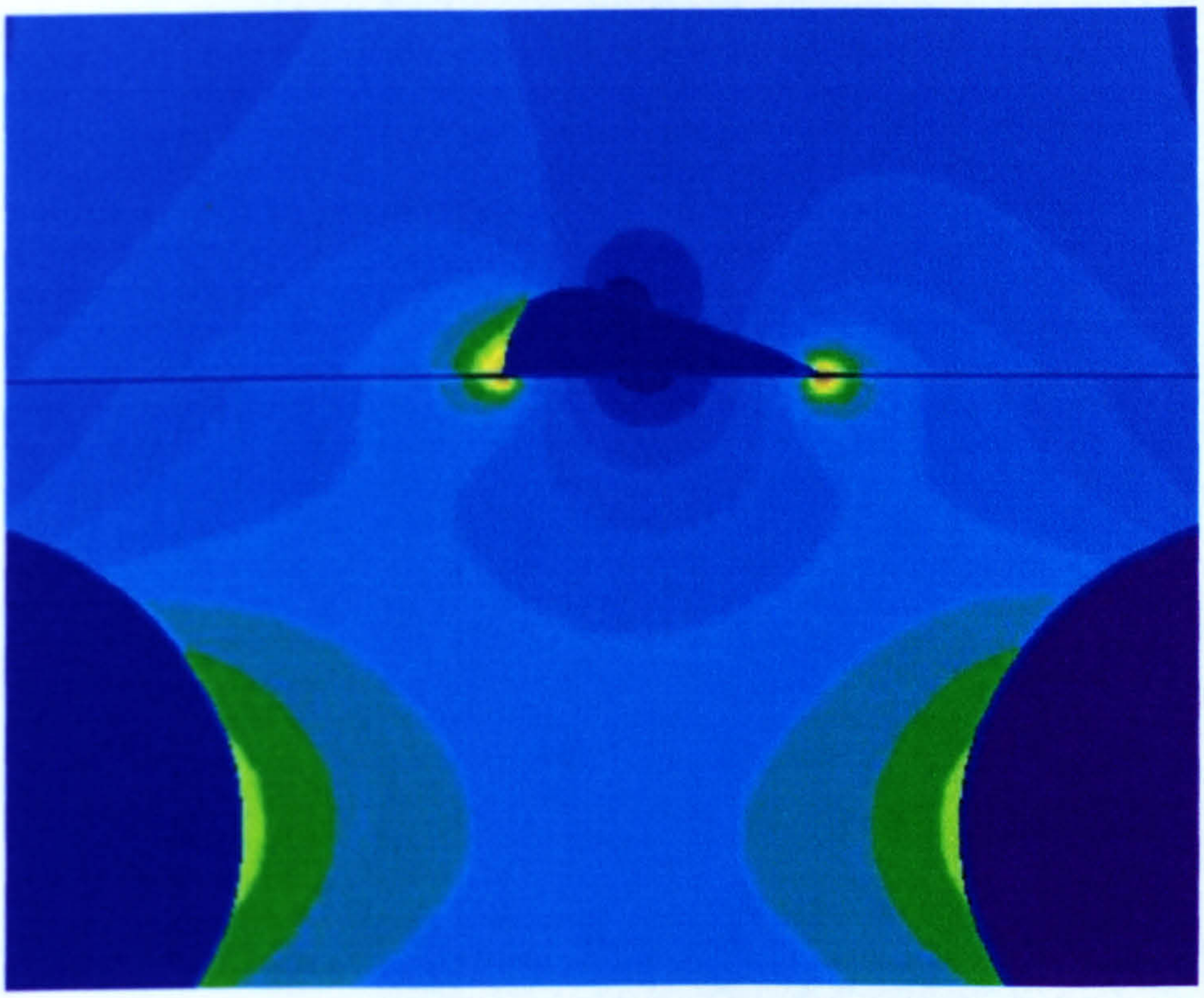

Figure 9.6 Illustrating the equipotential distribution around the droplet and the embedded electrodes.

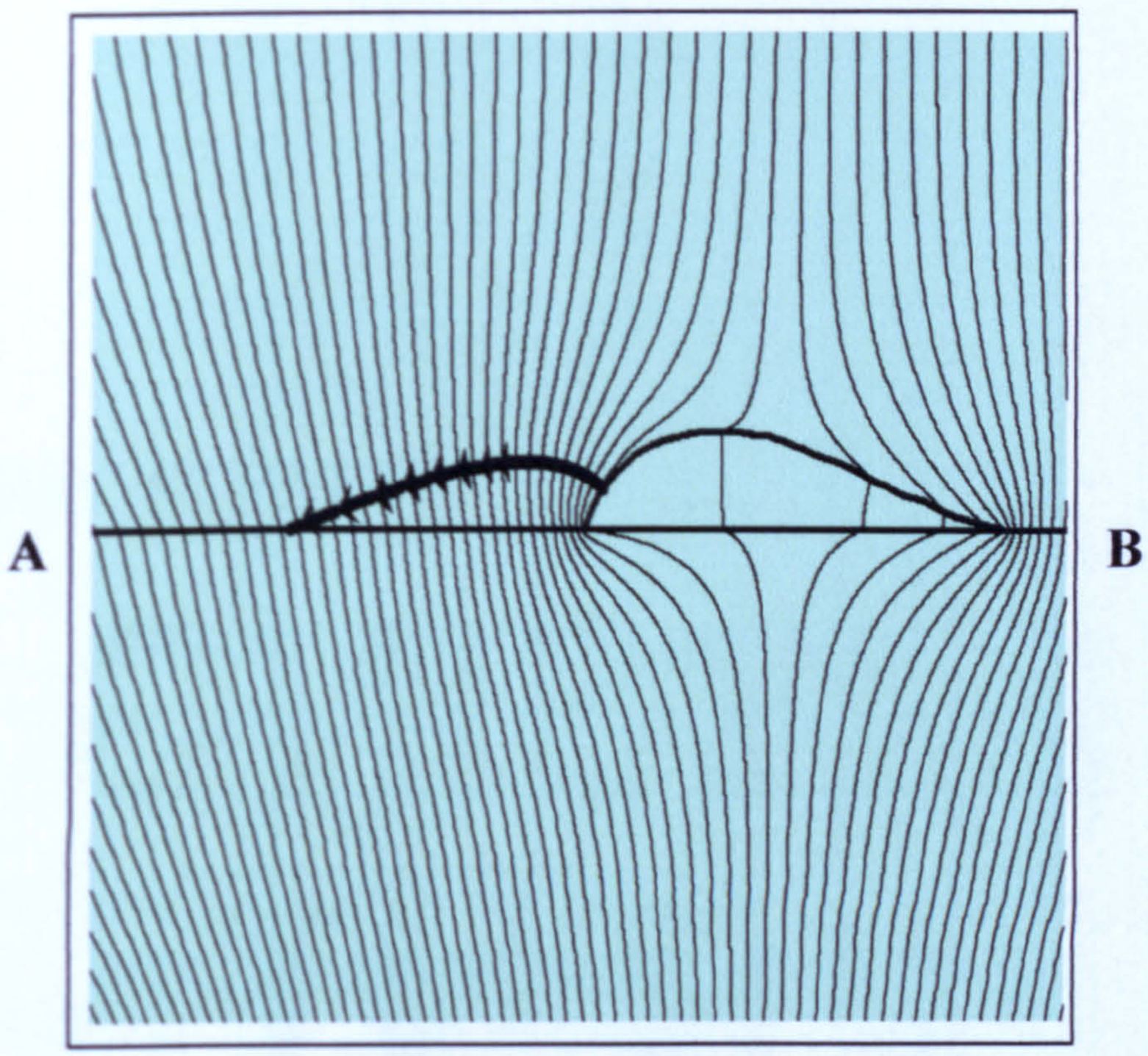

Fig (9.7) Detailed form of the equipotentials around a droplet on a PE plane inclined at 60°

Notes

1. The locations marked A and B identify points on the surface of the insulator referred to in the text..
2. The emphasized line depicts a field line extending from the droplet surface – also referred to in the text.

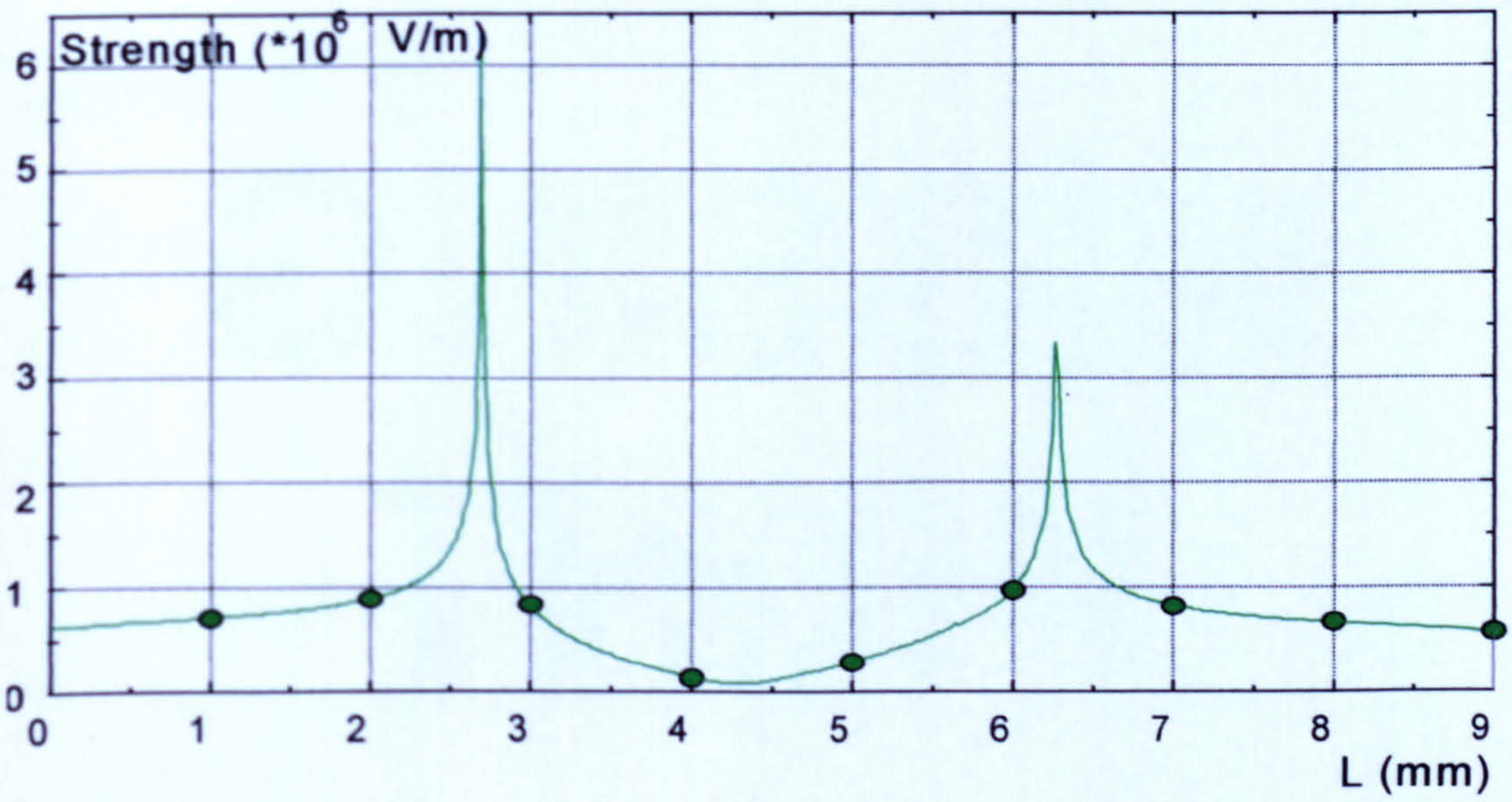

Fig (9.8) The electric field (E) between the locations A and B of Fig (9.7) with a water permittivity of 81.

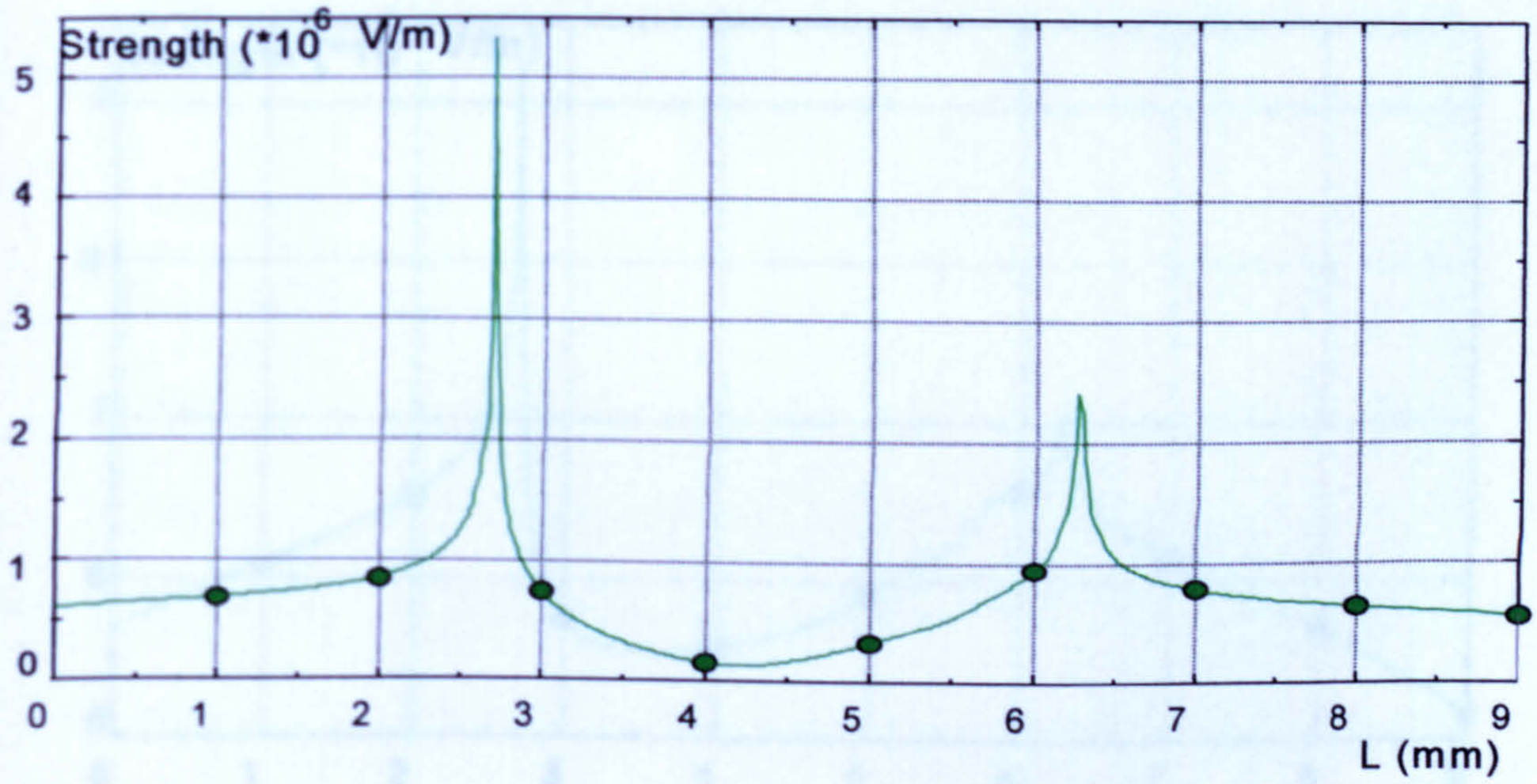

Fig (9.9) The electric field (E) between the locations A and B of Fig (9.7) the "water" permittivity of 40.

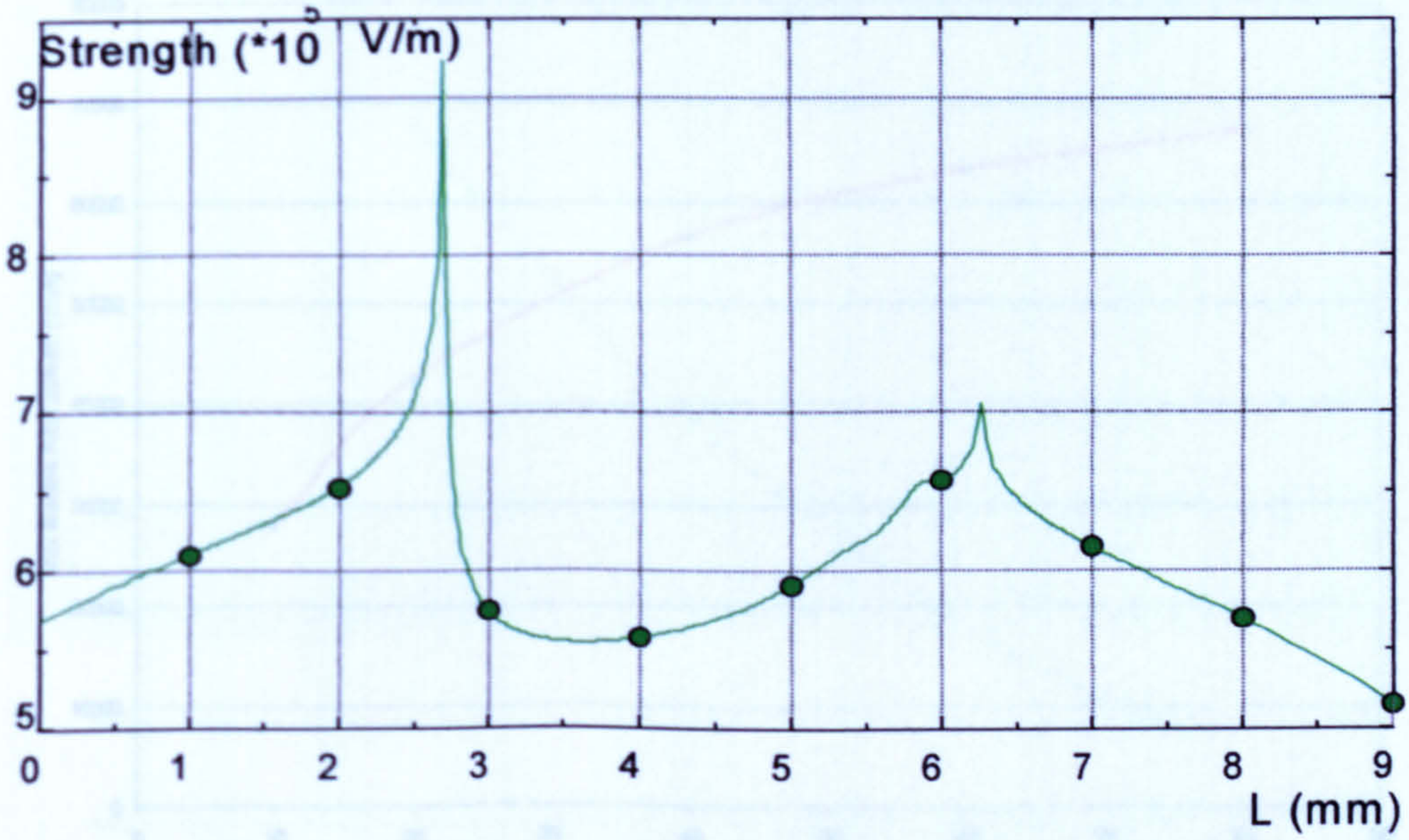

Fig (9.10) The electric field (E) between the locations A and B of Fig (9.7) the "water" permittivity of 2.35.

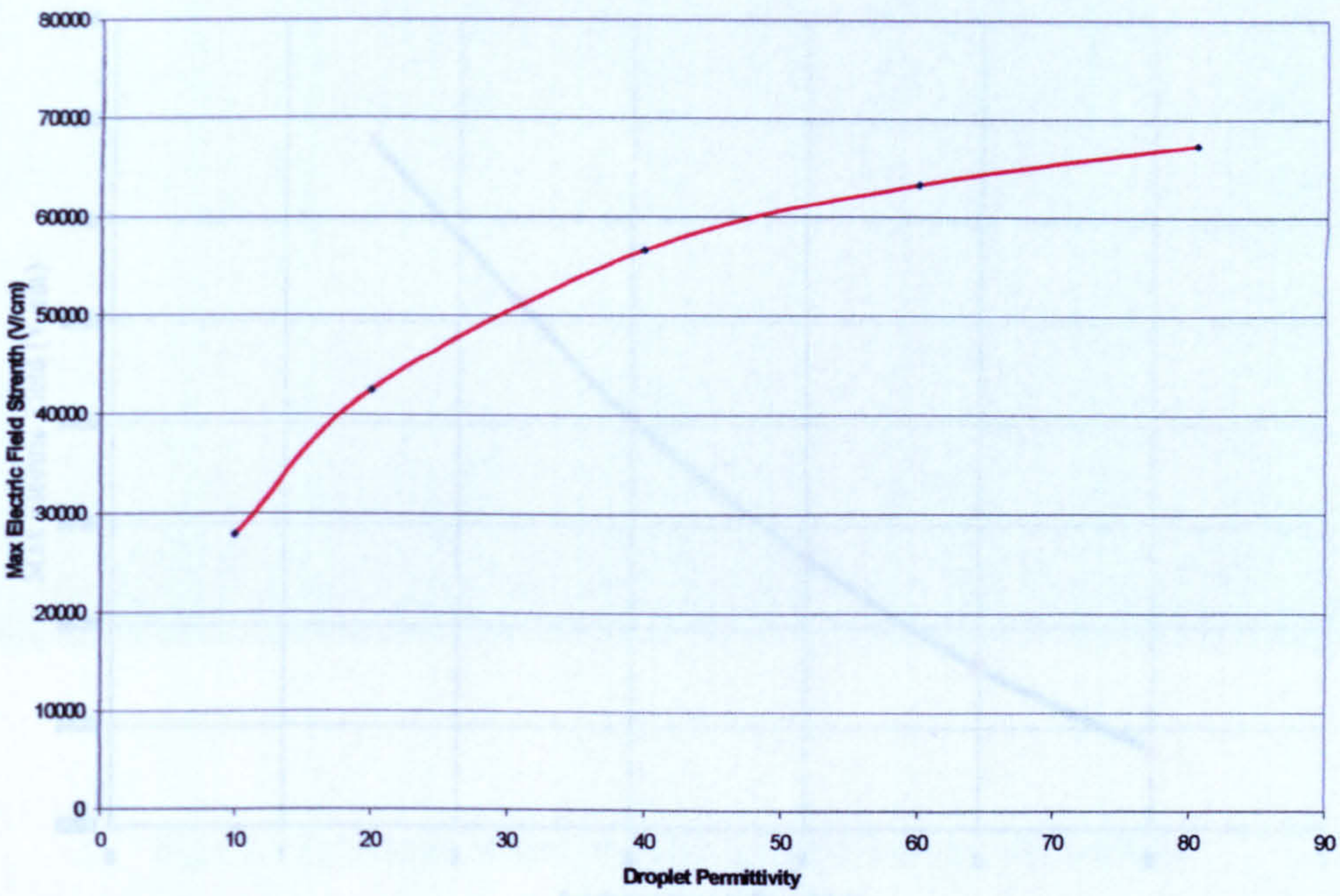

Fig (9.11) the relation between the electric field Strength and the droplet permittivity

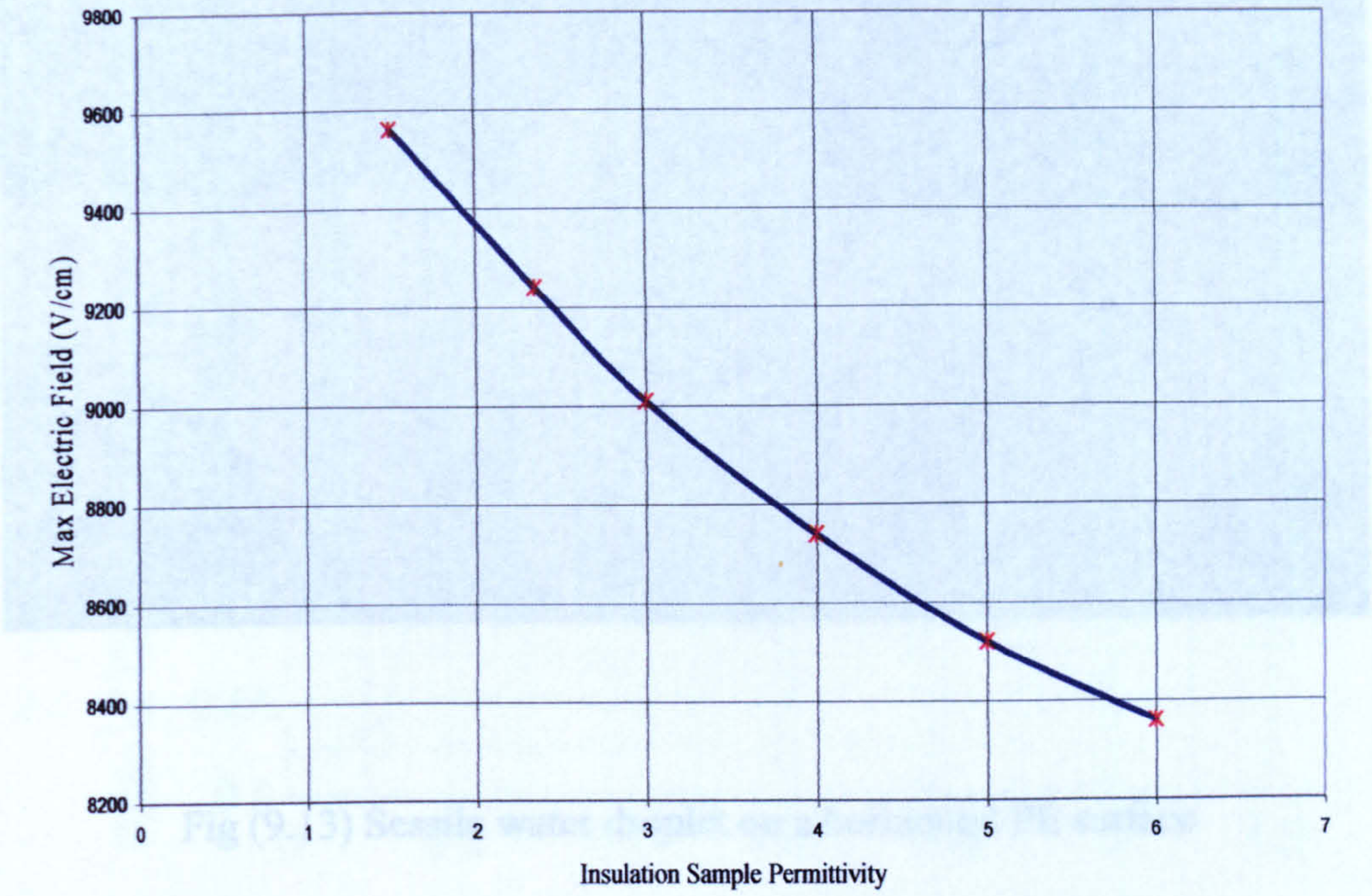

Fig (9.12) the relation between the electric field Strength and the insulation sample permittivity.

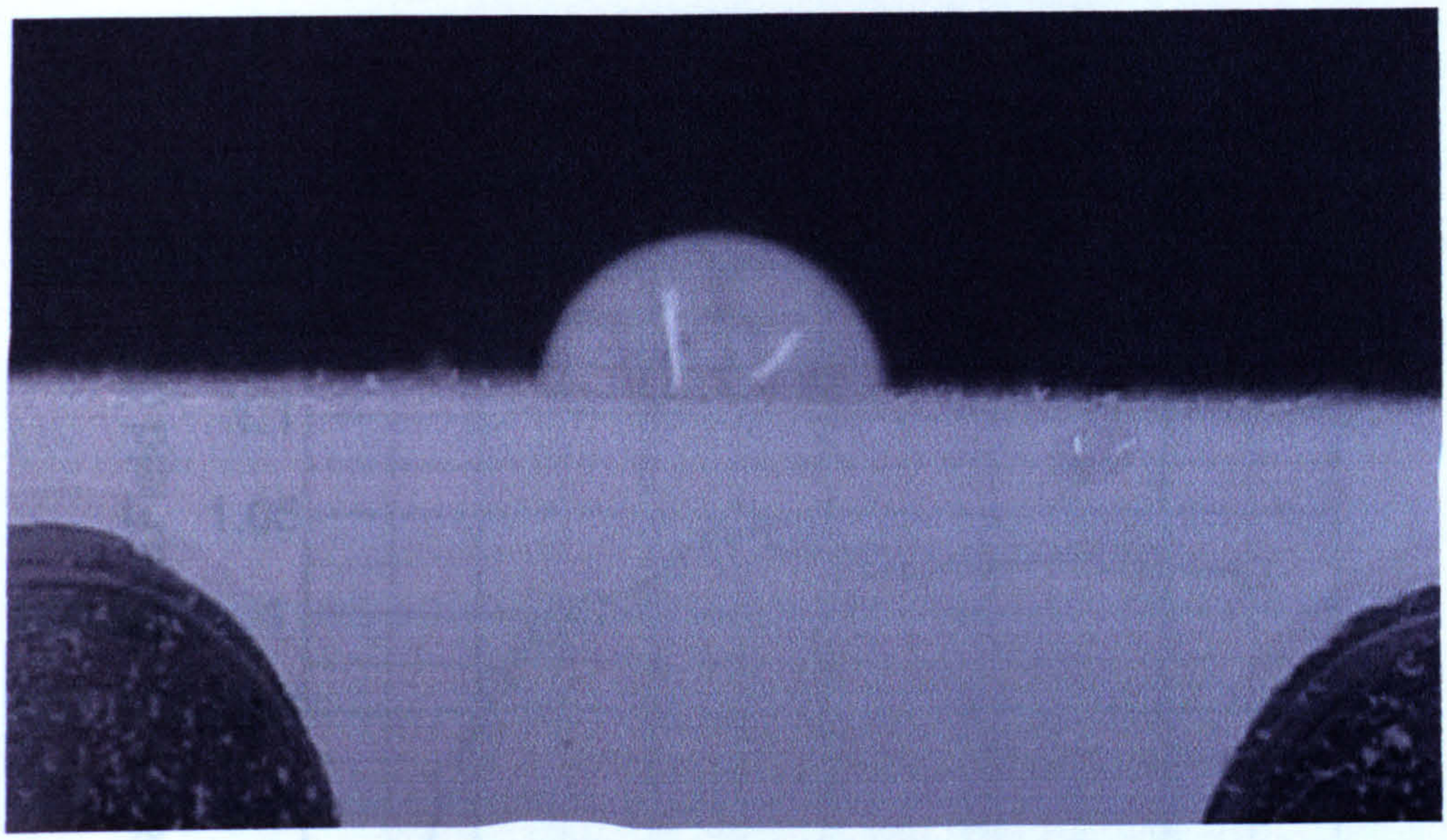

Fig (9.13) Sessile water droplet on a horizontal PE surface

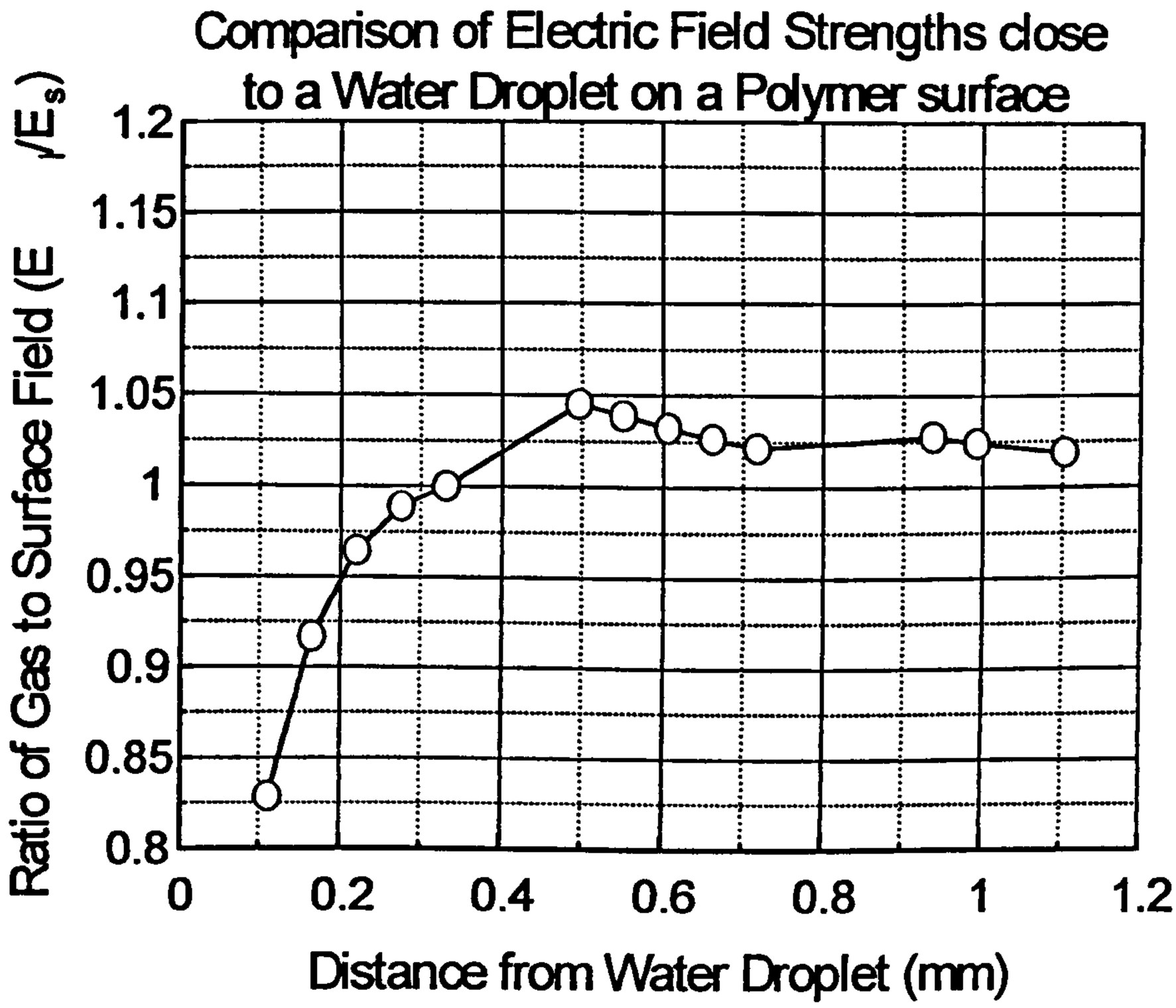

Fig (9.14) The ratio of E_l to E_s as a function of distance from droplet surface

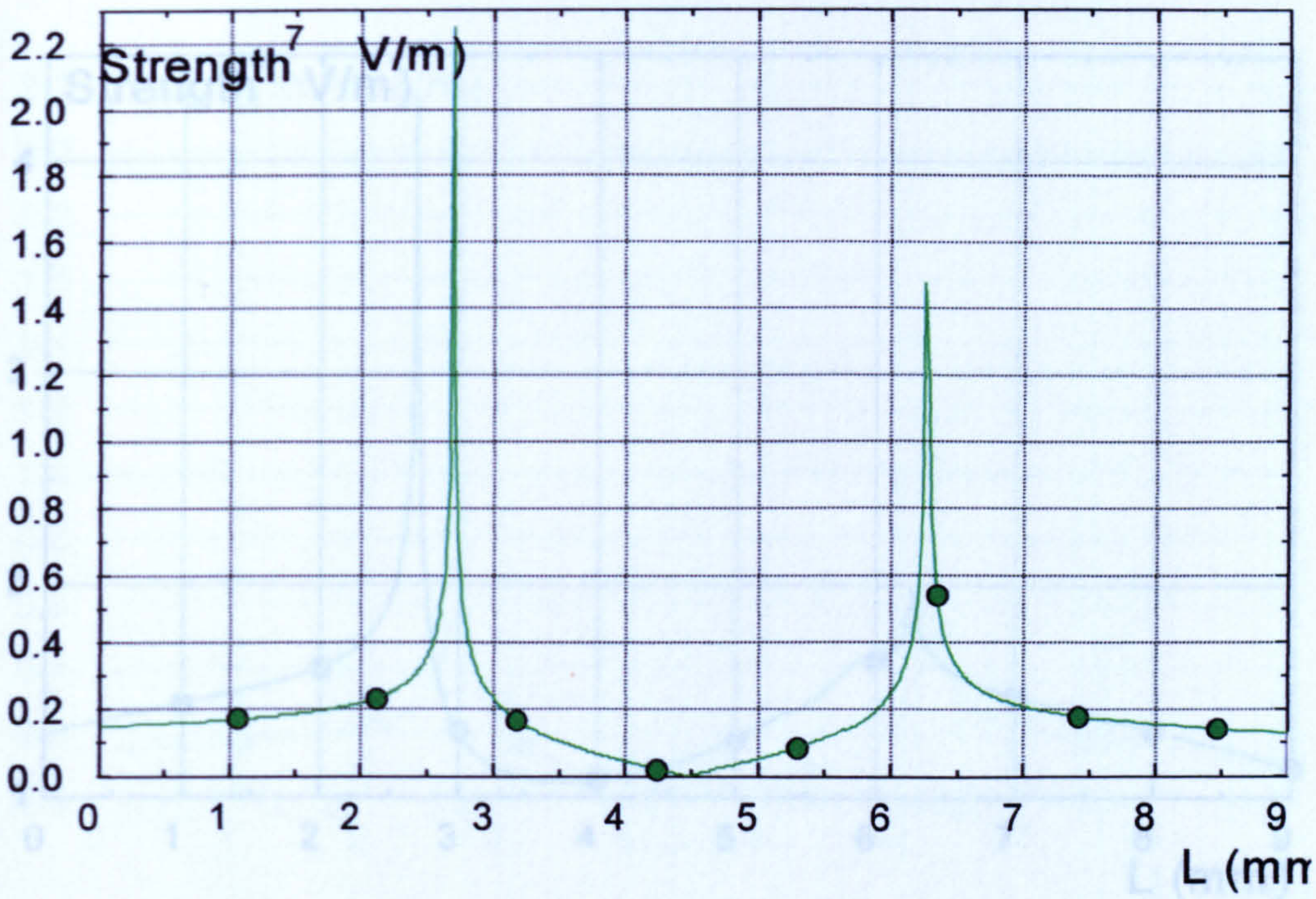

Fig (9.15) The electric field (E) between the locations A and B of Fig (9.7) the water resistivity was $1x10^6$ Ωm.

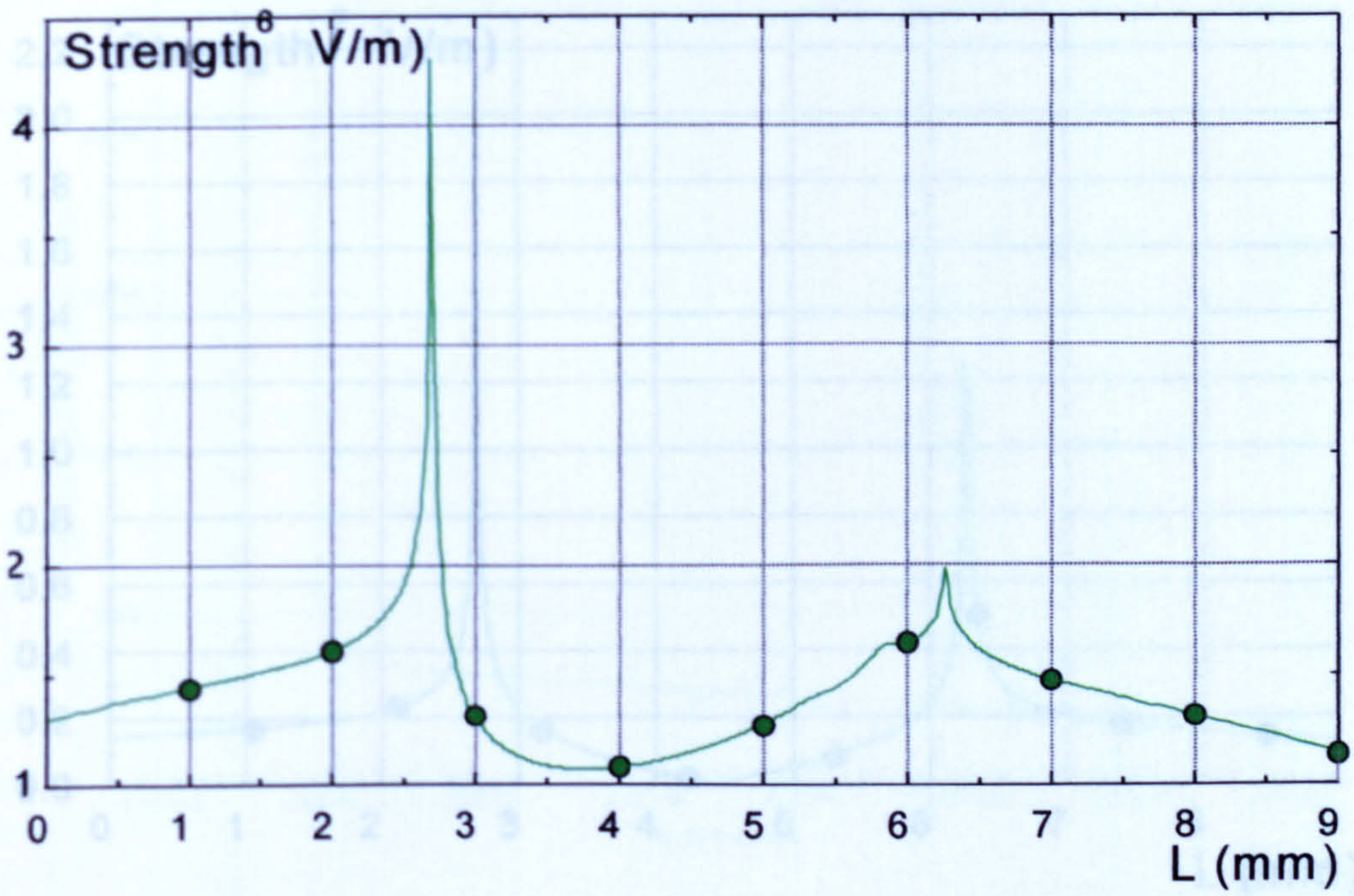

Fig (9.12) The electric field (E) between the locations A and B of Fig (9.7) the water resistivity was $1x10^{13}$ Ωm.

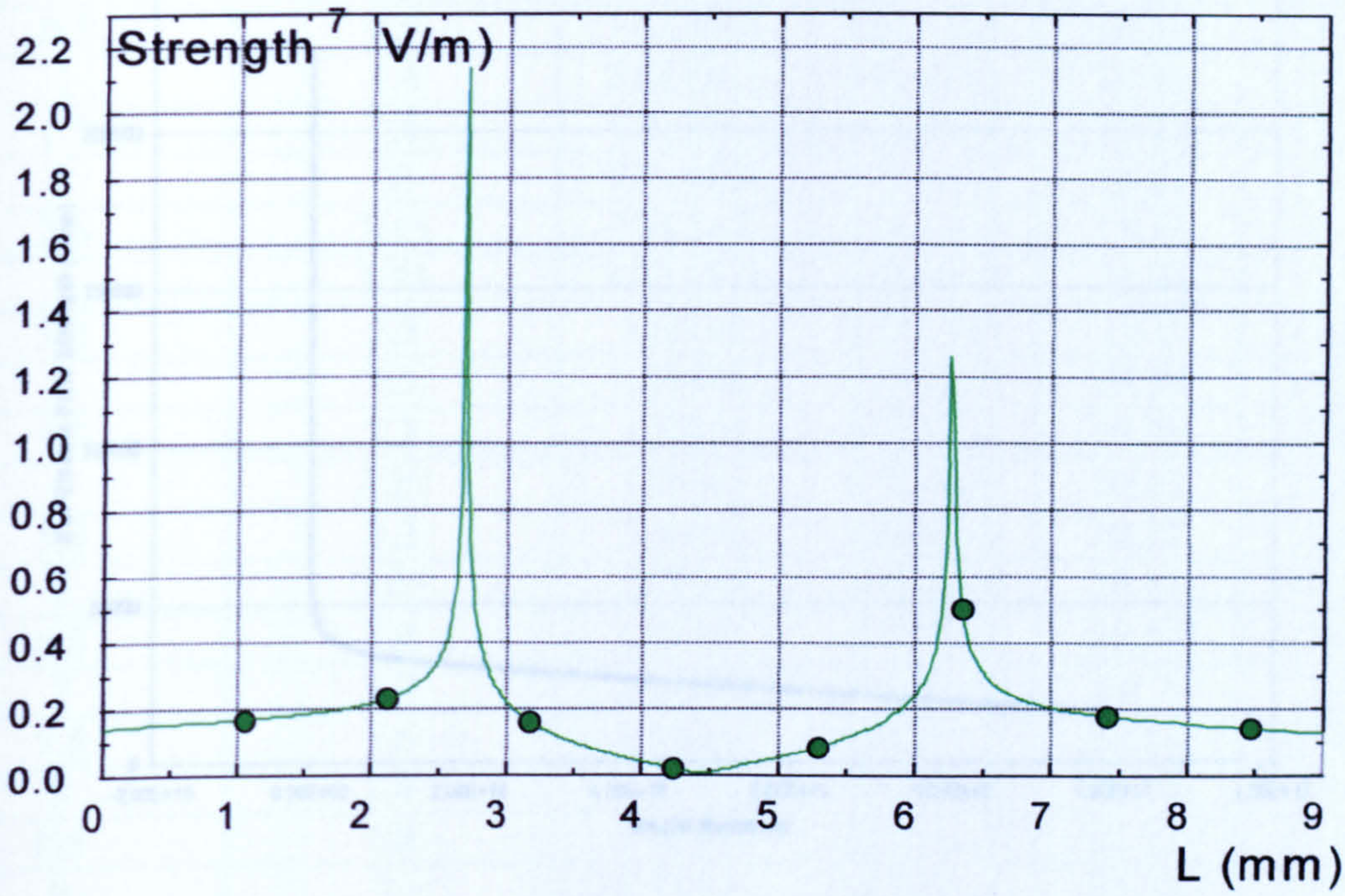

Fig (9.16) The electric field (E) between the locations A and B of Fig (9.7) the water resistivity was $1x10^{11}$ Ωm.

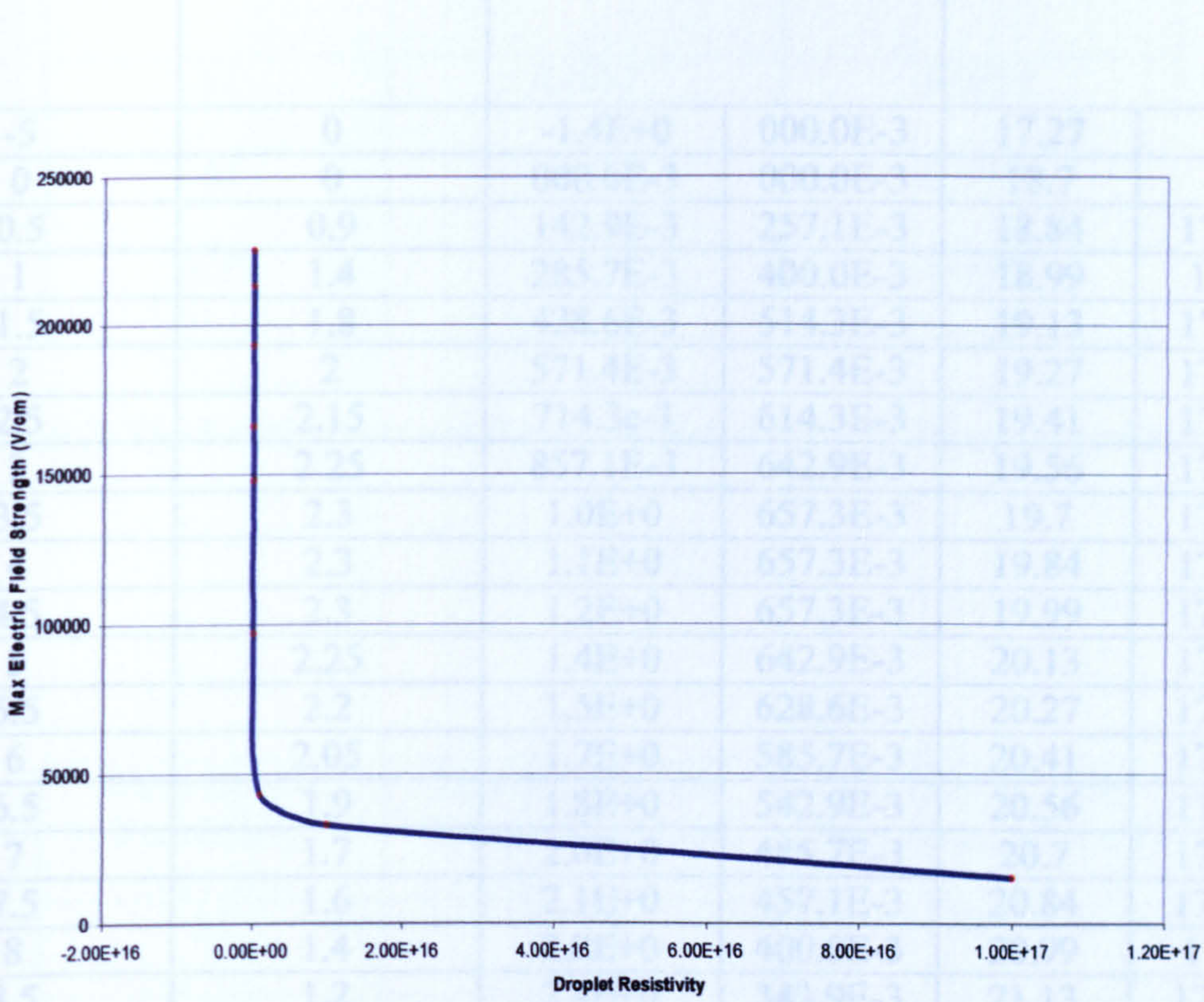

Fig (9.13) the relation between electric field strength and droplet resistivity

Distance along surface arbitrary unit	Drop height same units	Converted to mm		Converted to QuickField data points	
-5	0	-1.4E+0	000.0E-3	17.27	17
0	0	000.0E-3	000.0E-3	18.7	17
0.5	0.9	142.9E-3	257.1E-3	18.84	17.26
1	1.4	285.7E-3	400.0E-3	18.99	17.4
1.5	1.8	428.6E-3	514.3E-3	19.13	17.51
2	2	571.4E-3	571.4E-3	19.27	17.57
2.5	2.15	714.3e-3	614.3E-3	19.41	17.61
3	2.25	857.1E-3	642.9E-3	19.56	17.64
3.5	2.3	1.0E+0	657.3E-3	19.7	17.66
4	2.3	1.1E+0	657.3E-3	19.84	17.66
4.5	2.3	1.2E+0	657.3E-3	19.99	17.66
5	2.25	1.4E+0	642.9E-3	20.13	17.64
5.5	2.2	1.5E+0	628.6E-3	20.27	17.63
6	2.05	1.7E+0	585.7E-3	20.41	17.59
6.5	1.9	1.8E+0	542.9E-3	20.56	17.54
7	1.7	2.0E+0	485.7E-3	20.7	17.49
7.5	1.6	2.1E+0	457.1E-3	20.84	17.46
8	1.4	2.2E+0	400.0E-3	20.99	17.4
8.5	1.2	2.4E+0	342.9E-3	21.13	17.34
9	1	2.5E+0	285.7E-3	21.27	17.29
9.5	0.8	2.7E+0	228.6E-3	21.41	17.23
10	0.7	2.8E+0	200.0E-3	21.56	17.2
10.5	0.5	3.0E+0	142.9E-3	21.7	17.14
11	0.3	3.1E+0	85.7E-3	21.84	17.09
11.5	0.2	3.2E+0	57.1E-3	21.99	17.06
12	0.1	3.4E+0	28.5E-3	22.13	17.03
12.5	0	3.5E+0	000.0E-3	22.27	17
17	0	4.8E+0	000.0E-3	23.56	17

Table (9.1) Droplet profile taken from figure (9.4)
and adjusted as geometrical data for use with QuickField.

Water Droplet Permittivity	F_m in (HVED) With angle 0° (N)	F_m in (GED) With angle 180° (N)
81	0.0082	0.0063
40	0.0080	0.0061
2.35	0.0071	0.0055

Table (9.2) The Relation between the mechanical force and the droplet permittivity

Water Droplet Permittivity	Max Electric field Strength E_s (V/cm)	Min Electric field Strength E_s (V/cm)
81	63000	787
40	53210	1360
2.35	9120	5140

Table (9.3) The Relation between the Electric Field Strength and the droplet permittivity.

Insulation sample Permittivity	F_m in (HVED) With angle 0° (N)	F_m in (GED) With angle 180° (N)
1.5	0.0066	6.6e-4
2.35	0.0071	0.0055
4	0.0074	0.0058

Table (9.4) The Relation between the mechanical force and the insulation sample permittivity

Insulation sample Permittivity	Max Electric field Strength E_s (V/cm)	Min Electric field Strength E_s (V/cm)
1.5	9560	5040
2.35	9240	5150
4	8740	5180

Table (9.5) The Relation between the Electric Field Strength and the insulation sample permittivity.

Distance along field line s (mm)	Δs (mm)	Applied Field (kV mm^{-1})	Ionization Coefficient α (mm^{-1})	αΔs	ΣαΔs
0.000	0.216	5.739	7.418	1.600	1.600
0.216	0.216	5.686	7.094	1.530	3.130
0.431	0.216	5.627	6.770	1.460	4.590
0.647	0.216	5.564	6.398	1.380	5.970
0.863	0.216	5.499	6.028	1.300	7.270
1.078	0.216	5.435	5.657	1.220	8.490
1.294	0.216	5.371	5.332	1.150	9.640
1.510	0.216	5.306	5.007	1.080	10.720
1.725	0.216	5.242	4.683	1.010	11.730
1.941	0.216	5.178	4.404	0.950	12.680
2.157	0.216	5.114	4.126	0.890	13.570
2.372	0.216	5.051	3.848	0.830	14.400
2.588	0.216	4.988	3.570	0.770	15.170
2.804	0.216	4.925	3.338	0.720	15.890
3.020	0.216	4.862	3.106	0.670	16.560
3.235	0.216	4.800	2.875	0.620	17.180
3.451	0.216	4.739	2.689	0.580	17.760
3.667	0.216	4.679	2.504	0.540	18.300
3.882	0.216	4.619	2.318	0.500	18.800
4.098	0.216	4.559	2.133	0.460	19.260

Table (9.6) The growth of gas ionisation in air as a function of distance along a field line extending from the surface of a droplet. The final column shows that ΣαΔs exceeds 18 and therefore that avalanche growth satisfies the streamer criterion for breakdown.

Water Droplet resistivity (Ωm)	Max Electric field Strength E_s (V/cm)	Min Electric field Strength E_s (V/cm)
$1x10^{6}$	225000	7280
$1x10^{11}$	213000	8130
$1x10^{13}$	43100	10700

Table (9.7) The Relation between the Electric Field Strength and the droplet Resistivity.

Water Droplet resistivity (Ωm)	I_c Maximum A/m^2	I_c Minimum A/m^2
$1x10^{6}$	2.25e-6	7.28e-10
$1x10^{11}$	2.13e-6	5.13e-9
$1x10^{13}$	4.31e-7	1.07e-7

Table (9.8) The Relation between the current density and the droplet Resistivity

Insulation sample resistivity (Ωm)	Max Electric field Strength E_s (V/cm)	Min Electric field Strength E_s (V/cm)
$1x10^{6}$	44300	10600
$1x10^{11}$	223000	6220
$1x10^{13}$	225000	7280

Table (9.9) The Relation between the Electric Field Strength and the insulation sample Resistivity.

Insulation sample resistivity (Ωm)	I_c Maximum A/m^2	I_c Minimum A/m^2
$1x10^{6}$	4.43	1.06
$1x10^{11}$	2.23e-4	6.22e-8
$1x10^{13}$	2.25e-6	7.28e-10

Table (9.10) The Relation between the current density and the insulation sample Resistivity

Chapter 10

Conclusions and Suggestions for Future Work

10.1 General

In the context of high electrical stress applied to insulation exposed to hostile environmental conditions, the behaviour of water droplets on the insulation surface has been investigated in terms of droplet vibration, movement and spreading over the surface and also in terms of partial discharge activity at the edges of the water droplets. This behaviour has been investigated (a) optically, using a high speed-video camera, (b) electrically, using partial discharge detection and (c) theoretically using field modeling software.

As a result of this study, several conclusions have been drawn, and these have been identified and discussed at appropriate points in the text. In this chapter, the most salient conclusions are summarized and suggestions for the future work that might arise from the present study are identified and discussed.

10.2 Summary of Main Conclusions

In agreement with previous studies, it has been observed that as the level of applied 50-Hz, AC stress was increased at water droplets on a polymeric surface, the onset of partial discharge activity at the edge of the droplets was observed followed almost immediately by droplet vibration in a fixed position. The frequency of droplet vibration was measured to be 50Hz and, this being the applied frequency, it may be concluded that for the conditions studied, the mechanism of vibration is consistent with electrostatic attraction rather than a dielectrophoretic mechanism characterized by droplet vibration of double the applied frequency. Lateral spreading of the droplet in directions parallel to the applied field follows the onset of vibration, and the tendency for this to happen increases with increase in applied field above the vibration onset level. The onset of partial discharge activity was observed alongside vibration and it is

possible that vibration promotes partial discharges by altering the contact angle at the triple point and so increasing the curvature of the droplet and, consequently, the electric field in the air around the droplet.

Field calculations show the surface electric field reaches a narrow, local maximum at the triple junction. This is likely to promote surface electrical discharges there. However, calculations presented in this thesis consider a path in the air starting at a point on the droplet surface a significant distance above the triple junction and the polymer surface. Previous workers have reported the presence of partial discharges apparently along such a path and such discharges were also observes in the present study. This path is considered to extend along a field line through the air and to terminate on the polymer surface at some distance from the droplet. The present new calculations show that the magnitude of the electric field along such a field line can exceed that over an equivalent path on the polymer surface. Further calculations show that it is possible to satisfy the streamer criterion for gas breakdown along such a path. It is considered that if discharges do terminate some distance from the triple junction, then an evaluation of any effects they may have on surface hydrophobicity, and consequently on droplet spreading, may have to take this distance into account.

10.3 Suggestions for Future Work

In the present work a PE surface only has been examined, and even this surface could be more closely characterised. This limitation could be addressed by developing a test sample arrangement in which thin samples of various materials material, similar in geometry to a microscope slide, could be supported on an insulator backing. The surface condition of such slides could be highly defined and controlled. By studying a variety of insulation materials in this way, and by applying the experimental and theoretical techniques and procedures developed in this thesis, the significance of partial discharge location and their significance to such factors as insulator surface structure and hydrophobicity could be further studied.

By improving the control of the applied ac stress, it should be possible to more precisely determine the onset of partial discharge activity at a lower level of discharge

than that detected in the present study. By improving partial discharge detection, it should be possible to trigger the high-speed camera so obtain simultaneous records of discharge magnitude and visual location. Such improvements would allow the investigation of streamer breakdown away from the polymer surface to be more exhaustively conducted. This, in turn, would allow the connection between surface hydrophobicity changes caused by partial surface discharges and droplet movement to be more completely understood.

In this thesis, only liquid pollution was examined in the form of a single water droplet. This could be extended to multiple droplets that may interact and so behave closer to the practical case. Further, a study of solid pollution or a combination of solid and liquid pollution would again be of practical interest.

Following work on test samples of materials, it would be useful to study commercial outdoor insulators under high electrical stress, such as at 132kV or 500kV, with different types of environmental pollution. The behaviour of the pollution and the partial discharge activity could be investigated using the same procedures and techniques described in this thesis.

It would also be of interest to extend this work by applying AC stresses over a range of frequencies so that the characteristic resonance frequency of vibration of droplets could be determined. This information would be useful when considering droplet behaviour under the range of impulse and fault conditions encountered on practical power systems when applied stresses can contain a significant spectrum of frequencies.

Appendices

A STUDY OF WATER DROPLET BEHAVIOR ON INSULATOR SURFACES UNDER HIGH ELECTRICAL STRESS

UPEC 2001

B. H. Crichton and H. A. Gouda

Applied Electrical Technology Group, Institute for Energy and the Environment,
University of Strathclyde, Glasgow.

ABSTRACT

In this paper we study the behaviour of a single water droplet on an insulator surface under the influence of high, applied electric stress. Using a finite element method we have computed the associated field distribution. We have examined two cases: (1) Electrostatic analysis to calculate potential and field distributions and the associated force applied to the droplet; and (2) Current flow analysis to calculate leakage current density. The influence of water permittivity, observed droplet shape and position relative to the test electrodes is discussed. In each case, we calculate the resultant mechanical forces exerted on the droplet. These forces are found to depend on droplet shape such that its potential motion towards the electrodes will be influenced by this factor. This work forms part of a longer-term experimental study of droplet behaviour using high-speed digital camera techniques.

1. INTRODUCTION

Pollution phenomena constitute a serious problem, which must be taken into account in the design and the operation of HV insulating devices. Under severe environmental conditions, a pollution layer (dry or wet) is deposited on the insulator surface the leakage current begins to flow, leading to a total flashover [1]. The outdoor high voltage power plants, such as insulators, bushings, surge arresters and current transformers, etc. are exposed to various environmental conditions during their service life. In industrial, coastal and desert areas, for example, the surface of insulator can become heavily polluted. Contamination flashover may occur during period of wet weather and may cause power outages, which pose a particular threat to the reliability of the power supply [2] and the performance of a HV insulator under polluted condition is quite different from that under pollution-free conditions [3].

Considering the importance of pollution problems, continuous and intensive laboratory studies and field investigations have been taking place worldwide for many years. The work involves not only experimental investigations but also mathematical modeling to understand the different aspects of the contamination flashover mechanism [2].

On the other hand with the rise in transmission line voltage, importance of the research on insulator pollution has increased considerably, and pollution performance of insulators will be the co-ordination of insulation in UHV transmission lines. Research on insulator pollution is directly primarily to understanding the physics of growth of discharge and to develop a mathematical model, which can predict accurately the critical current [4].

2. POLLUTION OF INSULATION

When contamination is present, the response of external insulation to power frequency become an important consideration and may dictate external insulation design. It is known that flashover of insulation generally occurs when the surface is contaminated [5]. So the surface pollution can take a number of forms, including:

- Wetting by fog, dew, rain, snow or sea spray. This wetting may be affected by dissolved contaminants contained in the wetting agent, including salt and other chemical pollutants. Such pollution tends to form thin layers distributed over parts of the surface.
- Contamination by natural air-borne particles such as dust, sand or soot. In this case the pollution can be in form of discrete particles scattered over large areas of the insulator surface.

3. COMPUTATION OF ELECTROMAGNETIC FIELDS

Two cases are examined:

<u>Electrostatic analysis</u>

Is used to calculate the voltage, electric field, capacitance and electric force. Initial work in this programme has involved linear electrostatic analysis for 2-D and axisymmetric models. The work is based on finite-element solution to Poisson's equation with the following conditions:

- Material properties: air, orthotropic materials with constant permittivity.
- Loading sources: Voltage, and electric charge density.

<u>Current flow analysis:</u>

Is used to calculate the voltage, current density, electric field, and power loss (joule heat). Linear current flow

analysis is performed for 2-D and axisymmetric models with the following conditions:
- Material properties: air, orthotropic materials with constant resistively.
- Loading sources: Voltage, and electric charge density.
- Boundary conditions.

4. MODEL

The model, which was used to study the effect of the water droplet and a pollution layer under the water droplet on the polymer sample with diameter 1-cm (polyethylene), is shown in Fig (1). AC voltage was applied to the both electrodes (ring electrode with diameter 2-cm). The high voltage electrode is energized with a potential 20 kV, and the other is grounded. The droplet was assumed to be circular. The droplet conductivity (0.1 μS/cm) the conductivity of the air and polymer sample was taken 1e-15 S/cm and 1.2e-13 S/cm respectively. The relative permittivity of the water droplet was taken as 80.4 and the polymer sample as 2.35. The effect of the wet pollution layer with varying permittivity and conductivity on the electric field strength, the current density and the mechanical force was examined.

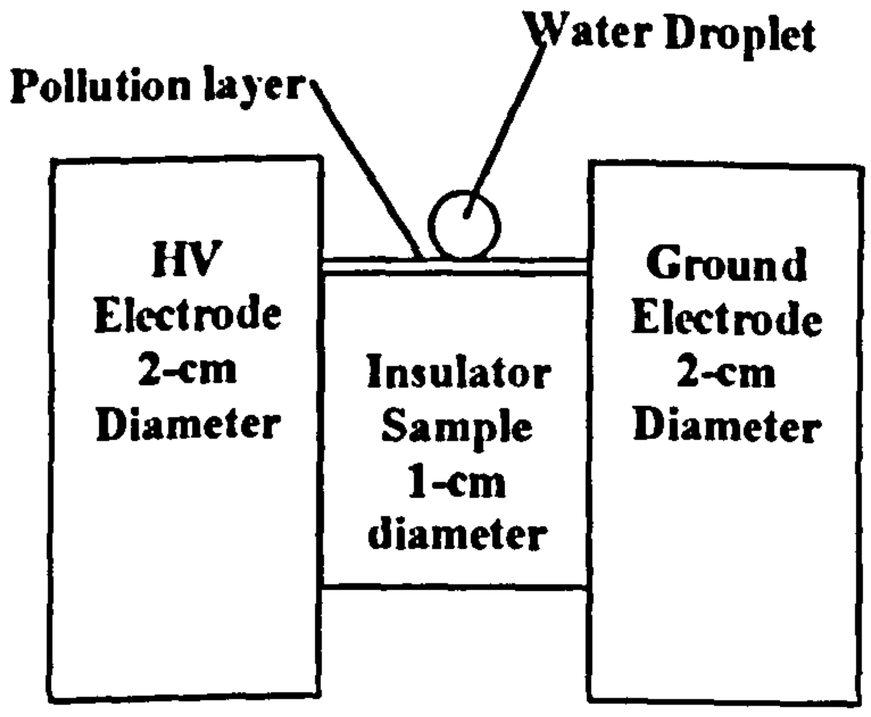

Figure (1)

5. ELECTROSTATIC ANALYSIS

In the electrostatic analysis we calculated the mechanical force and the electric field strength. First we considered the permittivity of the pollution layer to be the same as the insulation sample so there was effectively no pollution layer. The mechanical force and the electric field strength were calculated in two directions with respect to the water droplet position first in high voltage electrode direction (HVED) and in the ground electrode direction (GED). The values of the mechanical force Fm with water droplet permittivity equal 80.4 and different pollution layer permittivity was shown in the table 1.

wet Pollution layer permittivity	Fm in (HVED) With angle 0°	Fm in (GED) With angle 180°
(A) 2.35	0.0556 N	0.0549 N
(B) 40	0.0575 N	0.0565 N
(C) 80.4	0.0584 N	0.0579 N

Table (1) the mechanical force values

From the above table we can notice that the mechanical force in the HVED is bigger than in the GED this mean the water droplet would tend to move in the high voltage electrode direction. Also the mechanical force increases when the permittivity of the water droplet is equal to the permittivity of the wet pollution layer. The electric field strength values changed and we found the maximum value at the two sides of the water droplet. This means that, due to existing of the water droplet and the wet pollution layer, the electric field is about twice the average applied level (20kV/cm). The electric field strength (Es) maximum and minimum values are shown in table 2 at water droplet permittivity 80.4 and pollution layer permittivity 2.35, 40, and 80.4.

Pollution layer permittivity	Es Maximum V/Cm	Es Minimum V/Cm
(A) 2.35	41600	20700
(B) 40	45200	20806
(C) 80.4	46900	20900

Table (2) the electric field strength values

From the above table we can notice that the electric field strength increases when the permittivity of the pollution layer increases. The electric field strength over the surface of the insulation sample is shown in figure (2 A, B, and C). When the relative permittivity of the droplet decreased to 40 the mechanical force and the electric field strength values alter as shown in table 3 and 4 respectively.

wet Pollution layer permittivity	Fm in (HVED) With angle 0°	Fm in (GED) With angle 180°
(A) 2.35	0.0552 N	0.0546 N
(B) 40	0.0569 N	0.0561 N
(C) 80.4	0.0611 N	0.0604 N

Table (3) the mechanical force values

Pollution layer permittivity	Es Maximum V/Cm	Es Minimum V/Cm
(A) 2.35	41700	20700
(B) 40	45900	20900
(C) 80.4	48100	20700

Table (4) the electric field strength values

The values of the mechanical force increase when the permittivity increases and the mechanical force in the HVED is bigger than in the GED. This means that the water droplet tends to move towards the HVED.

Notes:

- All the maximum and minimum values of the mechanical, electric field strength and current density are calculated between the water droplet and the both two electrodes.
- All the figures are taken over the insulator surface.

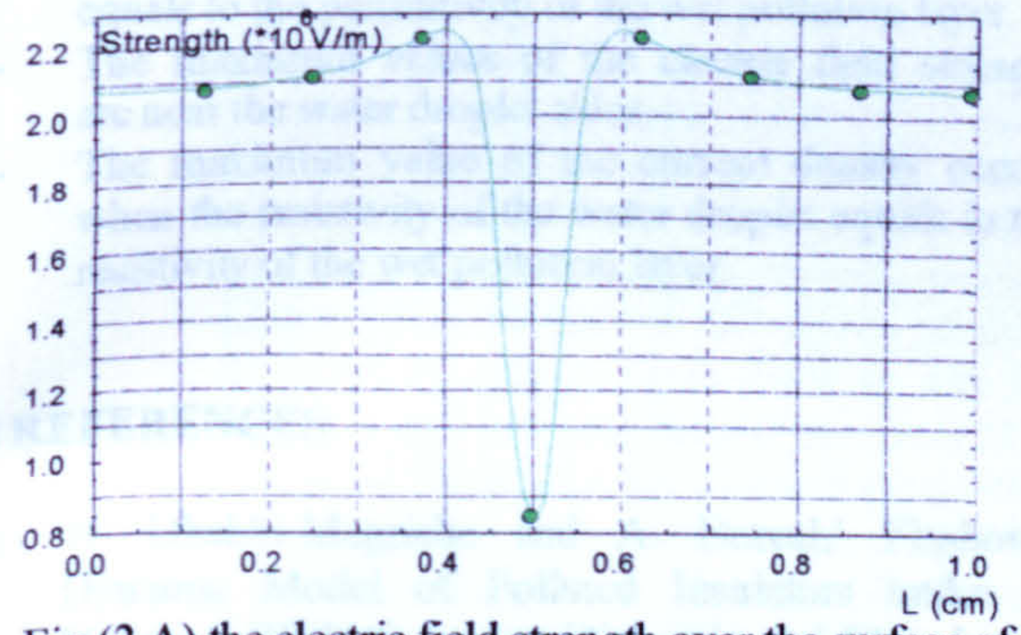

Fig (2 A) the electric field strength over the surface of insulation sample

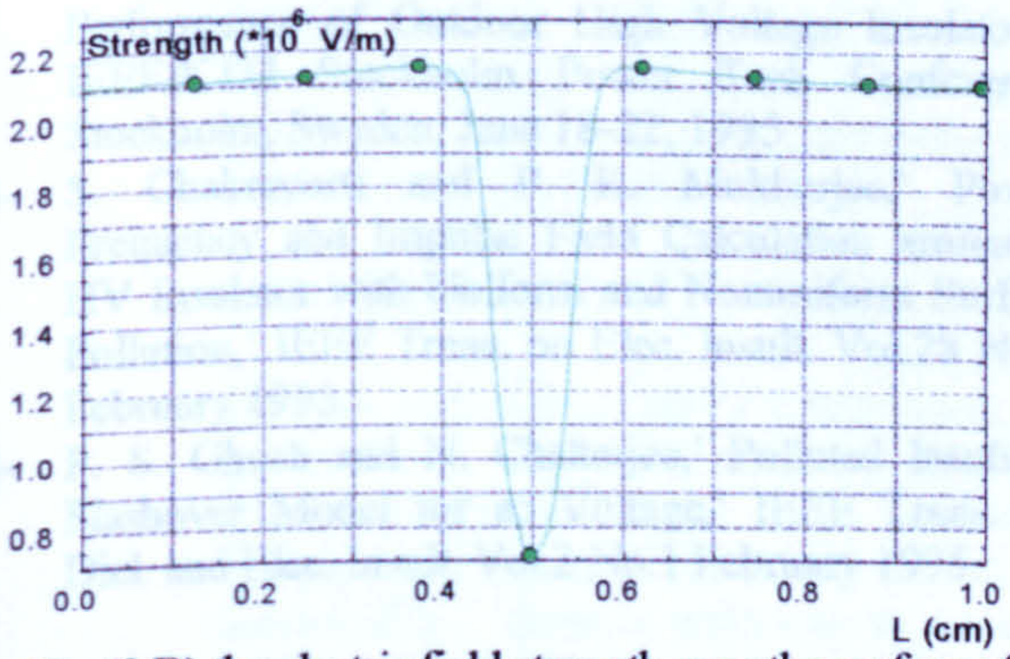

Fig (2 B) the electric field strength over the surface of insulation sample

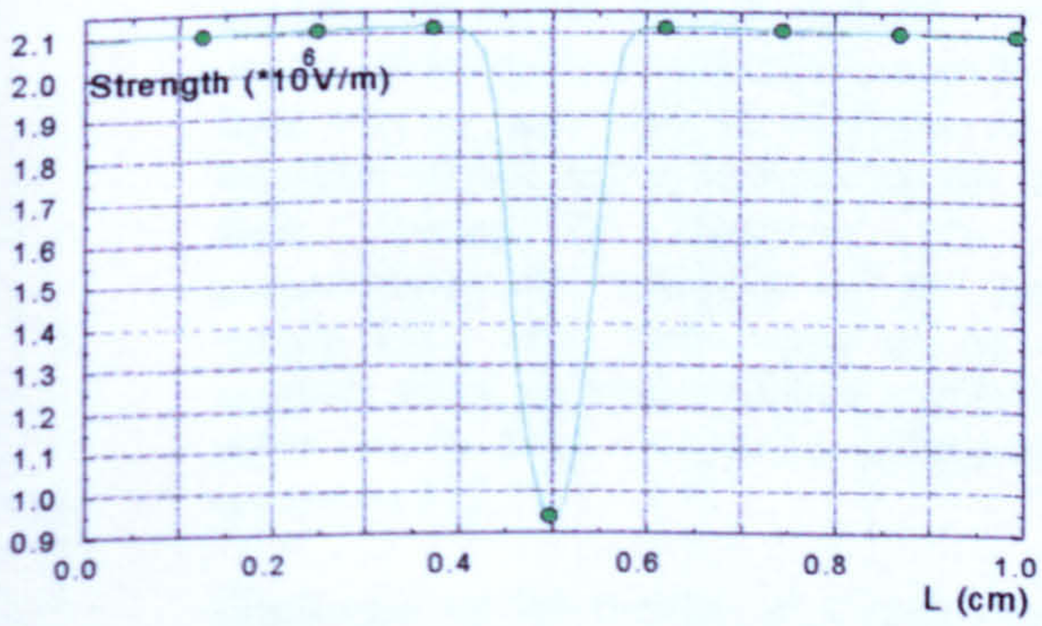

Fig (2 C) the electric field strength over the surface of insulation sample

6. CURRENT FLOW ANALYSIS

In the current flow analysis we study the effect of the water droplet and the pollution layer over the insulation surface on the leakage current density (Ic). The electrical resistance of the sample is 1e+13Ω and the water droplet is 1e+5Ω. First we considered that the wet pollution layer has no effect when its resistivity is equal to the sample resistivity. The maximum and minimum values of the current density are shown in table 5.

wet Pollution layer permittivity	Ic Maximum A/m^2	Ic Minimum A/m^2
(A) 1e+13	2.45e-7	8.59e-8
(B) 1e+10	2.18e-4	1.53e-5
(C) 1e+5	21.11	8.78

Table (5) the current density values

From the above we can see that the maximum value of the leakage current density passing through the water droplet and the polluted layer over the insulation surface. Also we can notice that the high current density occurs when the resistivity of the water droplet equal to the resistivity of the wet polluted layer. This current may be led to the flashover and then insulation failure. The current density over the surface of the insulation sample is shown in figure (3).

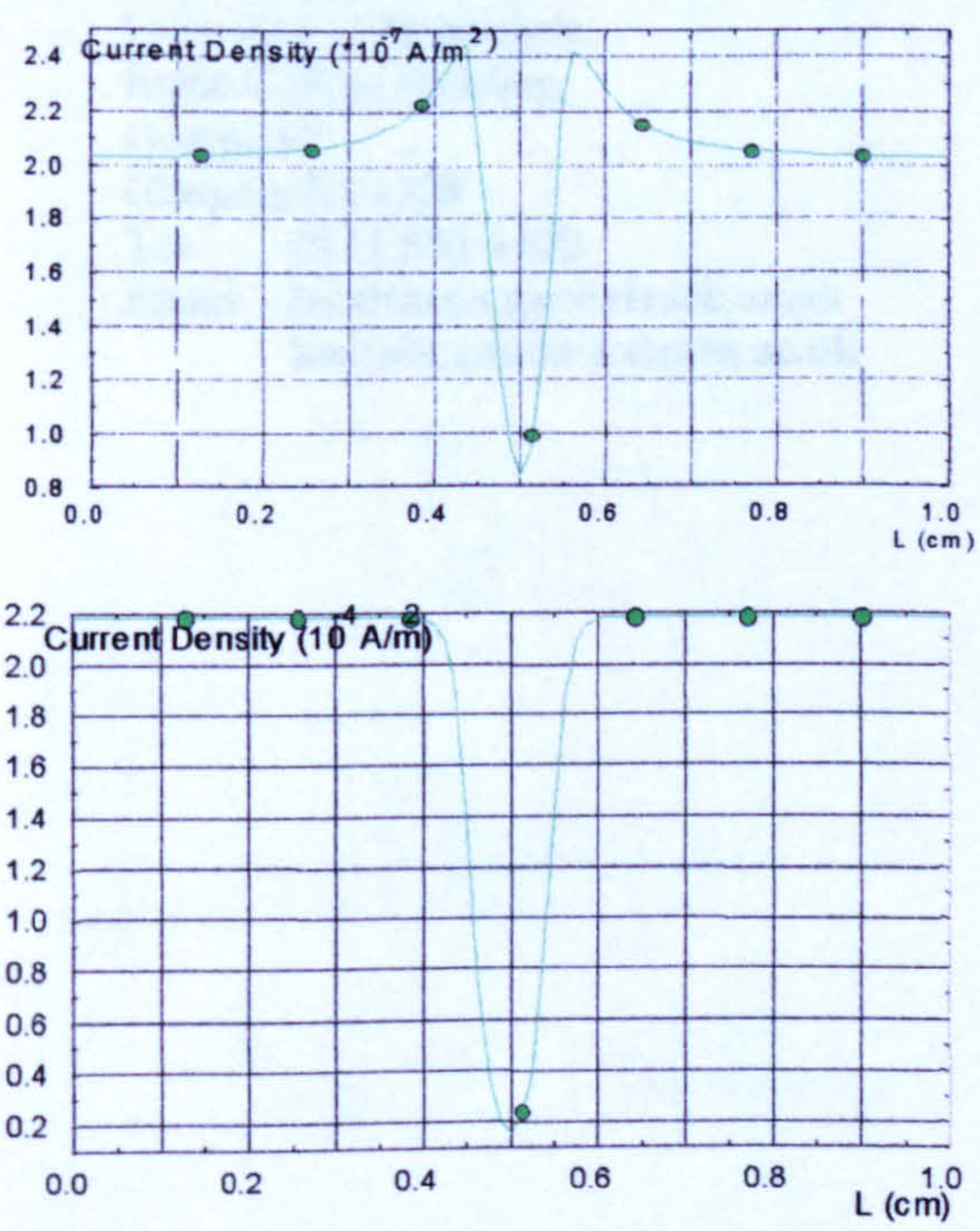

Fig (3) the current density over the surface of insulation sample

7. CONCLUSIONS

- The mechanical force and the electric field strength increase when the permittivity of the wet pollution layer increases.
- The mechanical force and the electric field strength increase when the permittivity of the water droplet decreases.
- The maximum value of the electric field strength occurs when the permittivity of the water droplet equals to the permittivity of the wet pollution layer.
- The maximum values of the electric field strength are near the water droplet sides.
- The maximum value of the current density occurs when the resistivity of the water droplet equals to the resistivity of the wet pollution layer.

8 REFERENCES

1- N. Dhahbi-Megriche and A. Boreal,' Flashover Dynamic Model of Polluted Insulators under ac Voltage', IEEE Trans. on Dielectric and Elec. Insult. Vol.7 No.2 April 2000.

2- S. Shihab and L. Zhou,' Simulation of Contamination Performance of Outdoor High Voltage Insulators,' IEEE/KTH Stockholm Power Tech Conference, Stockholm, Sweden, June 18-22, 1995.

3- S. Chakravorti and P. K. Mukherjee,' Power Frequency and Impulse Field Calculation around a HV Insulator with Uniform and Nonuniform Surface Pollution,' IEEE Trans. on Elec. Insult. Vol.28 No.1 February 1993.

4- P. S. Ghosh and N. Chatterjee,' Polluted Insulator Flashover Model for ac Voltage,' IEEE Trans. on Diel. and Elec. Insult. Vol.2 No.1 February 1995.

5- S. M. Ghufran Ali and H. M. Ryan,' Insulation Co – ordination under polluted conditions,' the 7th BEAMA International Electrical Insulation Conference.

6- B. F. Hampton,' Flashover Mechanism of Polluted Insulation,' Proc. IEE, Vol. 111, No 5, May 1964.

7- Md. Abdus Salam, Hussein Ahmad, Ahmad S. Ahmad, Tarmidi Tamsir, M. A. M. Piah and Z. Buntat,' Flashover Phenomena of Polluted Insulators Energized by AC Voltage,' IEEE conference on Electrical Insulation and Dielectric Phenomena 1999.

8- S. Keim and D. Koenig,' Study of the Behavior of Droplets on Polymeric Surfaces under the Influence of an Applied Electric Field,' IEEE conference on Electrical Insulation and Dielectric Phenomena 1999.

ACKNOWLEDGEMENTS

H.A.Gouda is grateful for financial support from the Ministry of Defence, Egypt.

B. H. Crichton and H. A. Gouda: -
Applied Electrical Technology Group,
Institute for Energy and the Environment,
Department of Electronic and Electrical Engineering,
University of Strathclyde,
Royal College Building,
George St
Glasgow G1 1XW
Tel 0141 552 4400
Email b.crichton@eee.strath.ac.uk
hossam.gouda@strath.ac.uk

Sessile Water Droplets on Insulating Surfaces Subject to High AC Stress: Effect of Contact Angle.

UPEC 2002

H. A. Gouda, B. H. Crichton, R. A. Fouracre and M. Stickland*

Applied Electrical Technology Group, Institute for Energy and the Environment,
University of Strathclyde, Glasgow, Scotland.
* Department of Mechanical Engineering, University of Strathclyde, Glasgow, Scotland.

Surface pollution of outdoor high-voltage insulators is an important cause of flashover. We have undertaken an experimental study of electrical breakdown at the edges of a sessile water droplet on a planar, polymeric, insulating surface when subject to AC stress, parallel to the insulator surface, up to 2MV/m. The static contact angle between droplet and surface was varied by controlling the physical properties of the droplet and by inclining the insulator plane from the horizontal. The partial discharge activity from the water droplet was investigated using a combination of high-speed video camera, operated at up to 3,000 frames per second, and an electrical partial discharge detection system. We have used this to examine the location of partial discharge at the edges of the water droplet.

1. INTRODUCTION

Outdoor high-voltage (HV) power plant, such as insulators, bushings, surge arresters and current transformers, etc. are exposed to various environmental conditions during their service life. Surface pollution is a serious problem for the design and operation of HV devices in many industrial, coastal and desert areas, for example, where the surface of insulator can become heavily polluted. Under severe environmental conditions, a pollution layer (dry or wet) may be deposited on an insulator surface and a leakage current may flow, leading to flashover [2] and compromising the reliability of the power supply [3]. The performance of an HV insulator under polluted condition is known to differ greatly from that under pollution-free conditions [4].

Discharges on the surface of a contaminated polymeric insulator are considered to be one of the ageing mechanisms responsible for the failure of the insulator and can occur between water drops on the surface of insulators, creating a number of radicals and ionized species that chemically react with the insulator surface and thus alter the original properties of the insulator material [1]. Considering the importance of pollution problems, continuous and intensive laboratory studies and field investigations have been taking place worldwide for many years. The work involves not only experimental investigations but also mathematical modeling to understand the different aspects of the contamination flashover mechanism [3].

2. EXPERIMENTAL PROCEDURE

The behaviour of a water droplet on the surface of a polymer sample was investigated using the apparatus shown schematically in Figure 1. It consisted of a polyethylene (PE) cylinder, diameter 20mm and length 30mm, with embedded electrodes. Up to 20kV, 50Hz was applied between the electrodeswith one of the electrodes effectively earthed.

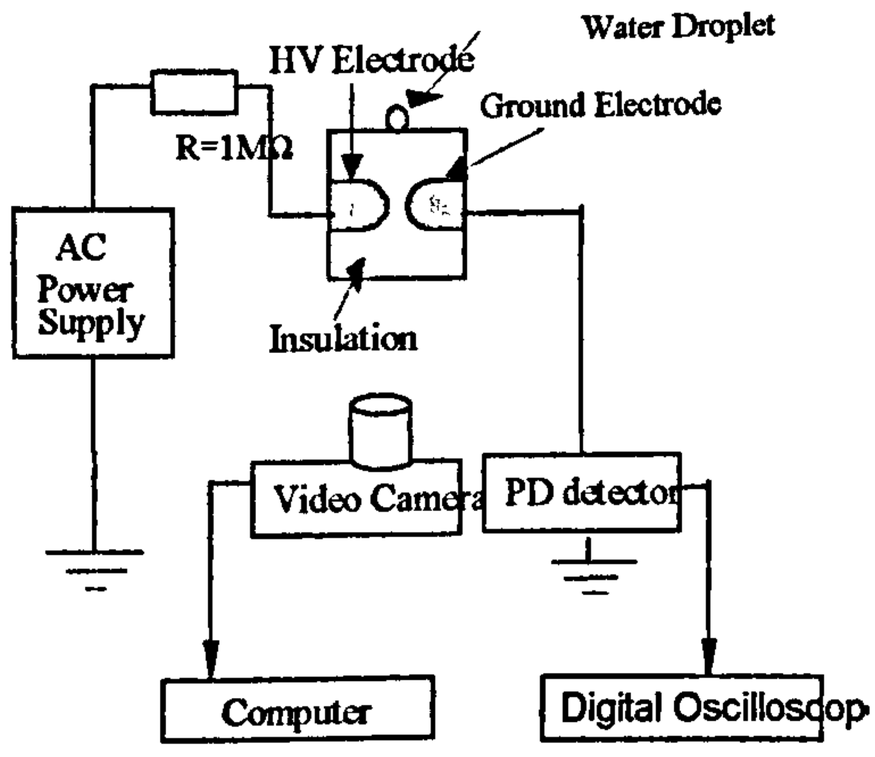

Figure 1. Schematic representation of experimental Set-up

A plane face was machined on the upper side of the cylinder and a single water droplet of volume 10μl was placed centrally on this surface. The tap water used had a resistivity of approximately $10^6\Omega m$ and a relative permittivity of approximately 80.4. The relative permittivity of the PE sample was assumed to be approximately 2.35.

The behavior of the droplet was observed using a Photron Fastcam Super 10k high-speed camera operating at 3000 frames per second. Partial discharge (PD) activity was determined by observing the electrical pulses generated across a 100-Ω resistor at the low-voltage electrode.

3. CONTACT ANGLE

Contact angle may be defined as the angle formed between the tangent to the water droplet at its point of contact and the planar surface on which it is placed. A measure of the hydrophobicity of the surface, is obtained by determining the contact angle when the contacting surface is horizontal [5]. In this study, the static contact angle was varied by tilting the insulator plane from the horizontal. This generated two separate contact angles, corresponding to the lowest and highest points of contact between the droplet and the plane surface, the lower point of contact giving the greater contact angle. The grater angle we designate angle A and the lesser angle (at the highest point) angle B.

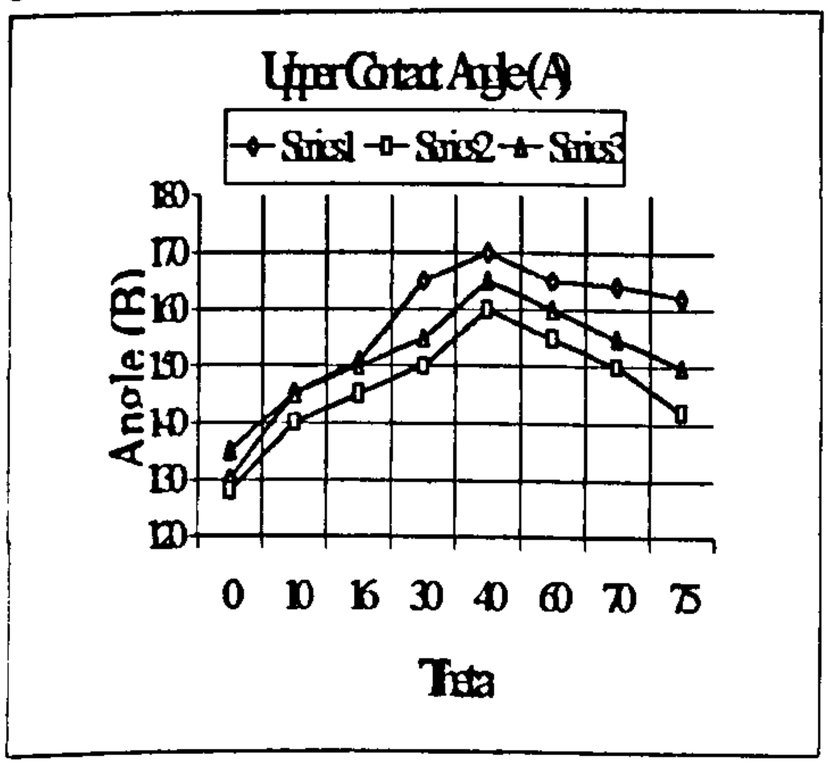

Figure 2. Upper Contact Angle A.
◊-tap water, Δ-salt water,
□-deionized water.

In the present work contact angles were measured for water droplets produced using tap water and, for comparison, nominally de-ionised water and tap water containing 1% saturated sodium chloride solution. These were chosen to represent three different water conductivities. All three conductivities show similarities in behaviour

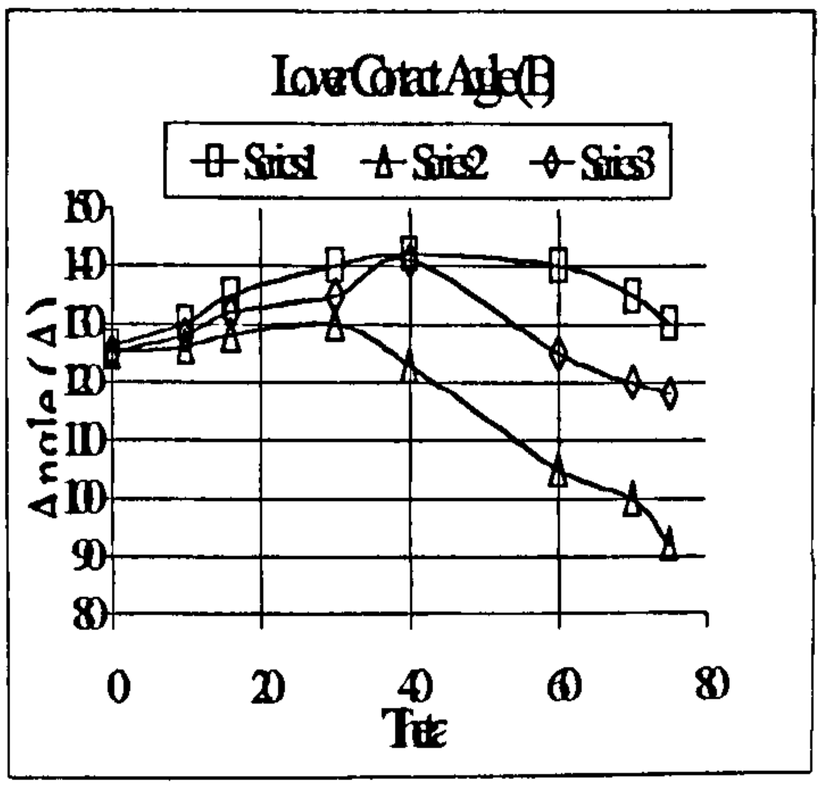

Figure 3. Lower Contact Angle B
□-tap water, ◊-salt water,
Δ-deionised water.

With increasing angle of inclination, θ, the angles A and B pass through a maximum as seen in Figures 2 and 3. When θ is zero the measured contact angles A and B show a small dependency on the conductivity but for a particular conductivity A and B are approximately the same. For larger values of θ the values of contact angle A are greater than the angle B, as might be expected. Tap water shows the largest measured contact angles although its conductivity lies between that of deionised water and water containing NaCl. However, it may be that the more complex nature of the dissolved content in the tap water droplets makes it difficult to compare the contact angle results directly with those for the other types of droplet.

4. PARTIAL DISCHARGE ACTIVITY

PD patterns were obtained for a 10μl droplet deposited in the middle of the flat portion of the sample. As described above, the PD activity was detected in two ways: electrically and visually by high-speed video camera.

4.1 Electrically detected partial discharges.

Figure 4 shows the PD activity generated by the system when no water droplet was present on the surface of the sample. The inception voltage was 8.25kV and discharges were observed on both half cycles close to the peak of the applied voltage waveform. The magnitude of these discharges does not appear to damage the sample and does not lead to breakdown if allowed to continue for a period of time.

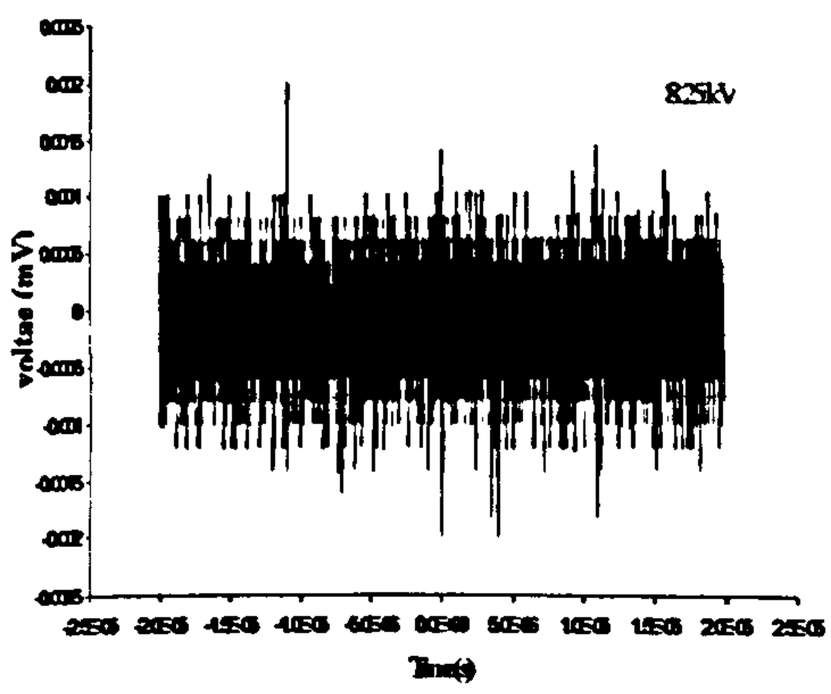

Figure 4. Partial discharge activity with no water droplet present.

When a water droplet was placed midway between the two electrodes on the flat horizontal polymer it was observed that surface partial discharge activity at the edges of the droplet was initiated when the applied voltage was raised to 11.7kV. Figure 5 shows the typical PD record obtained under these conditions.

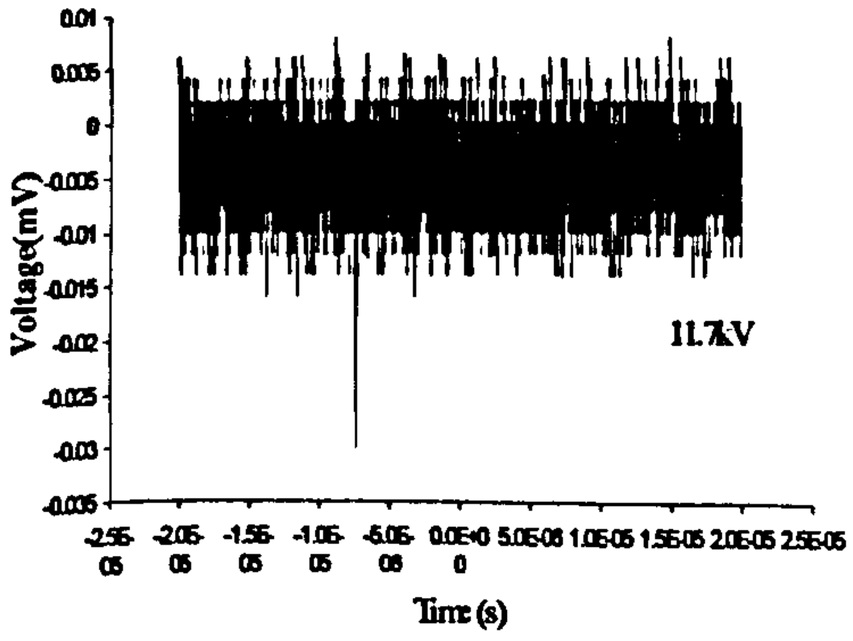

Figure 5. Partial discharge activity at the edges of a water droplet in the absence of droplet vibration.

The PDs in the negative half cycle appear to be larger than those in the positive half cycle. The magnitude of this negative PD is some 15 times greater than that observed without the presence of the droplet. Optical observation showed that the droplet was sessile and did not vibrate.

When the applied voltage was increased to 14.25 kV, the water droplet was observed to vibrate but without spreading. With the voltage raised to 16.8 kV, the droplet was observed to vibrate vigorously and then spread over the surface of the insulator. The measured PD activity at 16.8 kV is shown in figure 6. The peak magnitude was typically 25 times above the level observed without a water droplet. As before, PD activity is more pronounced during the negative half cycle. Under these conditions, the motion of the water droplet along the surface of the supporting insulator eventually lead to total breakdown along its surface

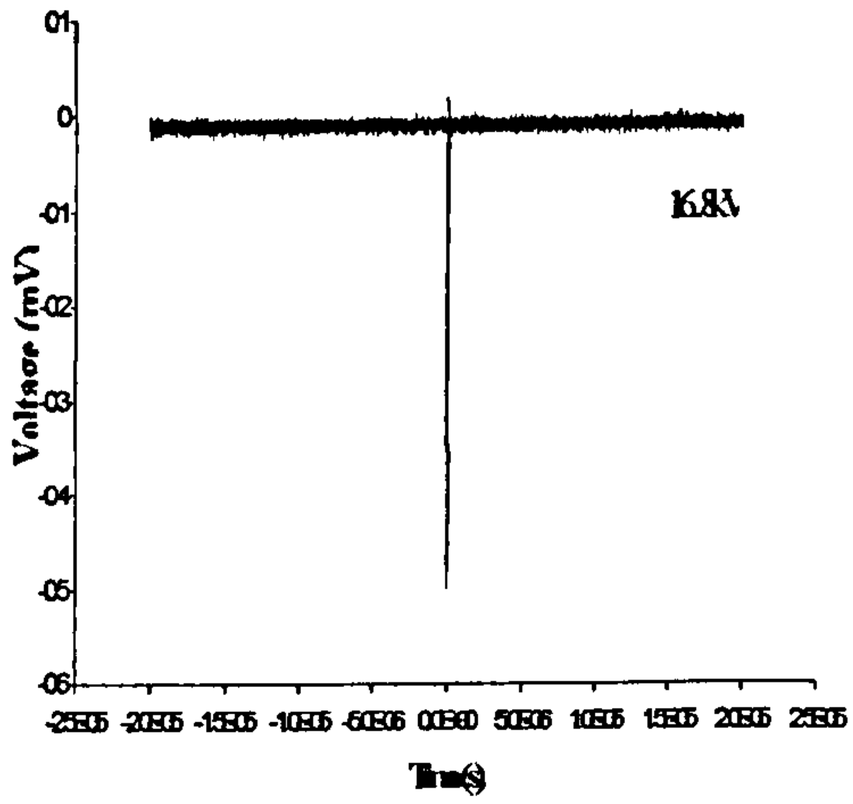

Figure 6. Partial discharge activity as the droplet spread over the surface.

4.2 Visual observation

Figure 7 shows a discharge at the edge of a droplet deposited on a level PE surface. The applied voltage was 16.8 kV and the water droplet had started to vibrate and expand. In the complete video sequence, the droplet is observed to vibrate and eventually spread over the whole sample as a wave-like vibration mode developed before complete electrical breakdown took place.

Figure 7. Discharge at the edge of a droplet spreading over the insulator surface..

5. ELECTRIC FIELD AROUND A DROPLET

When a droplet vibrates the contact angle varies considerably. As part of our study of this, we recorded a tap-water droplet on a PE surface inclined at 60° and computed the field around the resultant shape. Figure 8 shows the droplet profile and the computed equipotentials. From this computation, we have determined the variation in field along the surface of the PE between location s A and B shown on figure 10 for an average applied field of 2MV/m between the embedded electrodes

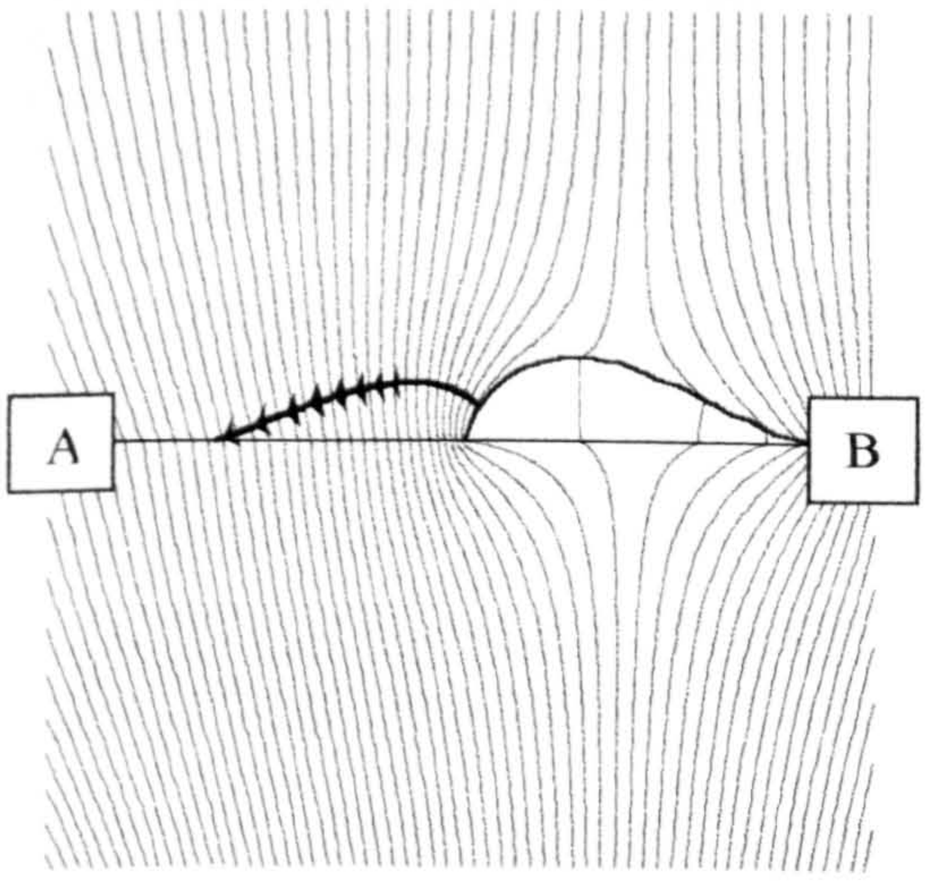

Figure 8. Equipotentials around a droplet on a PE plane inclined at 60°.

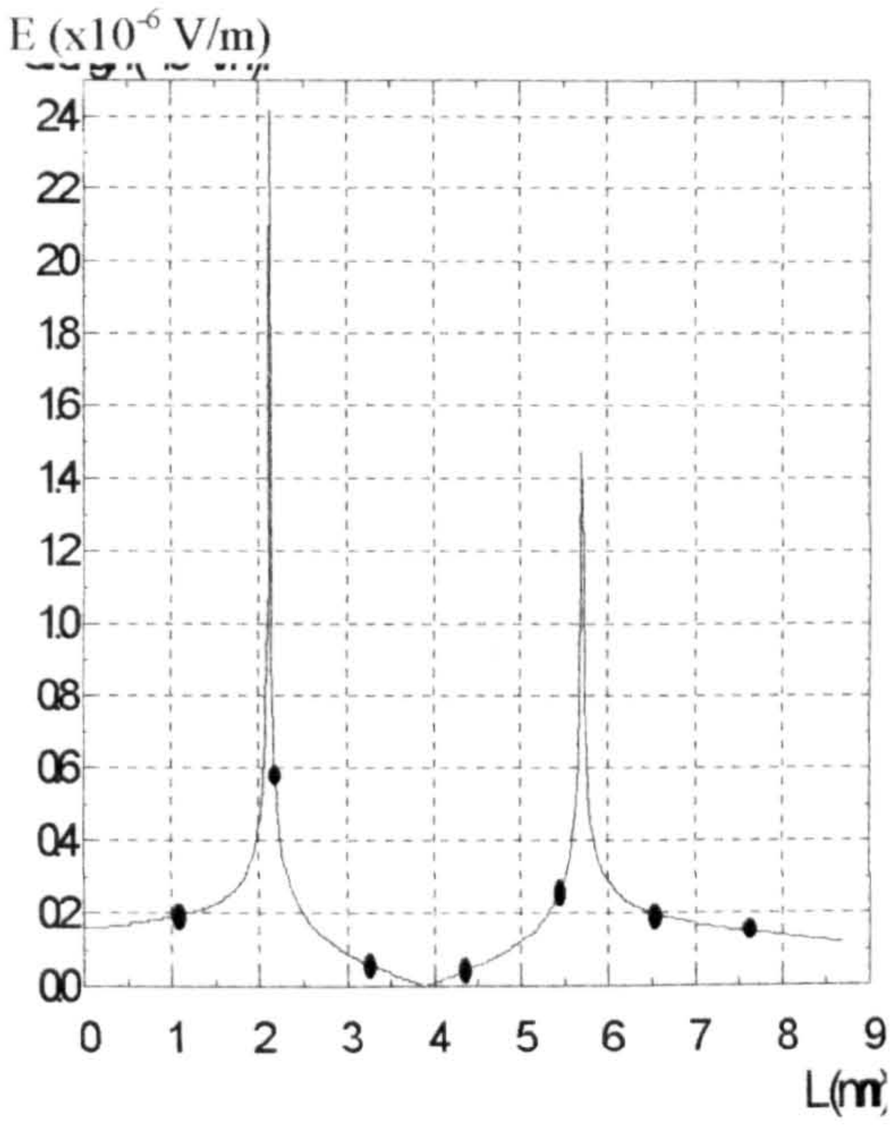

Figure 9. The electric field (E) between the locations A and B of figure 8.

. The results are presented in figure 9, which shows that, for the conditions studied, increasing the contact angle increases the field at the triple junction. It is reasonable to suggest that a similar increase can be expected when the droplet vibrates under an applied AC field. This effect is likely to contribute to the development of partial discharges around a vibrating droplet and to promote eventual full breakdown. It is intended to examine this point in more detail.

6. CONCLUSIONS

As an applied AC field is raised above a threshold level, a water droplet initially vibrates in a fixed position. As the field is raised, the droplet vibrates increasingly vigorously, spreads out and eventually extends over the surface. This process is associated with partial discharge activity at the edge of the droplet. The vibration of the droplet promotes partial discharges by altering the contact angle and so increasing the field near the triple point.

7. ACKNOWLEDGEMENTS

One of us (H.A.G.) wishes to acknowledge support from the Ministry of Defence, Armament Authority, Cairo – Egypt. We also acknowledge support from EPSRC for provision of the high-speed camera system.

8. REFERENCES

[1] A.Krivda and D.Birtwhistle, "Breakdown between Water Drops on Wet Polymer Surface", Ann Rep Conf EIDP, 2001.

[2] N.Dhahbi-Megriche and A.Boreal, " Flash-over Dynamic Model of Polluted Insulators under ac Voltage', IEEE Trans DEI, 17, No2, Apr 2000.

[3] S.Shihab and L.Zhou,"Simulation of Contamination Performance of Outdoor High Voltage Insulators,' IEEE/KTH Stockholm Power Tech Conf, Stockholm, June, 1995.

[4] S.Chakravorti and P.K.Mukherjee, "Power Frequency and Impulse Field Calculation around a HV Insulator with Uniform and Nonuniform Surface Pollution", IEEE Trans. on EI, Vol.28, No.1 Feb 1993.

[5] T.Tokoro and R.Hackam, "Loss and Recovery of Hydrophobicity and Surface Energy of HTV Silicone Rubber", IEEE Trans.DEI , Vol.8, No.6, Dec 2001.

Electrical Breakdown at Sessile Water Droplets on Insulating Surfaces Subject to High AC Stress.

GD 2002

B. H. Crichton, R. A. Fouracre and H. A. Gouda

Institute for Energy and the Environment,
University of Strathclyde, Glasgow, Scotland.

ABSTRACT

Electrical breakdown at the edges of sessile water droplets on a horizontal, insulating surface subject to high AC electrical stress has been studied experimentally. The behaviour of the water droplets under these conditions has been examined using a high-speed video camera and by detecting electrically partial discharge activity. Different modes of droplet vibration have been observed, some of which lead to transient changes in droplet contact angle at the insulator surface with concomitant changes in the electric field in the vicinity of the triple junction. These field effects have been calculated and their significance on partial electrical discharges discussed. Lateral spreading of water droplets has also been observed. It is considered this spreading is associated with the vibration and with the partial discharge activity.

1. INTRODUCTION

Surface pollution in the form of discrete water droplets is known to degrade the performance of high-voltage insulation. A water droplet plays a number of roles in the electrical breakdown at an air / insulator interference: it forms a stress enhancer because of its high permittivity; it deforms or may elongate under the influence of the electric field, through Coulomb and field-gradient forces, which can increase its stress-enhancing features; it can partly short out the insulating surface. Elongated droplets can coalesce to form a ribbon of water between the electrodes. The geometrical orientation and the hydrophilic or hydrophobic nature of an insulator surface can also affect the shape of a water droplet as can the presence of adhesive, cohesive and gravitation forces; crevices and ridges; pollution deposits; etc. See, for example [1, 2, 3, 4, 5, 6, 7].

Surface hydrophobicity is one of the factors known to influence insulator performance. Contact angle, defined as the angle formed between the tangent to the water droplet surface and the horizontal surface in the region of the contact [7], is used to give a measure of the hydrophobic property of a surface. During service conditions hydrophobicity may be lost, and insulator surface may become hydrophilic. It is known that hydrophilic surfaces have a poor performance under wet condition [8].

The present paper describes an experimental study of electrical breakdown at the edges of sessile water droplets on a PE surface subject to AC electrical stress up to a maximum of 20kV/cm (RMS) at 50 Hz. The study involves observing the vibration and other motion of discrete water droplets using a high-speed video camera operating at 3000 frames per second whilst electrically detecting any partial discharge activity in the vicinity of the droplets. The significance of the droplet vibration on electrical stress enhancement is investigated along with the effects on partial discharge activity. Lateral spreading of the water droplets is considered to be evidence of changes in the hydrophobic properties of the insulator surface brought about by the partial discharge activity.

2. EXPERIMENTAL PROCEDURE

Figure 1 illustrates the general experimental arrangement used to investigate the behaviour of discrete water droplets on a polyethylene surface under AC stress.

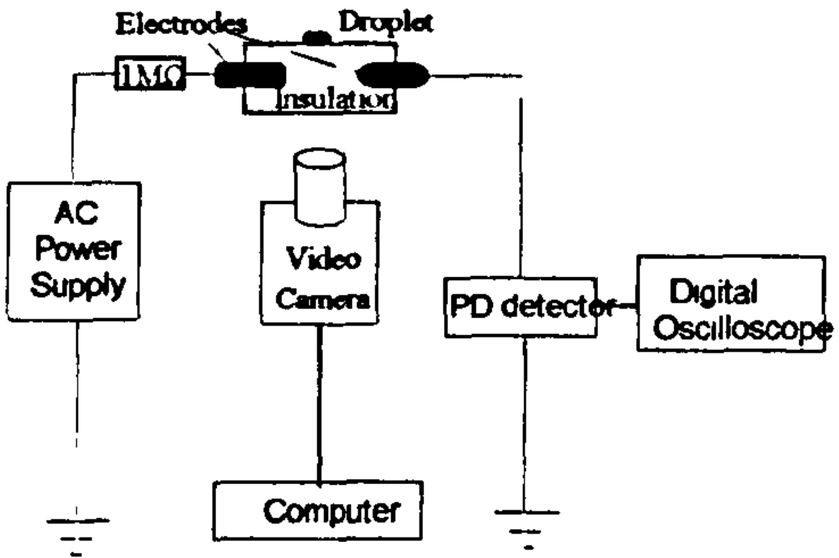

Figure 1. Schematic representation 0f the experimental arrangement.

The high voltage electrode was raised to a maximum of 20 kV AC, 50 Hz. The second electrode was effectively grounded through a low-value resistor used to allow the detection of partial discharges. The electrode arrangement allowed a high electrical field to be generated along the surface of the PE sample. This field was computed using a finite element program. The camera was interfaced to a computer which captured the camera output and subsequently stored the data on CDROM. With the present arrangement, good images were obtained up to a maximum of 3000 frames per second. The volume of the water droplet was typically 10μl and was placed on the PE surface using a syringe. For these initial studies, tap water was used with a conductivity of up approximately 100μs/cm.

Typically, the applied voltage was raised slowly until PD activity was detected. The level of PD activity was then monitored and recorded using the digital oscilloscope. The video camera was then used to detect the onset of vibration of the water drop and the vibration pattern was recorded. The applied stress was then raised until partial discharge activity around the droplet became visible. This activity was also recorded using the high-speed camera.

3. RESULTS AND DISCUSSION

Electrical detection of partial discharges. Figures 2, to 5 show the partial discharge (PD) activity detected electrically by placing a 100-Ω resistor in series with the test gap and observing the voltage pulses generated across it with a digital Oscilloscope.

Fig (2) Partial Discharge no Water Droplet

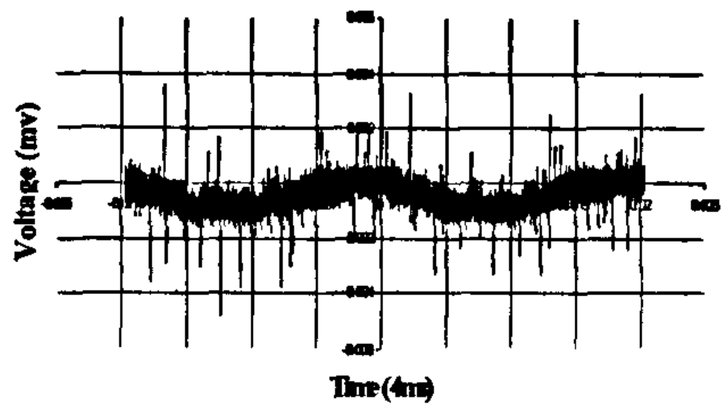

Fig (3) Partial Discharge with water droplet over the sample

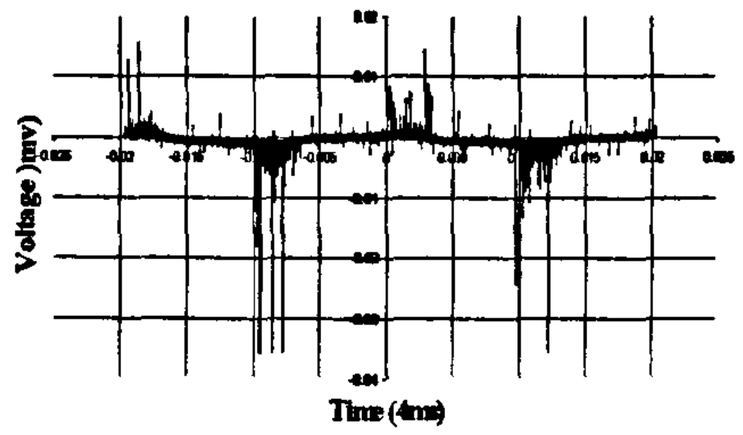

Fig (4) The Partial Discharge with the Water Droplet scattered over the sample

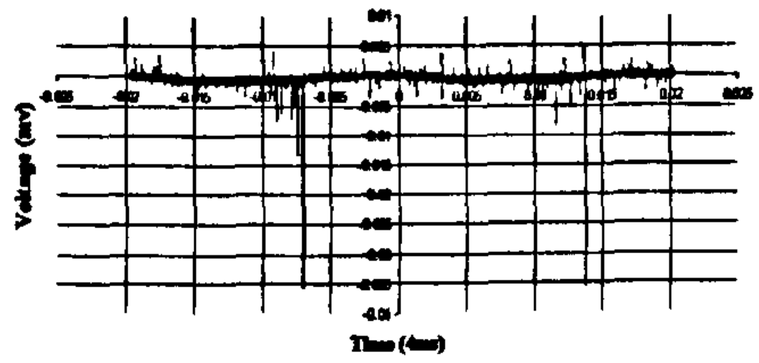

Fig (5) Break Down when the Water Droplet expanded

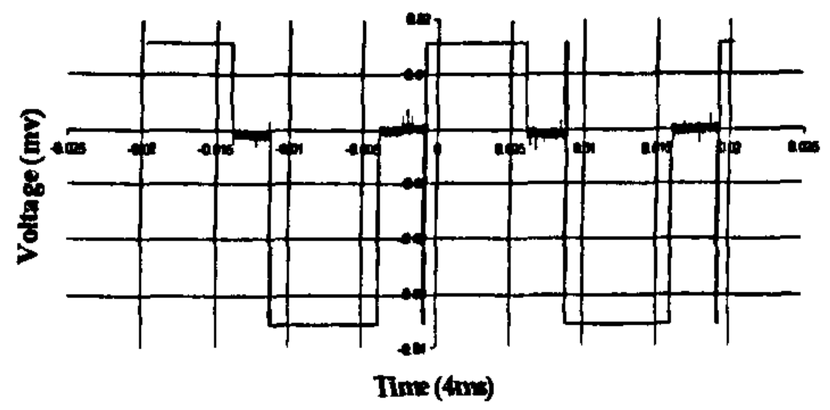

Figure 2 shows that, when no water droplet was present on the sample surface, the onset of PD activity was detected at about 9.5 kV. This PD activity occurs during both half cycles close to the peak value of the applied voltage. At this level of applied voltage, the PD activity was not strong enough to generate any visual damage to the sample or to lead to full breakdown, at least in the short term. In Figure 3, it is shown that when a water droplet is located at the centre of the test sample between the two electrodes, PD activity could be detected when the applied voltage was typically around 6.0 kV. However, at this level of stress no vibration or motion of the droplet

was observed. Partial discharges over the negative half cycle appear stronger than during the positive half cycle. These PD signals were used as a triggering signal for the high-speed digital camera. Figure 4 shows the level of PD activity when the voltage was increased to 7 kV. At this level of applied field, the water droplet was observed to vibrate and subsequently spread over the surface of the insulation sample. Again, the PD activity recorded during the negative half cycle is higher. Figure 5 shows the PD activity when the applied voltage is increased to 8.5 kV. In this case, vibration of the water droplet lead to a spreading over the sample until contact was made with one, or both electrodes, resulting in breakdown of the test sample with physical damage to its surface.

Observation of droplet motion. During the above electrical measurements of partial discharge activity, the mechanical activity undergone by the water droplets on the insulation surface was recorded using a high-speed digital video camera operating at up to 3000 frames per second. Figure 6 shows a sessile water droplet on the insulation surface under an applied voltage of 7kV at 50 Hz.

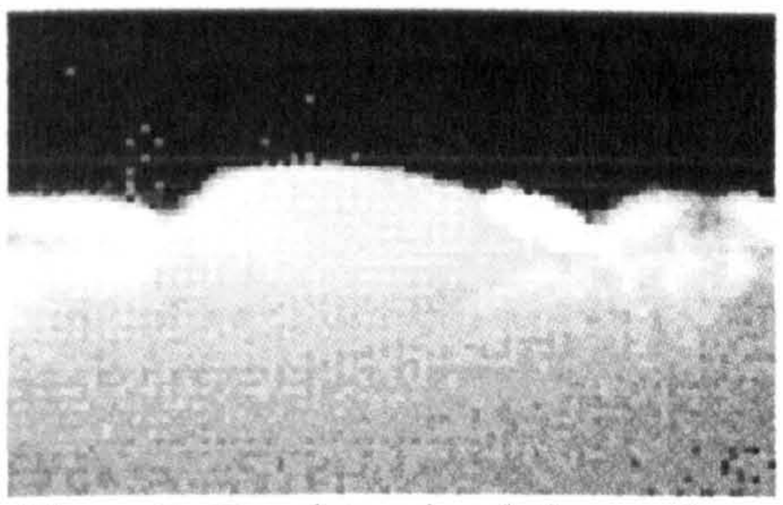

Figure 6. Droplet on insulation surface. Average applied stress 7kV/cm (RMS).

From the video camera records, vibration of the droplet was evident, as were partial discharges at the edges of the droplet nearest to the electrodes.

Electric field at the Edge of a water droplet. The electric field around a droplet on a flat insulating surface was computed in order to examine how electrical breakdown of the air surrounding the droplet might occur around the water droplet edge, as indicated in some of the digital camera records. Figure 7 shows the configuration of droplet examined in this way.

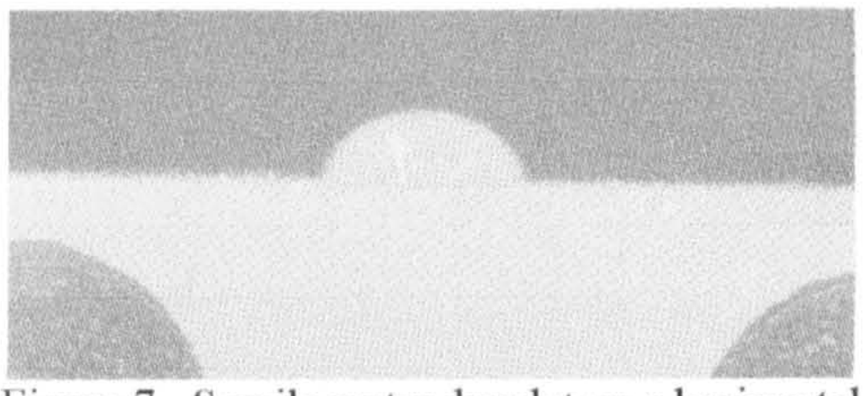

Figure 7. Sessile water droplet on a horizontal PE surface

To examine this, the field along the polymer surface (E_s) starting at the triple junction was compared with the field along a field line (E_l) starting on the droplet surface , but at a short distance away from the triple junction. Figure 8 shows the ratio of E_l to E_s as a function of distance from the droplet.

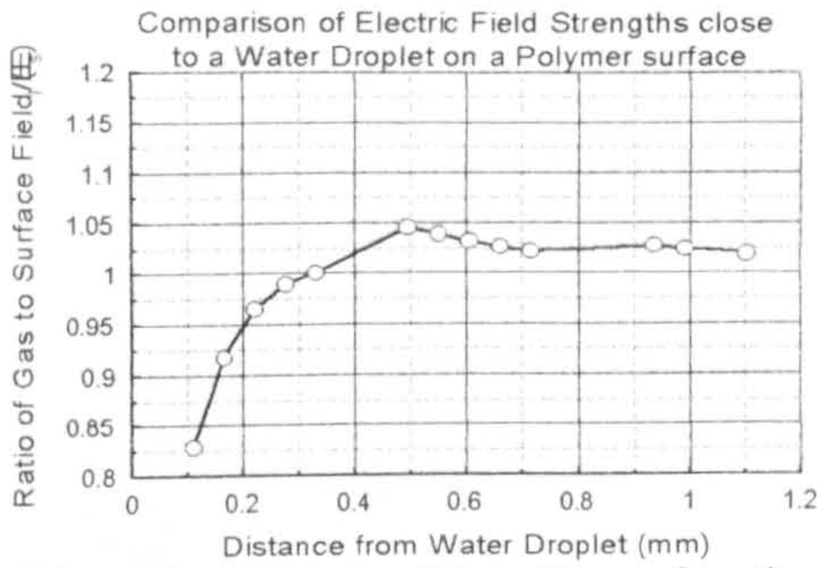

Figure 8. The ratio of E_l to E_s as a function of distance from droplet surface.

This shows that, for the droplet examined and at locations away from the droplet surface, E_l can exceed E_s. This suggests it may be possible to preferentially satisfy the conditions for electrical breakdown in the surrounding air at some distance away from the triple junction, as indicated by digital camera records. Further examination of this possibility is to be undertaken.

4. CONCLUSIONS.

For the conditions examined. With increasing applied AC stress, partial discharges precede the onset of droplet vibration. Lateral spreading of the droplet in the direction of the applied field follows the onset of vibration. There is evidence of partial discharge activity not associated with the triple junction and that, at the same locations, the electric field in the gas surrounding the droplet can exceed the field on the supporting surface.

5. ACKNOWLEDGEMENTS

One of us (H.A.G.) wishes to acknowledge support from the Ministry of Defence, Armament Authority, Cairo – Egypt.

6. REFERENCES

1- N. Dhahbi-Megriche and A. Boreal,' Flashover Dynamic Model of Polluted Insulators under ac Voltage', IEEE Trans. on Dielectric and Elec. Insult. Vol.7 No.2 April 2000.

2- S. Shihab and L. Zhou,' Simulation of Contamination Performance of Outdoor High Voltage Insulators,' IEEE/KTH Stockholm Power Tech Conference, Stockholm, Sweden, June 18-22, 1995.

3- S. Chakravorti and P. K. Mukherjee,' Power Frequency and Impulse Field Calculation around a HV Insulator with *Uniform and Nonuniform Surface* Pollution,' IEEE Trans. on Elec. Insult. Vol.28 No.1 February 1993.

4- D A Swift,' Flashover of an Insulator Surface in Air Due to polluted Water Droplets,' Proceeding of the 4th International Conference on Properties Applications of Dielectric Materials July 3-8, 1994, Brisbane Australia.

5- S. M. Ghufran Ali and H. M. Ryan,' Insulation Co – ordination under polluted conditions,' the 7th BEAMA International Electrical Insulation Conference.

6- B. H. Crichton and H. A. Gouda,' A Study of Water Droplet Behavior on Insulation Surface under High Electric stress,' UPEC 2001 Swansea University Wales.

7- T. Tokoro and R. Hackam,' Loss and Recovery of Hydrophobicity and Surface Energy of HTV Silicone Rubber,' IEEE Trans. on Dielectric and Elec. Insult. Vol.8 No.6 Dec. 2001.

8- Ivan J. S. Lopes, Shesha H. Jayaram and Edward A. Cherney,' A Study of Partial Discharges from Water Droplets on a Silicone Rubber Insulating,' IEEE Trans. on Dielectric and Elec. Insult. Vol.8 No.2 April 2001.